THE UNIVERSITY OF
SYDNEY

Selective Synthesis of Hydrogen from Aqueous-phase Reforming of Glycerol Over Supported Metal Catalysts

A thesis submitted in fulfillment of the requirements for the degree of Doctor of Philosophy by

MOHAMMAD MIZANUR RAHMAN

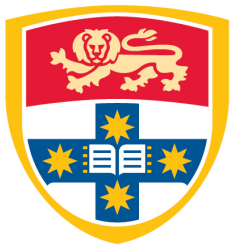

THE UNIVERSITY OF SYDNEY

School of Chemical and Biomolecular Engineering

UNIVERSITY OF SYDNEY

August 2014

DECLARATION

I certify that this thesis does not incorporate, without acknowledgement, any material previously submitted for a degree or diploma in any university. It does not contain any material previously published or written by another person except where due reference is made in the text.

Mohammad Mizanur RAHMAN

ABSTRACT

The current problem of the depletion of fossil-fuel reserves, along with the mounting environmental concerns associated with huge amounts of fossil fuel use, call for new energy systems based on renewable fuels. Hydrogen, a clean fuel that emits only water when combusted or used in PEM (proton exchange membrane) fuel cells, is in growing demand due to the technological advancements made in the fuel cell industry. Of the techniques available to synthesize H_2 sustainably, the aqueous-phase reforming (APR) process, pioneered by Dumesic group shows promise as it gives higher energy efficiency (mild reaction conditions, 200–250 °C at 20–50 bar) and a lower CO concentration (<300 ppm) in the product gas than the conventional processes. The ultimate objective of this project is to be able to feed the H_2 rich and CO free gas directly to PEM fuel cell, without the expense of intermediate gas cleaning or upgrading (CO removing), which was approached by the development of efficient and low cost catalysts.

Firstly, a series of Pt catalysts supported on alumina that was doped with different amounts of CeO_2 were developed, characterized and tested in the aqueous-phase reforming (APR) of glycerol to H_2. Several parameters like pressure, temperature, feed concentration and feed flow rate were optimized. The catalyst 3Pt/3CeAl, in which the support contained 3 wt% CeO_2, showed the highest active surface area and metal dispersion, also showed higher activity and selectivity towards H_2 production, for a 1 wt% glycerol fed with 0.05 mL/min at 240 °C under the corresponding system pressure. No CO could be detected (< 100 ppm) in the

product gas, meaning that the product may be directly useable in a PEM fuel cell.

Secondly, bimetallic Pt-Ni supported on 3 wt% CeO_2-doped Al_2O_3 (3CeAl) and multi-walled carbon nanotubes (MWNT) were studied. XRD, XPS and STEM-EDS analysis shows the evidence of Pt–Ni interaction which is thought to be responsible for their higher activity and selectivity in APR. A bimetallic catalyst – 1 wt% Pt and 3 wt% Ni supported on MWNT was then identified the best one compared to commercial Pt/Al_2O_3

Lastly, due to high cost of noble metals, non-noble based Cu-Ni alloy catalysts supported on MWNT were studied. Amongst the catalysts tested, bimetallic 1Cu–12Ni/MWNT catalyst gave the higher H_2 selectivity (86%) and glycerol conversion (84%). The presence of Cu in bimetallic catalysts resulted in suppression of undesirable methanation reaction. Catalysts characterized by XRD and XPS showed a significant peak shift of Ni in bimetallic Cu–Ni catalysts than the Ni catalyst, suggesting a strong interaction between Cu and Ni. Also H_2–TPR analysis showed that introducing Cu increased Ni reducibility. Though 1Cu–12Ni/MWNT catalyst showed slightly lower H_2 selectivity (86%) than the 1Pt-3Ni/MWNT catalyst (H_2 selectivity 91%), but the former is much cheaper compare to highly expensive Pt catalyst. This measure is crucial to the competitiveness of a catalyst in large-scale H_2 production.

The promising results regarding H_2 production and selectivity in this work mean that a high purity (CO free which is poison to PEM fuel cell anode) of H_2 could be obtainable in future investigations with optimized catalyst design and reaction parameters.

LIST OF PUBLICATIONS

Rahman, M. M., Church, T. L., Minett, A. I. & Harris, A. T. 2013. *Effect of CeO_2 Addition to Al_2O_3 Supports for Pt Catalysts on the Aqueous-Phase Reforming of Glycerol*. **ChemSusChem**, 6, 1006-1013

Rahman, M. M., Church, T. L., Variava, M. F., Minett, A. I. & Harris, A. T., *Bimetallic Pt-Ni composites on ceria-doped alumina supports as catalysts in the aqueous-phase reforming of glycerol*. **RSC advances**, 2014, 4, 18951-18960

Rahman, M. M., Church, T. L., Minett, A. I. & Harris, A. T. *Pt/CeO_2-Al_2O_3 catalyst for the Aqueous-Phase Reforming of Glycerol*. CSIRO Cutting Edge 2012 Symposium. 13-15th Nov. 2012, Victoria, Australia (Poster and Oral presentation)

Rahman, M. M., Church, T. L., Variava, M. F., Minett, A. I. & Harris, A. T., *Bimetallic Pt-Ni composites in the aqueous-phase reforming of glycerol*. International Conference on Mechanical, Industrial and Materials Engineering 2013, November 2013, Rajshahi, Bangladesh (Oral presentation).

Rahman, M. M., Church, T. L., Minett, A. I. & Harris, A. T., *Highly Active Pt-Ni Bimetallic Catalysts Supported on Multi-walled Carbon Nanotube for the Aqueous-Phase Reforming of Glycerol.* Chemeca 2013 Conference, 29 Sep-2 Oct, Brisbane, Australia. (Accepted for oral presentation)

Rahman, M. M., Church, T. L., Variava, M. F., Minett, A. I. & Harris, A. T*., Non-noble based Cu-Ni alloy catalyst in the aqueous-phase reforming of glycerol.* International Conference on Renewable Energy 2014, 10 April 2014, CUET, Bangladesh (Accepted for oral presentation)

ACKNOWLEDGEMENT

I would like to express my sincere gratitude to my supervisor Prof. Dr. Andrew T. Harris, Director of Laboratory for Sustainable Technology. His understanding, encouragement and support made my research experience quite enjoyable. My sincere thanks goes to my Associate supervisor Dr. Tamara L. Church for her detailed review, constructive criticism and excellent discussion during the preparation of my journal papers. Her great insight and logical way of thinking have provided a good basis and guidance throughout my PhD research. Also my sincere thanks to A/Prof. Dr. Andrew I. Minett, Co-Director of Laboratory for Sustainable Technology, for his valuable advice, encouragement and support throughout my PhD research.

I am also grateful for the financial support of University of Sydney International Scholarship, as well as the support from School of Chemical and Biomolecular Engineering at the University of Sydney. Thanks to Dr. Meherzad F. Variava for his cooperation in GC analysis and valuable advise throughout this work. Also I want to thank Dr. Jeffery, technical manager of the school, for his kind help in TOC, ICP-AES, and Porosity measurement experiments in the analytic labs. Furthermore I thank all of my colleagues of Laboratory for Sustainable Technology for all the help I received. It is really a pleasure to work in such comfortable and friendly environment.

I would like to give my special gratitude to my parents. My hearty thanks are due to my loving, encouraging and patient wife Suraia Parvin for her faithful support and inspiration during my PhD study. Without all their understanding it would have been impossible for me to finish this thesis. My special love to my sweet daughter Marwa Rahman Ushbah. Last but not least, I would like to give my deep love to my newborn daughter Umaiza Rahman.

Table of Contents

List of Figures

List of tables

This page intentionally left blank

Chapter 1

Chapter 1 outlined the background, objectives and scope of this research. Literatures were reviewed on previous studies on hydrogen production from aqueous-phase reforming of oxygenated hydrocarbon.

1 INTRODUCTION

1.1 Background

Today, human activities and anthropogenic emissions of green house gases (GHG) are widely regarded as responsible for global warming. The emission of green house gases, believed to be responsible for 0.75 °C increase in temperature with respect to level 1860-1900, is one of the most challenging environmental problem in our time (Energiloget, 2007). Although few debates still remain skeptical, the ambition to decrease GHG emissions has increased during recent years. This can be motivated by the precautionary principle, here representing the view that global warming should be mitigated until we are sure that it is not caused by human activities which for a long time has been very important for international environmental work. In the International Energy Agency's "Reference scenario", global energy related CO_2 emissions are predicted to increase by 55% between 2004 and 2030 (IEA, 2006). The largest part of global green house gas emissions comes from the burning of fossil fuels such as coal, oil and natural gas, which results in the large amounts of CO_2 emitted (57%) to the atmosphere. The second largest source of green house gas emissions (17%) is deforestation and decay of biomass etc. (IPCC, 2007).

At present, fossil fuels provide 81% of the total world's primary energy needs and generate 66.6% of the world's electricity demand. Under current global policies, the total world primary energy supply will reach 17,100 Mtoe by 2030, an increase of 50% over the 2005 energy supply (IEA, 2007a). With the predicted increase in

energy demand over the next 20-30 years, primarily supplied by fossil fuels, there is s need for technologies to address green house gas emissions. Considering the linear extrapolations of the rate of growth of oil consumption and the rate of increase of known oil reserves it can be deduced that the end of petroleum supply will be probably take place around 2050 (Turner, 1999). Natural gas appears as an alternative in the medium term, although a similar method of calculation predicts its total consumption will take place in 70-100 years. Only coal may retain for another couple of centuries.

The concern over energy security and climate change demonstrate the need for an energy economy where resources are renewable and green house gas emissions are reduced. Renewable energy resources such as biomass, solar, wind, geothermal, hydro and wave are capable of reducing green house gas emissions. So, a universal energy carrier derived from renewable sources, for example hydrogen, can address concerns regarding greenhouse gas emissions and reliable energy supply. Hydrogen is considered to be an ideal energy carrier in the future as the only by-product of hydrogen combustion is water vapor (if air is used for flame combustion of hydrogen small amounts of NO_x are produced). Hydrogen can be used as a fuel in furnaces, internal combustion engines, turbines and jet engines, and can also be converted directly to electricity in the fuel cells, with a variety of applications in transportation and stationary power generation. The only limitation in mobile applications is currently the storage of hydrogen. Hence, using renewable resources to produce hydrogen is one of the most promising alternatives for renewable energy sources in the period of diminishing fossil fuel reserves.

1.2 Hydrogen production from biomass

Concern about depletion of fossil fuel reserves and the pollution caused by continuously increasing energy demands make hydrogen an attractive alternative energy source (Cortright et al., 2002). Currently world hydrogen production is around $5x10^{11}$ Nm^3 per year, which corresponds to around 2% of primary energy demand. Figure 1-1 shows the principal production routes, indicating that 96% is produced from fossil fuel (Ewan and Allen, 2005).

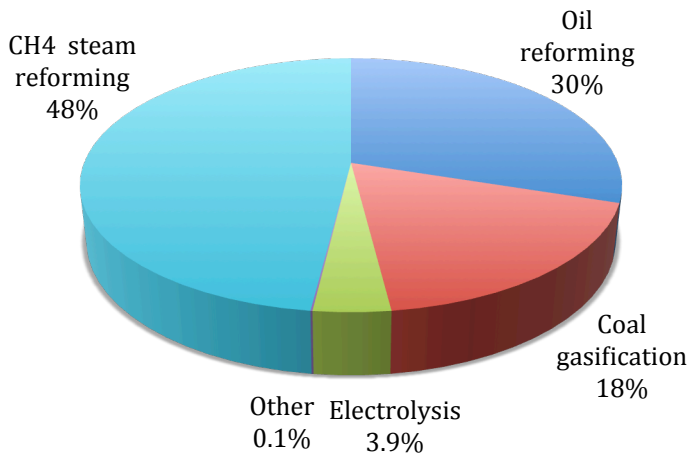

Figure 1-1 Present primary energy sources for hydrogen production (Data from Ewan and Allen, 2005)

However, hydrogen production can be environmentally friendly only if the resource used to produce hydrogen is carbon neutral. Biomass derived hydrogen production is classified as carbon neutral because the CO_2 released during hydrogen production is consumed by further biomass generation (Shapouri et al., 2002). Figure 1-2 illustrates the different routes, which can be adopted to produce

hydrogen from biomass. In addition to these, there are other biological routes to produce hydrogen.

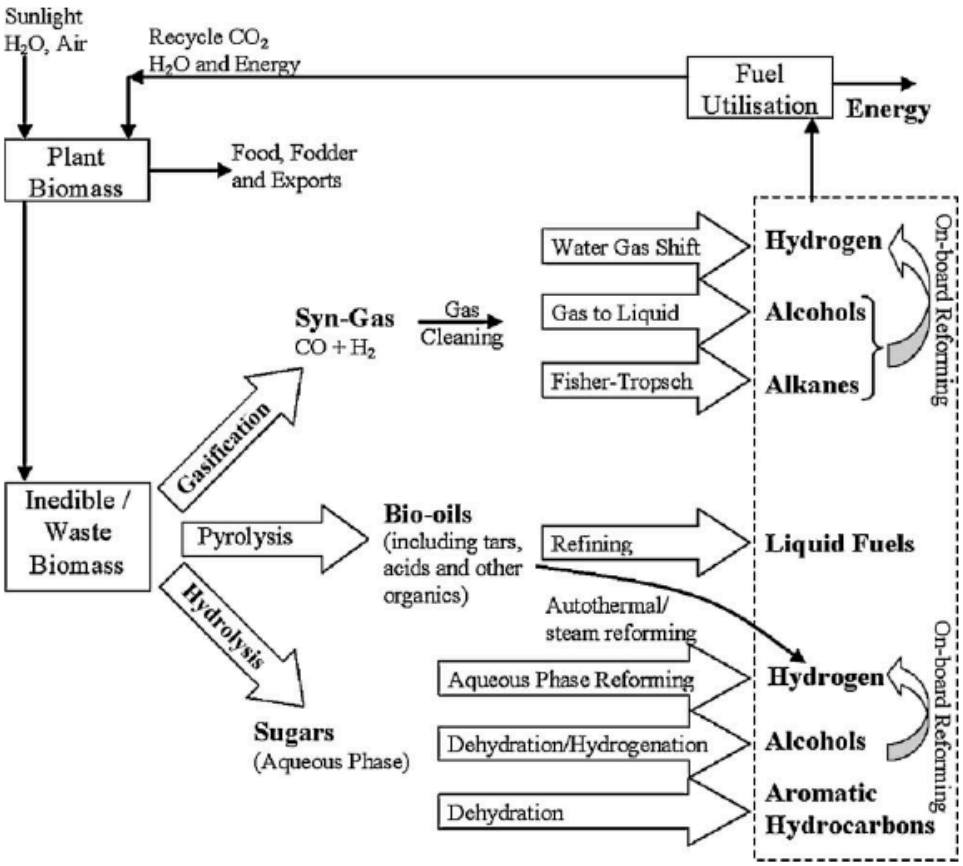

Figure 1-2 Hydrogen and liquid fuels production from biomass sources. The waste CO_2, H_2O and energy produced from these fuels can be utilized to produce further biomass. Reproduced from Tanksale (Tanksale et. al., 2010)

Wang et. al. (Wang et al., 1996) first introduced the hydrogen production concept from biomass. In their experiments, they used commercial Ni-based catalysts for the steam reforming of acetic acid and hydroxyacetaldehyde, which are major liquid products derived from the pyrolysis of carbohydrates in biomass. The yield of H_2 from hydroxyacetaldehyde and acetic acid was about 80 and 75%

respectively. Though, H_2 yield was almost similar, however, CH_4 yield from hydroxyacetaldehyde was much less than from acetic acid. They also studied ethanol, ethylene glycol, glycerol, and acetol steam reforming over the commercial nickel based catalyst called UCI G-90C. These reactants were almost completely converted at 400 $^{\circ}$C in a fixed bed reactor, the hydrogen yield varied between 94 and 100%. Chornet et al. (Chornet et al., 2002) studied hydrogen production from biomass based liquids including pyrolysis bio-oil from sawdust, hemicellulose, trap grease and crude glycerin. Crude glycrol from transesterification of vegetable oil contains 55% glycerin and methyl esters of fatty acids. The hydrogen yield from crude glycerin was around 77% of the stoichiometric amount. The total conversion of CO in the gas through water gas shift reaction would increase the hydrogen yield to 95% of the theoretically value. Moreover, the steam reforming of waste vegetable oils, particularly "trap grease", was examined by Chornet and co-worker (Chornet et al., 2002) recently in a fluidized bed reactor using a commercial nickel based catalyst. The conditions of steam reforming were temperatures slightly above 1073 K, a steam-to-carbon (S/C) ratio of 3-5 and a methane-equivalent space velocity of 900-1200 h^{-1}. Under such conditions, 100% of the tap grease was converted to gas. The hydrogen yield during the first 120 hours was 25 g per 100 g of grease, which is 74% of the possible stoichiometric conversion.

Also couple of vegetable oils, like, sunflower, rapeseed, corn and soybean oils were also investigated for the production of hydrogen by steam reforming. Marquervich et al. (1983) performed the experiments in an isothermal fixed-bed

tubular reactor, using both the laboratory and commercial Ni catalysts, at steam to carbon (S/C) ratios of 9, 6, and 3, at temperatures between 500 and 630 ºC and at a pressure of 1-2 bar. Results for the steam reforming of sunflower, rapeseed, corn, and soybean oils at the same catalyst temperature and S/C ratio showed that oil conversion to gases and hydrogen yields were not depended on the type of vegetable oil.

Recently, Dumesic and co-workers has reported that hydrogen rich syngas can be produced from the aqueous-phase reforming of oxygenated hydrocarbon at mild reaction conditions (Dumesic, 2010, Dumesic et al., 2009, Dumesic, 2012, Davda et al., 2005, Cortright et al., 2002, Dumesic et al., 2011). The most effective catalysts on aqueous-phase reforming of oxygenated hydrocarbon solutions were Pt/Al_2O_3, $NiSn/ Al_2O_3$, Raney-Ni, and Raney-NiSn catalysts. The APR process, pioneered by the Dumesic group, uses supported metal catalysts under mild reaction conditions (200–250 °C, 20–50 bar) for the production of hydrogen from oxygenated hydrocarbons in a single step (Cortright et al., 2002, Huber et al., 2004, Davda et al., 2003). The APR process is promising because it has several advantages over steam reforming process of hydrocarbons. APR eliminates the need to vaporize both water and the oxygenated hydrocarbon, which reduces the energy requirements for producing hydrogen. APR occurs at low temperatures that minimize undesirable decomposition reactions typically encountered when carbohydrates are heated to elevated temperatures. The oxygenated compounds are non-flammable and non-toxic, allowing them to be stored and handled safely. Additionally, since water-gas-shift (WGS) reaction is an exothermic reaction, it

favors low temperatures, resulting in low levels of CO (<300 ppm) than conventional steam reforming processes (Huber et al., 2006), a contaminant that poses well-known problems to the use of hydrogen in, for instance, fuel cell applications (Cortright et al., 2002, Davda et al., 2005).

1.3 Glycerol from bio-diesel

Glycerol is a valuable by-product of biodiesel industry, while doing transesterification (also called methanolysis when methanol is used) of vegetable oils or animal fats with methanol in the presence of acid or base catalysts. The overall transesterification reaction (Maris and Davis, 2007) can be described by three below reactions:

$$Triglyceride + ROH \underset{catalyst}{\leftrightarrow} Diglyceride + R^{'}COOR \quad (1\text{-}1)$$

$$Diglyceride + ROH \underset{catalyst}{\leftrightarrow} Monoglyceride + R^{''}COOR \quad (1\text{-}2)$$

$$Monoglyceride + ROH \underset{catalyst}{\leftrightarrow} Glycerol + R^{'''}COOR \quad (1\text{-}3)$$

where R= $-CH_3$ /C_2H_5, and $R^{'}$, $R^{''}$ and $R^{'''}$ are long-chain hydrocarbons which may be the same or different.

The first step is the conversion of triglycerides to diglycerides, followed by the conversion of diglycerides to monoglycerides and of monoglycerides to glycerol, yielding one methyl ester molecule per mole of glyceride at each step (Maris et al., 2007). Catalysts used for the transesterification of triglycerides are classified as

alkali, acid, enzyme or heterogeneous catalysts. Most commonly sodium hydroxide, sodium methoxide and potassium hydroxide are used as catalysts, which cause formation of several by-products such sodium salts in the crude glycerol. If the oil has a high content of free fatty acids and water, acid catalyzed transesterification is suitable. The common acids are sulfuric acid, phosphoric acid, hydrochloric acid or organic sulfonic acid.

The general industrial process of bio diesel production is shown in Figure 1-3 (Kuiper et al., 1973). The transesterification of the vegetable oils with methanol catalyzed by basic catalysts (NaOH) in a CSTR or plug flow reactor is the first step in the process.

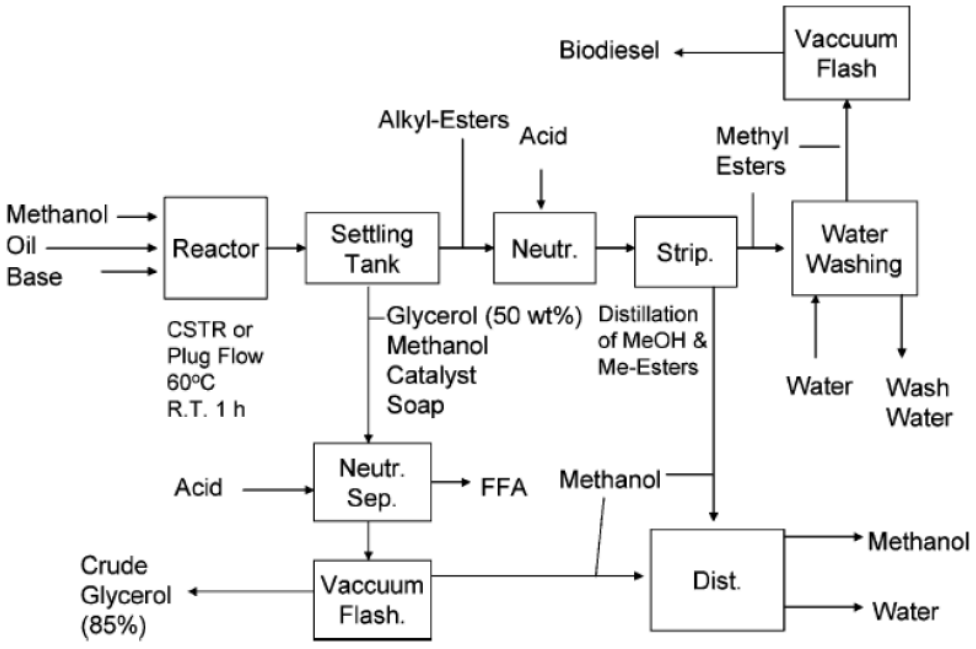

Figure 1-3 Basics of bio-diesel process. Reproduced from Kuiper (Kuiper et al., 1973).

The reaction is carried out at 60 °C under atmospheric pressure with a residence time of about 1 h. The products from the reaction are in two phases: a glycerol-rich phase and a methyl ester-rich phase, which are separated in a settling tank and a centrifuge. The glycerol stream contains mixture of approximately 50 wt% glycerol, the base catalyst and soap. The soap formation from base catalysts can be form via below equation.

$$R - COOH + NaOH \rightarrow R - COONa + H_2O \quad (1\text{-}4)$$

This fraction is neutralized with acid and the soap forms fatty acids, which are later separated from the glycerol stream. The fatty acid can be recycled and used for bio-diesel production. A vacuum flash process separates the methanol and glycerol phases, yielding 85 wt% crude glycerol. The methyl ester-rich stream, which also contains 2-3 wt% methanol, a small amount of base and small amounts of di- and monoglycerides, is neutralized prior to methanol removal, which removes the remaining catalyst and soap. The methanol in the methyl ester stream is then stripped by vacuum flash or in a falling film evaporator. Subsequent water washing removes salts and fatty acid from the methyl ester stream. The water remaining in the bio-diesel is removed during a final drying step in a vacuum flash process. Water is also removed from the methanol stream and the remaining methanol is recycled in the process.

As biodiesel production increases exponentially, the crude glycerol is also produced in a large amount. One ton of biodiesel yields about 110 kg of crude glycerol or about 100 kg of pure glycerol (Behr et al., 2008). Consequently, the

price of glycerol dropped down from $0.43/kg in 2003 to $0.18/kg in 2010 for pure glycerol, and to only $0.02/kg for crude glycerol (Maglinao and He, 2011). Therefore, it is imperative to find alternative uses for glycerol. A variety of chemicals and fuels including hydrogen can be produced from glycerol.

1.4 Hydrogen production from glycerol

Hydrogen can produce by using several processes as shown in Figure 1-2. Now we will discuss different generation methods used to produce hydrogen, using glycerol as a substrate.

1.4.1 Steam reforming (SR)

Steam reforming is a process operated at atmospheric pressure at high temperature (>400 °C) using catalysts based on nickel, cobalt or noble metals. Commercial steam reforming catalysts avoid the use of noble metals as the process is conducted at very high temperature. Ni is the metal preferred but can be promoted by addition of metal oxide from outside noble metal group. The most important parameters in the steam reforming process are temperature, steam-to-carbon (S/C) ratio and catalyst-to-feed ratio. Steam reforming of natural gas is carried out in the range of 800-900 °C, with a molar S/C ratio in the range of 3-5 and a space velocity (by weight) of 1500-2000 h^{-1}. High temperature and excess steam favorably shift the equilibrium and increase the rate of the reforming reaction. The reaction between CO and H_2O to H_2 and CO_2 (Water gas shift reaction) is carried

out in a separate reactor operating at a lower temperature. Oxygenated organic compounds such as methanol or acetic acid are more reactive than hydrocarbons and therefore, reforming can be carried out at lower temperatures. Steam reforming of oxygenated compounds has been described by Wang et.al., who studied the reforming of ethanol and other alcohols at 400-700 °C and pressures slightly above atmospheric pressure in a fixed-bed micro reactor. The industrial catalysts used, UCI G-90C, contained 15% Ni on a ceramic support ($Al_2O_3/CaAl_2O_4$). At 400 °C they observed almost the complete conversion of ethanol, ethylene glycol, glycerol, and acetol at a GHSV = 2240 h^{-1} (0.25 ml catalyst), S/C = 5 and a residence time of 0.02 s. The catalyst showed serious deactivation after a short period of high activity at this temperature (Wang et al., 1996).

Chornet et al. and Takanabe et al. (Chornet et al., 2002, Takanabe et al., 2004) studied on steam reforming of biomass-derived liquids with a fluidized-bed reactor, which provide the better-mixed regime than fixed bed reactor. The superheated steam at a pressure slightly above atmosphere was used as a fluidizing gas as well as a reactant in the reforming process. A nickel based catalyst from Sud-Chemie, designed for naphtha reforming in a fix bed reactor system, was used at 850 °C. A high hydrogen yield from crude glycerin was achieved and a deactivation of the catalyst during the glycerol steam reforming process was not observed.

The steam reforming reaction of oxygenated organic compounds (Wang et al., 1996) proceeds via reactions shown in (1-5) and (1-6):

• Complete steam reforming:

$$C_nH_mO_k + (n - k)\ H_2O \rightarrow CO + [(n + m/2 - k)]\ H_2 \quad (1\text{-}5)$$

• Partial thermal decomposition: (or cracking)

$$C_nH_mO_k \rightarrow C_xH_yO_z + \text{gas } (H_2, CO, CO_2, CH_4 \ldots .) + \text{coke} \quad (1\text{-}6)$$

Because of the excess of steam used in the process, carbon monoxide further undergoes the water gas shift reaction (1-7):

• Water gas shift reaction:

$$n\ CO + n\ H_2O \rightarrow n\ CO_2 + n\ H_2 \quad (1\text{-}7)$$

The sum of reaction in equation (1-5) and (1-7),

$$C_nH_mO_k + (2n - k)\ H_2O \rightarrow n\ CO_2 + [(2n + m/2 - k)]\ H_2 \quad (1\text{-}8)$$

Thus, the maximum (stoichiometric) yield of hydrogen that can be obtained by reforming and water gas shift (corresponding to the complete conversion of organic carbon to CO_2) equals 2 + m/2n – k/*n* moles per mole of carbon in the feed. In the case of glycerol, $C_3H_8O_3$, the yield of hydrogen is 2.33 moles per mole of carbon in the feed as described in reaction (1-9):

$$C_3H_8O_3 + 3\ H_2O \rightarrow 3\ CO_2 + 7\ H_2 \quad (1\text{-}9)$$

In reality, this yield will always be lower than the stoichiometric maximum because both the steam reforming and water gas shift reactions are reversible, resulting in the presence of some carbon oxides and methane (because of series selectivity issue with methanation reaction) in the product.

Also Dou et. al. (Dou, 2009) studied sorption-enhanced steam reforming of glycerol at atmospheric pressure within a temperature range of 400–700 °C. A commercial Ni-based catalyst and a dolomite sorbent were used for the steam reforming reactions and in situ CO_2 removal. The results showed that H_2 productivity was greatly increased with increasing temperature and the formation of methane by-product became negligible above 500 °C. The results suggested an optimal temperature of 500 °C for the glycerol steam reforming with in situ CO_2 removal using calcined dolomite as the sorbent, at which the CO_2 breakthrough time was longest and the H_2 purity was highest.

1.4.2 Partial oxidation (PO)

In the partial oxidation process, a substrate is reacted with oxygen at sub-stoichiometric ratios. The oxidation reaction results in heat generation and high temperature. The objective of reforming in the presence of the air is to balance the energy required for the process by oxidizing some of the substrate. If excess air is added, all the substrate will be oxidized and produce mainly carbon dioxide and water. The process can be shown as follows:

$$\text{Substrate } (C_nH_mO_k) + \text{Air} \rightarrow CO/CO_2 + H_2 + N_2;\ \Delta H < 0 \qquad (1\text{-}10)$$

This process may be conducted with or without catalysts. Gasification is an analogous example for the partial oxidation process. Dauenhauer et al. (Dauenhauer et al., 2006) had performed glycerol oxidation at various temperatures and C/O ratios over Pt/Al_2O_3 . The complete combustion of glycerol

occurs at C/O = 0.43. The hydrogen selectivity increased as the C/O increased from 1.0 and became flat and started decreasing as C/O increased further. The reduction of H_2 selectivity at higher C/O (less oxygen) is mainly due to reduction in temperature which results in lower glycerol conversion. At C/O ratio of 1.2, temperature = 1055 °C, complete glycerol conversion was achieved and the H_2 selectivity was 56% (Dauenhauer et al., 2006). Dalai and his coworkers (Valliyappan T, 2008) performed steam gasification of crude and pure glycerol at 800 °C at various steam to glycerol ratio with and without catalyst. Their study concluded that H_2 and total gas production was higher from crude glycerol than those from pure glycerol. That was probably due to the presence of potassium in the crude glycerol that tends to favor the gasification process.

1.4.3 Autothermal reforming (ATR)

Autothermal process combines the effect of partial oxidation and steam reforming by feeding fuel, air, and water together into the reactor. This process is carried out in the presence of a catalyst. The steam reforming process absorbs the heat generated by the partial oxidation process. The process can be depicted as follows:

$$\text{Substrate } (C_nH_mO_k) + \text{Air} + \text{steam} \rightarrow CO/CO_2 + H_2 + N_2;\ \Delta H = 0 \qquad (1\text{-}11)$$

Dauenhauer et al. (Dauenhauer et al., 2006) produced H_2 via autothermal steam reforming of glycerol over Rh-Ce/Al_2O_3 catalyst. Their study found that the addition of steam suppressed CO formation and Rh catalysts supported on Ce with Al_2O_3 washcoat exhibit higher H_2 selectivity. The main benefit of the autothermal

process is that, ideally, it should not require any energy for reaction to occur whereas steam reforming is highly an endothermic process. Although the autothermal steam reforming process has advantages over conventional steam reforming (Dauenhauer et al., 2006), the amount of hydrogen produced from autothermal reforming would be less (on a thermodynamic basis). Swami and Abraham (Swami et al., 2006) compared autothermal and conventional steam reforming of glycerol process over Al_2O_3 supported Pd/ Ni/Cu/K catalyst. The operating conditions were 550–850 °C, steam/carbon (S/C) = 3.0 and oxygen/carbon (O/C) = 0.3. Their study showed that the autothermal steam reforming process produced higher amounts of hydrogen, which was in contrast to the previous study (Rioche, 2005). However, higher temperatures favor hydrogen production in both cases. Douette et al. (2007) (Douette et al., 2007) performed glycerol reforming for hydrogen production at various ratios of O/C and S/C. Their study showed that 4.4 mol of hydrogen was produced per mole of crude glycerol under similar conditions but coking and catalyst deactivation was of great concern (Douette et al., 2007).

1.4.4 Aqueous phase reforming (APR)

Recently Cortright et al. have reported that hydrogen can be generated by catalytic reforming of biomass derived oxygenated hydrocarbons in liquid water at mild reaction conditions (200-250 °C, 20-50 bar) (Cortright et al., 2002). The preferred substrates for this reaction should contain a carbon to oxygen ratio of one in the

molecule. Therefore, chemicals which are easily available from renewable resources such as glucose, cellulose, ethylene glycol, glycerol, sorbitol represents an ideal feedstock for this reaction. Feedstock having lower number of C-atom favors hydrogen selectivity rather than alkane selectivity as shown in Figure 1-4 (Cortright, 2002).

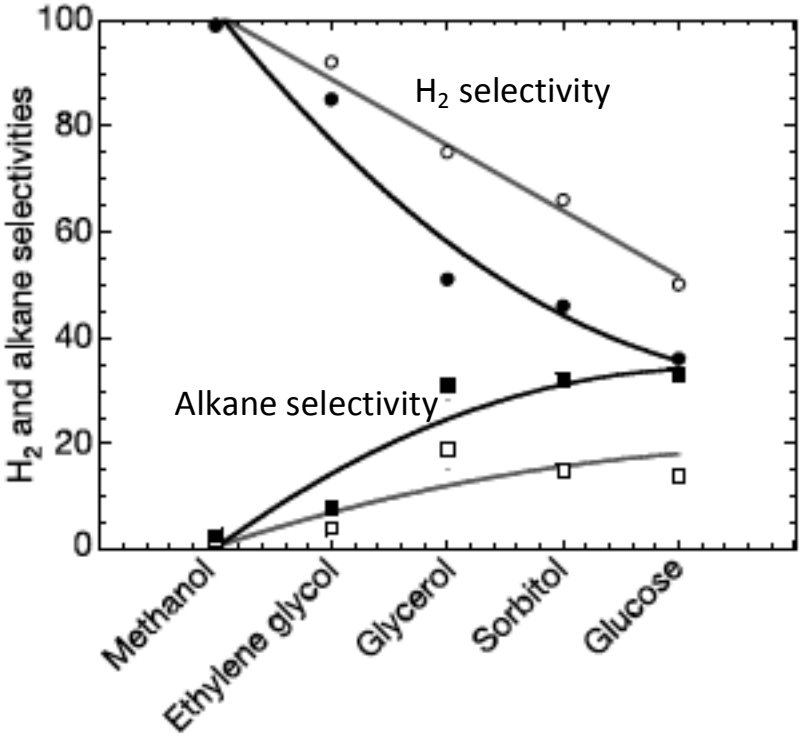

Figure 1-4 Selectivity versus oxygenated hydrocarbon. 1 wt% oxygenated hydrocarbon over $3Pt/Al_2O_3$ catalyst at 425 °C (opened symbols) and 538K (filled symbols). Reproduced from Cortright (Cortright et al., 2002).

The aqueous phase reforming (APR) process is a unique method that generates hydrogen from aqueous solutions of oxygenated compounds in a single step process compared to the three or more reaction steps required for the conventional gas phase reforming processes (Ewan and Allen, 2005). The major advantage of the APR process is that the reforming is done in the liquid phase at significant

lower temperatures (200–250 °C) where the water gas shift reaction is favorable, making it possible to generate hydrogen with low amounts of CO (< 300 ppm) in a single reactor. Furthermore, the APR process is possible at pressures from 15 to 50 bar where the hydrogen-rich effluent can be effectively purified using pressure-swing adsorption or membrane technologies. Additionally, the oxygenated compounds are nonflammable and non- toxic, allowing them to be stored and handled safely (Davda et al., 2005).

1.5 Basis of reforming process

1.5.1 Thermodynamic considerations

Steam reforming of hydrocarbons, oxygenated hydrocarbons having a C:O ratio of 1:1 and water-gas shift reaction to form CO_2 and H_2 from CO are according to reactions (1-12), (1-13) and (1-14) respectively.

$$C_nH_{2n+2} + nH_2O \Leftrightarrow nCO + (2n+1)H_2 \quad (1\text{-}12)$$

$$C_nH_{2y}O_n \Leftrightarrow nCO + yH_2 \quad (1\text{-}13)$$

$$CO + H_2O \Leftrightarrow CO_2 + H_2 \quad (1\text{-}14)$$

Figure 1-5 shows that steam reforming of oxygenated hydrocarbons to produce CO and H_2 is thermodynamically favorable at significantly lower temperatures than those required for alkanes (only at temperature higher than 675K) with similar number of carbon atoms. Figure 1-5 also shows that the value of $\Delta G^0/RT$

for water-gas shift of CO to CO_2 and H_2 is more favorable at lower temperatures. Therefore, it might be possible to produce H_2 and CO_2 from steam reforming of oxygenated compounds utilizing a single- step catalytic process, since the water-gas shift reaction is favorable at the same low temperatures at which steam reforming of carbohydrates is possible.

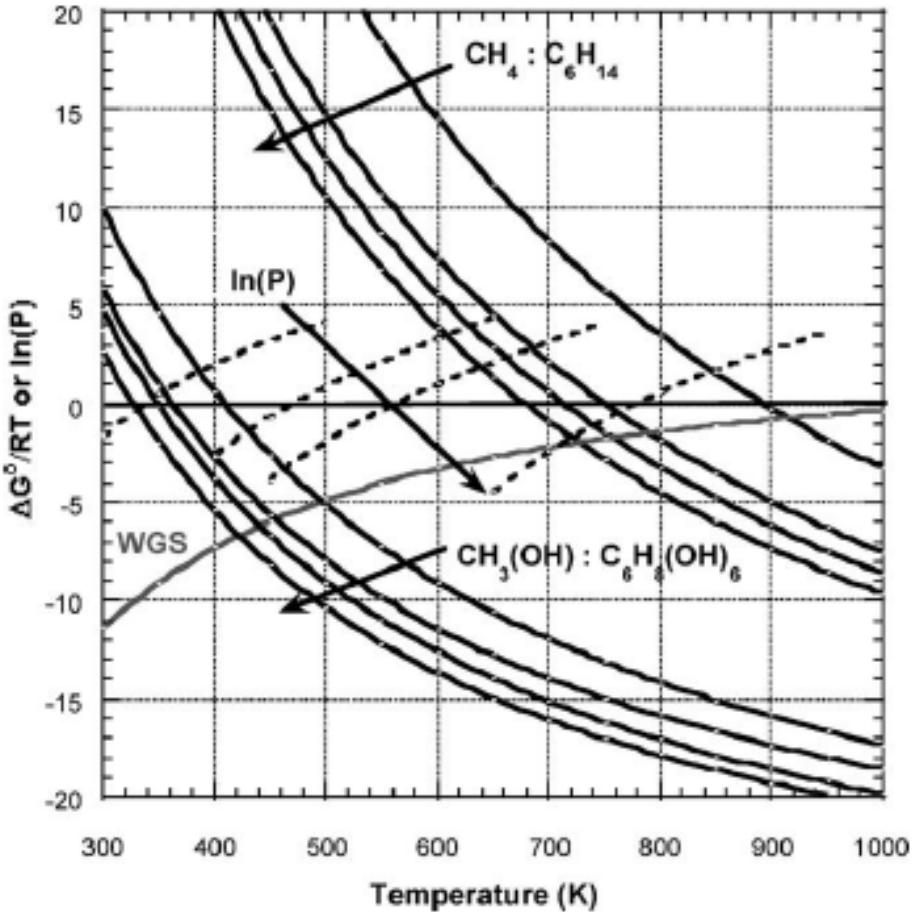

Figure 1-5 $\Delta G^0/RT$ vs. temperature for production of CO and H_2 from vapor-phase reforming of alkanes; oxygenated hydrocarbons; and water gas shift. Dotted lines show values of ln(P) for vapor pressure vs. temperature of $CH_3(OH)$, $C_2H_4(OH)_4$, $C_3H_5(OH)_3$ and $C_6H_8(OH)_6$ (pressure in units of atm). Reproduced from Davda (Davda et al., 2005)

Figure 1-5 also shows the plots of the logarithm of the vapor pressures (atm) versus temperature. It is apparent that the vapor-phase reforming of methanol, ethylene glycol, and glycerol can be carried out at temperatures near 550 K, since the values of $\Delta G^0/RT$ are favorable and the vapor pressures of these oxygenated reactants are higher than 1 atm at this temperature. In contrast, vapor-phase reforming of sorbitol must be carried out at temperatures near 750 K. Importantly, reforming of oxygenated hydrocarbons, if carried out in the liquid phase, would make it possible to produce H_2 from carbohydrate-derived feedstocks (e.g., sorbitol and glucose) that have limited volatility, thereby taking advantage of single-reactor processing at lower temperatures.

1.5.2 Kinetic considerations

According to the APR mechanism reported by Dumesic, a good APR catalyst should not only be active for the cleavage of the C–C bond, but also be active for the water–gas shift (WGS) reaction(Dumesic, 2010). Moreover, the catalyst should be inert to competing parallel and sequential reactions such as C–O cleavage and the methanation reaction ($H_2 + CO_2 \rightarrow CH_4 + H_2O$), which greatly deteriorate the yield of H_2. Sinfelt and Yates (Sinfelt, 1973), have studied the catalytic activities of different metals for C-C bond breaking during ethane hydrolysis, and the relative rates for different metals have shown in Figure 1-6 . Again Grenoble et al. (Grenoble et al., 1981), have studied the relative catalytic activities for WGS over different metals supported on alumina, and these data

have also shown in Figure 1-6. Among the metals tested, Cu exhibits highest WGS rates but this metal shows no activity for C-C bond cleavage. Figure 1-6 also shows the relative rates of methanation catalyzed by different metals supported on silica, as reported by Vannice (Vannice, 1977). Thus, upon comparing the catalytic activities of different metals in Figure 1-6, it can be concluded that Pt and Pd should show suitable catalytic activity and selectivity for production of hydrogen by APR of oxygenated hydrocarbons, which requires reasonably high activity for C-C bond breaking and WGS reactions, and low activity for methanation.

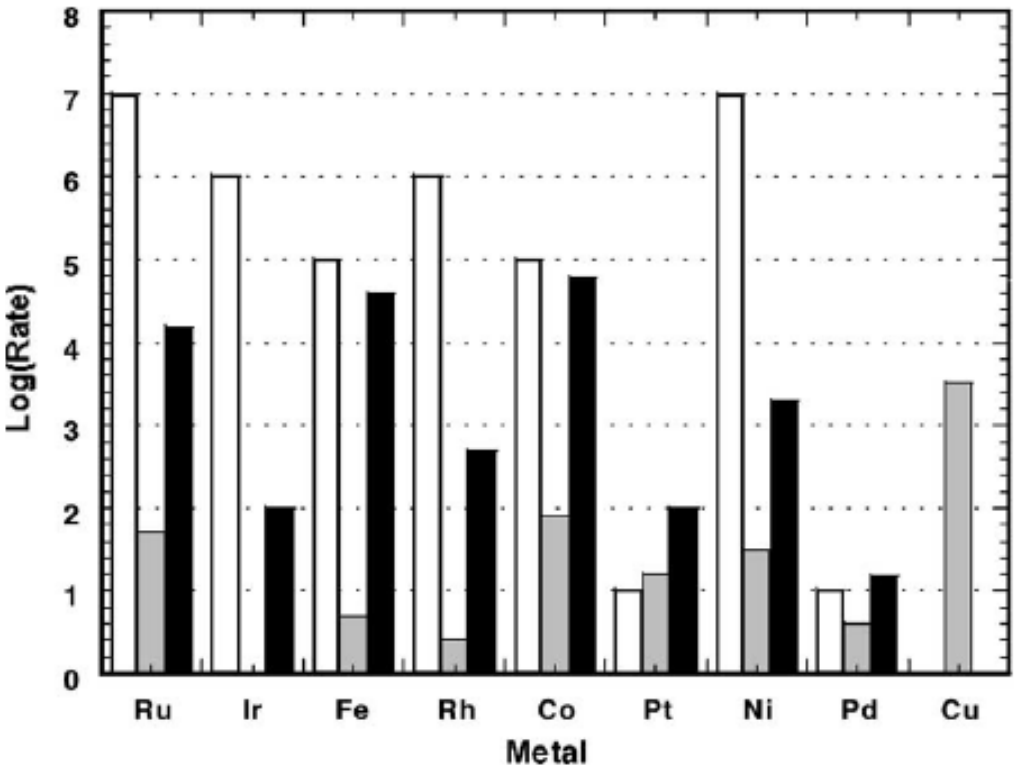

Figure 1-6 Relative rates of C-C bond breaking reaction by Sinfelt et al., 2006 (white), water-gas shift reaction by Grenoble et al., 1981 (grey), methanation reaction by Vannice, 1977 (black); In this figure, the rate of a particular reaction can be compared for different metals; however, for a specific metal, the absolute rates of the three different reactions cannot be compared relative to each other. Reproduced from Davda (Davda et al., 2003)

1.5.3 Selectivity challenges

Selectivity challenge must be overcome to generate hydrogen from oxygenated hydrocarbon, since the subsequent reaction of H_2 and CO_2 to form alkanes and water is also highly favorable at low temperatures. For example, the equilibrium constant for the liquid phase reforming of ethylene glycol at 227 °C is of the order of 10^7 and at same conditions the equilibrium constant for the conversion of CO_2 and H_2 to methane is of the order of 10^{10} mol^{-1} of CO_2 (Davda et al., 2003).

Figure 1-7 shows a schematic representation of the reaction pathways that is believed to be involved in the formation of H_2 and alkanes from oxygenated hydrocarbons over a metal catalyst. The reactant undergoes dehydrogenation steps on the metal surface to give absorbed intermediates before cleavage of C-C or C-O bonds. The absorbed species can be formed on the metal surface either by formation of metal-carbon bonds or metal-oxygen bonds. For example, on Pt catalyst, the absorbed species bonded to the surface is by Pt-C bonds, which is more stable than Pt-O bonds (Greeley, 2004). Subsequent cleavage of C-C bonds leads to the formation of CO and H_2 and CO reacts with water to form CO_2 and H_2 by the water-gas shift reaction (Grenoble et al., 1981).

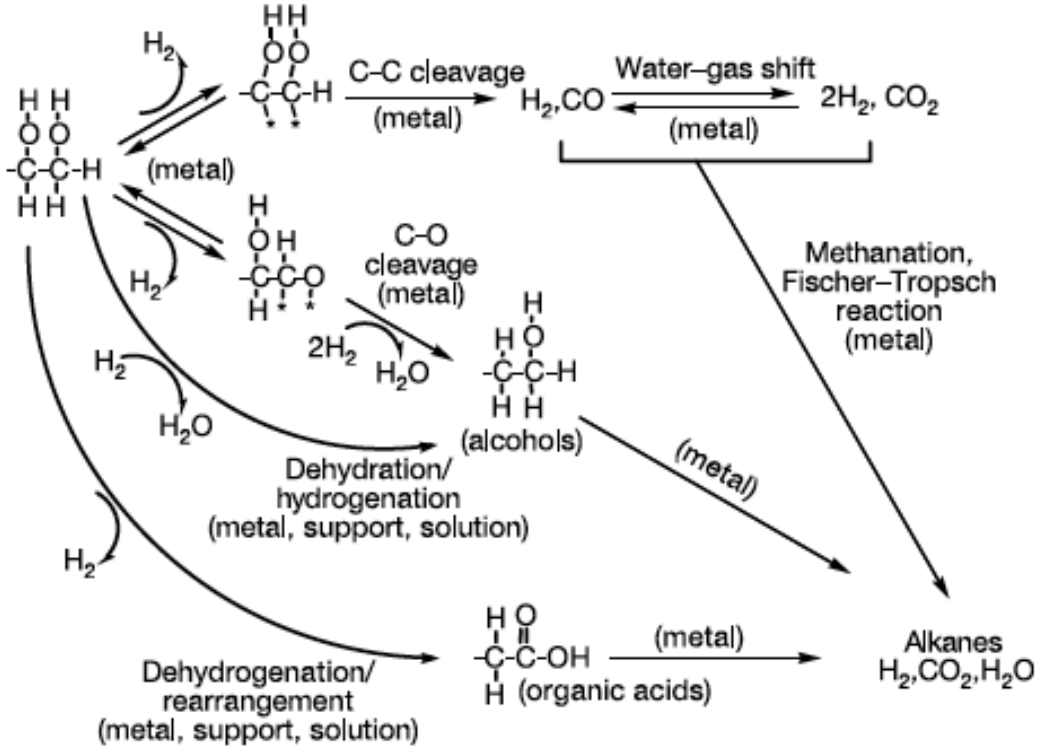

Figure 1-7 Reaction pathways and selectivity challenges for production of H_2 by reactions of oxygenated hydrocarbons with water. Reproduced from Cortright (Cortright et al., 2002)

The further reaction of CO or CO_2 with H_2 leads to alkanes and water by methanation and Fischer-Tropsch reactions (Iglesia et al., 1992), this H_2 consuming reaction thus represents a series selectivity challenge. In addition, undesirable alkanes can be formed on the catalyst surface by cleavage of C-O bonds, followed by hydrogenation of the resulting absorbed species. This process constitutes a parallel selectivity challenge. Another path way that contributes to this parallel selectivity challenge is cleavage of C-O bonds through dehydration reactions catalyzed by acidic sites associated with the catalyst support (Bates and

Van Santen, 1998), followed by hydrogenation reactions on the catalyst. This bi-functional dehydration/hydrogenation pathway consumes H_2, leading to decreased hydrogen selectivity and increased alkane selectivity.

In general, acidic supports such as SiO_2-Al_2O_3 are more alkane selective and basic/neutral supports such as Al_2O_3 and carbon are more H_2 selective. The pH of the solution should also be neutral for higher H_2 selectivity. H_2 selectivity also decreases with increasing number of carbon atoms in the feed molecule. H_2 selectivity decreases in the following order: methanol>ethylene glycol> glycerol>sorbitol> glucose (Cortright et al., 2002). H_2 selectivity can be increased by using bimetallic catalyst compared to mono-metalic catalyst (Huber and Dumesic, 2006).

1.6 Catalyst development for APR process

This literature review aims to report previous progress in the research on aqueous phase reforming of oxygenated hydrocarbons especially for hydrogen production. It will do so by focusing on research performed with similar variables. There are several factors, like metal components, alloying of catalyst metal, support type, nature of feed, catalyst preparation methods, controlling the activity and selectivity of APR of oxygenated hydrocarbons. A summery result for APR of glycerol has listed in Table 1-1. Highest hydrogen selectivity of 85% and glycerol conversion 45% was achieved for 3% Pt on alumina at reaction conditions: T=250 °C, P=20

bar, 10 wt% glycerol, 0.5 mL/min, 0.3 g catalyst. Also Nianjun and co-workers achieved same hydrogen selectivity of 85% for APR of glycerol on 2Ce-Ni-3Co/Al_2O_3 catalysts. A good APR catalyst should not only be active for C-C bond cleavage but also be active for WGS reaction. Moreover the catalyst should be inert to series and parallel competing reactions such as cleavage of C-O bond and methanation reaction, which greatly deteriorate the productivity of hydrogen. Several investigations have been done in this regard by Davda et al. (2003) and by Wen et al. (2008) (Davda et al., 2003, Wen et al., 2008). Here, the previously investigated APR catalysts are reviewed in three catagories: monometallic catalysts, bimetallic catalysts, and catalysts support.

Table 1-1 Comparisons of catalytic activities for APR of glycerol

Catalyst	Reaction Conditions for APR of glycerol	Best findings	Reference
$3Pt/Al_2O_3$	T=225 °C, P=30 bar, 10 wt% gly., 0.06 mL/min, 4.5 g cat.	H_2 sel. 75%, Gly. conv. 77%	Dumesic et. al., 2002
$1Pt/Al_2O_3$	T=220 °C, P=25 bar, 5 wt% gly., 0.05 mL/min, 1 g cat.	H_2 sel. 70%, CH_4 sel. 10%, C con. to gas 42%	Nianjun et. al., 2008
$3Pt/Al_2O_3$	T=250 °C, P=20 bar, 10 wt% gly., 0.5 mL/min, 0.3 g cat.	H_2 sel. 85%, Gly. conv. 45%	Lehnert et.al., 2008
$4.5Pt/Al_2O_3$	T=230 °C, P=32 bar, 10 wt% gly., LHSV 8.4 h^{-1}, 1.7 g cat.	H_2 mol% 70%, CO_2 mol% 25%, C con. to gas 19%	Wen et. al., 2008
$2Ce\text{-}Ni\text{-}3Co/Al_2O_3$	T=220 °C, P=25 bar, 5 wt% gly., 0.05 mL/min, 1 g cat.	H_2 sel. 85%, CH_4 sel. 27%, C con. to gas 45%	Nianjun et. al., 2010
3Pt/C	T=225 °C, P=30 bar, 10 wt% gly., WHSV 5 h^{-1}, 0.2 g cat.	H_2 sel. 57%, Gly. Con. 5.3%, C con. to gas 72%	David et. al., 2010
$17Ni/3MgO\text{-}Al_2O_3$	T=225 °C, P=30 bar, 1 wt% gly., WHSV 1.25 h^{-1}	Gly. conv. 15%, H_2 48%, CO_2 40%, CH_4 12% (mol%)	Iriondo et. al., 2008
$1Pt/Al_2O_3$	T=230 °C, P=40 bar, 5 wt% gly., WHSV 0.73 h^{-1}, 6.8 g cat.	Gly. conv. 25%, H_2 67%, CO_2 22%, CH_4 7 % (mol%)	Derya et. al., 2011

1.6.1 Monometallic catalysts

Several monometallic catalysts have been investigated in the APR of oxygenated hydrocarbon. Transitional metals are well known as good catalysts. Normally, they need to be loaded on support materials to prevent sintering and will also benefit from the activities of these materials in primary tars (heavy tars) cracking (Tanksale et al., 2010). Transition metals can absorb C–C bond selectively resulting in cleavage and formation of CH–OH group adsorbed on metal. CH–OH then dehydrogenates to produce CO and H_2 (Gursahani et al., 2001). They have shown superior activity and selectivity in breaking down C–C, C–O, and C–H bonds (Figure 1-7) mostly likely via the formation of metal carbide intermediates (McCarty and Wise, 1979; Trimm, 1999). Thus the transitional metals present advantages in the cracking (reforming in presence of H_2O) of oxygenated hydrocarbons compared with others metal catalysts.

Davda et al. (Davda et al., 2003) studied Ni, Pd, Pt, Ru, Rh and Ir catalysts supported on silica for APR of ethylene glycol (483 and 498 K, 22 bar). It was observed that the overall catalytic activity for ethylene glycol reforming, decreases in the following order for silica supported metals: Pt~Ni>Ru>Rh~Pd>Ir. The hydrogen selectivity for the metal decreases in the following order Pd>Pt>Ni>Ru>Rh. Pd/SiO_2 catalyst exhibited the highest selectivity (98%) for H_2 production and Ni/SiO_2 showed significant deactivation at high temperature of 225

°C. Ni and Ru exhibited relatively high rates of CO_2 production, although their selectivities for production of H_2 are relatively low. It was also observed that relatively low levels of CO were produced compared to the amount of CO_2 formed for APR of ethylene glycol. It was suggested that better catalyst may be obtained by the judicious use of metal alloys like Pt-Pd or Ni-Pd.

Wen et al. (Wen et al., 2008) studied the effect of metal component (e.g., Pt, Ni, Co and Cu) and as well as the effect of support (e.g., Al_2O_3, SiO_2, AC, MgO, HUSY and SAPO-11) on the activity and selectivity of hydrogen production by APR of glycerol using a fixed-bed flow reactor (503 K, 3.2 MPa, LHSV 8.4 h^{-1}). It was found that the activity of the metal catalysts increased in the order of Co<Ni<Cu<Pt. It was also found that the overall activity increased in the following order for supported Pt catalyst: SAPO-11<AC<HUSY<SiO_2<MgO<Al_2O_3. It was found that all of the supported Pt catalysts showed Pt sintering during the reaction. Trace amount of carbon deposition was also found on all of the supported Pt catalyst. However, no remarkable deactivation was observed over Pt/Al_2O_3, Pt/SiO_2, Pt/AC and Pt/HUSY catalysts. Moreover, Pt supported on basic support resulted in high activity and higher hydrogen molar concentration, whereas acidic support and neutral Al_2O_3 support tended to increase alkane formation.

As Pt shows highest activity and selectivity among the group VIII moles, so several studies have been performed using Pt supported catalyst to investigate the

effect of particle size, metal loading, reaction temperature, pressure, feed concentration, feed flow rate, LHSV. Luo et al. (Luo et al., 2008) studied APR of glycerol over supported Pt catalyst and the affect of metal loadings, operation conditions, feedstock concentration and liquid hourly space velocity (LHSV) have been examined. Among the four different metal loadings (0.3 wt%, 0.6wt%, 0.9wt% and 1.2wt%), the catalyst with 0.9wt% metal loading gave the highest hydrogen yield and carbon conversion to gas while 0.6 wt% and 1.2 wt% exhibited similar reforming activities. Since reforming of glycerol to generate hydrogen is an endothermic reaction, so higher reaction temperature and system pressure facilitated reforming process to produce higher hydrogen yield (Luo, 2008 #131). They studied two different concentrations of glycerol solution 5 wt% and 10 wt%. Experimental results showed that lower concentration have higher H_2 yield and higher carbon conversion to gas, while higher concentration have higher H_2 selectivity (95%) and lower methane selectivity. In this work, reforming results were compared for two different LHSV 1.56/h and 3.12/h. Lower LHSV of 1.56/h produced higher H_2 yield and higher H_2 selectivity as well as higher carbon conversion to gas. However, it produced higher methane selectivity. They found from XRD patterns, a new phase of boehmite Al(O)OH formed on used catalyst and from elemental analysis carbonaceous entities on the catalysts which may cause deactivation of catalyst during the reforming process.

Ana Valiente et al. (Ana Valiente et al., 2010) studied (500 K, 0.5 g catalyst, Liquid feeding rate = 1 mL/min) the influence of system pressure and catalyst weight/ethylene glycol flow rate ratio in the APR of ethylene glycol using Pt/Al_2O_3 catalyst. The result showed that carbon conversion to gas increased from 9.9% to 14.7% as the system pressure varies from 27 bar to 36 bar also H_2 and CO_2 yield increased with increased system pressure. Though H_2 selectivity increases from 96% to 98% for system pressure rises from 27 bar to 30 bar, in fact Shabaker et al. (Shabaker et al., 2004) showed that H_2 selectivity decreased and alkane selectivity increased significantly with the increase of system pressure using Sn-modified catalyst. They found that H_2 selectivity decreases with the increase of W/m_{eg} ratio. But Luo et al. (Luo et al., 2008) showed that H_2 selectivity increased as the space velocity (inverse of W/m_{eg} ratio) decreased in the APR of glycerol over Pt/Al_2O_3 catalyst. On the contrary, Shabaker et al. (Shabaker et al., 2004) observed a decrease in H_2 selectivity as the space velocity decreased in the APR of ethylene glycol using Ni catalysts.

Cortright et al. (Cortright et al., 2002) performed experiments (498-538 K, 29-56 bar, feeding rate 3.6 mL/h) on aqueous phase reforming of glucose, sorbitol, glycerol, ethylene glycol and methanol in a continuous flow tubular reactor using Pt/Al_2O_3 catalyst. They showed that the selectivity for H_2 production improves in the order glucose<sorbitol<glycerol<ethylene glycol<methanol. The lower H_2 selectivity is due to the undesirable homogeneous reactions of glucose in the aqueous phase. They found that lower glucose concentrations (1 wt%) correlated

with higher selectivities for hydrogen production than the higher concentrations (10 wt%). In case of sorbitol, glycerol, ethylene glycol and methanol, reactions at higher concentrations and lower conversion levels leads to higher rates of H_2 production.

Ozgur et al. (Özgür and Uysal, 2011) studied APR of glycerol with Pt/Al_2O_3 catalyst. They investigated the effects of reaction temperature (160-280 °C), feed flow rate (0.05-0.5 mL/min) and feed concentration (5-58 wt% glycerol) on product distribution. With the increase in temperature from 160 to 280 °C hydrogen composition decreased from 71 to 44%, CO_2 and other hydrocarbons concentration increased and total conversion of glycerol increased. The optimum temperature was determined as 230 °C and maximum gas production rate was found at feed flow rate 0.1 mL/min. They also found that hydrogen concentration in the gas product decrease as the glycerol concentration in the feed increases.

Shabaker et al. (Shabaker et al., 2003b) measured the rates of aqueous phase reforming of methanol and ethylene glycol to form H_2 and CO_2 under kinetically controlled reaction conditions over alumina supported Pt catalysts. It was found that the rates of formation of H_2 are similar for both of APR of methanol and ethylene glycol (from 1 to 10 wt%). Both oxygenated hydrocarbons showed nearly 100% H_2 selectivity over Pt/Al_2O_3.The rate of production of hydrogen is higher order in methanol (0.8) compared to ethylene glycol (0.3-0.5) and the reaction is weakly inhibited by hydrogen (-0.5 order) for both feedstocks. The rates of APR of methanol and ethylene glycol showed apparent activation barriers of 140 and 100 KJ/mol.

However, among the studied monometallic catalyst Pt supported on Al_2O_3 showed highest H_2 selectivity. As reaction temperature and feed concentration increases H_2 concentration in the product gas decreases but other hydrocarbons concentration increases and total feed conversion increases. Also, lower space velocity helps higher H_2 yield and higher H_2 selectivity as well as higher carbon conversion to gas but CH_4 selectivity increases.

1.6.2 Bimetallic catalysts

Also some studies have been performed using bimetallic catalysts incorporating Pt and another metal. Result shows that bimetallic catalysts are more active and selective than monometallic catalysts for H_2 production by APR process.

King et al. (King et al., 2010) studied the influence of Re addition in 3Pt/C catalyst for APR of glycerol for hydrogen production. In the APR of glycerol, a 3%Pt/C catalyst shows good selectivity towards H_2 but has relatively low activity. Addition of Re increased the activity of the catalyst and overall hydrogen productivity. They also studied addition of base (KOH) in an effort to decrease the acid-catalyzed dehydration and subsequent hydrogenation reactions pathways that lower selectivity towards hydrogen production in APR reaction. Addition of KOH resulted in a small increase in glycerol conversion, an increase in the gas phase product selectivity in terms of H_2/CO_2 ratio, and an increase in production of aqueous phase oxygenates. The highest hydrogen productivity among the catalyst was achieved with a 3%Pt-3%Re/C catalyst with added KOH base.

Miyao et al. (Miyao et al., 2006) studied APR of methanol over supported Pt-Ru bimetallic catalyst. Among the supports (SiO_2, TiO_2, Al_2O_3, MgO, CeO_2 and ZrO_2) used, TiO_2 supported Pt-Ru catalyst exhibited highest activity and selectivity for CO_2, and these were improved after reduction at higher temperature. The improved activity and selectivity were attributable to the occurrence of SMSI state and Pt-Ru alloy respectively. They found that basic oxide supports improves selectivity to CO_2, where as acidic supports suppressed the catalytic activity and selectivity.

Huber et al. (Huber et al., 2006) studied the activity of Pt and Pd bimetallic catalysts for APR of ethylene glycol. Alumina supported PtNi and PtCo catalysts with Pt to Co or Ni atomic ratios ranging from 1:1 to 1:9 had TOF_{H2} of 2.8-5.2 min^{-1} compared to a value of 1.9 min^{-1} for Pt/Al_2O_3 under similar reaction conditions. A $PtFe_9/Al_2O_3$ catalyst showed TOF_{H2} of 0.3 and 4.3 min^{-1} at 453 and 498K, and these values are about three times higher than Pt/Al_2O_3 under similar reaction conditions. A $PdFe_9/Al_2O_3$ catalyst had TOF_{H2} equal to 1.4 and 4.3 min^{-1} at 453 and 498K, and these values are about 36-46 times higher than Pd/Al_2O_3 under identical reaction conditions. They also tested a catalyst Pd/Fe_2O_3 that showed the highest TOF_{H2} equal to 14.6, 39.1 and 60.1 min^{-1} at temperature 180, 210 and 225 °C respectively. Unfortunately, the $PtFe_9/Al_2O_3$, Pd/Fe_2O_3 and $PdFe_9/Al_2O_3$ catalyst deactivated, losing 20%, 50% and 80% respectively of their activity after heated to 210 °C under APR reaction conditions.

Kunkes et al. (Kunkes et al., 2008) studied reaction kinetics to know the role of Re for APR of glycerol (30% and 80 wt%) over carbon supported Pt catalysts. Addition of Re to Pt increased the rates of water-gas shift reaction as well as alkane formation reactions. Re participated in glycerol conversion by weakening the binding energy of CO to neighboring Pt sites, increasing the rate of water-gas shift and facilitating hydrogenolysis of C-O bonds at elevated pressures. TEM study indicated that Pt-Re/C catalyst consisted primarily of bimetallic nanoparticles with size below 2 nm and Re inhibited the sintering of these nanoparticles during reaction conditions for glycerol conversion.

Platinum catalysts were identified as promising catalysts for the APR reactions (Davda et al., 2003). However, the high cost of Pt makes it advantageous to develop non-precious Ni catalysts. Although non-precious Ni catalyst showed high initial activity that was compared to Pt catalyst, significant deactivation was observed (Davda et al., 2003). Several efforts have been made to improve the catalytic activities of Ni by impregnating another metal components. Furthermore, modified skeletal Ni catalysts were developed by Shabaker et al. (Shabaker et al., 2004) to improve the stability of bimetallic catalysts.

Wen et al. (Wen et al., 2009) studied a APR of glucose over supported Ni catalyst and the effect of impregnation methods (single and two-step), high metal loadings, residence time, catalytic stability on catalytic performance have been examined. Among the series of catalyst, the 36 wt% and 48 wt% Ni/Al_2O_3 catalyst prepared by two-step impregnation showed higher Ni surface area and as well as Ni

dispersion. They showed that catalysts prepared by two-step impregnations exhibited smaller metallic Ni particle size than the corresponding catalysts prepared by single impregnations. They found that H_2 selectivity, H_2 yield, conversion of C to gas increases with the increase of Ni loadings both for single impregnations and as well as two-step impregnations. They also found that 36 wt% and 48 wt% Ni/Al_2O_3 catalyst prepared by two-step impregnation gave highest C to gas conversion, H_2 yields, H_2 selectivity, methane selectivity, as well as lowest CO molar concentrations. H_2 selectivity exhibited a maximum at residence time 60 min, and then decreased at longer residence time since methanation reaction seems gradually to be dominant at longer residence time. The hydrogen yield increased sharply in the range of 2-60 min, then gradually increased to 360 min. CO concentration decreases with the increase of residence time.

Shabaker et al. (Shabaker et al., 2004) reported results for aqueous phase reforming of sorbitol, glycerol and ethylene glycol over Pt/Al_2O_3, Ni/Al_2O_3, $NiSn/Al_2O_3$, Raney-Ni and Raney-NiSn catalysts. Al_2O_3 supported Ni and NiSn catalysts exhibit deactivation caused by sintering. Raney-Ni catalyst showed a medium H_2 selectivity of 47% and high alkane selectivity of 33%. The Sn-promoted Raney-Ni catalyst showed good activity, selectivity and stability for hydrogen production by APR. Addition of Sn to Ni improves the H_2 selectivity by APR of ethylene glycol from 35 to 51% at a Ni:Sn ratio of 270:1, while the alkane selectivity is reduced from 44 to 33%. At a Ni:Sn ratio of 14:1, the H_2 selectivity increased to 90%, while the alkane production is nearly eliminated. They found

that as the system pressure decreased to the bubble point of the feed (25.1 bar at 225 °C), alkanes selectivity decreased and H_2 selectivity increased accordingly also hydrogen selectivity is maximized by operation at higher reactor space velocities. Although the Pt/Al_2O_3 catalyst is more active in terms of specific activity, the Sn-modified Raney-Ni catalyst is less expensive, making it economically more competitive than the former in the APR of ethylene glycol.

Luo et al. (Luo et al., 2010) studied the influence of supported Ni-Co bimetallic catalyst prepared by urea matrix combustion method on the APR of glycerin for hydrogen production. A highest H_2 yield of about 40% was observed over Ni_1Co_3 (5 wt%Ni-15 wt%Co/Al_2O_3) among all the samples. Although Ni_1Co_5 possessed highest H_2 selectivity and lowest methane selectivity, the carbon conversion to gas was lowest, which implied low content of nickel is unfavorable for glycerin reforming process. They also studied the effect of Ce addition to Ni_1Co_3 catalyst. They found that 2 wt% Ce addition enhanced H_2 yield and decreased methane selectivity than Ni_1Co_3 catalyst, and also the higher level of Ce addition is unfavorable to H_2 yield. They concluded that the optimized ratio of Ni and Co is 1:3, and addition of 2 wt% Ce would improve its catalytic activity and suppress methane selectivity.

Tanksale et al. (Tanksale, 2010) studied APR of sorbitol using noble Ni and Ni-Pt catalysts supported on alumina nano-fiber (Alnf), ZrO_2 and mixed oxide of ceria-zirconia-silica (CZ_xS) using co-impregnation and sequential impregnation

methods. They tested the effect of sequence of impregnation and type of support on reducibility and activity of hydrogen production from APR of sorbitol. It was found that the promoting effect of Pt on Ni reducibility and activity can be greatly inhibited if Ni is impregnated first on Alnf. Sequentially impregnated Pt/Ni/Alnf catalyst did not form Ni-Pt bimetallic particles. Bimetallic catalyst supported on ZrO_2 and CZ_xS did not show any effect of sequence of impregnation. The concentration of silica in CZ_xS support play an important role for Ni reducibility. The rate of hedrogen production from APR of sorbitol was found to be highest for co-impregnated Ni-Pt/Alnf, followed by ZrO_2 and CZ_xS supported catalysts.

Ko et al. (Ko et al., 2006) showed that under the same pretreatment conditions, Pt-Ni bimetallic catalysts had more active sites than monometallic Pt or Ni catalysts.

Tupy et al. (Tupy et al., 2012) found that, after 24 h on stream in APR of ethylene glycol, a supported Pt-Ni catalyst was more active than a Pt catalyst because Ni segregation occurred and produced a Ni-enriched surface.

Huber et al. (Huber et al., 2006) suggested that the activity of Pt-based catalysts for APR could be increased by alloying Pt with Ni or Co, which decreased the strength with which CO and H_2 interacted with the surface, thereby increasing the fraction of catalytic sites available to react with ethylene glycol.

Manfro et al. (Manfro et al., 2013) studied APR of glycerol using Ni–Cu catalysts prepared from hydrotalcite-like precursors and showed that the high activity of Ni–Cu catalysts is related to the formation of alloy phase after reduction and

enhancement of metal dispersion and Ni reducibility. But they did not check catalyst stability for long run use.

Kim et al. (Ji Yeon Kim et al., 2013) studied APR of glycerol by using Cu-promoted Ni catalysts supported on $LaAlO_3$. The highest glycerol conversion and H_2 selectivity was observed for 15Ni-5Cu/$LaAlO_3$ catalyst and this was attributed due to smallest crystal size, highest metal dispersion and highest surface area. Also, Cu increased Ni reducibility.

1.6.3 Catalysts support

The activity and selectivity of metal catalysts also depends on the type of supports used. The H_2 selectivity for APR of ethylene glycol over silica supported Pt catalyst (Davda et al., 2003) is significantly lower than alumina supported Pt catalyst (Cortright et al., 2002). In general, acidic supports are more alkane selective and basic/neutral supports are more H_2 selective.

Lehnert et al. (Lehnert and Claus, 2008) studied the influence of support type and Pt catalyst particle size as well as nature of the catalyst precursor on the aqueous phase reforming of glycerol. Catalysts prepared from different metal precursors such as platinum ethanolamine, platinum (II)-nitrate, platinum sulfite and tetrammine platinum (II)-nitrate showed similar activities (glycerol conversion 45%) and identical hydrogen selectivity (85%). They showed that the selectivity of hydrogen increased with increasing particle size from 78% to 95%. They also

found that the variation of support material from pure γ-alumina to a mixture of γ, δ and θ phases led to an increase in hydrogen production from $1.2x10^{-3}$ to $7.6x10^{-3}$ mol min^{-1} g_{cat}^{-1}. In their study, they also investigated the influence of Pt loading. Catalyst with platinum loading of 10 wt% showed the highest rate of hydrogen production, which is $4.5x10^{-3}$ mol min^{-1} g_{cat}^{-1}. Furthermore, the production of hydrogen from crude glycerol was significantly lower ($1.0x10^{-3}$ mol min^{-1} g_{cat}^{-1}, TOF (H_2)=12 min^{-1}) than from pure glycerol ($7.6x10^{-3}$ mol min^{-1} g_{cat}^{-1}, TOF (H_2)=116 min^{-1}) in steady state.

Shabaker et al. (Shabaker et al., 2003b) studied the effects of the support on the activity and selectivity of Pt-based catalysts for aqueous phase reforming of ethylene glycol. They studied APR of 10 wt% ethylene glycol at temperature 210 and 225 °C over Pt-black and Pt supported on TiO_2, Al_2O_3, carbon, SiO_2, SiO_2-Al_2O_3, ZrO_2, CeO_2 and ZnO. A high turnover frequency of 8-15 min^{-1} at 225 °C was observed over Pt-black and Pt supported on TiO_2, carbon and Al_2O_3; a moderate turnover frequency near 5 min^{-1} over Pt supported on SiO_2-Al_2O_3 and ZrO_2; a lower turnover frequency over Pt supported on CeO_2, ZnO and SiO_2 for the production of hydrogen. Catalyst consisting of Pt supported on carbon, TiO_2, SiO_2-Al_2O_3 and Pt-black also lead to the production of gaseous alkanes and liquid-phase compounds that lead to alkanes at higher conversions. So, it can be concluded that Pt/Al_2O_3 and to a lesser extent Pt/ZrO_2 are active and selective catalysts for the production of hydrogen from APR of ethylene glycol.

Menezes et al. (Menezes et al., 2010) studied the effects of support on the activity and hydrogen production from glycerol by aqueous phase reforming on Pt-based catalysts. They measured the performance of Pt-based catalysts supported on different oxides (Al_2O_3, ZrO_2, MgO and CeO_2) in a batch reactor at 225 °C and autogenous pressure with stirring speed of 600 rpm using a mixture of 10 mg catalyst and 100 mL of 1wt% glycerol aqueous solution. Among the supports ZrO_2 and MgO showed higher production of hydrogen and lower concentration of undesired hydrocarbons.

Liu et al. (Liu et al., 2010) studied APR of ethylene glycol to hydrogen production on Pd/Fe_3O_4 catalyst prepared by co-precipitation method. Pd/Fe_3O_4 catalyst displayed superior catalytic performance compared to Pd catalyst supported on Fe_2O_3, NiO, Cr_2O_3, Al_2O_3, or ZrO_2 prepared by incipient wetness impregnation. Pd/Fe_3O_4 catalyst showed three times higher intrinsic activity than the second most active Pd/Fe_2O_3 catalyst. The conversion of EG to gas on the Pd/Fe_3O_4 catalyst was about 14.4% which is about 3.2 times than on the Pd/Fe_2O_3 catalyst. Pd/Fe_3O_4 catalyst accelerated the production rates of H_2 and CO_2 and at the same time it de-accelerated the production rates of CO and alkanes. The TOF of H_2 on the Pd/Fe_3O_4 catalyst was 109 min^{-1}, which is substantially higher than the best value (60.1 min^{-1}) ever reported in the literature obtained on Pd/Fe_2O_3 catalyst prepared by IWI. Pd/Fe_3O_4 catalyst retained ~80% of its initial activity after reaching the steady state. They reported that the excellent performance of the Pd/Fe_3O_4 catalyst was due to the enhanced synergistic effect between small Pd nano-particles and magnetite in promoting the WGS reaction.

Not many studies have been conducted on mixed oxide supports for APR (Liu et al., 2008). Liu et al., studied the performance of Pt catalyst supported on iron-chromium mixed oxides for APR of ethylene glycol. The iron-chromium mixed oxides support is prepared by solid thermal decomposition reaction. They reported that the addition of chromium compounds not only increased the BET surface area of the mixed oxides, but also affected the phase composition of iron oxide in the product. The catalytic activity reached maximum for the catalyst with a Cr/Fe molar ratio of 1:9.

But some mixed oxide support catalysts have been studied for steam reforming of glycerol and methane. Adhikari et al. (Adhikari et al., 2008) studied steam reforming of glycerin over CeO_2-Al_2O_3 supported Rh, Pt, Pd, Ir, Ru and Ni catalyst for H_2 production. Among the catalysts studued, Ni/Al_2O_3 and Rh/CeO_2-Al_2O_3 were found as the best performing catalysts in terms of hydrogen selectivity and glycerin conversion. It was found that with the increase in water to glycerin molar ratio, hydrogen selectivity and glycerin conversion increased. At 9:1 water to glycerin molar ratio, 900 C, and 0.15 ml/min feed flow rate, Ni/Al_2O_3 showed 80% hydrogen selectivity and Rh/ CeO_2-Al_2O_3 showed 71% hydrogen selectivity. At 3.5 wt% of metal loading, glycerin conversion was about 94% in both the catalysts but hydrogen selectivity was unchanged.

Feio et al. (Feio et al., 2007) studied steam reforming of methane over CeO_2-Al_2O_3 supported Pd catalyst. They found that the catalytic activities of Pd/CeO_2-Al_2O_3

catalysts in the steam reforming of methane depend strongly on the CeO_2 content. The CH_4 turnover rate of Pd/CeO_2-Al_2O_3 catalysts with ceria loading ≥12 wt% was around four orders of magnitude higher compared to that of Pd/Al_2O_3 catalyst. The increase of the activity of the catalysts was attributed to various effects of CeO_2 such as: (i) change of superficial Pd structure with blocking of Pd sites; (ii) the jumping of oxygen from ceria to Pd surface, which can decrease the carbon formation on Pd surface.

Damyanova et al. (Damyanova and Bueno, 2003) studied CO_2 reforming of CH_4 over mixed CeO_2-Al_2O_3 supported Pt catalyst. XPS result shows that the nature of Pt-Ce interaction varies with CeO_2 loading. Pt catalyst with 1 wt% of CeO_2 exhibited the highest specific activity and stability, due to the increase in the metal-support interface area, caused by the higher Pt dispersion.

However, the oxide supports are not very stable in the aqueous phase at these reaction conditions. Therefore, less reactive or inert catalyst supports are desired for APR. Wang et al. (Wang et al., 2009) studied both monometallic Pt and bimetallic Pt-Co catalysts supported on single walled carbon nanotubes (SWNT) prepared by wet-reduction method. Both of them showed higher APR activity than the Pt and Pt–Co catalysts supported on Al_2O_3. In addition, the catalytic activity and selectivity remained unchanged after a week of steady-state reaction.

van Haasterecht et al. (van Haasterecht et al., 2013) studied stability, catalytic activity and selectivity in the aqueous phase reforming of ethylene glycol over Ni, Co, Cu and Pt nanoparticles supported on carbon nano-fibers (CNF). The Pt/CNF

catalyst showed higher H_2 selectivities compared to Ni/CNF and Co/CNF due to the methanation activity of the latter two catalysts. Over the Co catalyst acids were formed in the liquid phase while alcohols were formed over Ni and Pt. Due to the low pH of the reaction mixture, especially in the case of Co (as a result of the formed acids), significant cobalt leaching occurs which resulted in a rapid deactivation of this catalyst. Table 1-2 shows APR catalyst for glycerol with advantages and disadvantages. The table also shows gap of these studies.

Table 1-2 Summery of APR catalyst with their advantages, disadvantages and gaps for APR of glycerol.

Reference/ Catalyst used	Reaction Conditions	Effects in the reaction	Disadvantages and gaps
Cortright et. al., 2002 3Pt/Al_2O_3 Luo et. al., 2008 1Pt/Al_2O_3	T=225 °C, P=30 bar, 10 wt% gly., 0.06 mL/min, 4.5 g cat. T=220 °C, P=25 bar, 5 wt% gly., 0.05 mL/min, 1 g cat.	Lower operating temperature and lower feed concentration resulted in higher H_2 selectivity. High reaction temperature and system pressure facilitated reforming process. Lower feed concentration gave higher H_2 yield and higher carbon conversion to gas, while higher concentration gave higher H_2 selectivity (95%) and lower methane selectivity.	Catalyst deactivation observed. Carbonaceous entities formed over the catalyst caused catalyst activity drop.
Lehnert et.al., 2008 3Pt/Al_2O_3	T=250 °C, P=20 bar, 10 wt% gly., 0.5 mL/min, 0.3 g cat.	Selectivity to H_2 increased with increasing particle size while the conversion of glycerol remained nearly constant. Also, variation of support material from pure γ-alumina to a mixture of γ-, δ- and θ-phases (Puralox_) led to an increase in H_2 production. Rate of H_2 was lower for crude glycerol than for pure glycerol due to impurities (e.g. NaCl)	For crude glycerol H_2 production rate decreased dramatically after about 4 h time on stream.
Wen et. al., 2008 Pt, Ni, Cu, Co/Al_2O_3, SiO_2, AC, MgO, HUSY, SAPO-11	T=230 °C, P=32 bar, 10 wt% gly.,LHSV 8.4 h^{-1}, 1.7 g cat.	Activity of the metal catalysts increased in the order of Co<Ni<Cu<Pt. Activity increased in the following order for supported Pt catalyst: SAPO-11<AC<HUSY<SiO_2<MgO<Al_2O_3. No remarkable deactivation was observed over Pt/Al_2O_3, Pt/SiO_2, Pt/AC and Pt/HUSY catalysts. Pt supported on basic support resulted in high activity and higher hydrogen molar concentration, whereas acidic support and neutral Al_2O_3 support tended to increase alkane formation.	All of the supported Pt catalysts showed Pt sintering during the reaction. Trace amount of C-deposition was found on all of the supported Pt catalyst.

Luo et. al., 2010 2Ce-Ni-3Co/Al_2O_3	T=220 °C, P=25 bar, 5 wt% gly., 0.05 mL/min, 1 g cat.	The optimized ratio of Ni and Co was 1:3, and addition of 2 wt% Ce would improve its catalytic activity and suppress methane selectivity. TPR profiles indicated a synergism between the metals.	Catalysts deactivated due to carbon deposition as plaques, and in some compositions due to sintering.
David et. al., 2010 Pt-Re/C	T=225 °C, P=30 bar, 10 wt% gly., WHSV 5 h^{-1}, 0.2 g cat.	Addition of Re significantly increased the conversion of glycerol, at some loss of hydrogen selectivity to light hydrocarbons and water-soluble oxygenates. Addition of 1%KOH to the feedstock resulted in a small increase in glycerol conversion with 3%Pt–3%Re/C, an increase in the gas phase product selectivity in terms of H_2/CO_2 ratio, and an increase in production of aqueous phase oxygenates.	Catalyst stability was not studied Optimization of base required.
Ozgur et. al., 2011 1Pt/Al_2O_3	T=230 °C, P=40 bar, 5 wt% gly., WHSV 0.73 h^{-1}, 6.8 g cat.	Optimum temperature for hydrogen production with APR was determined as 230 °C. Maximum gas production rate was found at the feed flow rates around 0.1 mL/min. It was also found that hydrogen concentration in the gas product increased with decreasing glycerol concentration in the feed.	Catalyst stability was not studied.
Manfro et. al., 2013 Cu-Ni catalyst	T=250-270 °C, P=35-50 atm, 10 wt% gly., 0.102 mL/min, 1.25 g cat.	Cu-Ni catalysts significantly reduced methane formation. Highly stable against oxidation with time on stream and no deactivation was observed in 6 h of reaction. The high activity and stability of the Ni–Cu catalysts was related to the formation of a Ni–Cu alloy after reduction and enhancement of the metal dispersion and Ni reducibility.	Although very active, it showed low selectivity for H_2 formation. Sintering of metal particles was observed.

Kim et. al., 2013 Cu-Ni/$LaAlO_3$	T=250 °C, P=20 bar, 15 wt% gly., 0.083 mL/min	Higher catalytic activity and selectivity was attributed due to smallest crystal size, highest metal dispersion and highest surface area. Also, Cu increased Ni reducibility.	Formation of the carbon of whisker type was observed. Catalytic stability was not examined with time –on-stream.

1.7 Objectives of the project

The production of hydrogen for fuel cell and other industrial application from renewable biomass-derived resources is a major challenge as global energy generation moves towards a hydrogen society. Nowadays the worldwide trend of increasing production of biofuel results in the overproduction of glycerol. The ideal alternative would be to produce hydrogen from glycerol in a single stage at the moderated reaction conditions. Thus, aqueous phase reforming of glycerol is an attractive technique due to low temperature requirements, less CO production and possible value added by-products formation. Author has put forward the hypothesis of selective H_2 synthesis via APR of glycerol. The ultimate aim by this is to be able to feed the generated H_2 directly to a fuel cell, without the expense of intermediate gas upgrading. Reviewing previous studies on APR of glycerol, has indicated that more efficient catalysts are still needed to maximize H_2 yield and minimize CO content (CO is a contaminant that poses well-known problems to the use of H_2 in fuel cell) rather than producing H_2 as part of a combustible gas mixture. Then, the main objectives of this project are:

(1) To develop supported catalysts with high H_2 yield, low CO content and low deactivation in APR of glycerol;

(2) To provide deeper fundamental insight into the interaction of the developed catalyst;

(3) To develop cheaper non-noble-metal based alloy catalyst with comparable performance to the highly expensive noble metal catalyst for economical hydrogen production in industrial scale.

1.8 Outline for the dissertation

Chapter 2 describes in detail the fabrication of APR test rig facility, different characterization techniques and activity assessment of samples.

Chapter 3 investigates the effect of ceria addition to the alumina supports of Pt catalysts on the aqueous-phase reforming of glycerol and compares the activity results with the bench mark catalyst Pt/Al_2O_3.

Chapter 4 investigates the effect of Ni addition to Pt catalysts supported on ceria doped alumina on the aqueous-phase reforming of glycerol.

Chapter 5 shows the support effects on the aqueous-phase reforming of glycerol and also investigates the advantages brought by Pt-Ni interaction on APR of glycerol.

Chapter 6 investigates the effect of Cu addition to Ni catalysts supported on carbon nanotubes on the aqueous-phase reforming of glycerol, also compares the results with the bench mark catalyst Ni/CNT.

Chapter 7 gives the conclusions for the whole PhD project and also point out the recommended work of next step.

Chapter 2

Chapter 2 described the methodology applied in this research.

2 METHODOLOGY

2.1 Catalyst Characterization

2.1.1 N_2 Physisorption analysis

The textural properties of the catalysts were measured by N_2 adsorption-desorption at liquid nitrogen temperature (−196 °C) using an Autosorb-IQ apparatus (Quantachrome). Prior to analysis, the samples were outgassed for 12 h at 140 °C. Then the volume of absorbed N_2 at different relative pressures (0-1) will be plotted to a close isothermal curve consisting of two parts of absorption and desorption. BET (Brunauer-Emmett-Teller) model was used to measure specific surface area (Brunauer et al., 1938), and BJH (Barret-Joyner-Halenda) model for the characterization of pores (total pore volume and pore sized distribution) (Barrett et al., 1951).

2.1.2 H_2 Chemisorption analysis

H_2 chemisorption was carried out using an Autosorb-IQ apparatus (Quantachrome Corporation) to measure the active surface area of the catalysts and calculate the dispersion and average crystallite size of the supported metals, at desired temperature. The calcined samples were loaded into a quartz U-tube and then outgassed. Prior to the chemisorption measurement, catalyst was first reduced, and then purged with He, and finally cooled to room temperature. Two chemisorption isotherms were generated; the first corresponded to the combined (strong and weak) adsorption, and the second corresponded only to weak adsorption. Both

isotherms were extrapolated to P = 0, characteristic of monolayer chemisorption (Shen et al., 2008), with the former corresponding mostly to fast, strong adsorption on metal sites and the latter corresponding to slow, weak adsorption on the metal oxide support. However, the data used here, was calculated on the basis of monolayer adsorption of H_2 on the metal sites only; that is, only strong H_2 adsorption was considered.

The adsorption equilibration time was set at 30 minutes to approach full monolayer coverage (Shen et al., 2008). The monolayer chemisorbed volume, V_m, was derived by extrapolation to P = 0 in isothermals of H_2 chemisorption. Based on the assumption of full monolayer coverage, the number of exposed metal sites was then calculated from V_m, enabling the estimation of the active metal surface area (M_{area}, m^2/g), percent metal dispersion (M_{disp}, %) and average crystallite size (d, nm) via Eqs. 2-1 to 2-3.

$$M_{area} = \frac{N_m S A_m}{166} \tag{2-1}$$

$$M_{disp} = \frac{N_m S M}{100 L} \tag{2-2}$$

$$d = \frac{100 L f}{M_{area} \times Z} \tag{2-3}$$

N_m (μmol/g) refers to the number of adsorbed gas molecules; S (=2 atoms/molecule) refers to the number of surface atoms covered by each chemisorbed gas molecule; A_m ($Å^2$/atom) refers to the cross-sectional area occupied by each active surface atom; '166' in Eq. 2-1 is related to the units

calculation; M refers to molecular weight of supported metal; L refers to percent loading of supported metal; f refers to particle shape correction factor (= 6 for spherical particles).

2.1.3 X-ray diffraction (XRD)

The crystalline structure of the supported catalysts was determined by X-ray diffractometry using Cu Kα radiation (λ = 0.1542 nm) and a graphite monochromator (model S6000, Shimadzu). The instrument was operated at 40 kV and 40 mA. Scans were recorded over the range $2\theta = 10–85°$ in steps of 0.01°, and data for each point was collected for 1 s. The average crystal size of the supported metal particles was estimated using the Scherrer equation (Scherrer, 1918):

$$D_{XRD} = \frac{\lambda K}{\beta Cos\theta} \tag{2-4}$$

In Eq. 2-4, K refers to shape factor (≈ 0.9), λ is the wavelength, β is the line broadening at half the maximum intensity (FWHM) in radians, and θ is the Bragg angle. Also dispersion was estimated according to Eq. 2-5 (Anderson, 1975):

$$M_{disp} = \frac{6V_m}{dA_m} \tag{2-5}$$

Where V_m is the Ni atomic volume, d is the crystallite size and A_m is the surface area of a single atom.

2.1.4 Transmission electron microscopy (TEM)

Transmission electron microscopy (Philips CM120 Biofilter) is used to gain insight into the inner pore structure and distribution of metal sites in that.

2.1.5 STEM-EDS

Scanning tunneling electron microscopy (STEM, JEOL 2200FS) coupled with X-ray energy dispersion spectroscopy (EDS) is used to carry out the visual confirmation of the alloying effect of bimetallic catalyst.

2.1.6 SEM-EDS

Scanning electron microscopy (SEM) (FESEM, Zeiss Ultra+) is used to image the morphology of the samples surface. The coupled X-Ray energy dispersion spectroscopy (EDS) enables a qualitative and quantitative analysis upon the elemental components on the surface of the particles.

2.1.7 H_2-TPR

The reducibility of the catalysts was carried out, in a microflow reactor operating at atmospheric pressure, by the temperature-programmed reduction with H_2 (H_2-TPR). At first, the samples (~50 mg) were dehydrated at 300 °C for 2 h under inert atmosphere (Ar gas). Then a mixture of 1.6% H_2 in Ar, flowed at 30 sccm through

the sample, raising the temperature to 900 °C at a heating rate of 10 °C min^{-1}. The out flowing gas was detected by a thermal conductivity detector (TCD).

2.1.8 Thermogravimetric analyser (TGA)

Thermogravimetric analysis (TGA Q500) is done to check carbon deposition on spent catalyst and also to check metal loading on the support. Also catalyst reducebility was studied by using SDT Q600. The reducibility characteristics of samples can be obtained from the curve of weight loss vs. temperature when the samples are undergoing a standard reduction procedure in TG. Comparison between actual weight loss by H_2 reduction and stoichiometric value can tell the reduction degree of the samples, and the derivative weight loss curve (DTG) presents the information of reducibility.

2.1.9 X-ray photoelectron spectra (XPS)

X-ray photoelectron spectra were recorded on an ESCALAB250Xi (Thermo Scientific, UK) using a monochromated Al Kα source (1486.68 eV) operating at 164W (10.8 mA and 15.2 kV) and under a vacuum of $\leq 2 \times 10^{-9}$ mbar. Binding energies were referenced to the adventitious hydrocarbon C1*s* signal at 285.0 eV.

2.1.1 ICP

Inductively coupled plasma–atomic emission spectrometry (ICP-AES, Vista AX, Varian) was used to verify any leaching to metal particals from the catalyst bed into the liquid effluent.

2.2 APR activity tests

2.2.1 APR test rig

Figure 2-1 shows the apparatus used to study the aqueous-phase reforming of glycerol. The catalyst was loaded into a 5 mm i.d. stainless steel tubular reactor and held in position with quartz wool plugs. Reaction temperature was measured by a K-type thermocouple that was placed inside the reactor, very close to catalyst bed. The reactor was mounted in a MTI GSL-1100X tube furnace.

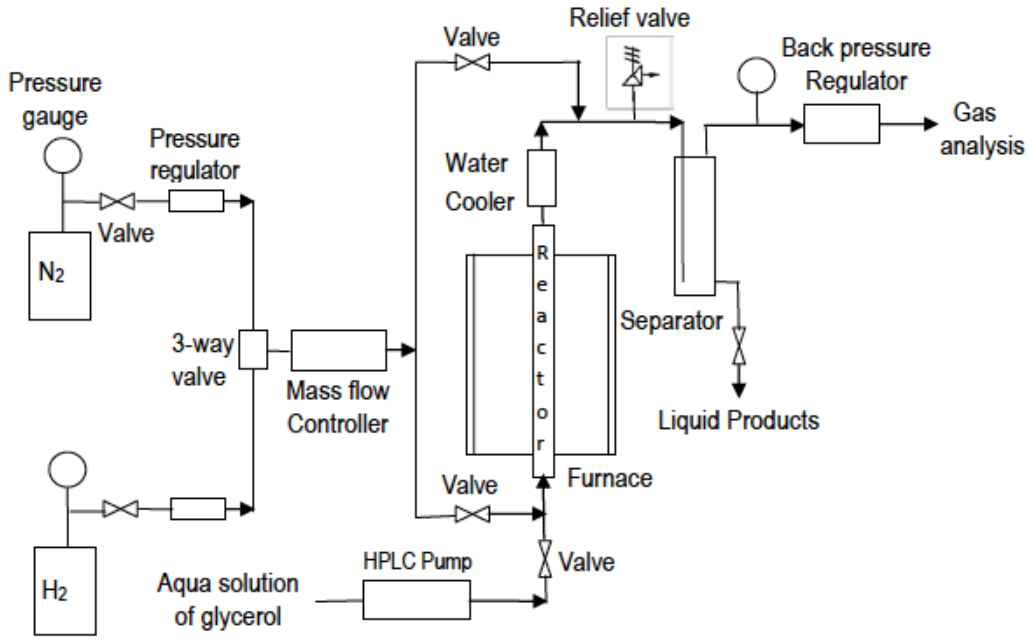

Figure 2-1 Schematic of apparatus used for APR studies

Prior to each reaction, the fresh catalyst was reduced in flowing H_2 at atmospheric pressure. After reduction, 100 mL/min N_2 or Ar was passed through the reactor for 8 h in order to cool and flush the reactor to remove all absorbed elements. A

Swagelok backpressure regulator attached to a pressure gauge was used to pressurize the system, typically at 30~50 bar. After cooling, reactant (aqueous glycerol) was introduced by a Waters 510 HPLC digital pump, and the catalyst bed was heated. When the reactor reached at specified temperature and pressure, 50 sccm N_2 or Ar were introduced continuously using a Bronkhorst mass-flow controller to carry the product gas mixture. The system was allowed to stabilize for about 2 h before the reaction products were analyzed.

The catalysts were evaluated on the bases of H_2 yield, CO yield, CO_2 yield, CH_4 yield, and carbon conversion to gas, H_2 selectivity and glycerol conversion efficiency, which were calculated according to:

$$\text{Yield of species } x = \frac{\text{moles of } x \text{ produced experimentally}}{\text{moles of } x \text{ produced theoretically}} \times 100\%$$

$$\text{C conversion to gas} = \frac{\text{moles of C in the gas products}}{\text{moles of C fed into the reactor}} \times 100\%$$

$$H_2 \text{ selectivity} = \frac{2 \times \text{moles of } H_2 \text{ produced experimentally}}{\text{Total H atoms in the gas products}} \times 100\%$$

$$\text{Glycerol conversion} = \left[1 - \frac{\text{moles of glycerol in liquid products}}{\text{moles of glycerol in feed}}\right] \times 100\%$$

For calculating yield of H_2, CO_2, CO, and CH_4, we considered the theoretical production of 7,3,3 and 3 moles respectively for per mole of complete glycerol reforming (Eq. 3-2).

2.2.2 GC analysis of gas phase

Gas products were analyzed at 25-min intervals using an online Varian CP-3800 gas chromatograph equipped with one Hayesep N, 60/80 Mesh, 5 m x 1/8″ SST column and one Molsieve 5Å, 60/80 Mesh, 1 m x 1/8” column, connected in series. Thermal conductivity (TCD) and flame ionization (FID) detectors were used to analyze H_2 and carbon compounds, respectively. The GC was calibrated using highly pure gas (grade 5.0) from Coregas. For each reading, ten successive injections were made and checked for relative standard deviations. The calibration curves were developed, and the samples were analyzed, with the TCD at 200 °C and the FID at 300 °C.

2.2.3 HPLC analysis of liquid phase

The liquid products of the APR reaction were collected in a condenser downstream of the reactor bed (Figure 2-1), and aliquots of the condensed liquid were analyzed with a Shimadzu HPLC, comprising a degasser (DGU-20A5), a pump (LC-20AD), an autosampler (SIL-20A HT), an oven (CTO-20A), and a refractive index detector (RID-10A). A Rezex RCM-Monosaccharide column (300 × 7.8 mm) was used for analyte separation. Ultrapure DI water (flow rate 0.5 mL/min) was used

as the eluent.

2.2.4 TOC analysis of liquid phase

Shimadzu TOC-L (with auto sampler ASI-L) was used to know the total organic carbon content of the liquid phase.

Chapter 3

Chapter 3 described the effect of ceria addition to alumina support of Pt catalyst on the aqueous phase reforming of glycerol. Catalysts were characterized and tested in a continuous flow packed bed reactor and the gas products were analyzed by a on line GC. The influence of CeO_2 addition to the Al_2O_3 support in Pt/Al_2O_3 catalysts on the yield, gas phase conversion and selectivity of the aqueous phase reforming of glycerol.

This chapter is based on:

Rahman, M. M., Church, T. L., Minett, A. I. & Harris, A. T. 2013. Effect of CeO_2 Addition to Al_2O_3 Supports for Pt Catalysts on the Aqueous-Phase Reforming of Glycerol. ChemSusChem, 6, 1006-1013

3 Pt catalyst supported on ceria-doped alumina

3.1 Introduction

The APR process (§1.4.2) is promising because it gives higher energy efficiency and a lower CO concentration (<300 ppm) in the product gas than conventional steam reforming processes (Huber et al., 2006). According to the APR mechanism reported by Davda (§1.5.2), a good APR catalyst should be active not only for the cleavage of the C–C bond, but also for the water–gas shift (WGS) reaction (Davda et al., 2005). Moreover, the catalyst should be inert to competing parallel and sequential reactions such as C–O cleavage and the methanation reaction (Eq. 3-1), which greatly deteriorate the yield of H_2.

$$H_2 + CO_2 \Leftrightarrow CH_4 + H_2O \qquad (3\text{–}1)$$

The activity of any supported catalyst depends critically on the metal and on the support itself (Rodriguez et al., 2007), and a high-performance catalyst can be designed by taking into account the significant contribution of the support (Panagiotopoulou and Kondarides, 2004, Boga et al., 2012). Shabaker et al. (Shabaker et al., 2003b) studied Pt catalysts supported on TiO_2, Al_2O_3, C, SiO_2, Al_2O_3-SiO_2, ZrO_2, CeO_2 and ZnO for the production of H_2 by APR (Shabaker et al., 2003b); TiO_2-supported Pt was the most active. Wen et al. studied Pt, Ni, Co and Cu catalysts supported on Al_2O_3, active C, SiO_2, MgO, HUSY (SiO_2/Al_2O_3 = 4.8) and SAPO–11. Among these, Pt/Al_2O_3 was the most active for the APR of glycerol (Wen et al., 2008). On the other hand, Menezes et al. (Menezes et al.,

2010) found Pt/MgO to perform better than Pt supported on Al_2O_3, ZrO_2, or CeO_2, and attributed its success to the basic nature of MgO. Boga et al. (Boga et al., 2013) found that bimetallic Pt-Cu catalyst supported on a Mg(Al)O mixed-oxide support showed higher hydrogen selectivity and lower methane production than Pt/Al_2O_3. Luo et al. (Luo et al., 2010) stated that adding 2 wt% ceria with a bimetallic Ni–Co catalyst supported on alumina improved its catalytic activity and resistance to sintering in the APR of glycerol. Pt catalysts supported on Al_2O_3 may suffer from severe deactivation due to coke deposition, oxidation or sintering (Comas et al., 2004, Gorte and Zhao, 2005).

Catalysts, particularly noble metals (Pt, Pd, Rh), containing ceria as a support or promoter are very important due to the unique acid–base and redox properties of ceria (Trovarelli, 1996). These can affect the thermal resistance of the support (Piras et al., 2000), the dispersion of supported metals, the oxidation and reduction of supported noble metals (Tiernan and Finlayson, 1998) and the catalytic behavior of metal crystallites. Ceria can also decrease coke formation on a catalyst surface due to its high oxygen storage capacity, which results from oxygen vacancies at the metal–oxide interface of reduced ceria (Wang and Lu, 1998). Pt/CeO_2 is an active catalyst for the WGS reaction (Barbier Jr and Duprez, 1993, Mendelovici and Steinberg, 1985, Whittington et al., 1995), as is $Pt/CeO_2/Al_2O_3$ (Germani and Schuurman, 2006). However, ceria alone is not a suitable support due to its low surface area and lower hydrothermal stability (Shabaker et al., 2003b). Therefore, combining alumina with ceria permits the development of new materials that combine the high surface area of alumina with the unique properties

of ceria.

Considering that the thermal resistance, catalyst dispersion, catalytic activity for the WGS reaction, and coking-resistance of ceria, as well as its ability to minimize methanation, would be very useful in the APR of glycerol, a series of Pt catalysts supported on ceria-doped alumina was prepared and tested. The CO_2 reforming of CH_4 with similar catalysts has been reported (Damyanova and Bueno, 2003), as has the APR of glycerol over Pt/Al_2O_3 (Wen et al., 2008, Menezes et al., 2010, Luo et al., 2008), over Ni/CeO_2 (Manfro et al., 2011), over $Ce\text{-}Ni\text{-}Co/Al_2O_3$ (Luo et al., 2010) and over Pt/CeO_2 (Menezes et al., 2010).

3.2 Experimental

3.2.1 Catalyst preparation

The CeO_2–Al_2O_3 supports with different amounts of CeO_2 were prepared by impregnating alumina (Sigma) with aqueous diammonium hexanitrate cerate, $(NH_4)_2[Ce(NO_3)_6]$ (99%, Aldrich). Specifically, for the synthesis of 1 wt%CeO_2-Al_2O_3 (1CeAl), 2.0 g of dried (120 °C overnight) alumina was impregnated with a solution prepared by dissolving 66.4 mg $(NH_4)_2[Ce(NO_3)_6]$ in 10 mL of deionized water in a 100-mL glass vial. The mixture was then stirred overnight at room temperature, and the water was allowed to evaporate. The sample was then dried in air at 120 °C for 12 h and calcined under flowing air at 550 °C for 3 h (ramp rate of 1.5 °C /min). The 3, 6 and 9 wt% CeO_2-Al_2O_3 supports were prepared analogously. Pure CeO_2 (S_{BET} = 8 m^2/g) was purchased from Aldrich.

Pt/CeO_2-Al_2O_3 and Pt/Al_2O_3 catalysts were prepared by impregnating the supports with aqueous tetraammine platinum nitrate (Strem Chemical). Specifically for the preparation of 3Pt/1CeAl, 1 g of calcined $1CeO_2$-Al_2O_3 support was impregnated with a solution prepared by dissolving 62.6 mg of $[Pt(NH_3)_4](NO_3)_2$ into 5 mL of deionized water in a 100-mL glass vial. After the mixture was stirred overnight at room temperature, the water was allowed to evaporate in the fume hood. The samples were dried at 120 °C for 12 h and calcined at 550 °C for 3 h under air (ramp rate of 1.5 °C/min). The prepared catalysts are denoted Pt/Al or *y*Pt/*x*CeAl, where *x* is the concentration of CeO_2 (wt%) in the Al_2O_3 support and *y* is the Pt loading (usually 3 wt%).

3.2.2 APR activity test

The APR of glycerol (Eq. 3-2) was studied in a continuous-flow, fixed-bed-type reactor system (§2.2.1).

$$C_3H_8O_3 + 3H_2O \Leftrightarrow 3CO_2 + 7H_2 \quad (3\text{-}2)$$

Prior to each reaction, the fresh catalyst was reduced in flowing H_2 (25 vol.% in N_2) at atmospheric pressure at 500 °C for 90 min (ramp rate of 1.5 °C/min). After reduction, 100 mL/min N_2 was passed through the reactor for 8 h in order to cool and flush the reactor to remove all absorbed elements. After cooling, a 5-wt% glycerol solution was introduced by a Waters 510 HPLC digital pump at a rate of 0.01 or 0.05 mL/min. A representative GC curve (Figure 3-1) shows only four peaks, representing H_2, N_2, CH_4 and CO_2, respectively, for each injection of

product gas.

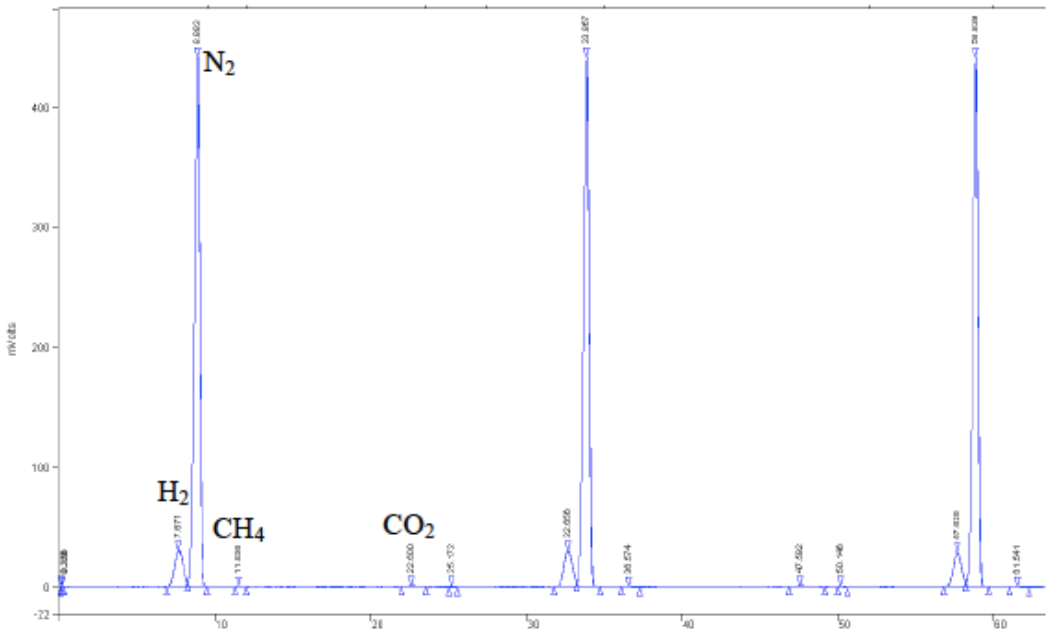

Figure 3-1 A representative GC curve from the APR of glycerol over 3Pt/6CeAl as measured on the in-line Varian CP-3800 gas chromatograph. The product gas was sampled every 25 min; three successive injections are shown here

The liquid products, collected in a condenser downstream of the reactor bed, were analyzed by a Shimadzu HPLC (§2.2.3). A representative HPLC curve is shown in Figure 3-2. The catalysts were evaluated on the bases of H_2 yield, H_2 selectivity, CH_4 selectivity, carbon conversion to gas and glycerol conversion efficiency (§2.2.1).

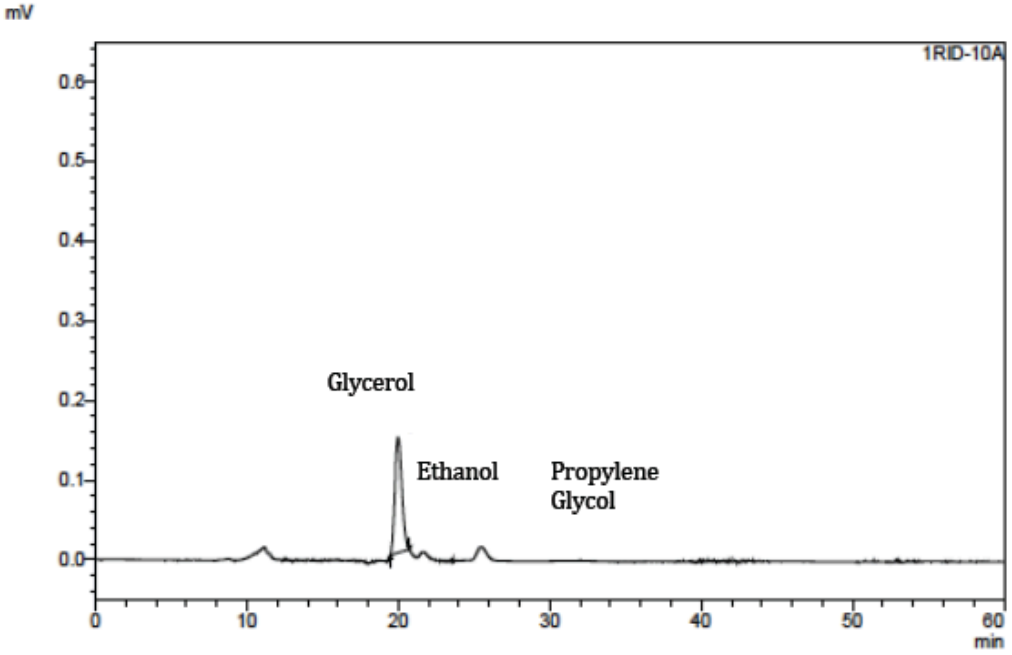

Figure 3-2 A representative HPLC curve for the APR of glycerol over 3Pt/3CeAl, reaction was carried out at T= 240 ^{0}C, P= 40 bar, flow rate 0.05 mL/min of 1 wt% aqueous glycerol

3.3 Results and Discussions

3.3.1 Catalyst characterization

The textural properties of the catalysts and supports were evaluated from nitrogen adsorption-desorption isotherms at −196 °C, using an Autosorb-IQ or Autosorb 1 apparatus (§2.1.1); the results are given in Table 3-1. Specific surface areas were determined from the linear portion of the adsorption isotherm (P/P_0 = 0.05–0.35), and the pore volume was calculated at P/P_0 = 0.995. The pore-size distribution was calculated from the adsorption isotherm using the Barrett–Joyner–Halenda (BJH) formula. Isotherms are shown in the Figure 3-3 and 3-4.

Table 3-1 Textural properties of supports and catalysts, measured by N_2 adsorption/desorption. Unless otherwise noted, the supports and catalysts were calcined in air at 550 °C for 3 h.

Support	S_{BET} (m^2/g)[a]	V_{Pore} (cm^3/g)[b]	D_{Pore} (nm)[c]	Catalyst	S_{BET} (m^2/g)[a]	V_{Pore} (cm^3/g)[b]	D_{Pore} (nm)[c]
Al_2O_3	155	0.26	4.30	3Pt/Al	155	0.25	4.88
$(Al_2O_3)_{por.}$[d]	267	0.38	6.12	$3Pt/(Al)_{por.}$[d]	205	0.38	4.90
1CeAl	158	0.27	4.88	3Pt/1CeAl	143	0.25	4.86
3CeAl	162	0.28	4.88	3Pt/3CeAl	150	0.25	4.88
				1Pt/3CeAl	149	0.25	4.84
6CeAl	157	0.25	4.86	3Pt/6CeAl	140	0.23	4.86
9CeAl	148	0.23	4.88	3Pt/9CeAl	134	0.22	4.88

[a] Specific surface area (S_{BET}) was determined from the linear portion of the isotherm (P/P_0 = 0.05–0.35).

[b] Pore volume (V_{pore}) was calculated at P/P_0 = 0.995 of the desorption branch of isotherm.

[c] Predominant pore size (volume basis) (D_{pore}) was calculated from the adsorption isotherm using the Barrett–Joyner–Halenda (BJH) formula (Barrett et al., 1951).

[d] Prepared according to a published procedure (Li et al., 2010) and calcined in air at 500 °C for 2 h.

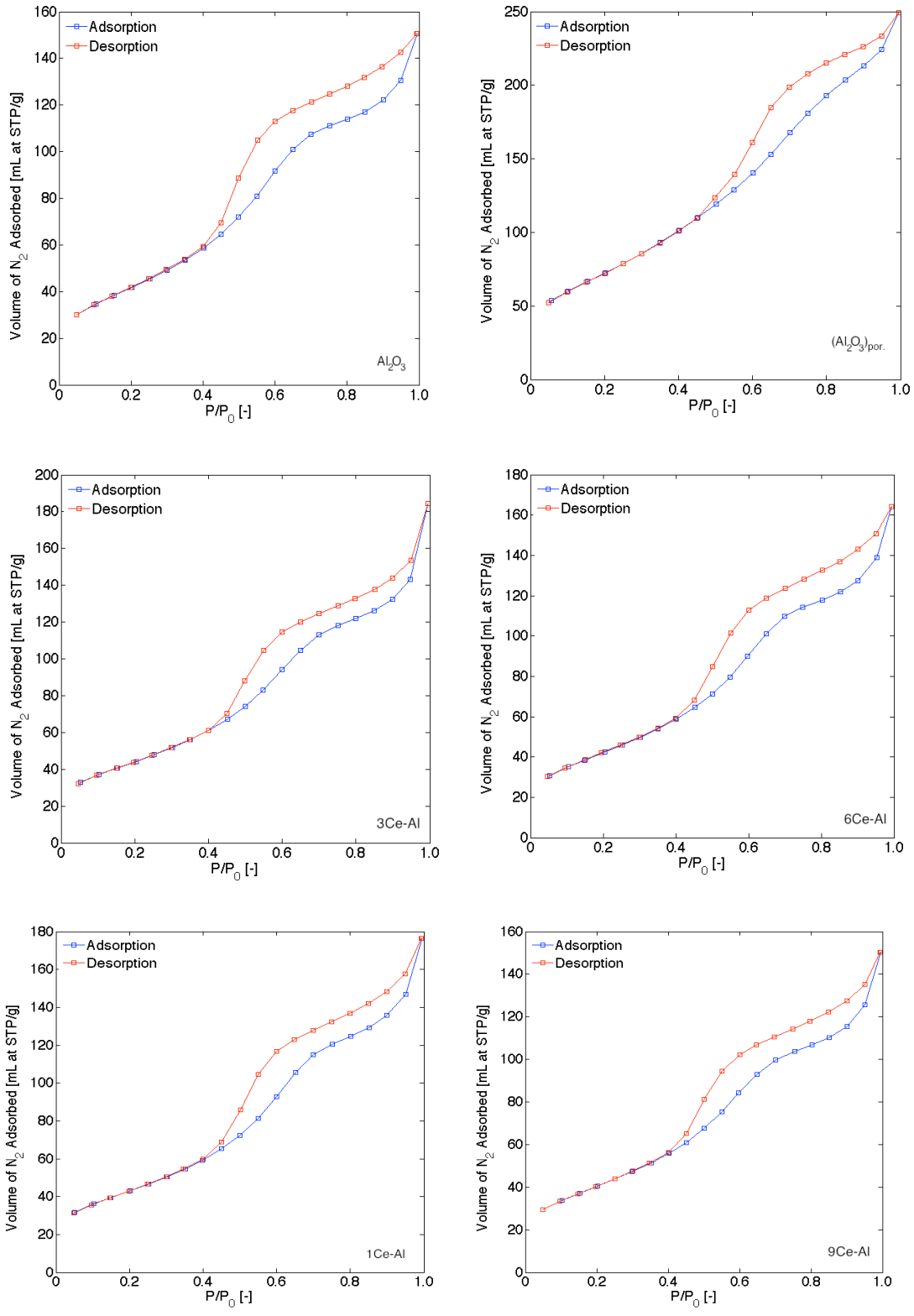

Figure 3-3 N_2 physisorption isotherms of Al_2O_3 and CeO_2-Al_2O_3 supports. Isotherms were collected on an Autosorb iQ or Autosorb 1 instrument (Quantachrome) at –196 ^{0}C

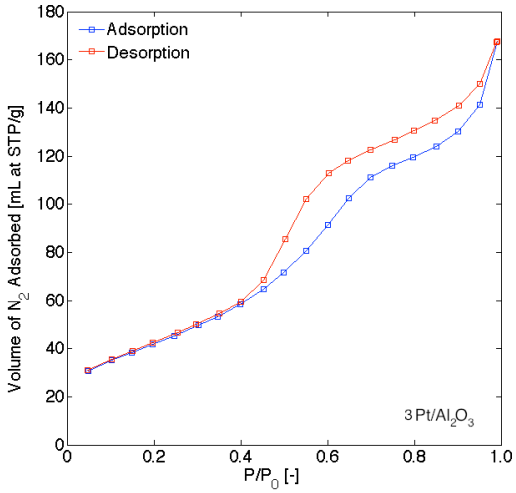
Adsorption
Desorption
Volume of N2 Adsorbed [mL at STP/g]
P/P0 [-]
3 Pt/Al2O3

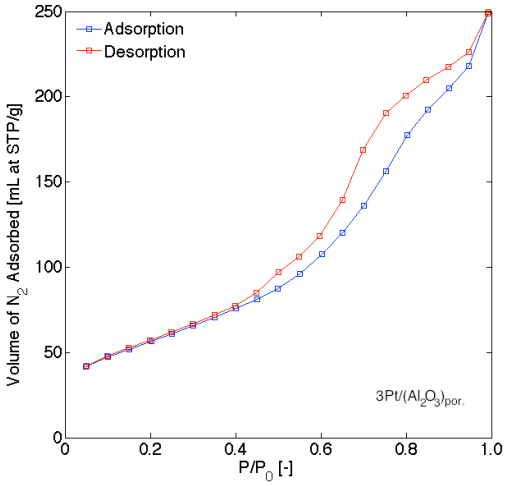
Adsorption
Desorption
Volume of N2 Adsorbed [mL at STP/g]
P/P0 [-]
3Pt/(Al2O3)por.

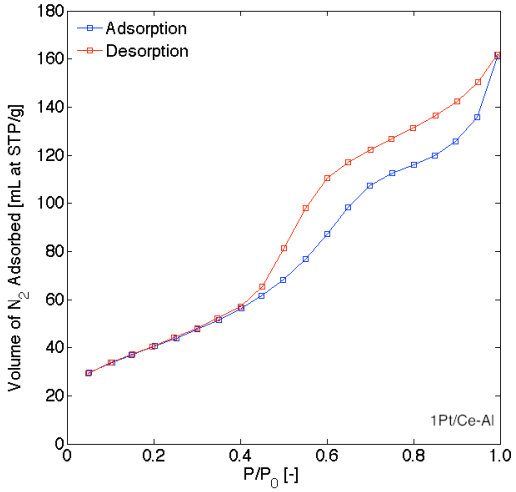
Adsorption
Desorption
Volume of N2 Adsorbed [mL at STP/g]
P/P0 [-]
1Pt/Ce-Al

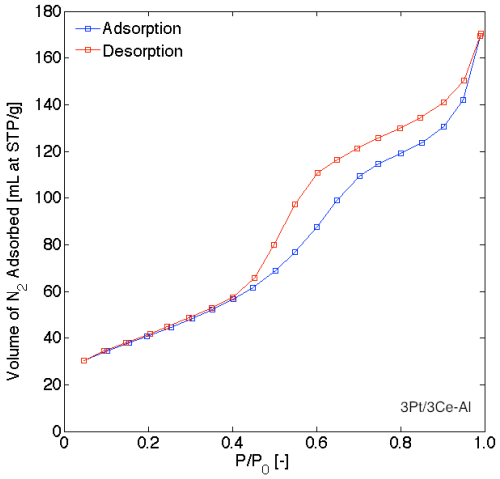
Adsorption
Desorption
Volume of N2 Adsorbed [mL at STP/g]
P/P0 [-]
3Pt/3Ce-Al

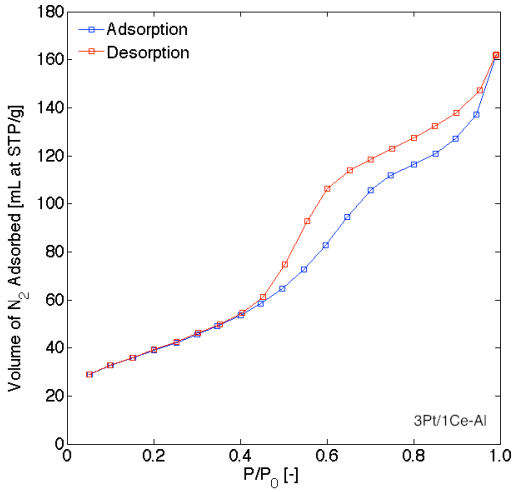
Adsorption
Desorption
Volume of N2 Adsorbed [mL at STP/g]
P/P0 [-]
3Pt/1Ce-Al

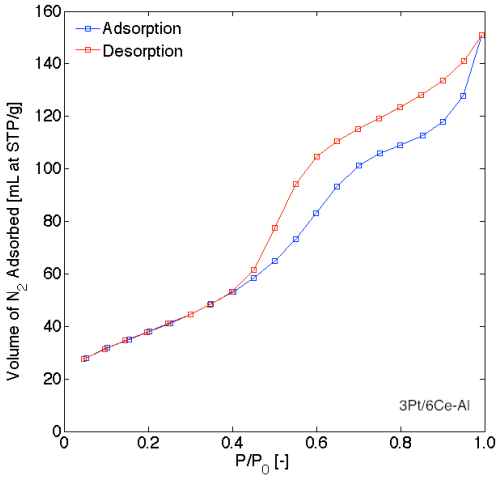
Adsorption
Desorption
Volume of N2 Adsorbed [mL at STP/g]
P/P0 [-]
3Pt/6Ce-Al

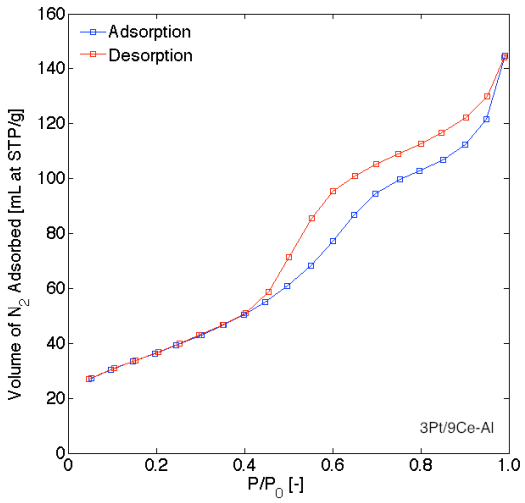

Figure 3-4 N_2 physisorption isotherms of Pt/Al_2O_3 and Pt/CeO_2-Al_2O_3 catalysts. Isotherms were collected on an Autosorb iQ instrument (Quantachrome) at –196 °C. Catalysts were calcined, but not reduced, prior to measurement

The surface area of the Al_2O_3 support after calcination at 550 °C increased slightly when 1 or 3 wt% ceria was added; whereas Al_2O_3 with 6 wt% CeO_2 showed the same surface area as the alumina support. A ceria loading of 9 wt% decreased both the surface area and pore volume of the Al_2O_3, possibly due to the plugging of pores with cerium oxide species. Notably 9CeAl, with an average Ce content of 3.5 µmol/m^2, is expected to be the only support that contains bulk-like ceria particles (CeO_2 is well-dispersed on Al_2O_3 for Ce content <2.5 µmol/m^2(Yao and Yao, 1984)). Bulk ceria (S_{BET} = 8 m^2/g) and 9CeAl showed the lowest surface areas. Ceria may stabilize alumina against surface area loss by preventing the transformation of γ-Al_2O_3 to α-Al_2O_3, which is dependent on the wt% of ceria loading (Ozawa and Kimura, 1990, Blom et al., 1994). Impregnating Al_2O_3 and CeAl supports with Pt had little effect on their surface areas, pore volumes and

pore sizes (Table 3-1).

XPS of the calcined catalysts, prior to reduction, showed that the oxidation state of Pt on the surface, and thus the reducibility of Pt, depended on the ceria content of the support (Figures 3-5 and 3-6). On pure Al_2O_3, the calcined Pt was mostly present as Pt^{4+} ($BE_{Pt4f7/2}$ = 73.6 eV), presumably PtO_2 (Shyu and Otto, 1989), though ~15 atom% metallic Pt was also detected ($BE_{Pt4f7/2}$ = 70.8 eV). When 3 or 6 wt% CeO_2 were present in the support, the fraction of metallic Pt ($BE_{Pt4f7/2}$ = 71.1 eV) in the calcined samples was much higher (54 or 52 atom%, respectively), with the remaining Pt existing as Pt^{4+} ($BE_{Pt4f7/2}$ = 74.3 and 74.2 eV, respectively). On 9CeAl, however, the majority of the Pt did not appear to be Pt(0). The oxidation state of the oxidized Pt was indistinct; although the position of the Pt $4d_{5/2}$ peak was consistent with Pt^{2+} ($BE_{Pt4d5/2}$ = 315.9 eV), the Pt 4*f* signals appeared to show Pt^{4+}. The broad nature of the former peak, and the overlap of the latter with the Al 2*p* peak, complicates the assignment of the oxidation state of this catalyst.

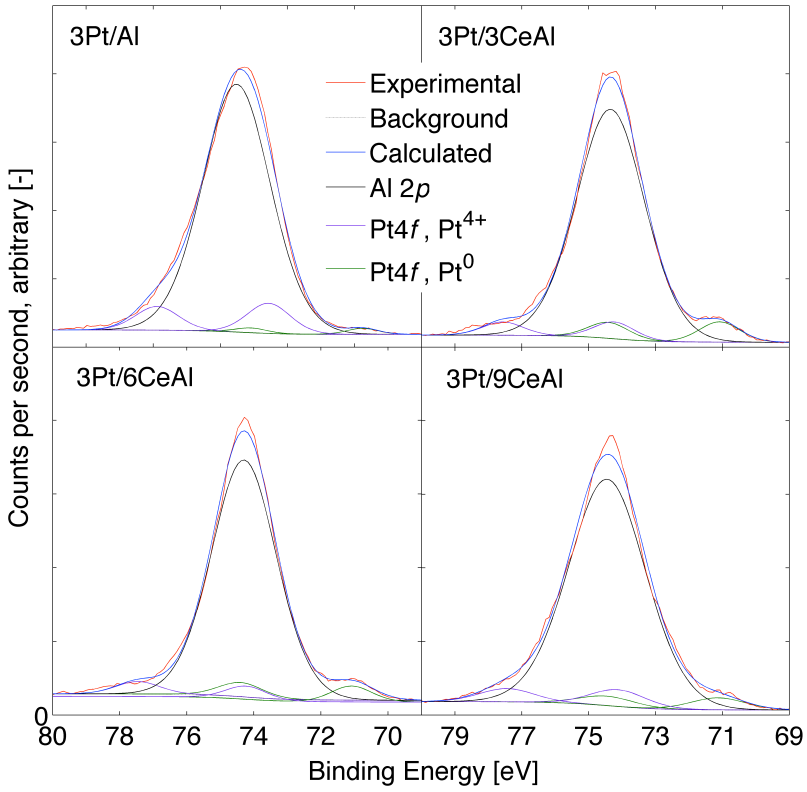

Figure 3-5 XPS in the Al 2*p*/Pt 4*f* region of the Pt catalysts supported on alumina and ceria-doped alumina supports. Catalysts were calcined, but not reduced, prior to measurem

The presence of strong Pt–CeO_2 interactions such as those described by Shyu and Otto could explain the appearance of Pt^{2+} (Shyu and Otto, 1989); however, the lower calcination temperatures used here disallow direct comparison. The Ce 3*d* region of the XPS spectra (Figure 3-6) showed that Ce^{3+} and Ce^{4+} species co-existed in all of the CeO_2–Al_2O_3 and Pt/CeO_2–Al_2O_3 samples. Quantification of species in this region is non-trivial (Bak and Hilaire, 1993) and was not attempted.

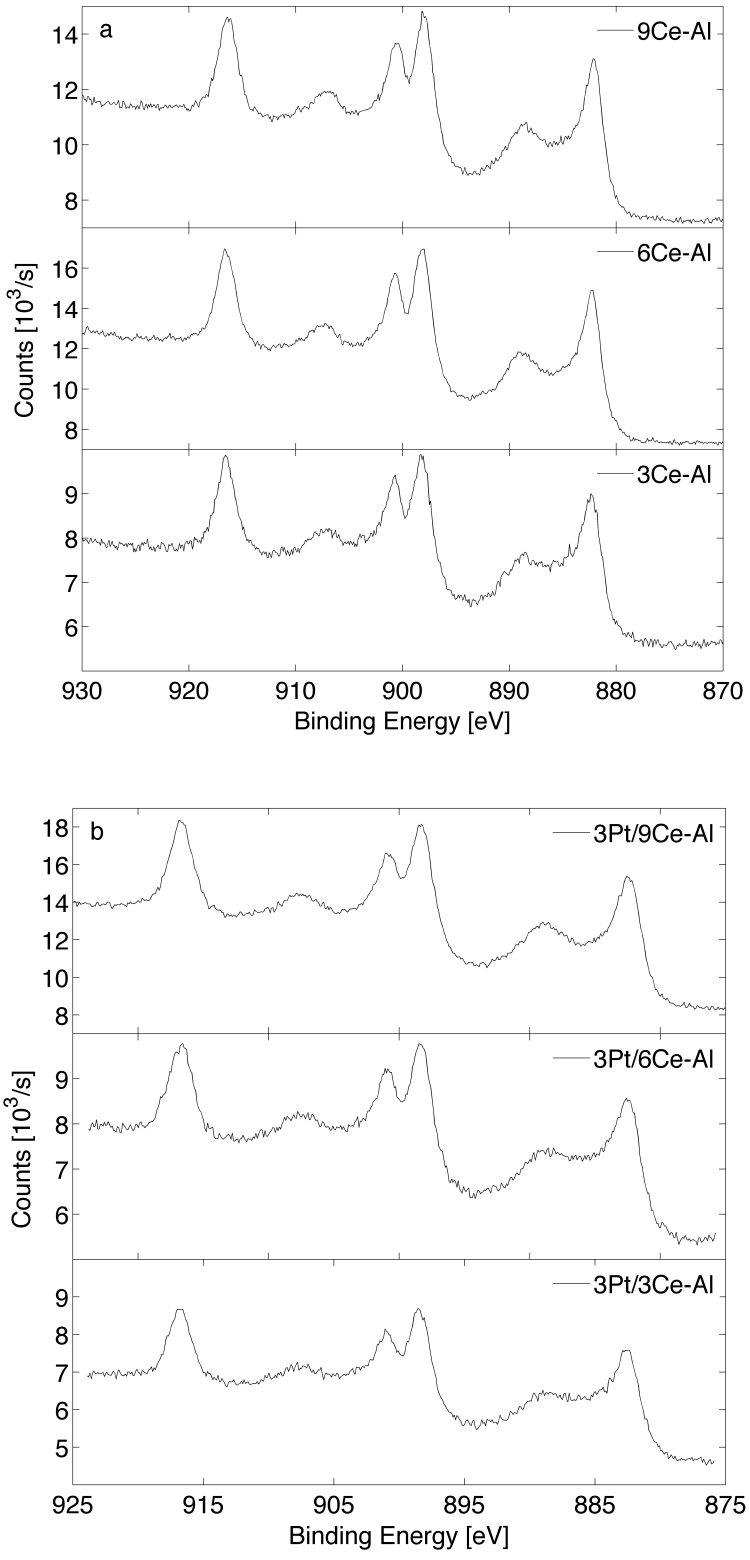

Figure 3-6 XPS in the Ce3$d_{5/2}$ region of (a) the ceria-doped alumina supports, and (b) the Pt catalysts supported on ceria-doped alumina supports. Catalysts were calcined, but not reduced, prior to measurement

Table 3-2 H_2 chemisorption results for the supported catalysts

Catalyst	H_2 uptake (μmol/g)[a]	M_{area}[b] (m^2/g)	M_{disp}[b] (%)	Ave. crystal size (nm)
3Pt/Al	41	3.9	53	21
3Pt/$(Al)_{por.}$[c]	42	4.1	55	20
3Pt/3CeAl	45	4.3	58	19
3Pt/6CeAl	34	3.2	44	26
3Pt/9CeAl	21	2.0	27	43
1Pt/3CeAl	22	2.1	85	13

[a]Based on extrapolation of the strong adsorption isotherm to P = 0. Prior to testing, each catalyst was reduced in situ at 400 °C for 40 min in 50 mL/min H_2. [b] $\mathbf{M_{area}}$ = metal surface area; $\mathbf{M_{disp}}$ = metal dispersion on support. [c] Prepared according to a published procedure (Li et al., 2010) and calcined in air at 500 °C for 2 h.

H_2 chemisorption (§2.1.2) was carried out using an Autosorb-IQ apparatus (Quantachrome Corporation), and measuring at dry ice temperature (−78.5 °C) to avoid H_2 spillover onto the ceria (Salasc et al., 1999, Perrichon et al., 2004). Two chemisorption isotherms were generated; the first corresponded to the combined (strong and weak) adsorption, and the second corresponded only to weak adsorption. Both isotherms were extrapolated to P = 0, characteristic of monolayer chemisorption (Shen et al., 2008), with the former corresponding mostly to fast, strong adsorption on metal sites and the latter corresponding to slow, weak adsorption on the metal oxide support. However, the data in Table 3-2 was calculated on the basis of monolayer adsorption of H_2 on the metal sites only; that is, only strong H_2 adsorption was considered. Prior to the chemisorption

measurement, about 100 mg catalyst was first reduced in situ at 400 °C for 40 min in 50 mL/min pure H_2, then purged with 50 mL/min He for 30 min, and finally cooled to room temperature. The H_2 chemisorption data is summarized in Table 3-2, and the isotherms are shown in Figure 3-7

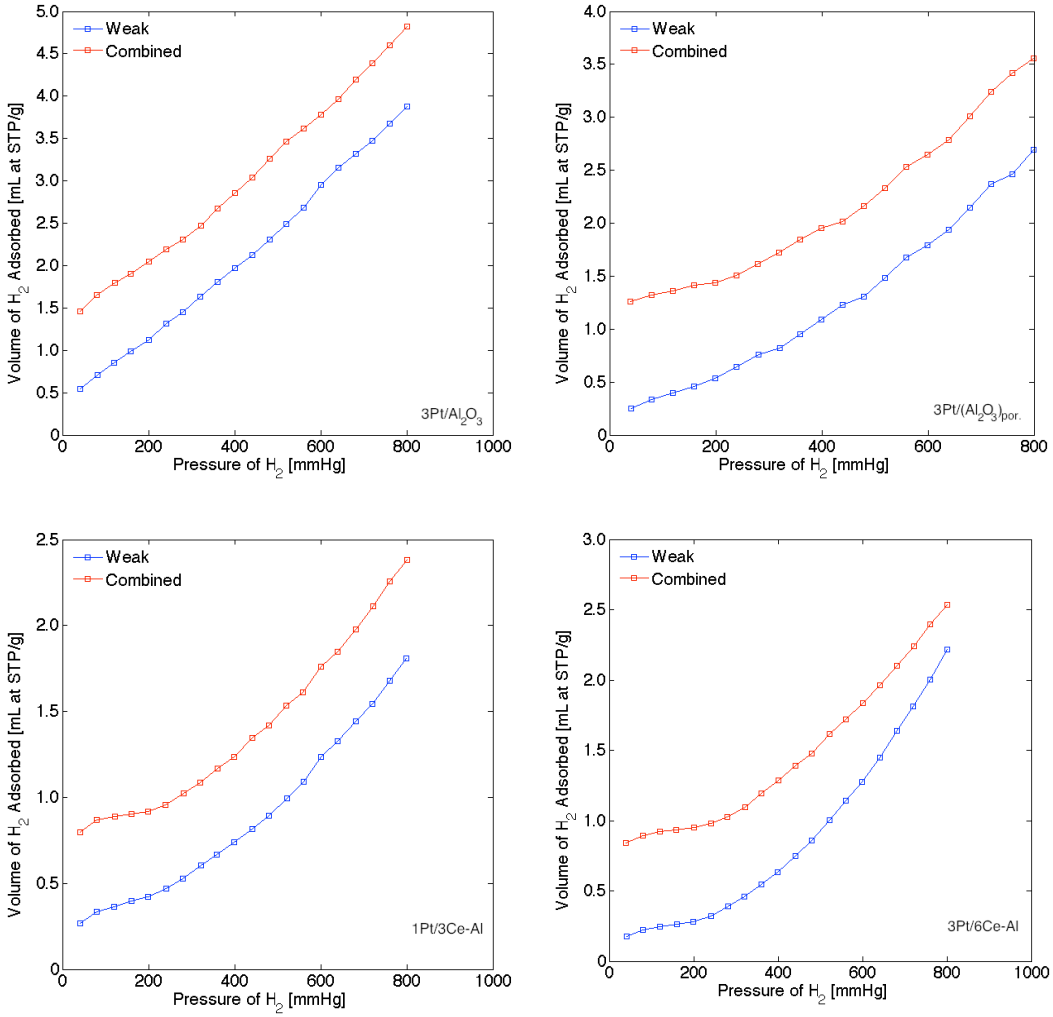

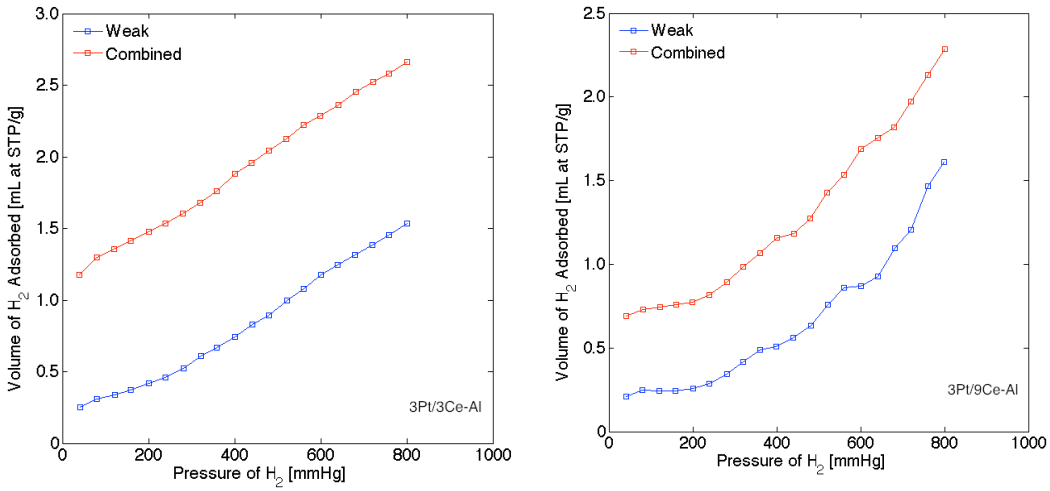

Figure 3-7 H_2 chemisorption isotherms of Pt/Al_2O_3 and Pt/CeO_2-Al_2O_3 catalysts. Isotherms were collected on an Autosorb iQ instrument (Quantachrome) at –78 ^{0}C. Prior to the chemisorption measurement, the sample was reduced in situ at 400 ^{0}C for 40 min in 50mL/min H_2, then purged with 50 mL/min He for 30 min, and finally cooled to room temperature.

Both active surface area and metal dispersion benefitted from the introduction of small amounts of CeO_2, as they increased by a small amount when 3 wt% ceria was added. However higher ceria loadings decreased both the active surface area and the metal dispersion noticeably; these were lowest for 3Pt/9CeAl. The 3Pt/xCeAl catalysts showed similar trends for S_{BET}, M_{area} and $M_{disp.}$, as well as for monolayer hydrogen uptake (Tables 3-1 and 3-2). The high active metal surface area and metal dispersion (4.3 m^2/g and 58%, respectively) exhibited by 3Pt/3CeAl are therefore related to the surface area of 3CeAl (162 m^2/g), which was the highest among the supports. A large surface area of the support was not sufficient, though, to produce a high active metal surface area, as the active metal surface area was slightly lower on $3Pt/(Al)_{por}$ than on 3Pt/3CeAl. The composite

with 1 wt% Pt loading on 3CeAl support (1Pt/3CeAl catalyst) showed significantly elevated metal dispersion (85%) and the lowest average crystal size (13 nm), but had a lower active metal surface area of 2.1 m^2/g, presumably because it contained less Pt.

The XRD patterns of the supported Pt catalysts after calcination and reduction are shown in Figures 3-8 and 3-9, respectively. 3Pt/1CeAl, which had the lowest ceria loading, did not show any clear diffraction peaks for crystalline CeO_2, but the characteristic diffraction lines of the CeO_2 fluorite structure at 2θ = 28.5, 33.3, 47.5 and 56.4° (Fathi et al., 2000, Kim, 1968) were well-defined for catalysts with higher ceria loadings (≥3 wt%). These peaks were broader for CeO_2-doped Al_2O_3 than for pure CeO_2, meaning that the CeO_2 crystallites were smaller in the CeO_2-Al_2O_3 samples, as expected. No bulk crystalline phases corresponding to mixed cerium-aluminium oxides were detected at these calcination and reduction temperatures (Figures 3-8 and 3-9). Prior to reduction, two clear diffraction peaks for platinum oxide species were observed at 2θ = 39.9 and 46°.

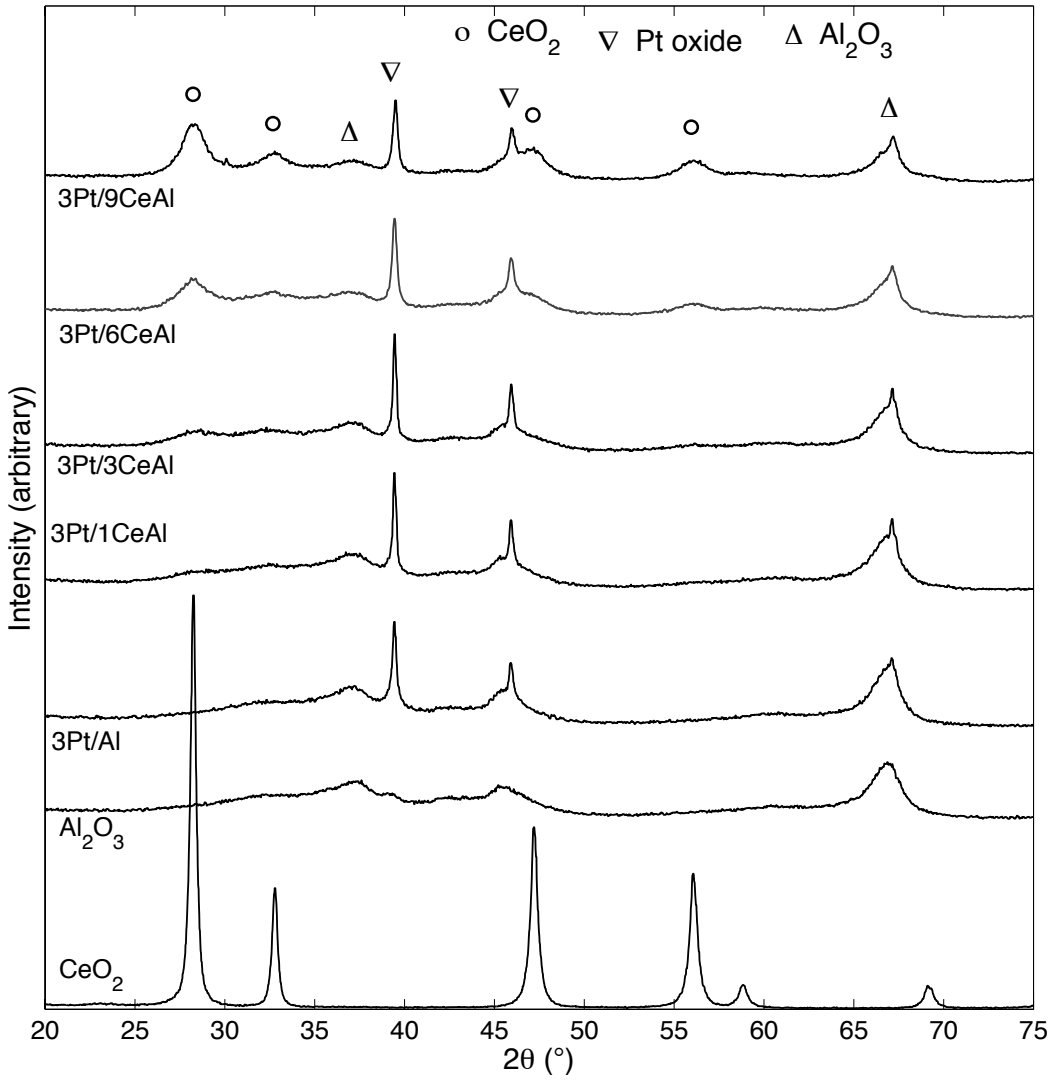

Figure 3-8 X-ray diffraction patterns of pure CeO_2 and Al_2O_3 as well as of the Pt/Al and Pt/CeAl catalysts with different CeO_2 loadings. Samples were calcined at 550 ^{0}C for 3 h under air (ramp rate of 1.5 ^{0}C/min)

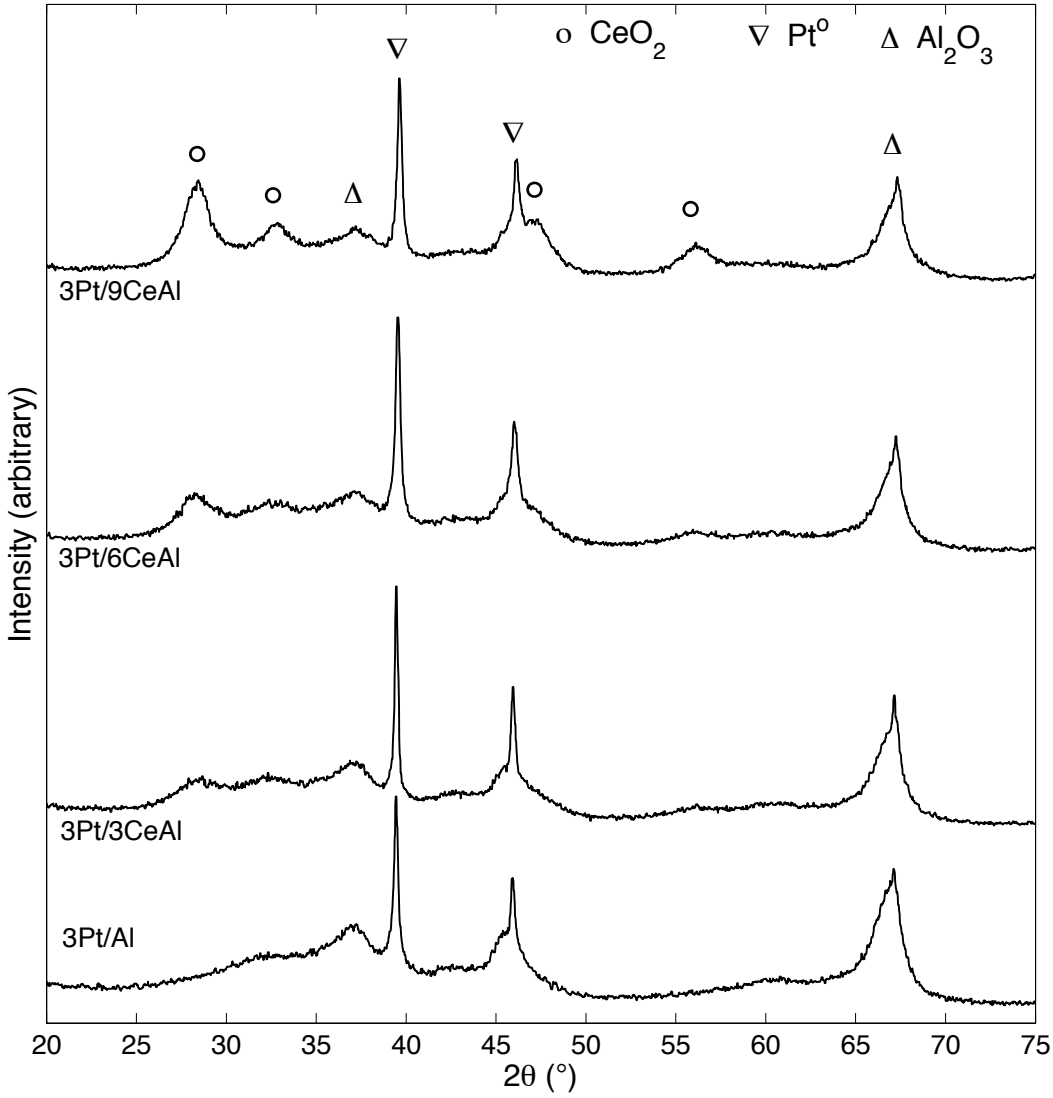

Figure 3-9 X-ray diffraction patterns of the 3Pt/Al and Pt/CeAl catalysts with different CeO_2 loadings. Catalysts were reduced in flowing H_2 (25 vol.% with N_2) at 500 ^{0}C for 90 min (ramp rate of 1.5 ^{0}C/min)

Also the reducibility of the catalysts was studied with results shown in Figure 3-10. It is clear that Pt-oxide reduction was promoted by the wt% of ceria addition. This result is consistent with XRD (Figure 3-9) and XPS (Figure 3-7).

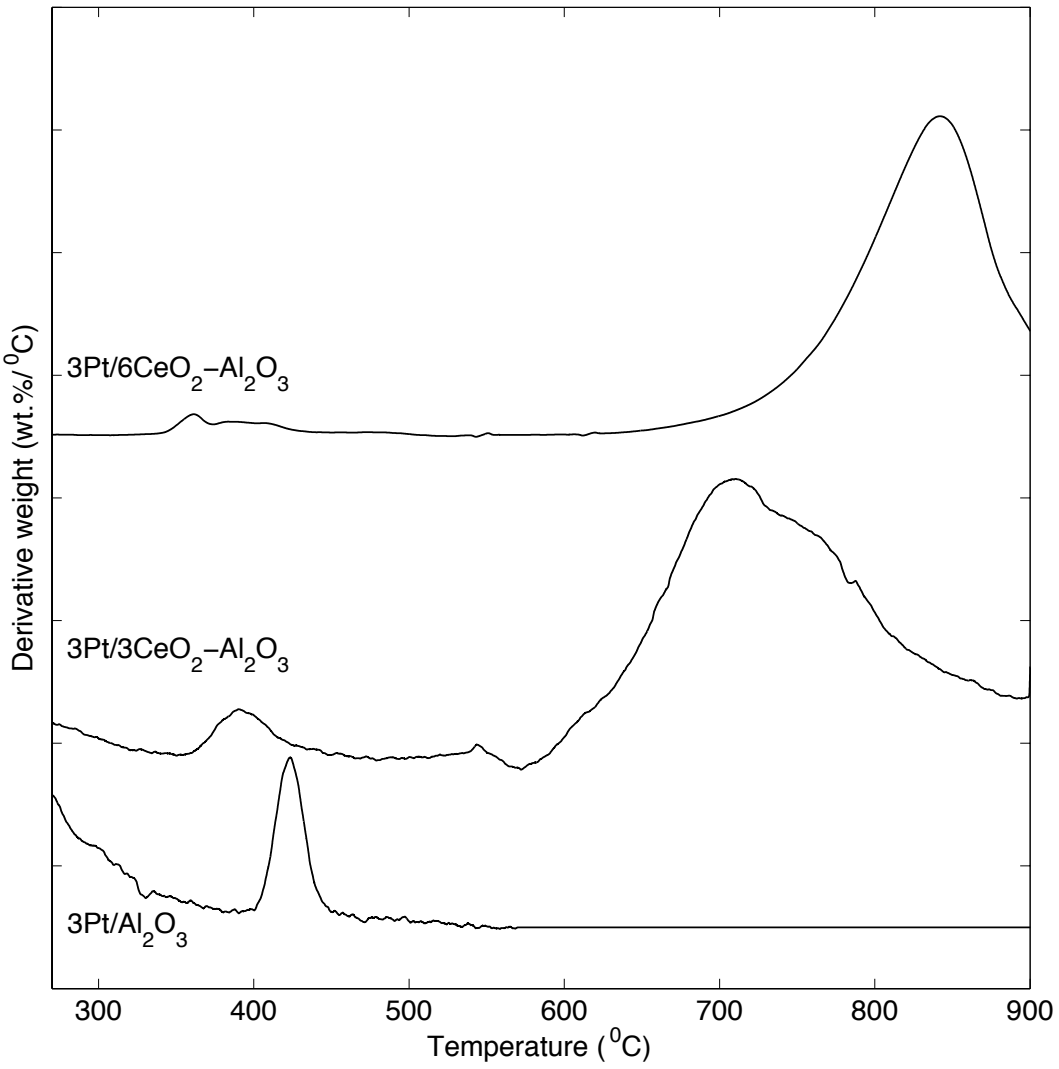

Figure 3-10 TGA study of catalyst reduction by H_2 (25 vol.% in N_2) at 1.5 ^{0}C/min.

3.3.2 Catalytic test

3.3.2.1 Effect of ceria loading on catalytic activities

An aqueous solution of 1 wt% glycerol was in initial tests of catalyst performance. The reaction data presented in Figures 3-11 and 3-12 showed that the aqueous-phase reforming of glycerol over all of the studied catalysts indeed leads to a hydrogen-rich gas phase. The yield of H_2 during the APR of glycerol over the catalyst was the ratio of the amount of H_2 produced divided by the amount of H_2 that could have been produced if all of the glycerol was completely reformed (i.e. 7 theoretical mol H_2/mol glycerol; refer to Eq. 3-2). Pt catalysts supported on Al_2O_3 with 3 and 6 wt% CeO_2 both gave higher H_2 yields than the one on unpromoted Al_2O_3 (Figure 3-11), and the highest H_2 yield (56% from 3Pt/3CeAl) was significantly higher than the yield (36%) observed using the catalyst on unpromoted alumina (3Pt/Al). The catalyst with the highest CeO_2 content, 3Pt/9CeAl, produced less H_2 (25% yield). 1Pt/3CeAl gave less H_2 (29% yield) than Pt on unpromoted Al_2O_3, but also yielded higher carbon conversion to gas and less CH_4 yield. Higher methane yields were observed for the catalysts with 3 and 6 wt% ceria loading in the alumina support. The lowest CH_4 yield, 3%, was produced by 1Pt/3CeAl.

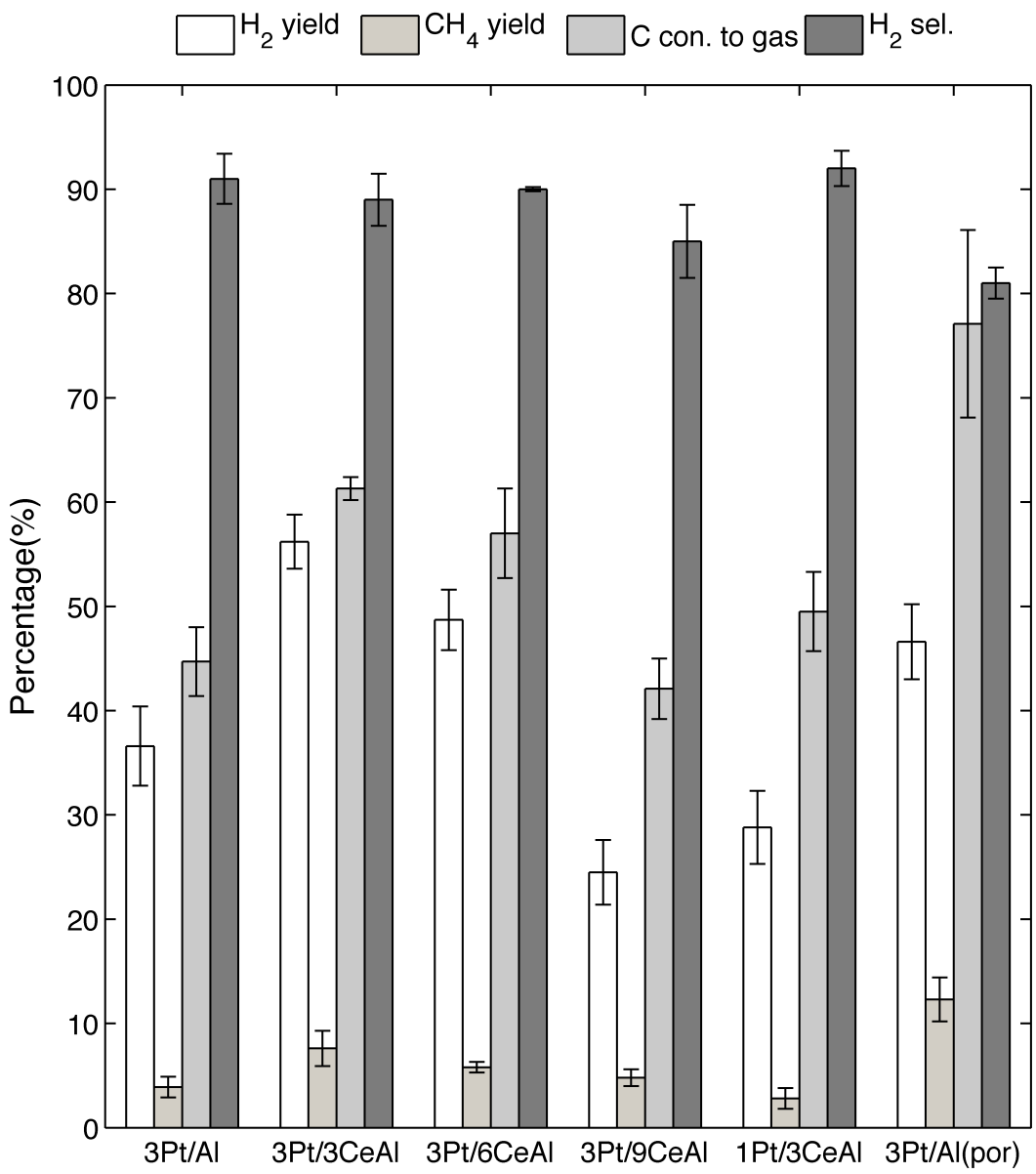

Figure 3-11 Effect of CeO_2 addition to the Al_2O_3 support in Pt/Al catalysts on the yield, gas phase conversion and selectivity of the aqueous phase reforming of glycerol (220 ºC, 30 bar, 5 wt% glycerol, 0.01 mL/min, 250 mg catalyst); data are mean values over t = 3–20 h). Error bars indicate one standard deviation; each bar is the average of ≥2 experiments

The highest carbon conversion (§2.2.1) to gas, 61%, was achieved for 3Pt/3CeAl (Figure 3-11). All catalysts on ceria-doped supports produced higher carbon conversions to gas phase than 3Pt/Al. Thus, including CeO_2 in the Al_2O_3 support for APR catalysts improved both the H_2 yield and carbon conversion to gas phase, and the magnitude of the effect varied with CeO_2 loading. All of the catalysts showed similar H_2 selectivity. Although 1Pt/3CeAl produced the highest hydrogen selectivity, it gave lower H_2 yield and carbon conversion to gas phase than 3Pt/3CeAl. H_2 selectivity, yield, and carbon conversion to gas decreased with increasing ceria loading above 3 wt%, which could be due to the loss of surface area and metal dispersion with higher ceria loading (Tables 3-1 and 3-2). Additionally, the negative effects of adding more than 3 wt% ceria to the catalyst support may be caused by interactions between the ceria and platinum; such interactions can facilitate the oxidation of surface Pt sites (Zhuang et al., 1991). Yu-Yao has suggested that the increased oxidation state of Pt in Pt/CeAl catalysts produces less active metal surface (Yao, 1980), which is problematic because the activity of noble-metal reforming catalysts is related to their reducibility, i.e. to the quantity of Pt^0 present on the surface. This may explain why ceria loadings $\geq$6 wt% did not significantly increase the catalytic activity of CeAl-supported Pt catalysts in aqueous-phase reforming, and is consistent with the lower active metal surface areas measured for 3Pt/6CeAl and 3Pt/9CeAl.

We noted that 3CeAl had the highest surface area, and considered the possibility that this was the source of the favourable catalytic properties of 3Pt/3CeAl. Therefore, to examine the effect of the surface area and porosity of the support on

the reforming reaction, a highly porous Al_2O_3 support (S_{BET} = 267 m^2/g, V_{pore} = 0.38 cm^3/g) support was synthesized and impregnated with 3 wt% Pt. The resulting catalyst, $3Pt/(Al)_{por.}$, had similar Pt dispersion to Pt/Al (Table 3-2). It produced a much higher carbon conversion to gas than 3Pt/Al catalyst (Figure 3-11); however, this came largely in the form of CH_4, as the catalyst produced a somewhat higher H_2 yield but the highest CH_4 yield (12%) and lowest H_2 selectivity (81%). Thus, the increase in surface area that occurred when 1–3 wt% CeO_2 was added to the Al_2O_3 support may have contributed to the increase in H_2 yield from Pt-catalyzed APR, but was clearly not sufficient to explain it. Interestingly, increasing the surface area of the support had little impact on dispersion, but decreased the H_2 selectivity by ~9%; this complements a report that a significant change in Pt dispersion and active metal surface area on Al_2O_3 barely impacted the selectivity of the APR of ethylene glycol (Shabaker et al., 2003b).

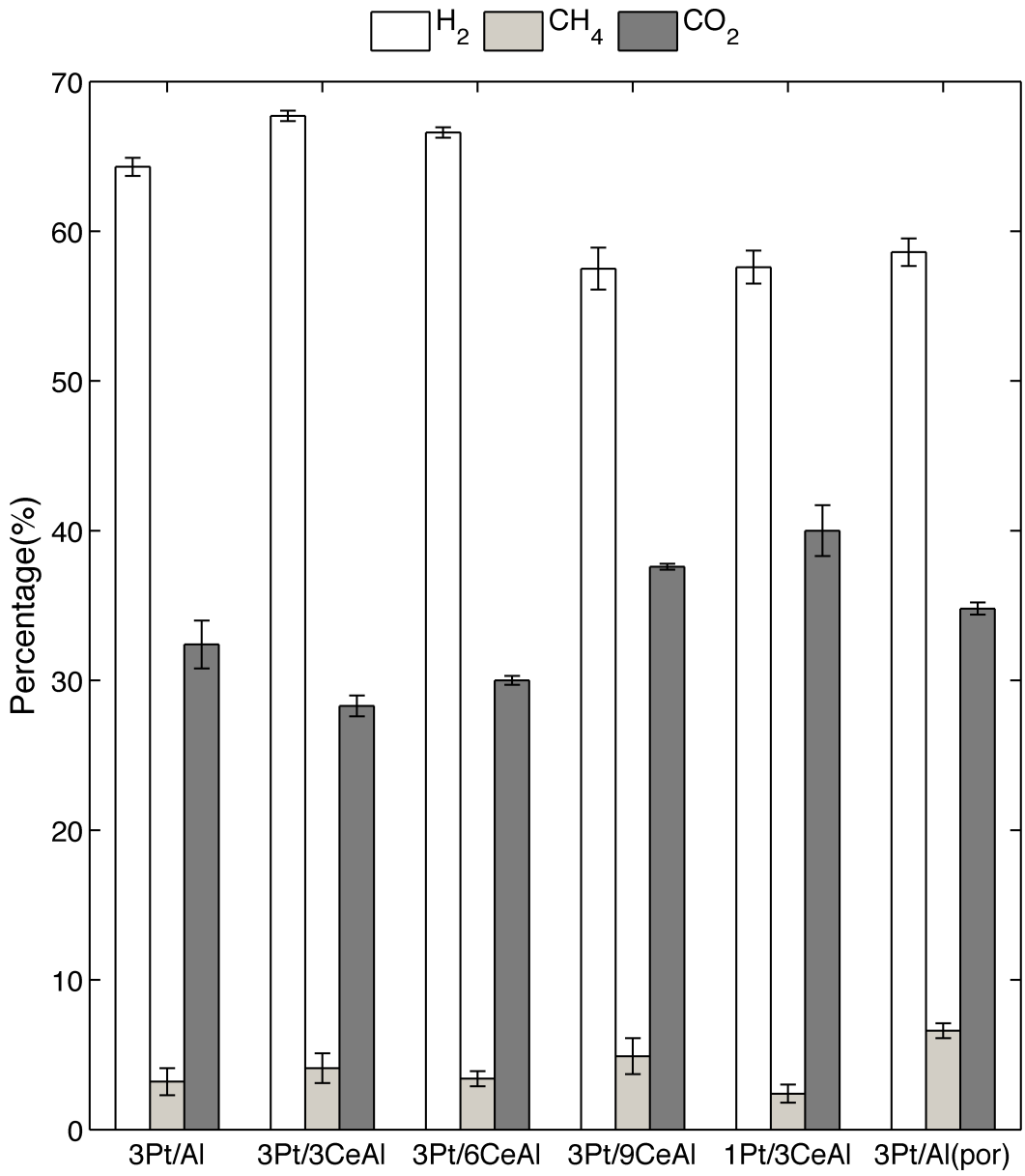

Figure 3-12 Effect of CeO_2 addition to the Al_2O_3 support in Pt/Al catalysts on the distribution of gaseous products from the aqueous phase reforming of glycerol (220 ºC, 30 bar, 5 wt% glycerol, 0.01 mL/min, 250 mg catalyst); data are mean values over t = 3–20 h). Error bars indicate one standard deviation; each bar is the average of ≥2 experiments

The distributions of gaseous products from the APR of 5 wt% glycerol are illustrated in Figure 3-12. H_2, CO_2 and CH_4 were the only products identified in the gas phase. No CO was detected, indicating that CO concentration in the

product gas was below the GC detection limit (i.e. [CO] ≥ 100 ppm). It is clear that, as the ceria content in the catalyst support increased above 3 wt%, the fraction of H_2 in the product decreased gradually. Catalysts 3Pt/3CeAl and 3Pt/6CeAl generated the most H_2-rich gas streams, being 68 and 66 mol% H_2, respectively (cf. 64 mol% H_2 obtained using 3Pt/Al). Notably, in the series 3Pt/xCeAl (i.e. not including 3Pt/$(Al)_{por.}$), the fraction of H_2 in the product gas was strongly correlated with the active metal surface area in of the catalyst (see Figure 3-13a), confirming the contribution of Pt particle size to the improvements in catalyst performance. Additionally, the fraction of CO_2 in the product gas increased with the ceria loading in the catalyst support, indicating that higher ceria loading favoured the WGS reaction. Though the gas product from APR over 1Pt/3CeAl contained less H_2 (57 mol%), it also contained less CH_4 and more CO_2, meaning less methanation and a higher yield from the WGS reaction. It also showed the highest normalized rate of H_2 production, 261 mmol H_2 gPt^{-1} h^{-1}. APR over 3Pt/$(Al)_{por.}$ produced less H_2 (58 mol%) than the reaction over 3Pt/Al, but higher fractions of both CH_4 and CO_2 (Figure 3-12), meaning that the porosity and high surface area of the support favoured both methanation and the WGS reaction.

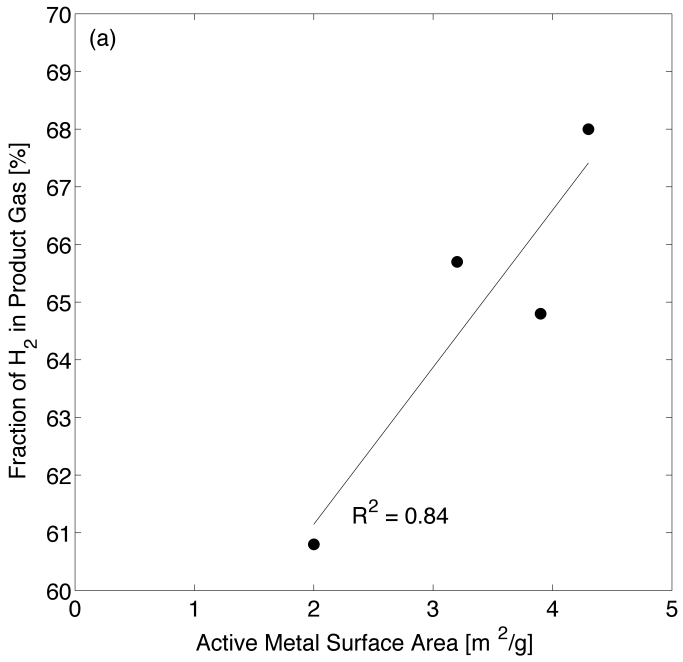

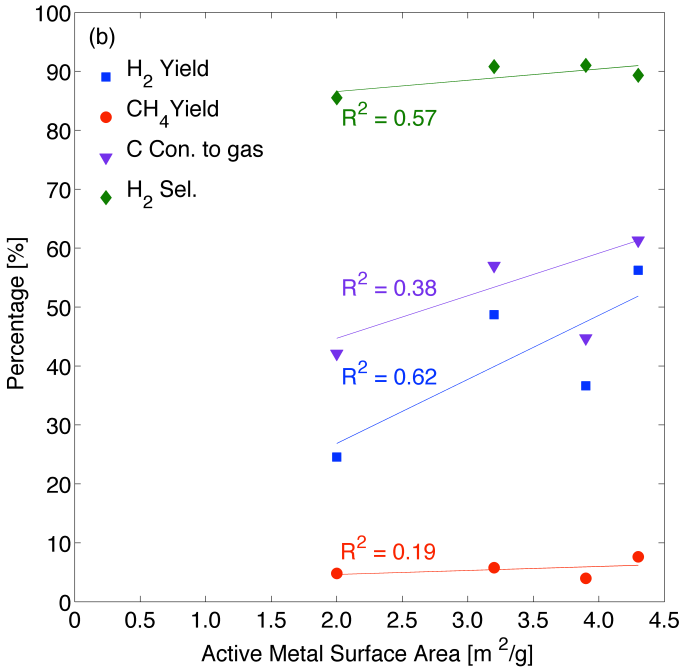

Figure 3-13 Correlation between active metal (Pt) surface area and the results of aqueous phase reforming. (a) Correlation with fraction of H_2 in the product gas; only catalysts 3Pt/xCeAl are considered. Active metal surface areas were measured by H_2 chemisorption at –78 °C, and aqueous phase reforming was performed using 5 wt% aqueous glycerol as the feedstock. T = 220 ºC, P = 30 bar, flow rate = 0.01 mL/min, mcatalyst = 250 mg, data averaged over t = 3–20 h. (b) Correlation with gas yields and selectivity

From the above analysis it is evident that among the catalysts tested, those with 3 wt% CeO_2 doping in the Al_2O_3 support showed the best performance. 3Pt/3CeAl showed the highest H_2 yield of all the catalysts tested, producing 55% more H_2 than 3Pt/Al. Even 1Pt/3CeAl showed higher H_2 selectivity and carbon conversion to gas, as well as much lower CH_4 yield, than 3Pt/Al. This clearly evinces the advantage of adding 3 wt% CeO_2 to the alumina catalyst support in the Pt-catalyzed APR of glycerol. Moreover, it suggests that using CeO_2 in the catalyst support may permit the loading of Pt, an expensive noble metal, to be lowered without compromising catalyst performance.

Though the catalyst support 3CeAl had a slightly larger surface area than Al_2O_3, experiments using a catalyst on porous Al_2O_3, which had a higher surface area, gave an H_2 yield intermediate to those on Al_2O_3 and 3CeAl, and produced a high CH_4 yield. Moreover, the addition of 3 wt% ceria to the alumina support had only a minor effect on the active surface area of the deposited Pt (Table 3-2). Nevertheless, H_2 yield was correlated to active surface area, with each additional m^2/g of active metal contributing an additional 10% to H_2 yield (Figure 3-13b, $R^2 = 0.7$).

H_2 yield was also improved when the fraction of reduced Pt in the calcined catalyst increased, at least in the cases of 3Pt/3Ce-Al and 3Pt/6Ce-Al. The addition of 3 or 6 wt% CeO_2 to the support greatly increased this fraction (see XPS data in Figure 3-6), indicating that dispersed CeO_2 promoted the reduction of Pt^{4+} to Pt^0 (Figure 3-10). This may have been related to the oxygen-storage capacity of CeO_2, which

is enhanced by noble metals (Yao and Yao, 1984), and which would have been increased upon the reduction treatment as surface O atoms were removed. The oxidation state(s) of Pt in calcined Pt/9CeAl, however, could not be determined reliably, so it is unclear whether this trend held when more CeO_2 was added to the support.

Thus, overall, adding CeO_2 to the Al_2O_3 supports of Pt-containing APR catalysts affected the APR reaction in several ways. The clearest of these was that CeO_2 increased the active surface area of the Pt catalyst (Table 3-2), as this value was directly correlated to the fraction of H_2 in the product gas (Figure 3-13a). It was also correlated, though less strongly, to H_2 yield (Figure 3-13b). The impact of the total support surface area was less clear. Increasing the amount of CeO_2 in the catalyst support also increased the fraction of CO_2 in the product gas (Figure 3-12), presumably due to the ability of CeO_2 to catalyze the WGS reaction (Figure 3-17). Adding CeO_2 to the support also improved the reducibility of the supported platinum oxides (Figure 3-10).

In a test of catalyst stability, we also studied H_2 formation by the continuous APR of glycerol over 3Pt/3CeAl for 135 h. A catalyst mass of 150 mg and a reaction temperature of 200 °C were used, and a stable H_2 yield of 37% was obtained (Figure 3-14), indicating that the catalyst was stable over a period of days.

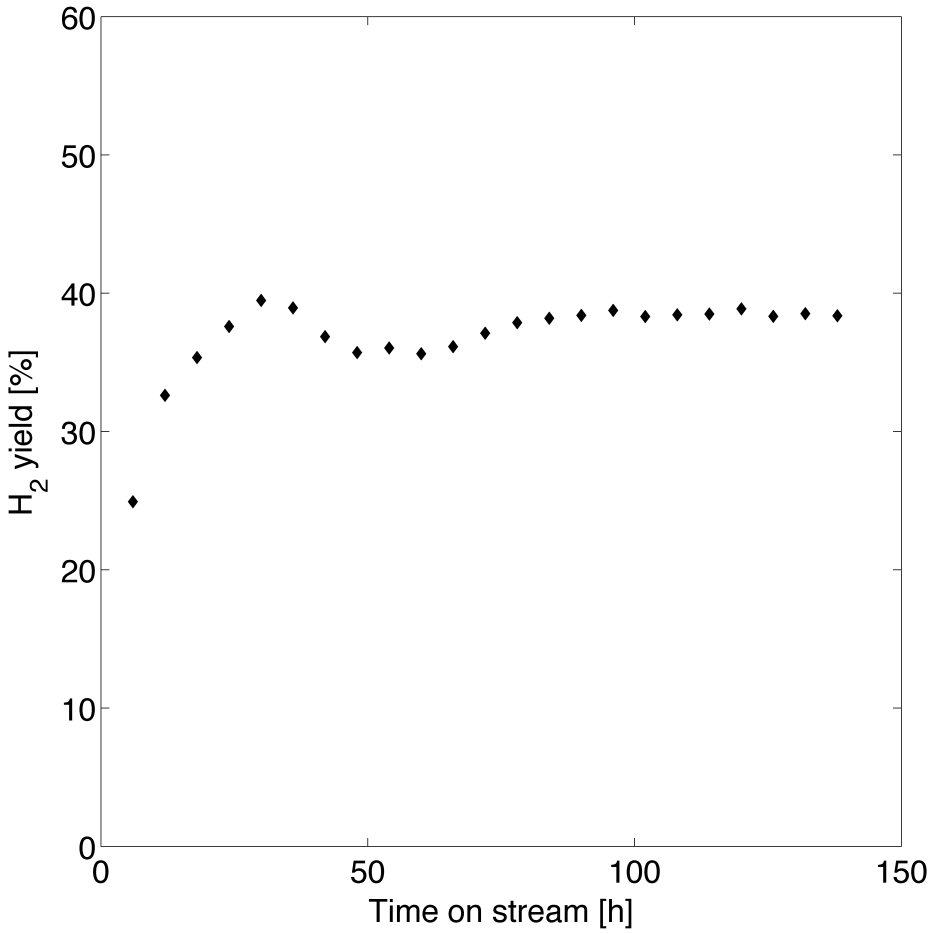

Figure 3-14 H_2 formation by the continuous APR of glycerol over 3Pt/3CeAl for 135 h. T = 200 °C, P = 20 bar, flow rate 0.01 mL/min of 5 wt% aqueous glycerol, and 150 mg catalyst was used

3.3.2.2 Effects of various reaction conditions on catalytic activities

The catalyst 3Pt/3Ce-Al, which produced the highest H_2 yield from the APR of glycerol in the catalyst-screening studies, was used to investigate the effect of various reaction conditions on the reaction, as the contact time between reactants and catalyst are expected to significantly impact catalytic activity. The impacts of feedstock concentration and feed flow rate were explored first. Figure 3-15

compares the results from the APR of glycerol solutions with three different feedstock concentrations (1, 5 and 10 wt%) and two feed flow rates (0.01 and 0.05 mL/min). As the flow rate of the reaction was varied, three different weight hourly space velocities (WHSV), 0.024, 0.12 and 0.24 h^{-1}, were also studied. Though a feedstock of 5 wt% glycerol, delivered at 0.01 mL/min (WHSV = 0.12 h^{-1}), produced slightly higher hydrogen yield and selectivity than a 1-wt% feedstock delivered at 0.05 mL/min, it also gave lower carbon conversion to gas and fraction of CO_2 in the product. The APR of glycerol at WHSV = 0.12 h^{-1} produced significantly higher H_2 yield and carbon conversion to gas than the other WHSV values tested. On the other hand, when the feedstock was 10 wt% glycerol (WHSV = 0.24 h^{-1}), the H_2 yield and carbon conversion to gas were much lower compared to the 1 and 5 wt% feedstocks, but the H_2 selectivity was better for the 10 than the 1 wt% feedstock. This was because, at WHSV = 0.24 h^{-1}, CH_4 yield was lower, indicating that methanation was mitigated, and the WGS reaction was favoured. Although CH_4 yield (7.5%) was high at WHSV = 0.12 h^{-1}, conversion of glycerol was facilitated and the reforming ratio (mol H_2/mol CO_2) was also very close to the theoretical value of 2.33. Where as this was not observed at the lower (0.024 h^{-1}) or higher (0.24 h^{-1}) WHSV. This can be attributed to the sufficient contact between the glycerol reactant and the catalyst, which allowed the reforming reaction to take place; the shorter contact time (i.e. for WHSV = 0.24 h^{-1}) only allowed the partial conversion of glycerol (Montoya et al., 2000, Bradford and Albert Vannice, 1999). Overall, the high carbon conversion to gas and the better catalysis of the WGS reaction (as shown by CO_2 yield) motivated us to use 1 wt%

glycerol and a feed flow rate of 0.05 mL/min for further experiments. Figure 3-15 also shows that H_2 selectivity under all the conditions presented here are within the range of error bars. Therefore it could be concluded that the selectivity was largely independent of the WHSV used.

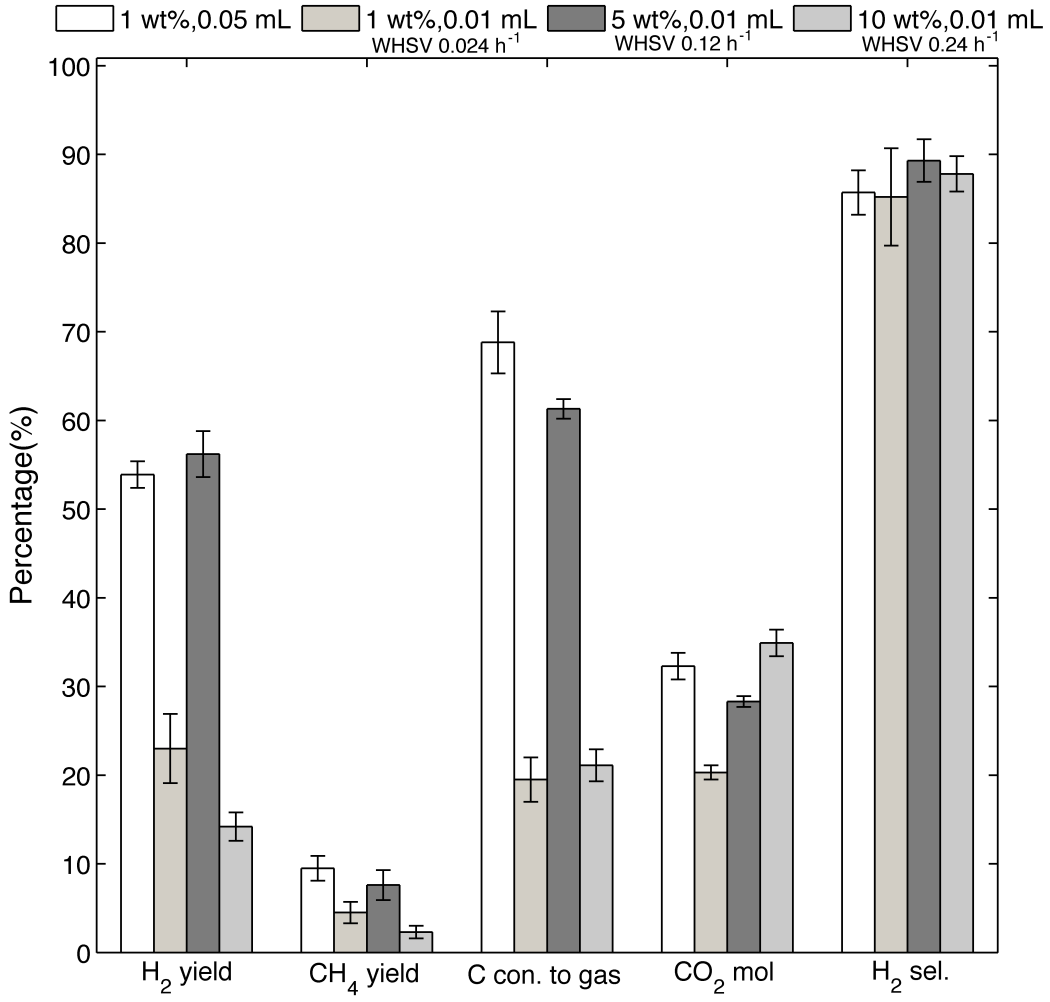

Figure 3-15 Effect of the concentration and feed flow rate of glycerol on its APR over 3Pt/3CeAl (220 ºC, 30 bar, 250 mg catalyst; data are mean values over t = 3–20 h). Error bars indicate one standard deviation; each bar is the average of ≥2 experiments

The effect of reaction temperature and corresponding system pressure on the APR of glycerol (1 wt% in H_2O, 0.05 mL/min) was also examined over 3Pt/3CeAl. Under these conditions, we also studied the glycerol conversion efficiency by measuring the amount of unreacted glycerol in the product. Increasing the reaction temperature and corresponding system pressure favoured much higher H_2 yield, carbon conversion to gas and glycerol conversion efficiency (Figure 3-16). At the highest temperature tested (240 $^{\circ}$C), the gas phase carbon conversion reached 85%, but was significantly lower than the glycerol conversion efficiency (95%). Thus, other hydrocarbons may have been formed but not detected by GC. Apart from unreacted glycerol, the liquid phase from this reaction contained small traces of other compounds, particularly ethanol and propylene glycol, but these were not quantified. The normalized rate of H_2 generation was also higher at 240 $^{\circ}$C (311 mmol gPt^{-1} h^{-1}); however, the higher conversion and H_2 yield came at the cost of selectivity; evidently, methanation was significantly increased and the WGS reaction was decreased.

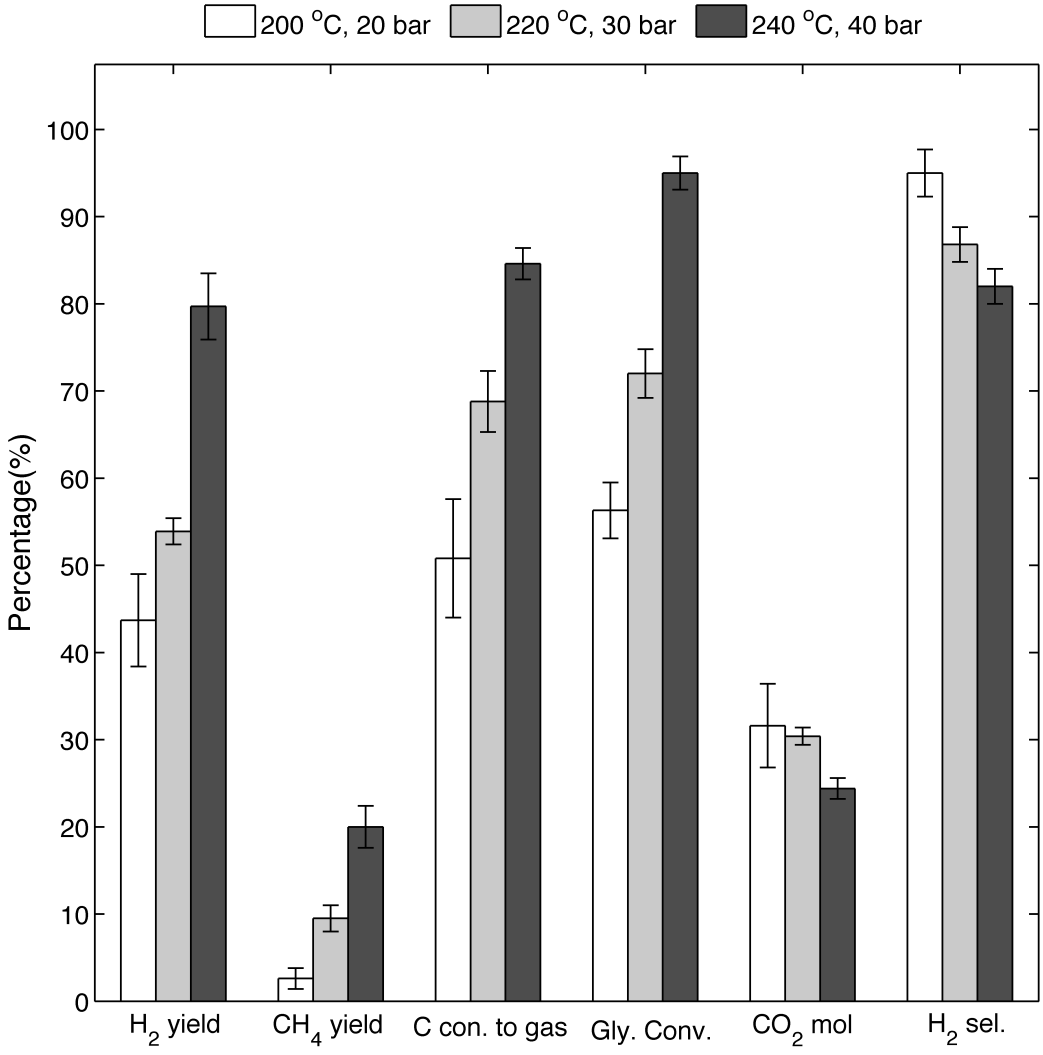

Figure 3-16 Effect of temperature and pressure on the APR of glycerol (1 wt% glycerol, 0.05 mL/min, 250 mg of 3Pt/3CeAl catalyst; data are mean values over t = 3–20 h). Error bars indicate one standard deviation; each bar is the average of ≥2 experiments

3.3.2.3 Effect of WGS reaction on H_2 yield in ARR

An important advantage of APR (Eq. 4-3) is the ability of producing 7 moles of hydrogen per 1 mole of glycerol, 4 moles from glycerol reforming (Eq. 4-1) and 3 moles from WGS reaction (Eq. 4-2). To investigate the fact, WGS reaction was

studied using the same reactor system and same reaction conditions (240 °C, 40 bar, 250 mg catalyst) was applied for APR process to investigate the catalyst performance. Instead of using 1 wt% glycerol in DI water, 0.05 ml min^{-1} DI water and 0.39 ml min^{-1} CO was introduced in the reactor as the reactant. The produced gas mixture was analyzed using an online gas chromatograph (Varian CP-3800) equipped with one Hayesep N, 60/80 Mesh, 5 m x 1/8″ SST column and one Molsieve 5Å, 60/80 Mesh, 1 m x 1/8" column, connected in series. Thermal conductivity detector (TCD) and flame ionization detector (FID) in series were used to analyze H_2 and hydrocarbons, respectively. The carbon balance agreed within ±5 mol.%. Figure 3-17 shows the total CO conversion, H_2 yield and CH_4 yield. Catalysts showed higher CO conversion and H_2 yield compare to WGS reaction without catalyst. In the case of 3Pt/3CeAl, higher CO conversion and H_2 yield was observed compare to 3Pt/Al catalyst. When carrying out the WGS reaction, methane can be formed by CO/CO_2 hydrogenation in a methanation reaction (Haryanto et al., 2009). CH_4 yield tends to decrease as ceria was added with 3Pt/Al catalyst. The presence of ceria produced favorable structural and electronic effects for enhancing the WGS activity.

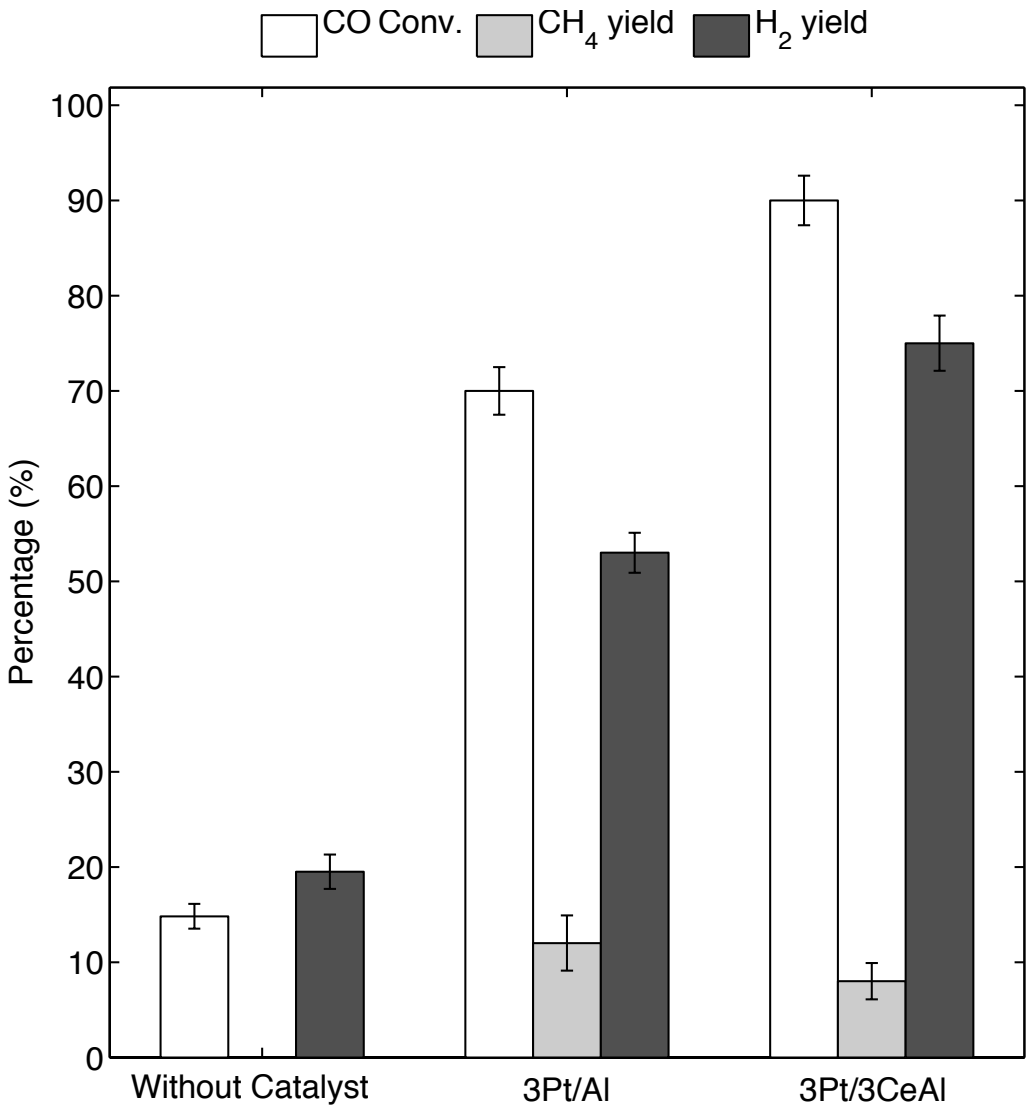

Figure 3-17 WGS study without catalyst and with catalysts (240 °C, 40 bar, 0.05 mL min−1 DI water, 0.39 mL/min CO, 100 mg catalyst; data are mean values over t = 3–20 h). Error bars indicate one standard deviation; each bar is the average of ≥2 experiments

3.4 Conclusions

A series of Pt catalysts supported on Al_2O_3 doped with different amounts (in wt%) of CeO_2 were developed and tested in the aqueous-phase reforming of glycerol to H_2. The catalyst 3Pt/3CeAl showed the highest glycerol conversion (95%), carbon

conversion to gas (85%) and hydrogen yield (80%) for a 1 wt% solution of glycerol fed at 0.05 mL/min, at 240 °C under the corresponding system pressure. Compared to 3Pt/Al, 1Pt/3CeAl showed higher H_2 selectivity and carbon conversion to gas, as well as much lower CH_4 yield, clearly evincing the effect of adding 3 wt% ceria to the alumina catalyst support in the Pt-catalyzed APR of glycerol. H_2-chemisorption results showed that highest metal dispersion (58%) and active surface area (4.3 m^2/g) was achieved for 3 wt% CeO_2 doping in the alumina support, and these are thought to be partly responsible for the high hydrogen yield and carbon conversion to gas. No CO could be detected in the product gas, meaning that it may be directly useable in a PEM fuel cell. Thus, Pt supported on ceria-doped alumina had both higher catalyst activity and higher selectivity towards H_2 generation from the APR of glycerol than an unpromoted alumina-supported Pt catalyst.

Chapter 4

Chapter 4 described the effect of Ni addition to Pt catalyst on the aqueous phase reforming of glycerol. Catalysts were characterized and tested in a continuous flow packed bed reactor. From the XRD and XPS analyses, it was clear that adding Ni impacted both the crystallite and electronic structure of Pt. These effects would be expected to impact the reactivity of the metal, and likely conspired to produce high glycerol conversion and gas phase C yield and, ultimately, the high H_2 yield observed.

This chapter is based on:

M. M. Rahman, Tamara L. Church, Meherzad F. Variava, Andrew T. Harris, and Andrew I. Minett, Bimetallic Pt-Ni composites on ceria-doped alumina supports as catalysts in the aqueous-phase reforming of glycerol. RSC advances, 2014,4,18951-18960

4 Bimetallic Pt-Ni composites on $3CeO_2$-Al_2O_3

4.1 Introduction

In chapter 3, we reported that Pt supported on alumina doped with 3 wt% ceria gave significantly higher H_2 yield and selectivity from the APR of glycerol than Pt on alumina (Rahman et al., 2013). The improved performance of these catalysts was attributed to their higher coking resistance and oxygen storage capacity, as well as to enhanced catalysis of the WGS reaction and lower methanation activity under APR conditions (Wang, 1998)(Whittington, 1995). Although Pt catalysts are highly active for APR (Davda et al., 2005), the high cost of Pt makes catalysts based on non-precious metals desirable. Also, Pt catalysts supported on Al_2O_3 may suffer from severe deactivation due to coke deposition, oxidation or sintering (Comas et al., 2004, Gorte and Zhao, 2005). Ni has shown initial APR activity comparable to that of Pt, but was subject to significant deactivation (Davda et al., 2003). Thus, efforts have been made to improve the catalytic activities of the Ni catalysts by impregnating them with other metallic elements (Shabaker et al., 2004).

The activity of APR catalysts, as well as of other supported-metal catalysts, can be enhanced by adding an additional metal (§1.6.2) (Çağlayan et al., 2005, Rynkowski et al., 1995, Dal Santo et al., 2012). It has been suggested that adding noble metal promoters to a Ni catalyst for dry methane reforming may reduce coke deposition and therefore provide stability (Crisafulli et al., 2002). Relevant to C–C bond cleavage, adding Pd to a Ni/SiO_2 catalyst increased the amount of gas

produced from cellulose pyrolysis; this was attributed to greater tar-cracking activity (Widyaningrum et al., 2013). The Pt-Ni system in particular has been extensively studied in a range of applications because of its synergetic catalytic effect (Baker et al., 1986). Kunkes et al. reported the conversion of glycerol by APR over carbon-supported Pt and Pt-Re catalysts. The addition of Re led to an increase in the production of H_2, CO, CO_2, and light alkanes (primarily methane), ultimately leading to better hydrogen selectivity (Kunkes et al., 2008). Wang et al. showed that adding Co to a Pt-based APR catalyst significantly increased its activity without impacting the selectivity for H_2 (Wang et al., 2009). Manfro et al. (Manfro et al., 2013) added Cu to a Ni catalyst and obtained decreased CH_4 formation, which increased H_2 selectivity. Ko et al. (Ko et al., 2006) showed that, under the same pretreatment conditions, Pt-Ni bimetallic catalysts had more active sites than monometallic Pt or Ni catalysts. Tupy et al. (Tupy et al., 2012) found that, after 24 h on-stream in the APR of ethylene glycol, a supported Pt-Ni catalyst was more active than a Pt catalyst because Ni segregation occurred, producing a Ni-enriched surface. Huber et al. (Huber et al., 2006) suggested that the activity of Pt-based catalysts for APR could be increased by alloying Pt with Ni or Co, which would decrease the strength with which CO and H_2 interact with the surface, thereby increasing the fraction of catalytic sites available to react with ethylene glycol. Boga et al. found that bimetallic Pt-Cu catalyst supported on a Mg(Al)O mixed-oxide support showed higher hydrogen selectivity and lower methane production than Pt/Al_2O_3 (Boga et al., 2013). Luo et al. stated that adding 2 wt% ceria with a bimetallic Ni–Co catalyst supported on alumina improved its catalytic

activity and resistance to sintering in the APR of glycerol (Luo et al., 2010). In this chapter, bimetallic Pt-Ni catalysts supported on 3-wt%-ceria-doped alumina have been prepared and tested for APR of glycerol. The ratio of Pt to Ni on the support was optimized and the catalyst characterized to better understand the system.

4.2 Experimental

4.2.1 Catalyst preparation

The 3-wt% CeO_2–Al_2O_3 supports were prepared by impregnating 2.0 g of dried (120 °C overnight) γ-Al_2O_3 (Sigma) with a solution prepared by dissolving 197 mg of $(NH_4)_2[Ce(NO_3)_6]$ (99%, Aldrich) in 10 mL deionized water in a 100-mL glass vial. The mixture was stirred overnight at room temperature, and the water was allowed to evaporate. The sample was then dried in air at 120 °C for 12 h and calcined under flowing air at 600 °C for 3 h (heating rate 1.5 °C/min).

$[Pt(NH_3)_4](NO_3)_2$ (Strem Chemical) and $Ni(NO_3)_2•6H_2O$ (Sigma–Aldrich) were dissolved, individually or together, into a minimum amount of deionized water to make monometallic or bimetallic catalysts, respectively. These were deposited on 3-wt% CeO_2–Al_2O_3 supports (3CeAl) using a conventional impregnation technique. Specifically, to prepare 1Pt-3Ni/3CeAl, 2.205 g of calcined 3CeO_2–Al_2O_3 support was impregnated with a solution prepared by dissolving 43.1 mg $[Pt(NH_3)_4](NO_3)_2$ and 324.5 mg of $Ni(NO_3)_2·6H_2O$ in 10 mL of deionized water in a 100-mL glass vial. The mixture was then stirred overnight at room temperature, and the water was allowed to evaporate. The sample was then dried in air at 120

°C for 12 h and calcined under flowing air at 600 °C for 6 h (heating rate 1.5 °C/min). Catalysts were reduced ex situ in flowing hydrogen (50 mL/min) at 800 °C for 60 min (heating rate 1.5 °C/min) at atmospheric pressure and stored under vacuum prior to use.

For comparison, a mixed "1Pt/3CeAl + 6Ni/3CeAl" catalyst was also prepared. In order to prepare this physical mixture of catalysts with a total of 1 wt% Pt and 6 wt% Ni, catalysts 2Pt/3CeAl and 12Ni/CeAl were independently prepared, then mixed in a 1:1 ratio by mass.

4.2.2 Catalyst testing

The APR of glycerol was studied in a continuous-flow fixed-bed reactor system (§2.2.1). The catalyst (250 mg) was loaded into a 5-mm i.d. stainless steel tubular reactor and held in position with quartz wool plugs. The system was allowed to stabilize for about 2 h before analysis of the reaction products began. Gas products were analyzed at 25-min intervals using an online gas chromatograph, Varian CP-3800 (§2.2.2). The GC was calibrated using highly pure gases (grade 5.0) from Coregas. For each reading, ten successive injections were made and the relative standard deviations were measured. The calibration curves (Figure 4-1) were developed, and the samples were analyzed, with the TCD at 200 °C and the FID at 300 °C. A representative GC curve (Figure 4-2) shows only four peaks, representing H_2, N_2, CH_4 and CO_2, respectively, for each injection of product gas.

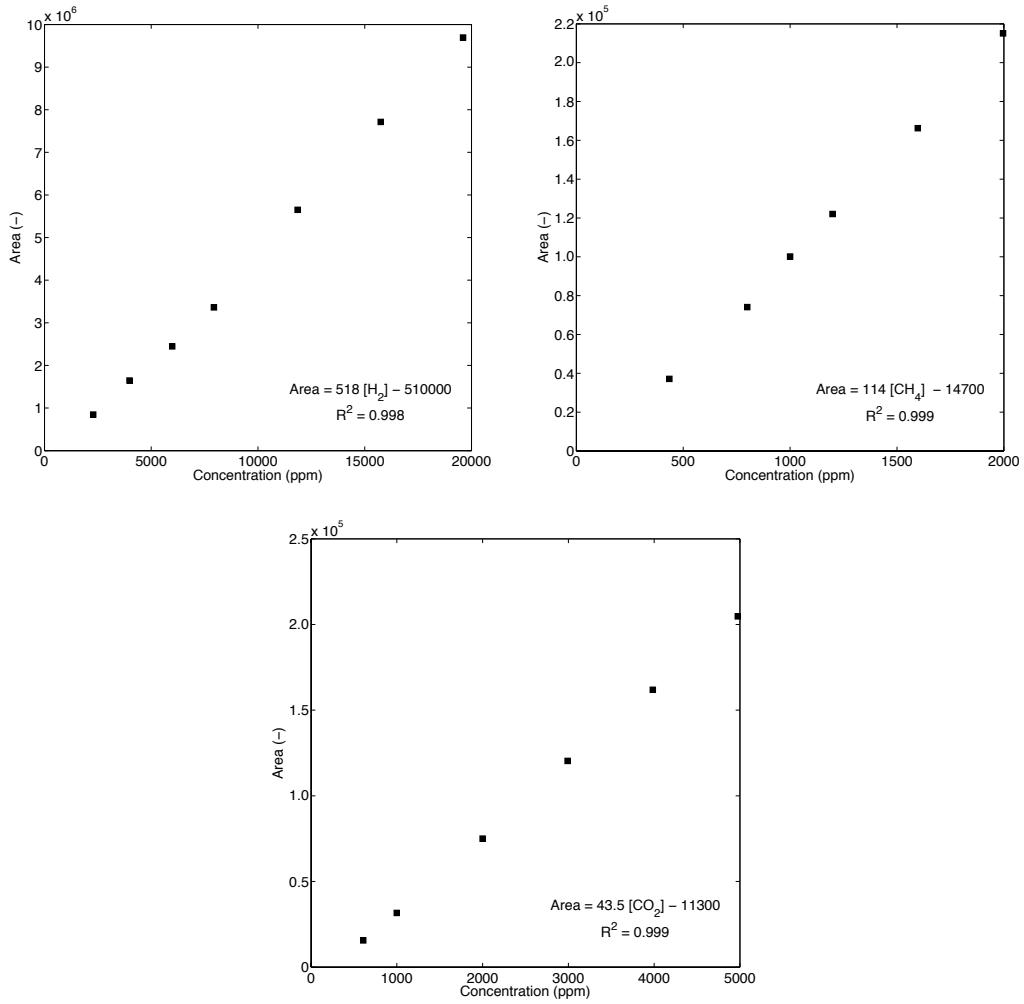

Figure 4-1 GC calibration curves for hydrogen, methane and carbon dioxide

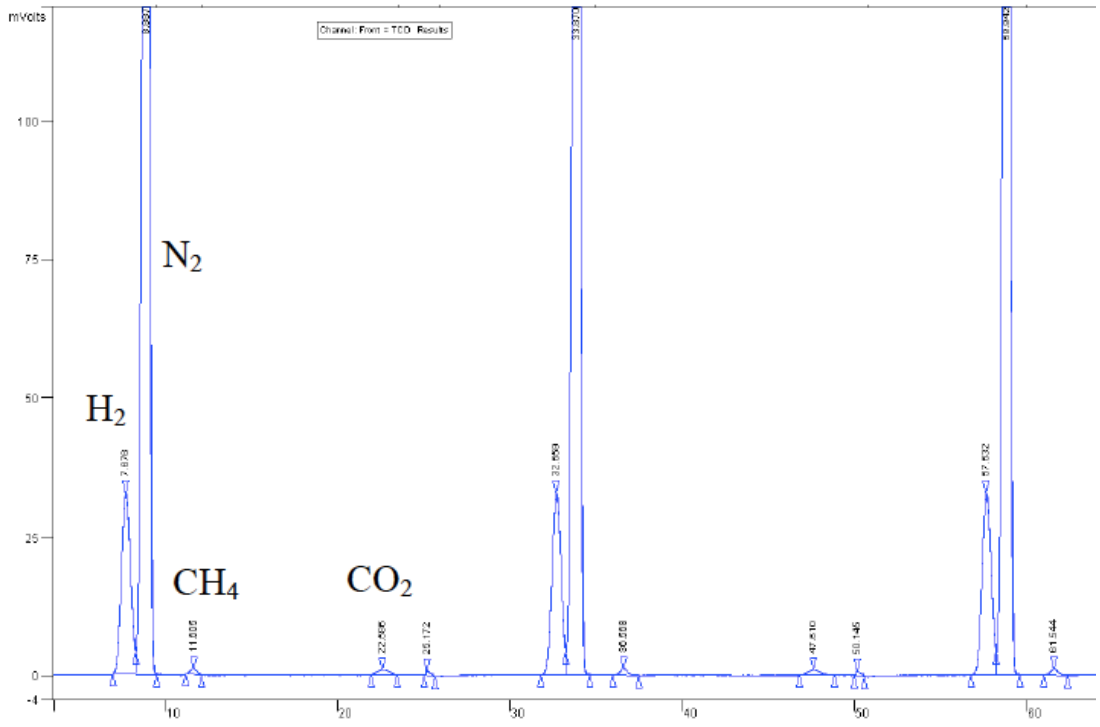

Figure 4-2 A representative GC curve from the APR of glycerol over 1Pt-12Ni/3CeAl, as measured on the in-line Varian CP-3800 gas chromatograph. The product gas was sampled every 25 min; three successive injections are shown here

The liquid products of the APR reaction were collected in a condenser downstream of the reactor bed (Figure 2-1), and aliquots of the condensed liquid were analyzed with a Shimadzu HPLC (§2.2.3). A representative HPLC trace and a calibration curve are shown in Figure 4-3.

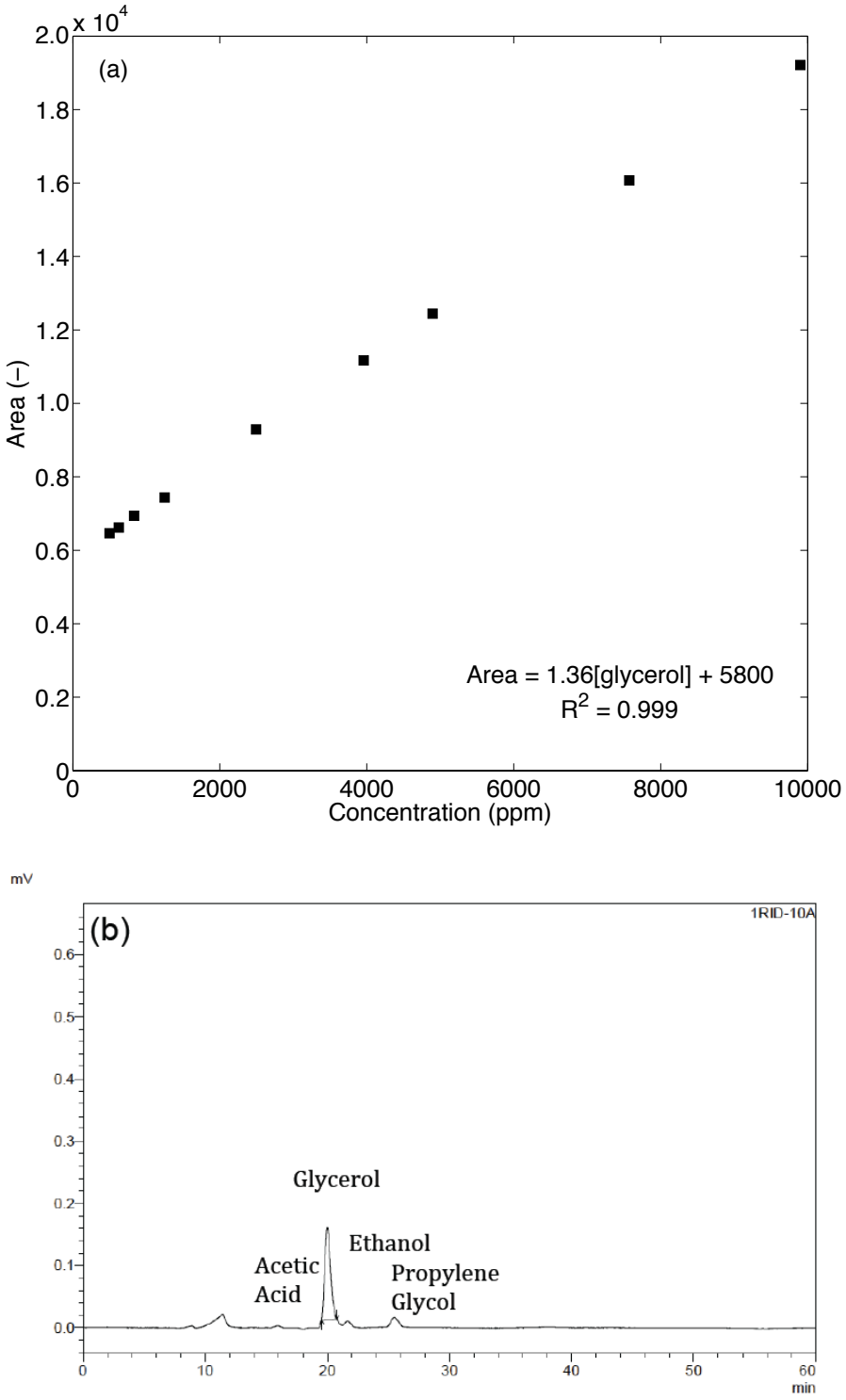

Figure 4-3 (a) HPLC calibration curve for glycerol to measure unreacted glycerol; and (b) a representative HPLC analysis of the liquid product of APR over 1Pt-6Ni/3CeAl.

The catalysts were evaluated on the basis of H_2, CO_2 and CH_4 yield, as well as carbon conversion to gas, H_2 selectivity and glycerol conversion efficiency (§2.2.1).

4.3 Results and Discussions

4.3.1 Catalyst characterization

The textural properties of the catalysts were measured by N_2 adsorption-desorption at liquid nitrogen temperature (−196 °C) using an Autosorb-IQ apparatus (Quantachrome) (§ 2.1.1). Prior to analysis, the samples were outgassed for 12 h at 140 °C. The results are summarized in Table 4-1. The support, composed of 3 wt% CeO_2 in Al_2O_3, had S_{BET} = 162 m^2/g (Rahman et al., 2013). Adding 6 wt% Ni lowered the surface area to 125 m^2/g, whereas adding Pt (1 or 3 wt%) caused a smaller loss of surface area, to ~150 m^2/g (Rahman et al., 2013). As Ni was added to 1Pt/3CeAl, S_{BET} and V_p gradually decreased. D_p decreased significantly when 12 or 18 wt% Ni was present.

Table 4-1 Textural properties of catalysts[a]

Supports/Catalysts	S_{BET}	V_P	D_P	Particle size (nm)[e]		M_{disp}
	(m^2/g)[b]	(cm^3/g)[c]	(nm)[d]	Pt (111)	Ni (200)	(%)[f]
$3CeO_2$–Al_2O_3 (3CeAl)	162	0.28	4.9	NA	NA	-
1Pt/3CeAl	149	0.25	4.8	11	NA	10
6Ni/3CeAl	125	0.22	4.9	NA	-[g]	-
1Pt-3Ni/3CeAl	139	0.23	4.9	8.8	-[g]	13
1Pt-6Ni/3CeAl	120	0.20	4.9	4.6	-[g]	25
1Pt-12Ni/3CeAl	116	0.19	4.3	8.1	12	14
1Pt-18Ni/3CeAl	109	0.18	4.3	6.7	21	17

[a] Measured by N_2 adsorption/desorption at −196 °C. Prior to measurement, samples were calcined in air at 600 °C for 6 h.
[b] Specific surface area (S_{BET}) was determined from the linear portion of the isotherm ($P/P_0 = 0.05$–0.35) (Brunauer et al., 1938).
[c] Pore volume (V_p) was calculated at $P/P_0 = 0.995$.
[d] Predominant pore size (D_p, volume basis) was calculated from the adsorption isotherm using the Barrett–Joyner–Halenda (BJH) formula (Barrett et al., 1951).
[e] Calculated by applying the Scherrer equation (Scherrer, 1918) to the XRD peak generated from the (111) plane of Pt and (200) lane of Ni in the reduced catalysts (Figure 4-5).
[f] M_{disp} = metal dispersion of Pt and Pt-Ni, calculated according to the method of Anderson (Anderson, 1975).
[g] Peak was too small and broad to be measured reliably.

The crystalline structures of the supported catalysts were determined by X-ray diffractometry using Cu Kα radiation (λ = 0.1542 nm) and a graphite monochromator (Shimadzu S6000) (§2.1.3). The XRD patterns of the catalysts after calcination and reduction are shown in Figures 4-4 and 4-5, respectively. As expected, the characteristic peaks of NiO in the patterns of the calcined catalysts intensified and became sharper as the Ni content increased from 3 to 18 wt%, indicating that both the relative amount of crystalline NiO and its crystallite size increased with increasing Ni content. At higher Ni loading (≥12 wt%), three clear

diffraction lines of the NiO fluorite structure were observed at 2θ = 37.2, 43.3, and 62.9° representing the (111), (200), and (220) planes, respectively (Iriondo et al., 2008, Manfro et al., 2011); the last one in particular was difficult to discern at lower Ni loadings. Two clear diffraction peaks representing the (111) and (200) planes, respectively, of metallic platinum (Sherrell et al., 2012) were observed at 2θ = 39.9 and 45.9°. Neither PtO (JCPDS 43-1100) nor PtO_2 (JCPDS number 23-1306) were present in significant amounts. Three broad peaks at 2θ = 37.5, 46, and 67° in the XRD pattern indicated the presence of γ-Al_2O_3 (Wen et al., 2009), and those at 2θ = 28.6, 33.3, and 56.4° represented the fluorite-structured CeO_2 (Damyanova and Bueno, 2003).

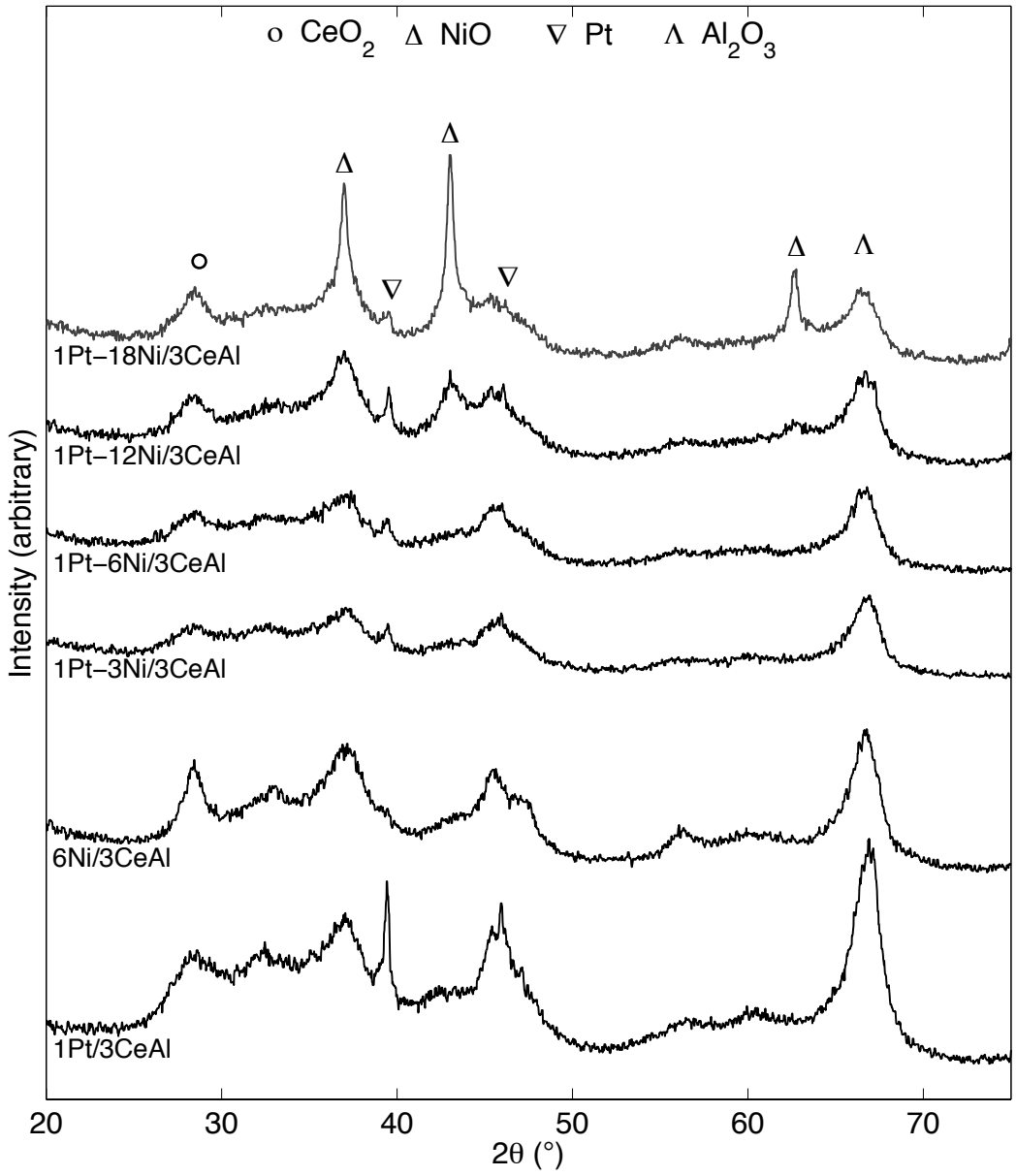

Figure 4-4 X-ray diffraction (XRD) patterns of Pt-Ni/3CeAl catalysts that had been calcined at 600 °C for 6 h under air (heating rate 1.5 °C/min)

Figure 4-5 shows the XRD patterns of the catalysts following reduction at 800 °C. These demonstrated that NiO was completely reduced to Ni^0, with diffraction peaks at 2θ = 44.5 and 51.8° corresponding to the (111) and (200) planes,

respectively.(Iriondo et al., 2008) The amount of detectable crystalline Ni^0 increased with increasing Ni content, as did the Ni^0 crystallite size. The diffraction peak representing the Pt (111) reflection occurred at higher 2θ in all Pt-Ni samples than in monometallic 1Pt/3CeAl ($2\theta = 39.9°$), as shown in Figure 4-5 (inset).

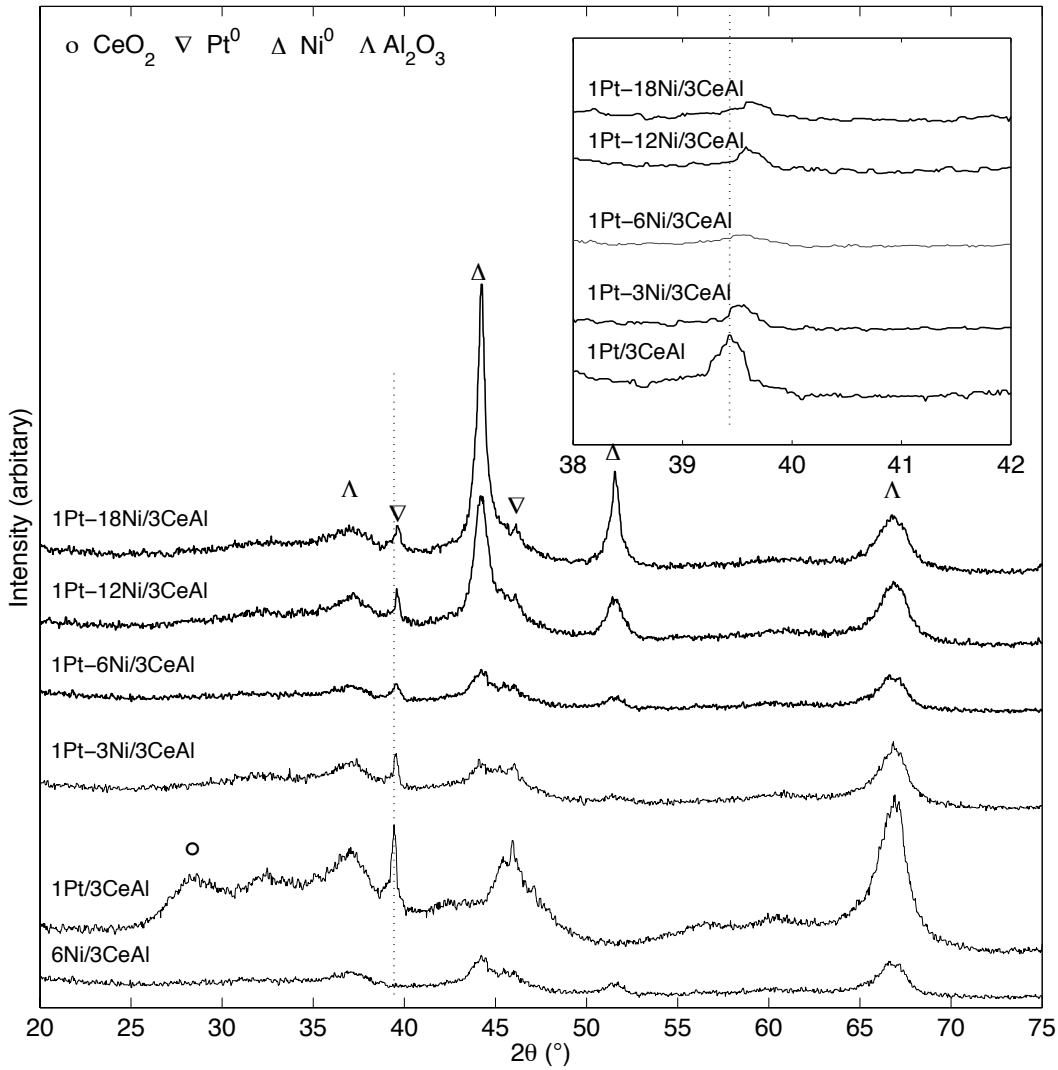

Figure 4-5 X-ray diffraction patterns of catalysts that had been reduced in flowing H_2 (50 vol.% in N_2) at 800 °C for 60 min (heating rate 1.5 °C/min). 1Pt/3CeAl was reduced at 500 °C. Inset shows the Pt (111) peak region

This type of peak shift, which has also been observed by Tegou et al. for Pt-Ni particles (Pt/Ni ~ 4) (Tegou et al., 2011) and by Fu et al. (Fu et al., 2009) for Ni@Pt core-shell nanoparticles at high Ni/Pt ratios, can indicate the formation of a solid solution, i.e., an alloy. Two thermodynamic alloys of these metals, NiPt and Ni_3Pt, are known, and can be produced in ordered form at 645 and ~580 °C, respectively (Nash and Singleton, 1989); thus both could have formed under the catalyst-reduction conditions used here. Diffraction peaks at 2θ = 41.1 (Esch and Schneider, 1944) or 41.6° (Park et al., 2002) have been assigned to the (111) reflection of NiPt; whereas a peak at 2θ = 40.1° (Park et al., 2002) has been assigned to Ni_3Pt. Though neither of these alloys appeared as bulk phases in any of our samples (see Figure 4-5, inset), near-surface alloys of Ni and Pt may have produced the observed shift in 2θ for Pt (111), (Tegou et al., 2011) and would be expected to impact the reactivity of the metal (Greeley, 2004, Frühberger et al., 1997, Hwu et al., 2002).

In addition to a shift in its position, the Pt (111) peak varied in breadth among the XRD patterns of our supported Pt–Ni materials. The mean diameter of the Pt (or Pt-Ni) crystallites was calculated by applying the Scherrer equation (Eq. 2-4) to this peak, and the results are shown in Table 4-1. Also the corresponding Pt (or Pt-Ni) dispersions was calculated by Eq. 2-5, where V_m is the Pt atomic volume (0.0151 nm^3), d is the crystallite size (nm) and A_m is the surface area of a single Pt atom (0.080 nm^2) (Anderson, 1975). Notably, all of the bimetallic Pt-Ni catalysts bore smaller crystallites than the monometallic Pt catalyst; thus, adding Ni to the

catalysts reduced the crystallite size from 11 nm for 1Pt/3CeAl to as low as 4.6 nm for 1Pt-6Ni/3CeAl. Larger amounts of Ni (12 and 18 wt%) did not promote further reduction in crystallite sizes of the Pt-Ni. As the catalyst with 1 wt% Pt and 6 wt% Ni showed the greatest peak width at half height for Pt (111), it had the greatest calculated metal dispersion (M_{disp} = 25%, Table 4-1). Auspiciously, this value was significantly higher than that for the Pt-only catalyst (M_{disp} = 10%). Even in the case that these Pt particles contained dissolved Ni atoms, Pt atoms are expected to form the surface layer of a solid Pt–Ni solution (Greeley, 2004), so greater dispersion indicates that a greater fraction of the Pt atoms in the sample existed on the particle surfaces.

X-ray photoelectron spectra were recorded on an ESCALAB250Xi (Thermo Scientific, UK) using a monochromated Al Kα source (see §2.1.9). As shown in Figure 4-6, the Pt $4f_{7/2}$ XPS peaks of Pt-Ni catalysts occurred at higher binding energies than that of 1Pt/3CeAl; thus, the electronic environment of Pt was modified when Ni was introduced. A similar effect has been observed in the X-ray photoelectron spectra of core-shell Pt-coated Au nanoparticles (Zhao and Xu, 2006). On the other hand, nanoparticles of Pt/Ni alloys have actually shown lower Pt $4f_{7/2}$ binding energies than Pt nanoparticles synthesized according to the same methods (Park et al., 2002, Fu et al., 2009).

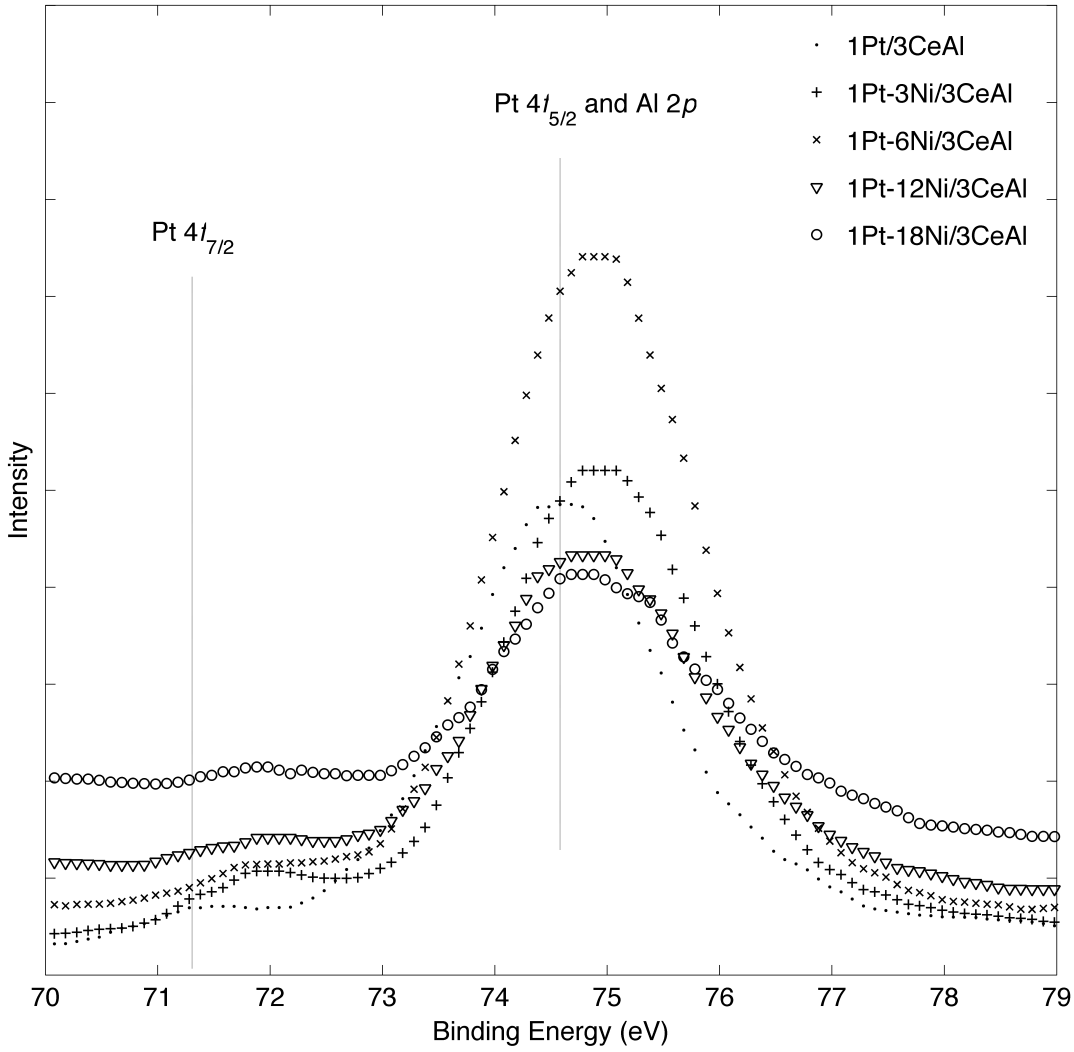

Figure 4-6 The Pt 4*f* and Al 2*p* region of the X-ray photoelectron spectra of xPt-yNi/3CeAl catalysts that had been reduced in flowing H_2 (50 vol.% in N_2) at 800 °C for 60 min (heating rate 1.5 °C/min). 1Pt/3CeAl was reduced at 500 °C

Among our 1Pt-yNi/3CeAl samples, Ni addition had the greatest impact on the Pt $4f_{7/2}$ binding energy in 1Pt-3Ni/3CeAl and 1Pt-6Ni/3CeAl ($BE_{Pt\ 4f(7/2)}$ = 71.94 and 71.90 eV, respectively; cf. 71.35 eV for 1Pt/3CeAl), suggesting that electronic impacts of Ni-Pt interactions were most significant in those samples. In the future, EXAFS or XANES studies may shed further light on the nature of the interactions

between Ni and Pt on CeO_2–Al_2O_3 supports (Boga et al., 2013, Tupy et al., 2012); however, it is clear from the XRD and XPS evidence that adding Ni impacted both the electronic and crystallite structure of Pt. Further, energy-dispersive spectroscopy (EDS) analysis of 1Pt-6Ni/3CeAl confirmed that Ni and Pt co-existed on that material (Figure 4-7). Also EDS analysis of 1Pt-12Ni/3CeAl and 1Pt-18Ni/3CeAl showed co-existance of Ni and Pt in several areas on the material. TEM images of 1Pt-6Ni/3CeAl and 1Pt-18Ni/3CeAl catalysts are shown in Figure 4-8.

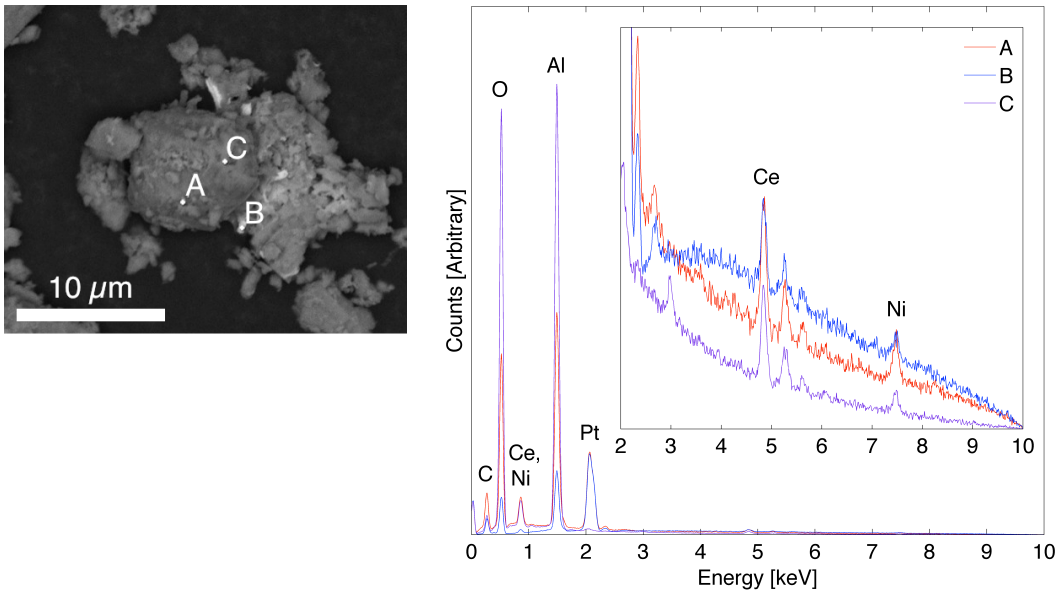

Figure 4-7 EDS spectra of three spots on a 1Pt-6Ni/3CeAl catalyst that was reduced in flowing H_2 (50 vol% in N_2) at 800 °C for 60 min (heating rate 1.5 °C/min)

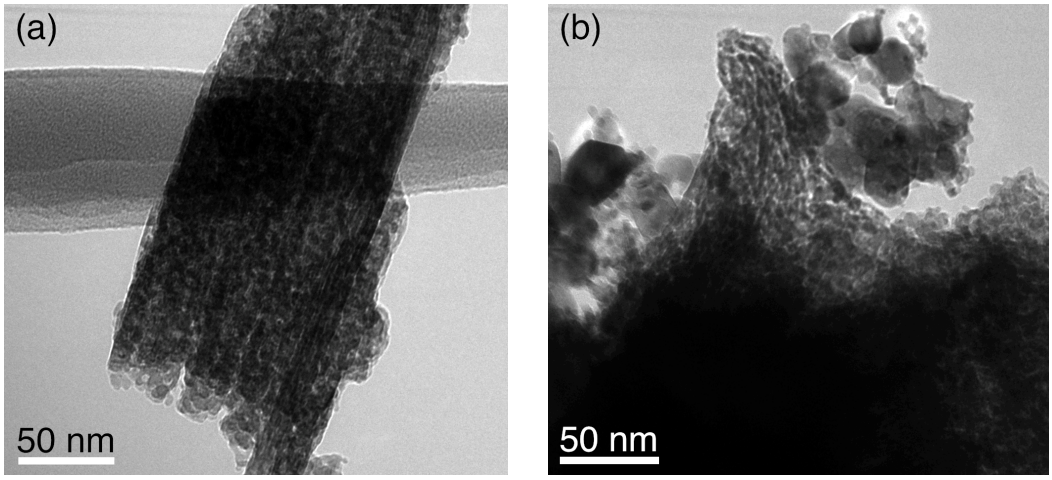

Figure 4-8 Transmission electron images of (a) 1Pt-6Ni/3CeAl and (b) 1Pt-18Ni/3CeAl catalysts reduced in flowing H_2 (50 vol.% in N_2) at 800 °C for 60 min (heating rate of 1.5 °C/min)

4.3.2 Catalytic tests

An aqueous solution with 1 wt% glycerol was used to evaluate the performance of the catalysts. All reactions were performed at 240 °C, 40 bar, and with a feed flow rate of 0.05 mL/min, irrespective of the catalyst used. The reaction data presented in Figures 4-9 and 4-10 show that the aqueous-phase reforming of glycerol over any of the studied catalysts indeed leads to a hydrogen-rich gas phase. Alkanes larger than methane (i.e. ethane) were only detected in trace amounts and were not quantified. No CO was detected, indicating that CO concentration in the product gas was below the GC detection limit (i.e. [CO] ≤ 100 ppm) in all reactions.

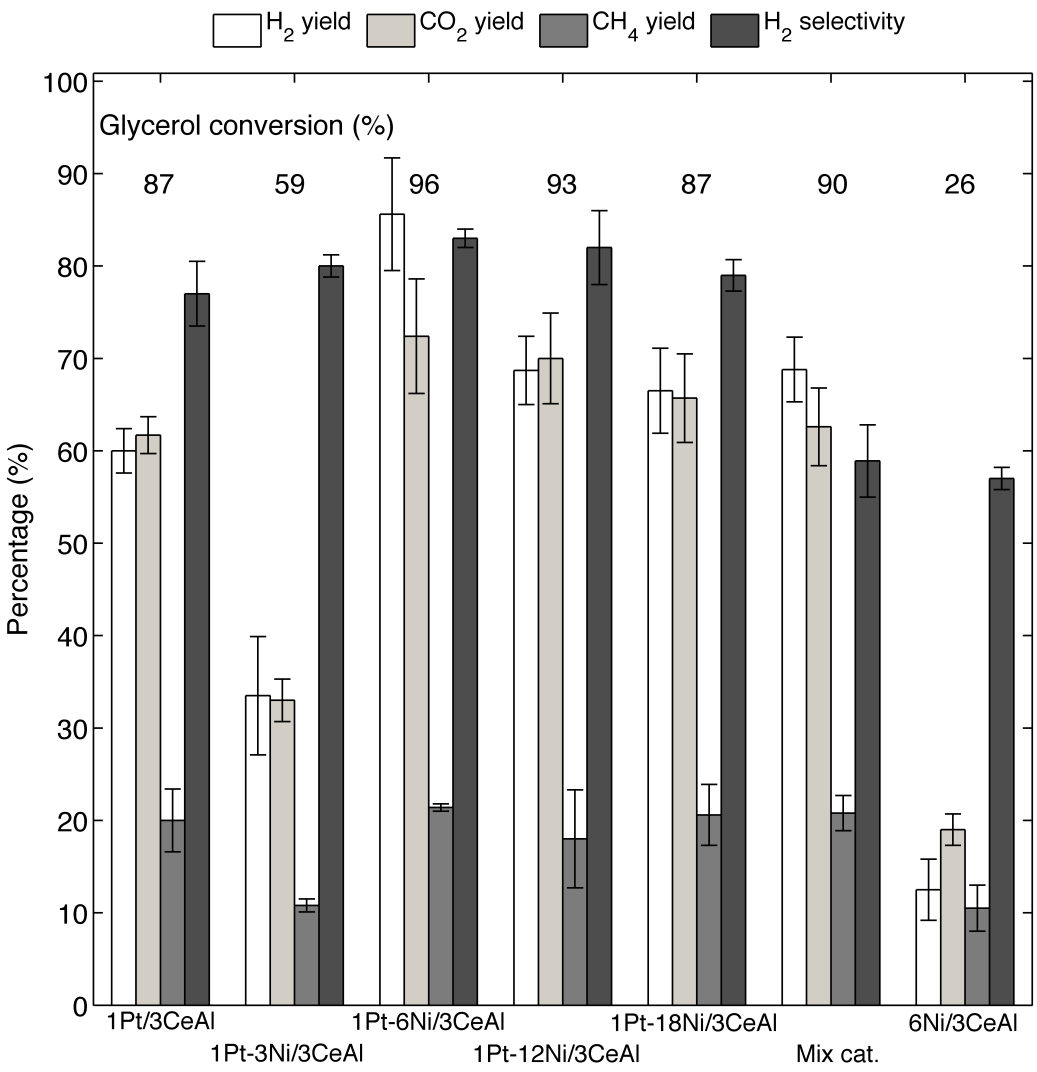

Figure 4-9 Effect of adding Ni to Pt/3CeAl catalysts on yields, selectivity and glycerol conversions in the aqueous phase reforming of glycerol (240 °C, 40 bar, 1 wt% glycerol, 0.05 mL/min, 250 mg catalyst; data are mean values over t = 5–20 h). Error bars indicate one standard deviation; each bar is the average of ≥2 experiments. Mix cat. = mixture of separate Pt/3CeAl and Ni/3CeAl catalysts with a total of 1 wt% Pt and 6 wt% Ni

The H_2 yields (Figure 4-9) and concentrations in the gaseous products (Figure 4-10) from glycerol reforming over three of the nickel-containing catalysts, 1Pt-6Ni/3CeAl, 1Pt-12Ni/3CeAl and 1Pt-18Ni/3CeAl, were similar to those obtained over our reported 3Pt/3CeAl catalyst (78 and 69%, respectively) (Rahman et al.,

2013), despite that these catalysts contained one third as much Pt. Among these three nickel-containing catalysts, the H_2 yield decreased with increasing Ni loading. Thus the highest H_2 yield (86%) and selectivity (83%) were observed for APR over 1Pt-6Ni/3CeAl. The lowest H_2 yield (13%) and H_2 selectivity (57%) among any of the catalysts was observed over Pt-free 6Ni/3CeAl. The H_2 selectivity obtained from 1Pt-6Ni/3CeAl was quite similar to those reported by Lehnert and Claus (Lehnert and Claus, 2008) for 3 wt% Pt catalysts supported on alumina (highest H_2 selectivity, 85%, obtained at 250 °C/20 bar, 10 wt% glycerol flowing at 0.5 mL/min) and by Cortright et al. (Cortright et al., 2002) for 3 wt% Pt catalysts supported on nanofibers of γ-alumina (highest H_2 selectivity was 75%, obtained at 225 °C/29 bar, 10 wt% glycerol flowing at 0.06 mL/min). Moreover, the APR of glycerol over 1Pt-6Ni/3CeAl, 1Pt-12Ni/3CeAl and 1Pt-18Ni/3CeAl produced higher H_2 selectivity than that over the C-supported Pt and Pt-Re catalysts reported by King et al. (King et al., 2010), who obtained 56% selectivity for H_2 when flowing a 10-wt% glycerol solution through 200 mg catalyst at 225 °C and 30 bar.

Notably, the APR of glycerol over 1Pt-6Ni/3CeAl, 1Pt-12Ni/3CeAl and 1Pt-18Ni/3CeAl produced more CO_2 than that over 1Pt/3CeAl (Figure 4-9), or even 3Pt/3CeAl, which produced 62% CO_2 yield (Rahman et al., 2013). This is consistent with the higher activity of Ni as a WGS (Eq. 4-2) catalyst (Grenoble et al., 1981), and may help to explain why similar H_2 yields were generated by these 1Pt-xNi/3CeAl catalysts and by 3Pt/3CeAl, despite the much lower Pt content of the bimetallic catalysts. However, the increased WGS activity that was provided

upon Ni addition was not sufficient to explain the high H_2 yield and selectivity of the best catalyst, 1Pt-6Ni/3CeAl, as a mixture of separate Pt/3CeAl and Ni/3CeAl catalysts with a total of 1 wt% Pt and 6 wt% Ni did not perform as well. Despite that Ni also favors methanation (Vannice, 1977), the APR of glycerol over 1Pt-6Ni/3CeAl, 1Pt-12Ni/3CeAl and 1Pt-18Ni/3CeAl showed similar CH_4 yields to the reaction over 1Pt/3CeAl (20%). This could be due to an interaction between Pt and Ni; an interaction between Pt and Cu has been credited for lowering methane production in the APR of glycerol over catalysts supported on magnesium/aluminium oxides (Boga et al., 2013). Nevertheless, the highest fraction of CH_4 in the gas product (18%) was obtained using 6Ni/3CeAl as the catalyst (Figure 4-10).

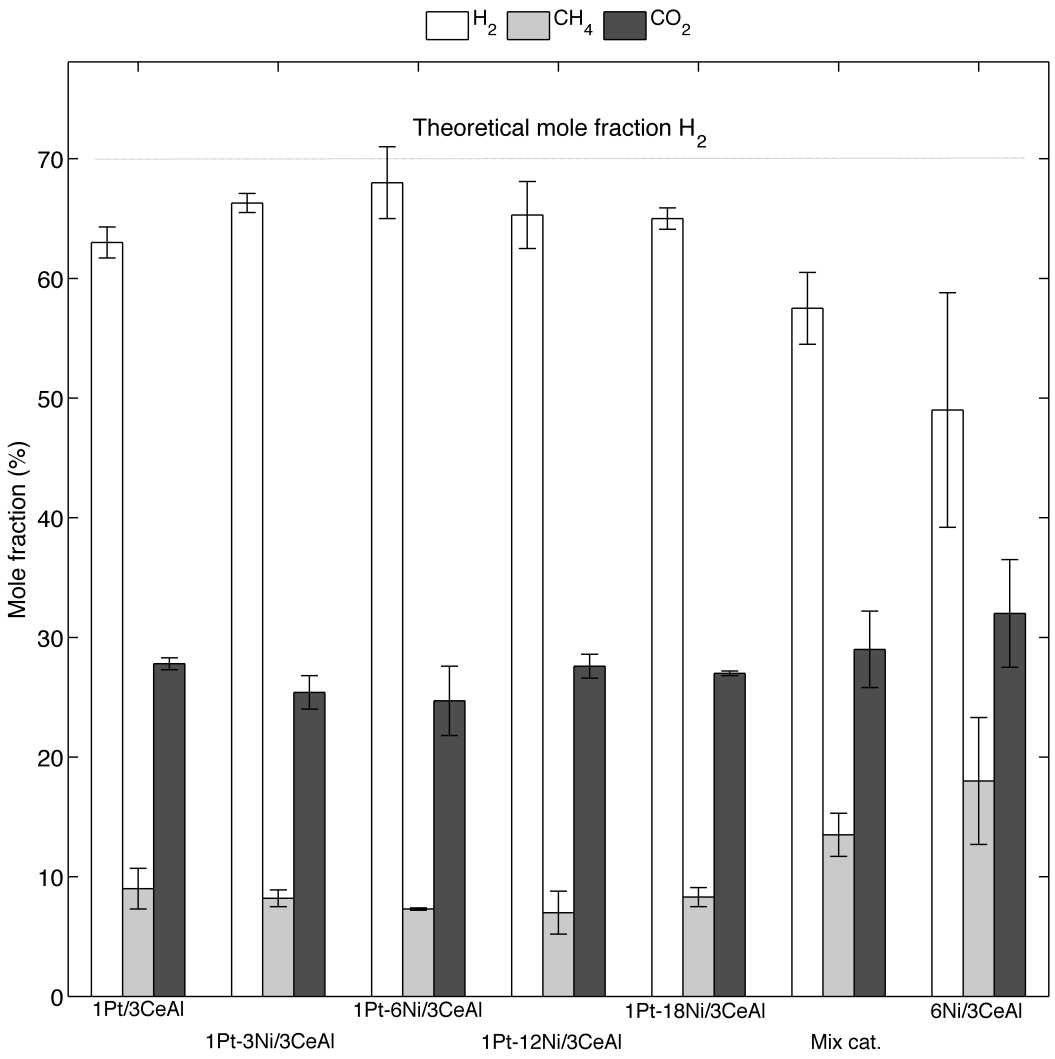

Figure 4-10 Effect of Ni addition to Pt/CeAl catalysts on the distribution of gaseous products from the aqueous phase reforming of glycerol (240 °C, 40 bar, 1 wt% glycerol, 0.05 mL/min, 250 mg catalyst; data are mean values over t = 5–20 h). Error bars indicate one standard deviation; each bar is the average of ≥2 experiments. Mix cat. = mixture of separate Pt/3CeAl and Ni/3CeAl catalyst with a total of 1 wt% Pt and 6 wt% Ni.

Some authors have correlated the activity and H_2 selectivity of supported-metal APR catalysts with metal particle size and dispersion. Wawrzetz et al. (Wawrzetz et al., 2010), showed that H_2 formation from the APR of glycerol decreased with

increasing Pt particle size. On the other hand, Lehnert and Claus (Lehnert and Claus, 2008) showed that bigger Pt particles produced higher H_2 selectivity (but similar activity), and concluded that the adsorption of glycerol occurred preferentially at face positions of the metal crystallite. Iriondo et al. (Iriondo et al., 2011) observed that less-dispersed Ni and PtNi catalysts were more active for the APR of glycerol. In our case, the 1Pt-6Ni/3CeAl catalyst, which had the smallest Pt metal particles (4.6 nm) and highest dispersion (25%), showed the highest H_2 selectivity (83%) and yield (86%).

The liquid phase after the reaction over each of the catalysts was also analyzed in order to examine the formation of larger byproducts. Apart from unreacted glycerol, we identified traces of some other compounds, particularly ethanol, propylene glycol, and acetic acid. These were not quantified. The APR of 1 wt% glycerol over catalysts 1Pt-6Ni/3CeAl, 1Pt-12Ni/3CeAl and 1Pt-18Ni/3CeAl produced similar glycerol conversions and gas phase carbon yields as that over 3Pt/3CeAl, though both quantities decreased as the Ni content increased from 6 to 18 wt%.

In order to evaluate the activity and efficiency of each catalyst, the rates of H_2 formation were normalized to the mass of catalyst or Pt used (Figure 4-11). Catalysts 3Pt/3CeAl and 1Pt-6Ni/3CeAl produced almost the same amount of H_2 per gram of catalyst per hour, despite that the latter contained less Pt. Thus the amount of expensive metal could be reduced significantly by adding Ni, and with a

slight *improvement* in catalytic activity; this translated to a three-fold improvement in the H_2 generated per gram of Pt. Conversely, 1Pt/3CeAl and 1Pt-6Ni/3CeAl contained the same amount of Pt, but the latter produced H_2 approximately twice as quickly. Overall, 1Pt-6Ni/3CeAl combined the highest glycerol conversion with the greatest rate of H_2 production and H_2 selectivity, which could make it competitive for large-scale H_2 production. Based upon the characterization and catalytic data, a few inferences can be drawn regarding the mechanism(s) by which the addition of 6 wt% Ni enhanced catalyst activity. First, Ni itself contributed to the H_2 yield by catalyzing the WGS reaction; however, this was insufficient to explain the exceptional activity of 1Pt-6Ni/3CeAl, as a mixture of separate Pt/3CeAl and Ni/3CeAl catalysts containing a total of 1 wt% Pt and 6 wt% Ni was not nearly as effective. Further, 1Pt-6Ni/3CeAl bore the smallest and most-dispersed Pt nanoparticles, and thus had more Pt atoms located at the particle surfaces than the Ni-free catalyst with the same Pt loading. Shabaker et al. have also noted a correlation between Pt dispersion and the apparent activation energy in APR, albeit on a range of different supports (Shabaker et al., 2003b).

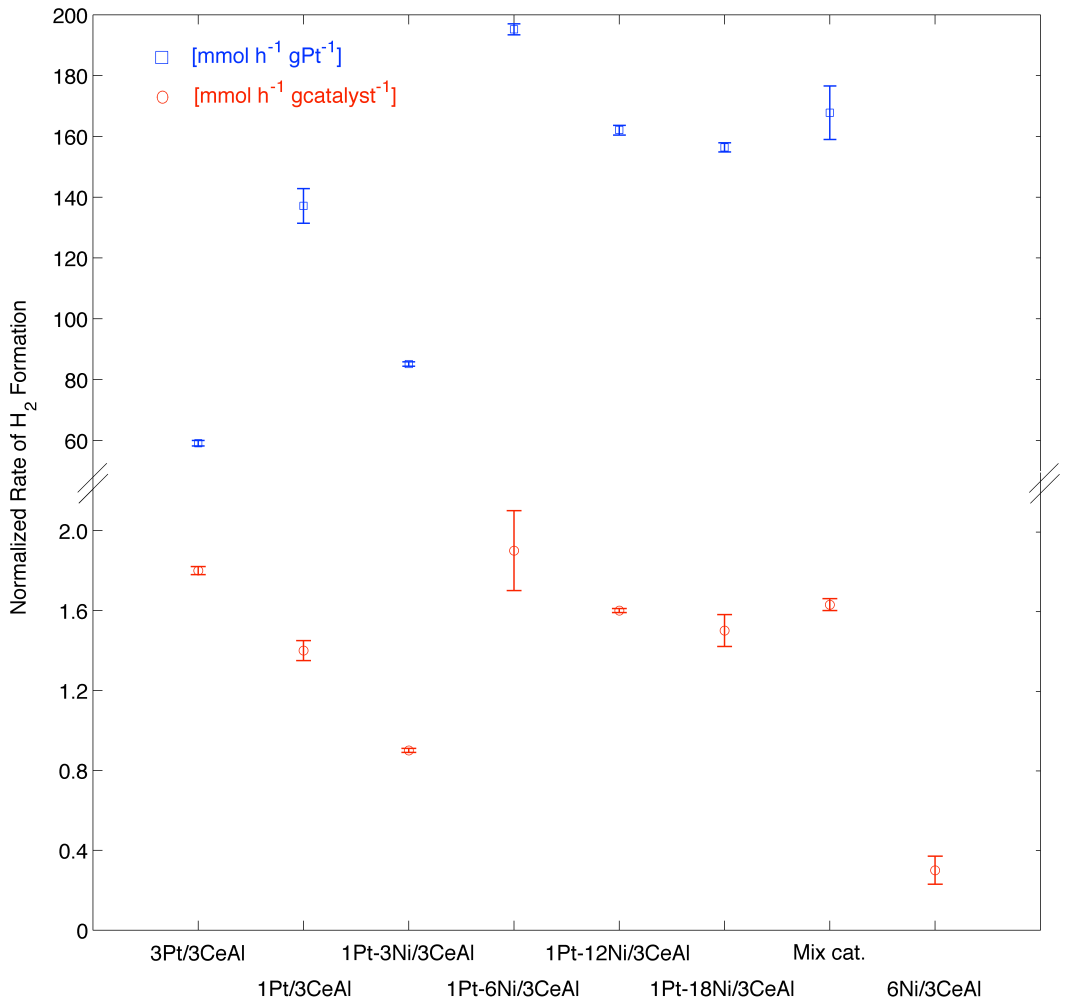

Figure 4-11 Rate of H_2 production from the APR of glycerol (240 °C, 40 bar, 1 wt% glycerol, 0.05 mL/min, 250 mg catalyst; data are mean values over t = 5–20 h), normalized to the mass of catalyst or Pt used. Error bars indicate one standard deviation; each data point is the average of ≥2 experiments

Finally, the XRD pattern and X-ray photoelectron spectrum of 1Pt-6Ni/3CeAl pointed to interactions between Pt and Ni (see above), including the dissolution of some Ni atoms in the Pt (i.e. surface, though not bulk, alloy formation); both computational (Greeley, 2004) and experimental studies (Hwu et al., 2002, Frühberger et al., 1997), have demonstrated that surface Pt-Ni alloys bind H_2 less

strongly than Pt^0. The importance of H_2 binding strength has been demonstrated by Shabaker et al. (Shabaker et al., 2003a), who showed that hydrogen inhibits the APR of oxygenated hydrocarbons on Pt catalysts, likely by occupying and thus blocking Pt active sites. Similarly, Huber et al. (Huber et al., 2006) speculated that supported PtNi and PtCo catalysts, which outperformed a supported Pt catalyst, had lower heats of H_2 and CO adsorption than pure Pt, and thus more unoccupied active sites accessible to reactants. The similar phenomenon was also observed by Tanksale et. al. on Pt-Ni catalysts using microcalorimetry study (Tanksale, 2008 #198). Thus the exceptional activity of 1Pt-6Ni/3CeAl was likely caused by a confluence of factors; in particular, it offered the best balance of advantageous Ni–Pt interactions and high Pt dispersion. It is noted that metal dispersion calculated by chemisorption is more accurate than by XRD. But due to bimetallic complexcity in this chapter we used XRD data for dispersion calculaton (Table 4-1) rather than chemisorption data (Table 3-2).

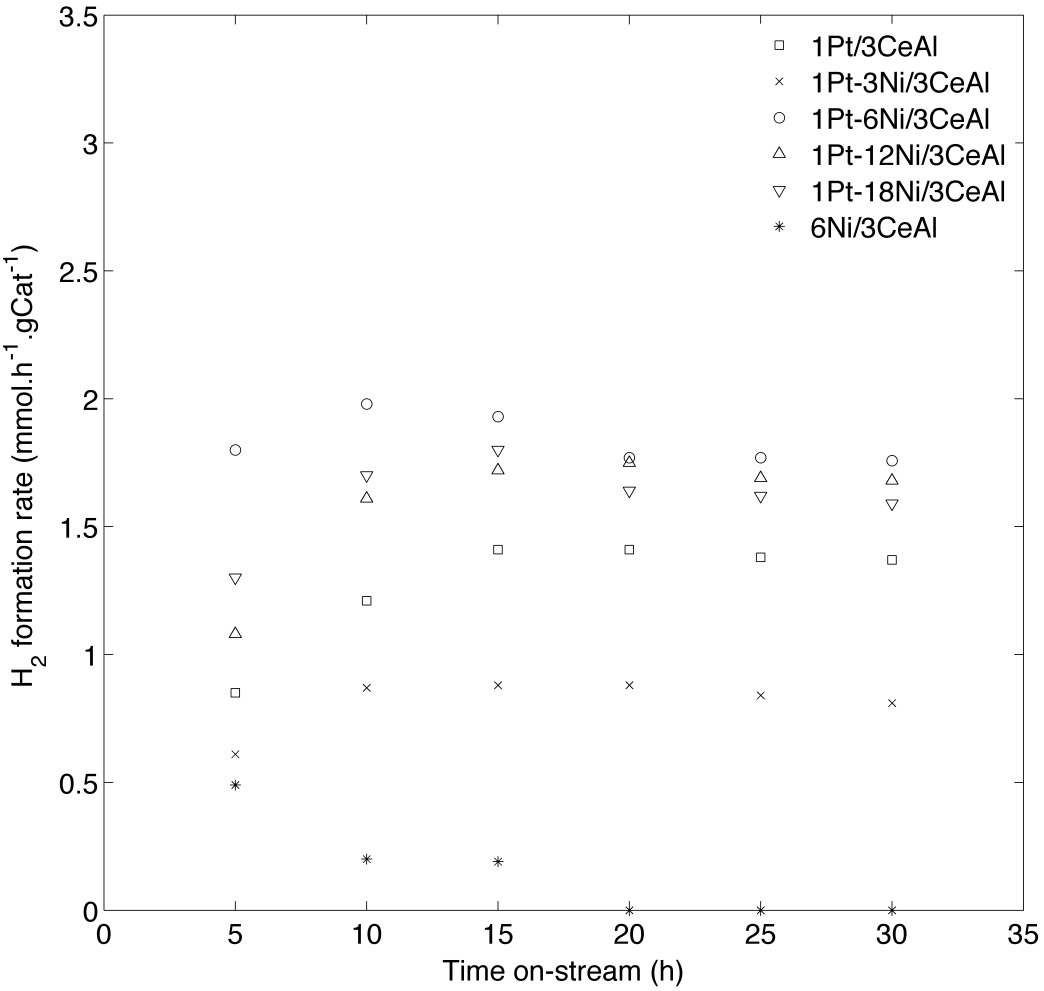

Figure 4-12 Variation of H_2 formation rate with time on-stream in the APR of glycerol (240 °C, 40 bar, 1 wt% glycerol, 0.05 mL/min, 250 mg catalyst). Each value is the average of ≥2 experiments.

One of the major problems related to the operation of heterogeneous catalysis is the loss of catalytic activity, i.e. "deactivation", over time, and Ni catalysts are generally more susceptible than noble-metal catalysts. Figure 4-12 shows the stability of the ceria–alumina-supported catalysts in the APR of glycerol over 30 h on-stream. Only catalyst 6Ni/3CeAl was severely deactivated; it ceased to produce a detectable H_2 peak after 15 h on-stream.

Two main causes of catalyst deactivation in APR are carbon deposition and the sintering of the active phase (Shabaker et al., 2004), and we therefore examined the catalysts for signs of these problems. Figure 4-13 presents the XRD patterns of the fresh and spent 1Pt-6Ni/3CeAl catalysts. No carbon formation (expected at 2θ = 25.5°) (Comas et al., 2004) or oxidation of metallic Ni phase (expected at 2θ = 37.2 and 62.9°) (Wen et al., 2008, Iriondo et al., 2008) were observed on the spent catalyst after 30 h on-stream. The only difference observed was in the widths of the Pt^0 and Ni^0 peaks, which were slightly sharper in the XRD pattern of spent 1Pt-6Ni/3CeAl. This could have indicated a very small amount of particle agglomeration/sintering (based on the Pt (111) peak, calculated particle sizes were 4.6 and 4.9 nm, respectively, for the fresh and spent catalysts). However, despite this sintering, no deactivation was observed with time on-stream, even upto 85 h as shown in Figure 4-14, for 1Pt-6Ni/3CeAl catalyst.

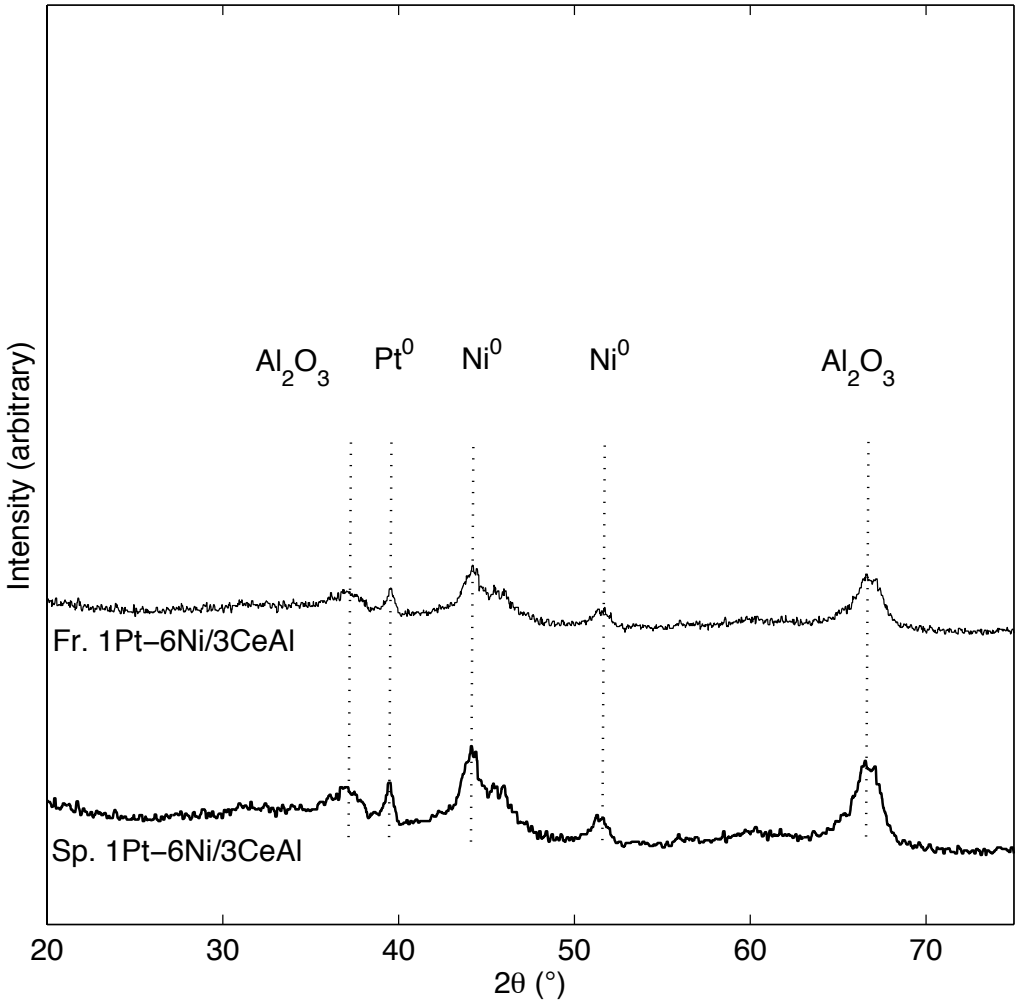

Figure 4-13 XRD patterns of 1Pt-6Ni/3CeAl catalyst freshly reduced in flowing H_2 (50 vol% in N_2) at 800 °C for 60 min, and spent after 30 h on-stream (240 °C, 40 bar, 1 wt% glycerol, 0.05 mL/min, 250 mg catalyst)

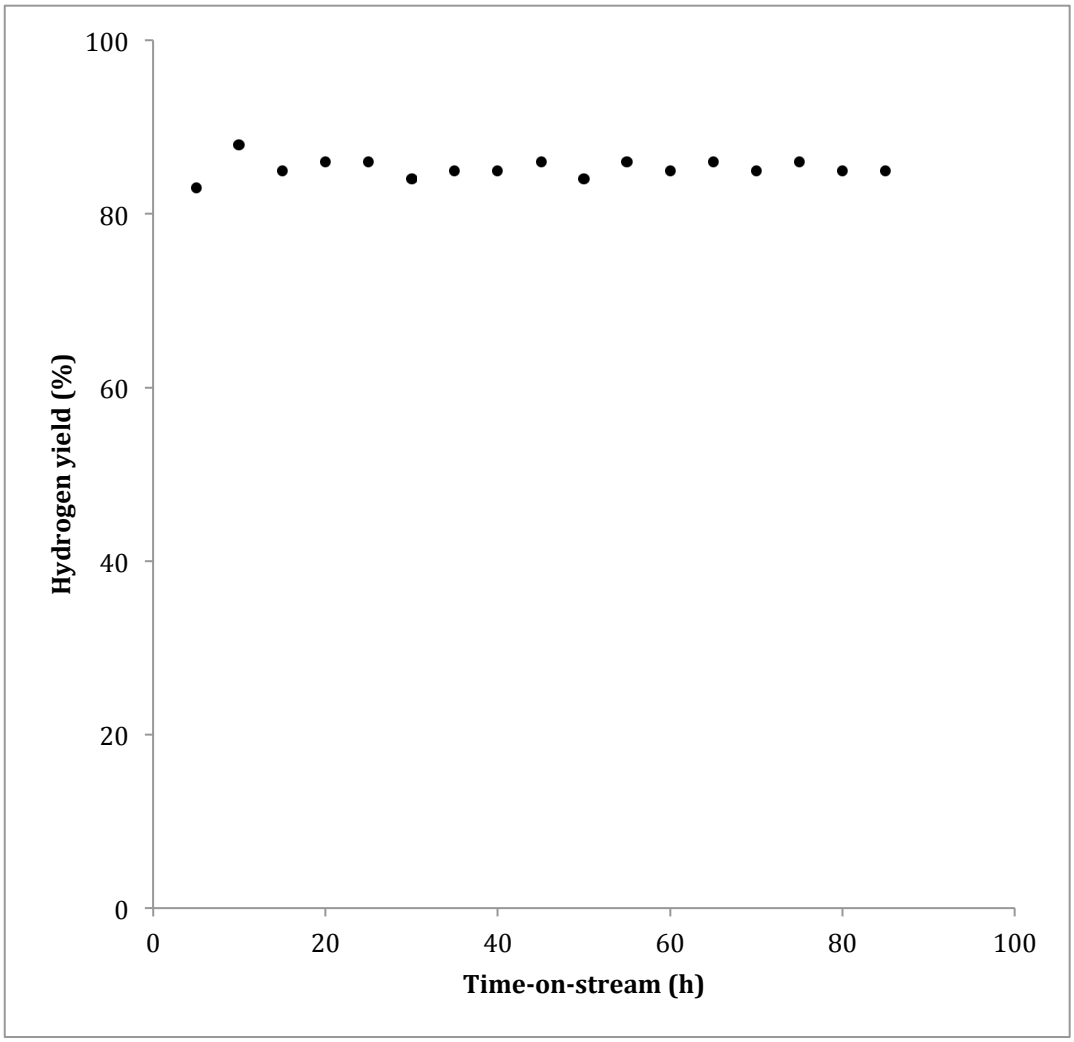

Figure 4-14 H_2 yield with time-on-stream for APR of glycerol over 1Pt-6Ni/3CeAl catalyst (240 ºC, 40 bar, 1 wt% glycerol, 0.05 mL/min, 250 mg catalyst, 85 h on-stream)

No evidence of weight loss due to carbon combustion was observed during thermogravimetric analysis (Figure 4-15). TGA curves for the other spent catalysts did not show any weight loss except 6Ni/3CeAl and Mix cat., which showed significant weight loss due to the burning of coke at 550 °C (Figure 4-16). Inductively coupled plasma atomic emission spectrometry

(ICP–AES) analysis of the liquid effluent showed no measurable leaching of Pt and Ni.

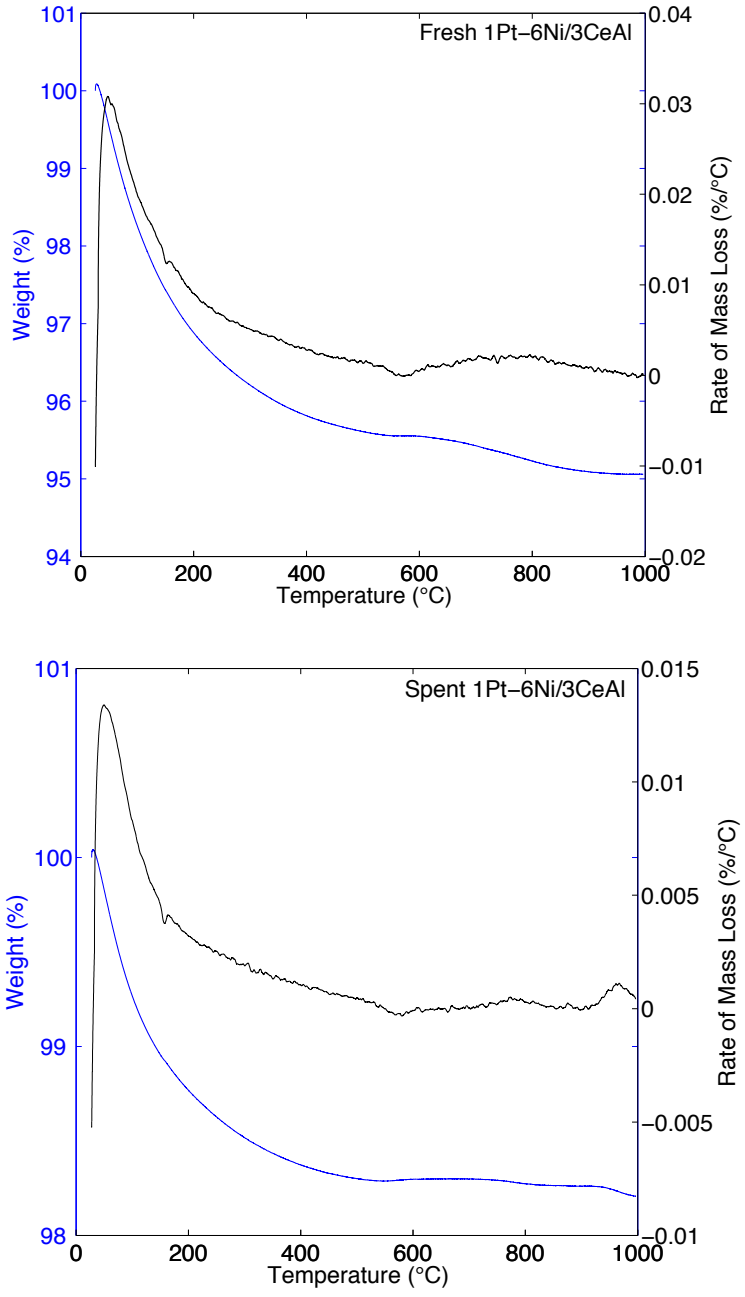

Figure 4-15 Thermogravimetric analysis of fresh (reduced: 50 vol% H_2 in N_2, 800 °C, 60 min) and spent (after reaction: 240 °C, 40 bar, 1 wt% glycerol, 0.05 mL min^{-1}, 30 h) 1Pt-6Ni/3CeAl. Samples were heated at 10 °C min^{-1} in instrument air (40 vol% in N_2)

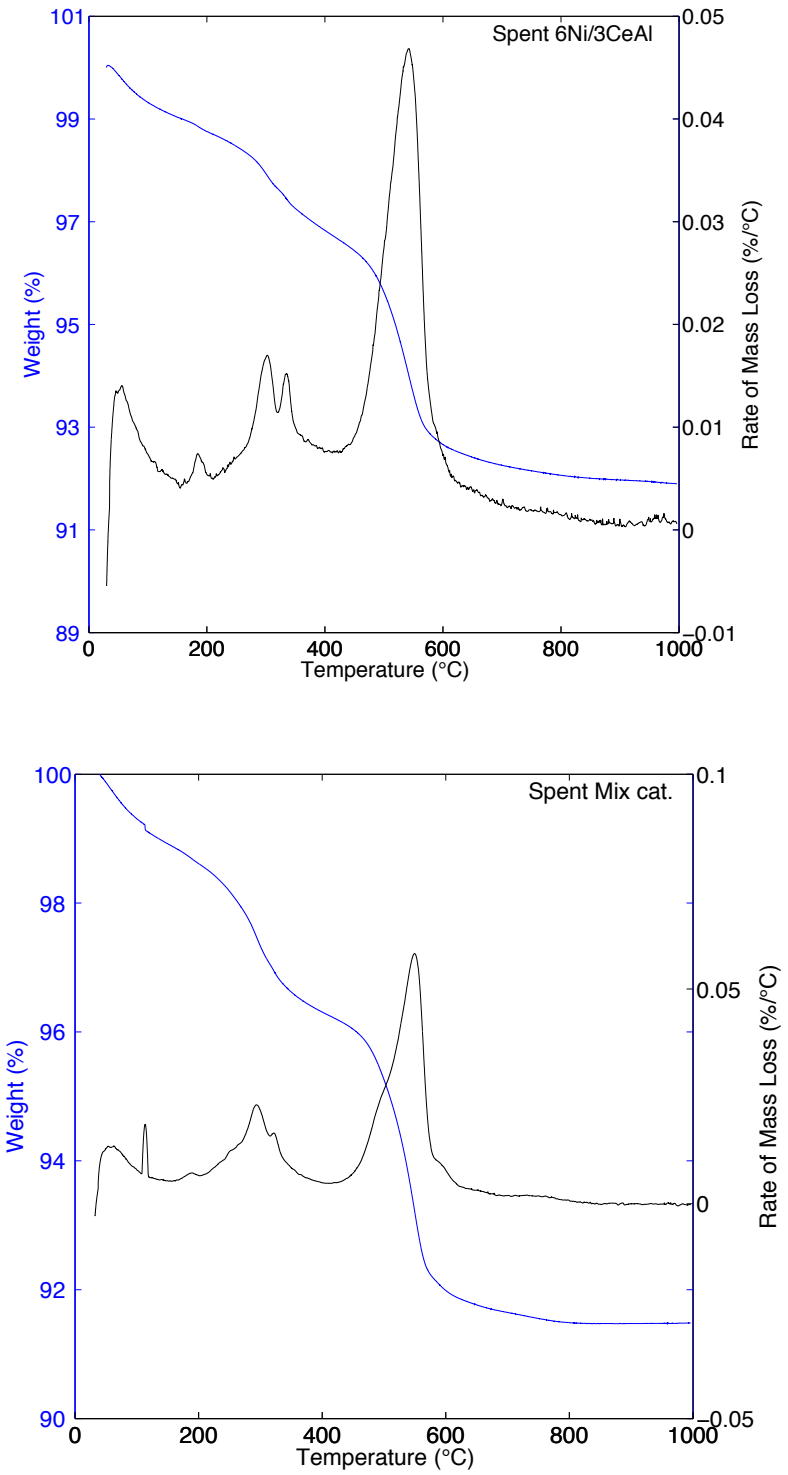

Figure 4-16 Thermogravimetric analysis of spent (after reaction: 240 °C, 40 bar, 1 wt% glycerol, 0.05 mL min^{-1}, 30 h) 6Ni/3CeAl and Mix cat. Samples were heated at 10 °C min^{-1} in instrument air (40 vol% in N_2)

4.4 Conclusions

In the APR of glycerol, our reported 3Pt/3CeAl catalyst showed better activity and selectivity towards H_2 production than 3Pt/Al_2O_3 did (Rahman et al., 2013). Although Pt catalysts are highly active for APR, the high cost of Pt makes catalysts based on non-precious metals desirable. A bimetallic Pt-Ni catalyst showing good activity for the APR of glycerol to produce H_2 was developed in this work. Bimetallic 1Pt-6Ni/3CeAl showed the highest H_2 yield and gas phase C yield, and produced three times as much H_2 per gram of Pt as 3Pt/3CeAl. The favourable characteristics of 1Pt-6Ni/3CeAl could not be attributed to a single factor, but rather appeared to stem from smaller crystallite size (4.6 nm), higher metal dispersion (25%) and higher electronic interaction ($BE_{Pt\ 4f(7/2)}$ = 71.94 eV). Further, the 3-wt%-CeO_2-doped Al_2O_3 support enhanced both the activity and selectivity towards H_2 production. As a result 1Pt/3CeAl showed higher glycerol conversion and H_2 yield than the benchmark catalyst, 3Pt/Al_2O_3 (Rahman et al., 2013).

This page intentionally left blank

Chapter 5

Chapter 5 describes Pt-Ni alloy catalyst supported on multi walled carbon nanotubes (MWNT) in the APR of glycerol. Catalyst characterization by XRD, XPS showed a peak shift of Pt in bimetallic Pt-Ni catalyst than the monometallic Pt catalyst. Also the presence of Pt and Ni emission lines, in STEM-EDS spectra, from both the bulk and the single crystal particles strongly suggests that Pt is present in close vicinity of Ni particle. The bimetallic interaction between Pt and Ni is thought to be responsible for the high glycerol conversion and gas phase C yield and, ultimately, the high H_2 yield observed.

5 Bimetallic Pt-Ni catalyst supported on MWNT

5.1 Introduction

Chapter 4 reports bimetallic Pt-Ni/3CeO_2-Al_2O_3 catalysts that significantly enhanced the activity and selectivity of H_2 production from APR of glycerol. So far, however, very few articles have described bimetallic catalysts supported on carbon nanotubes for the APR of glycerol. Carbon nanotubes, an inert or less reactive catalyst support, place a great role in reaction mechanism due to it's high porosity and hydropobic nature (van Haasterecht et al., 2013, Shabaker et al., 2003b). Wang et al. (Wang et al., 2009) studied both monometallic Pt and bimetallic Pt-Co catalysts supported on single walled carbon nanotubes (SWNT) prepared by wet-reduction method. Both of them showed higher APR activity than Al_2O_3 supported catalyst. In addition, the catalytic activity and selectivity remained unchanged after a week of steady-state reaction. Shabaker et al. (Shabaker et al., 2003b) have compared a variety of supports for Pt APR that included activated carbon, which had comparable activity to an alumina support. King et al. (King et al., 2010) studied APR of glycerol on Pt-Re bimetallic catalyst supported on porous carbon. In this work, bimetallic Pt-Ni catalysts supported on multi-walled carbon nanotubes have been synthesized and tested for APR of glycerol. Also have compared MWNT support with two others commercial oxide supports, Al_2O_3 and MgO. Also, a comparison with the best performing catalyst (1Pt-6Ni/3CeAl) of chapter 4 is reported.

5.2 Experimental

5.2.1 Catalyst preparation

The highly pure MWNT (carbon content ≥ 98%) (Figure 5-1) used in this research was purchased from SWeNT (SMW100). The surface area of the MWNT is 296 m^2/g, the pore volume is 1.6 cm^3/g and the pore diameter is 3.2 nm. The carbon nanotubes were sonicated in 1M HNO_3 at 25 °C (Branson sonifier 450) at 20 kHz for 15 min. The objectives were to obtain good dispersion of MWNT in solution and to ensure surface modification of the outer layer of the MWNT with functional groups (i.e. –COOH and –OH) to provide nucleation sites for the deposition of Pt and Ni nanoparticles. The surface modification of MWNT is necessary for metal deposition onto carbon (Ebbesen et al., 1996, Yu et al., 1998). The nanotubes were then filtered and dried for further use.

$[Pt(NH_3)_4](NO_3)_2$ (Strem Chemical) and $Ni(NO_3)_2{\cdot}6H_2O$ (Sigma–Aldrich) were dissolved, individually or together, into ethanol to make monometallic or bimetallic catalysts, respectively. These were deposited on refluxed MWNT using a conventional impregnation technique. Specifically, to prepare 1Pt-3Ni/MWNT, 0.5 g of refluxed MWNT was impregnated with a solution prepared by dissolving 10.44 mg $[Pt(NH_3)_4](NO_3)_2$ and 78.98 mg of $Ni(NO_3)_2{\cdot}6H_2O$ in 50 mL of ethanol in a 100-mL glass vial. The mixture was then stirred overnight at room temperature, and the ethanol was allowed to evaporate. The sample was then dried in air at 120 °C for 12 h and calcined under flowing NO (1.5 vol.% in Ar) at 500 °C for 60 min (heating rate 5 °C min^{-1}). Catalysts were reduced in situ in flowing

H_2 (25 vol.% in Ar) at 650 °C for 30 min (heating rate 5 °C min^{-1}) at atmospheric pressure.

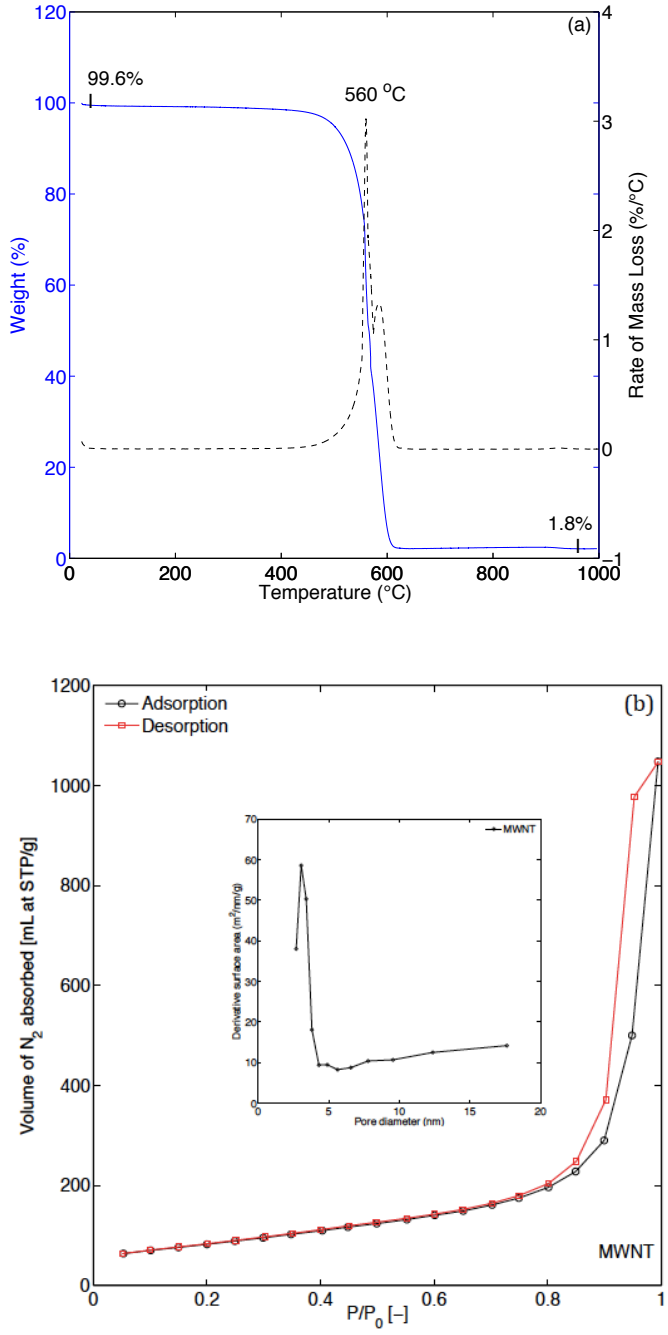

Figure 5-1 For MWNT support material (a) TGA oxidation curve showing it's carbon content, and (b) N_2 physorption isotherms. Inset shows pore size distribution (BJH model, desorption data was used)

5.2.2 Catalyst testing

The APR of glycerol was studied in a continuous flow type fixed bed reactor system (see §2.2.1). The catalyst (100 mg) was loaded into a 5-mm i.d. stainless steel tubular reactor and held in position with quartz wool plugs. A backpressure regulator (0 to 1000 psig, Swagelok) attached to a pressure gauge was used to pressurize the system with Ar to 40 bar. The system was allowed to stabilize for about 2 h before analysis of the reaction products began. Gas products were analyzed at 25-min intervals using an online gas chromatograph (Varian CP-3800, see §2.2.2). A representative GC curve (Figure 5-2) shows only three peaks, representing H_2, CH_4 and CO_2, respectively, for each injection of product gas. Liquid products were analyzed with a Shimadzu HPLC (see §2.2.3). Also Shimadzu TOC-L (with auto sampler ASI-L) was used to know the total organic carbon content of the liquid phase.

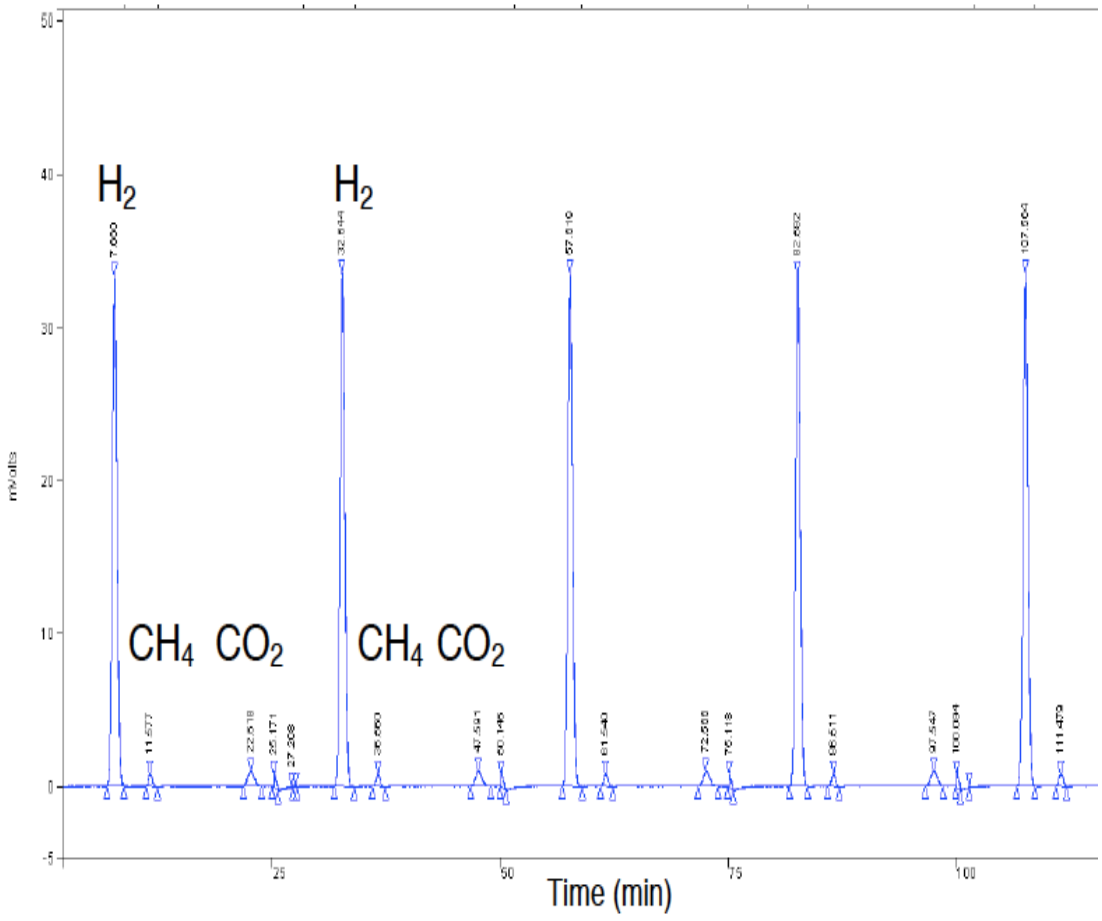

Figure 5-2 A representative GC curve from the APR of glycerol over 1Pt-12Ni/MWNT catalyst, as measured on the in-line Varian CP-3800 gas chromatograph. The product gas was sampled every 25 min; five successive injections are shown here

The catalysts were evaluated on the bases of H_2 yield, CO_2 yield, CH_4 yield, carbon conversion to gas, H_2 selectivity and glycerol conversion efficiency (see §2.2.1).

5.3 Results and Discussions

5.3.1 Catalyst characterization

The specific surface area (Brunauer-Emmett-Teller, S_{BET}) (Brunauer et al., 1938), pore size (Barrett–Joyner–Halenda, BJH, adsorption branch) (Barrett et al., 1951), and pore volume were measured by N_2 adsorption at liquid nitrogen temperature (−196 °C) using an Autosorb-IQ apparatus. The results are given in Table 5-1. Specific surface areas were determined from the linear portion of the adsorption isotherm (P/P_0 = 0.05–0.35), and the pore volume was calculated at P/P_0 = 0.995. Results showed that both the surface area and pore volume decreases with the increase of metal loadings. No significant change of pore diameter was observed. Impregnation, calcination and higher-temperature reduction caused destruction in the structure of the MWNT support to a degree (Table 5-1). However, most of the surface area and pore volume was retained.

Table 5-1 Textural properties of catalysts; C–prior to reduction, R–after reduction

Catalysts	S_{BET} ($m^2\ g^{-1}$)[b]		V_P ($cm^3\ g^{-1}$)[c]		D_P (nm)[d]	
	C[a]	R[e]	C	R	C	R
1Pt/MWNT	296	292	1.6	1.55	31.9	31.8
1Pt-3Ni/MWNT	290	289	1.58	1.58	31.6	31.6
1Pt-6Ni/MWNT	284	285	1.55	1.54	31.3	31.4
1Pt-12Ni/MWNT	269	261	1.40	1.32	31.0	31.1
12Ni/MWNT	272	251	1.41	1.30	31.0	31.0

[a] Measured by N_2 adsorption/desorption at −196 °C. Prior to measurement, samples were calcined under flowing NO (1.5 vol.% in Ar) at 500 °C for 60 min (heating rate 5 °C/min).

[b] Specific surface area (S_{BET}) was determined from the linear portion of the isotherm (P/P_0 = 0.05–0.35) (Brunauer et al., 1938)

[c] Pore volume (V_p) was calculated at P/P_0 = 0.995.

[d] Predominant pore size (volume basis) (D_p) was calculated from the adsorption isotherm using the Barrett–Joyner–Halenda (BJH) formula (Barrett et al., 1951)

[e] Catalysts were reduced in flowing H_2 (25 vol.% in Ar) at 650 °C for 30 min (heating rate 5 °C/min) at atmospheric pressure.

H_2 chemisorption was carried out using an Autosorb-IQ apparatus (Quantachrome Corporation) (see §2.1.2), and measureing at water bath temperature of 60 °C. Two chemisorption isotherms were generated; the first corresponded to the combined (strong and weak) adsorption, and the second corresponded only to weak adsorption. Both isotherms were extrapolated to P = 0, characteristic of monolayer chemisorption (Shen et al., 2008), with the former corresponding mostly to fast, strong adsorption on metal sites and the latter corresponding to slow, weak adsorption on the metal oxide support. However, the data in Table 5-2 was calculated on the basis of monolayer adsorption of H_2 on the metal sites only;

that is, only strong H_2 adsorption was considered (van Haasterecht et al., 2013). Prior to the chemisorption measurement, 100 mg catalyst was first reduced in situ at 650 °C (Pt-Ni) or 350 °C (Pt only) for 30 min in flowing pure H_2 (25 mL/min), then purged with 50 mL/min He for 30 min, and finally cooled to room temperature. The highest metal dispersion, 45.7%, was observed for the introduction of 3 wt% Ni into 1Pt/MWNT catalyst, even though metal dispersion decreased with higher Ni loading. This highest metal dispersion (45.7%) could be partly responsible for higher H_2 yield (Figure 5-9) and glycerol conversion (Table 5-6) observed by 1Pt-3Ni/MWNT catalysts.

Table 5-2 H_2 chemisorption results for the supported catalysts

Catalysts	H_2 uptake (μmol/g)	M_{disp} (%)	Crystal size (nm)
1Pt/MWNT	21	38	10.3
1Pt-3Ni/MWNT*	28.3 (27.8)	45.7 (45.1)	3.8 (3.9)
1Pt-6Ni/MWNT	26	41	5.9
1Pt-12Ni/MWNT	22	32	7.8
12Ni/MWNT	15	29	19

* the value in parenthesis is after 5th run.

The crystalline structure of the supported catalysts was determined by X-ray diffractometry using Cu Kα radiation (λ = 0.1542 nm) and a graphite monochromator (model S6000, Shimadzu) (see §2.1.3). Figure 5-3 shows that Pt

(111) diffraction peak positions of the bimetallic 1Pt-12Ni/MWNT catalyst (and possibly the 1Pt-3Ni/MWNT catalyst, though the Pt (111) peak was barely visible in the XRD pattern of that sample) slightly moved to higher position compared to monometallic Pt catalyst, indicating an interaction between Pt and Ni. The similar phenomenon of bimetallic interaction between Pt and Ni (Tegou et al., 2011), Pt and Cu (Fu et al., 2009), Pt and Co (Boga et al., 2013, Park et al., 2002) were observed and confirmed in the previous reports. The bimetallic interaction between Pt and Ni is thought to be responsible for the higher catalytic activity and selectivity towards H_2 production than the monometallic Pt and Ni catalysts.

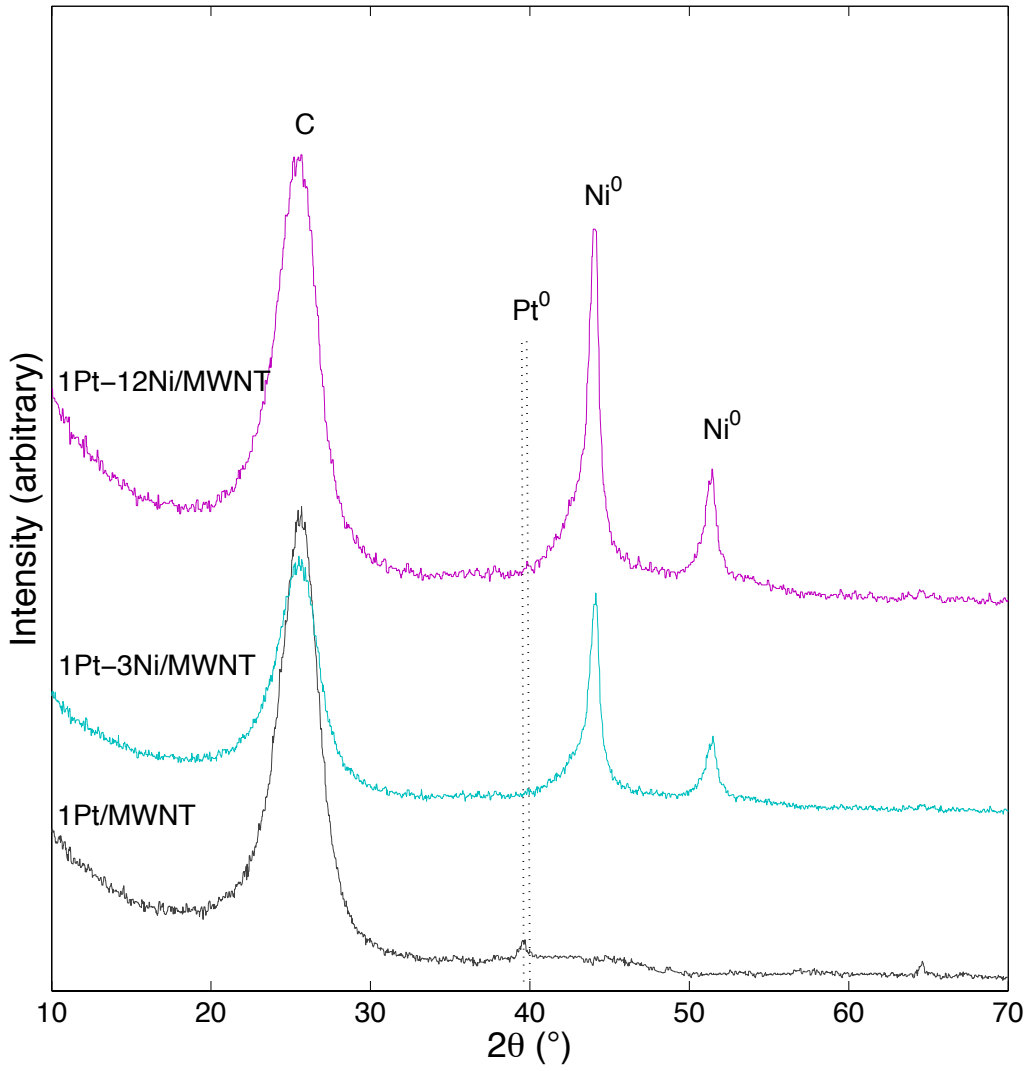

Figure 5-3 X-ray diffraction patterns of catalysts that had been reduced in flowing H_2 (25 vol.% in Ar) at 650 °C for 30 min (heating rate 5 °C/min). 1Pt/MWNT was reduced at 350 °C.

X-ray photoelectron spectra (XPS) were recorded on an ESCALAB250Xi (Thermo Scientific, UK) (see §2.1.9). As shown in Figure 5-4, the Pt 4*f* XPS peaks of Pt-Ni catalysts (1Pt-3Ni/MWNT and 1Pt-6Ni/MWNT) have shifted to low binding energy compared to pure Pt catallyst, in particular for 1Pt-3Ni/MWNT sample. On the other hand,1Pt-12Ni/MWNT has shifted to slightly higher binding

energy, indicating that the electronic structure of Pt was modified when Ni was introduced. This result is consistent with XRD result of Figure 5-3. Also Ni 2*p* peak intensity decreases as the Pt/Ni atomic ratio increases. This result is similar to the results of Pt coated Au nanoparticles with core-shell structure (Zhao and Xu, 2006).

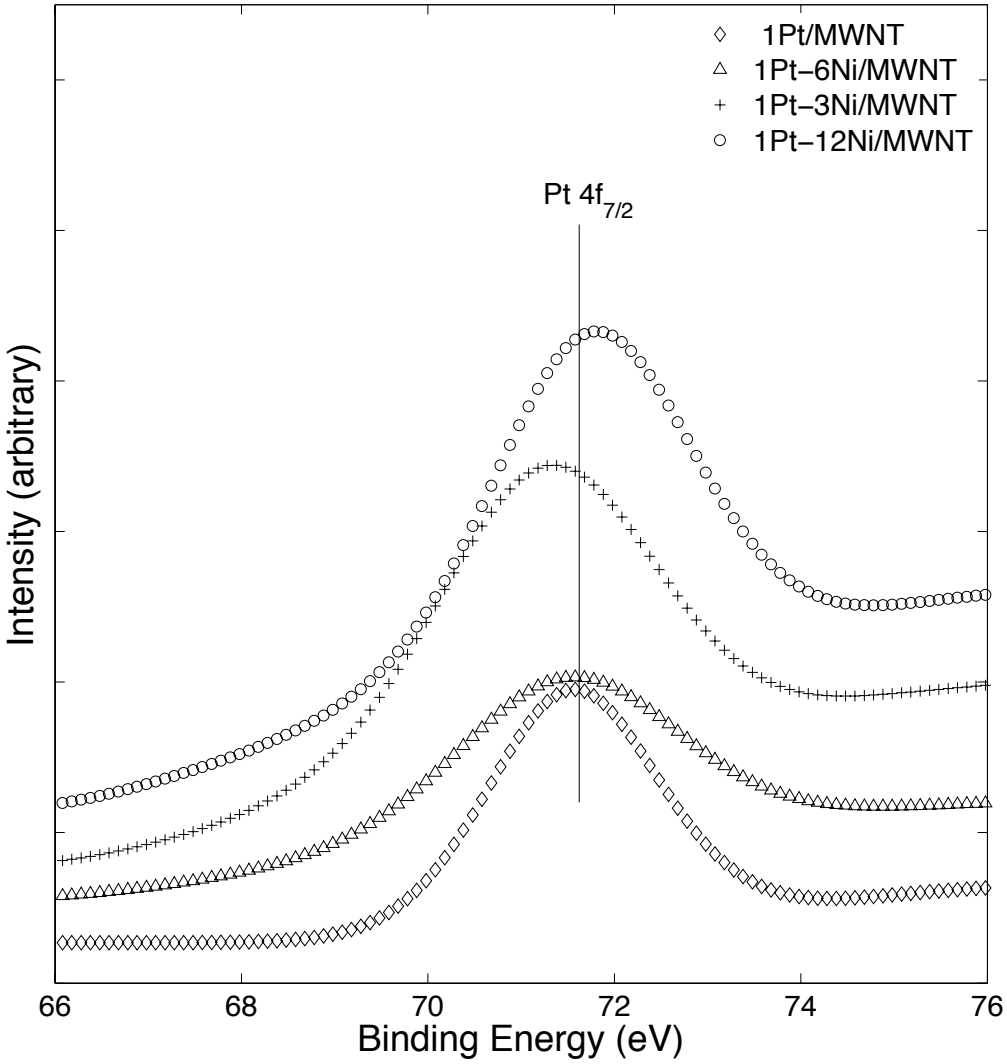

Figure 5-4 XPS patterns of Pt and Pt-Ni catalysts. Samples were calcined at 500 ºC for 60 MIN in flowing NO (1.5 vol.% in Ar)

The calcined catalysts were suspended on a 3 mm holey carbon support film on a copper grid and were analysed in a JEOL 2200FS transmission electron microscope (TEM). Energy dispersive X-ray spectrometer (EDX) was used in scanning tunneling electron microscope (STEM) mode. TEM micrographs and EDX analysis of the bimetallic catalysts were carried out to visually confirm the alloying effect of Pt on Ni. Figure 5-5 illustrates the TEM micrographs of 1Pt-3Ni/MWNT (a) and the STEM dark field image of 1Pt-3Ni/MWNT (b) and the corresponding EDX spectra (c) of the three points shown on the STEM micrograph. TEM micrographs [Figure 5-5 (a)] showed some unattached particles, which could be due to sonication while preparing TEM sample. Though some particles have been dislodged during the sonication. But that doesn't mean that they would be dislodged during APR as well. Also ICP analysis of liquid effluent showed no measureable leaching of Pt or Ni particles. Point 2 was chosen to be on a bulk particle and Point 1 and 3 were on single crystals. This was chosen because we wanted to observe the distribution of Ni and Pt on the catalyst. The size of the EDX beam was ca. 5 nm. All the TEM micrographs taken were of unreduced catalysts, and therefore a decrease in agglomeration can be expected after the catalysts are reduced. The presence of Pt and Ni emission lines from both the bulk and the single crystal particles strongly suggests alloy formation (Tanksale et al., 2008). Since the catalyst was not reduced before EDX study, It is assumed that Pt and Ni exist as solid solution in mixed oxide form. In Figure 5-5b, the Pt peaks tend to be difficult to read since single crystal particles (points 1 and 3) and bulk particle (point 2) have represented on the same scale. Indeed Pt was detected along

with Ni. So, it seems that Pt is present in close vicinity of Ni particle. The similar phenomenon was also observed for 1Pt-6Ni/MWNT catalysts as well.

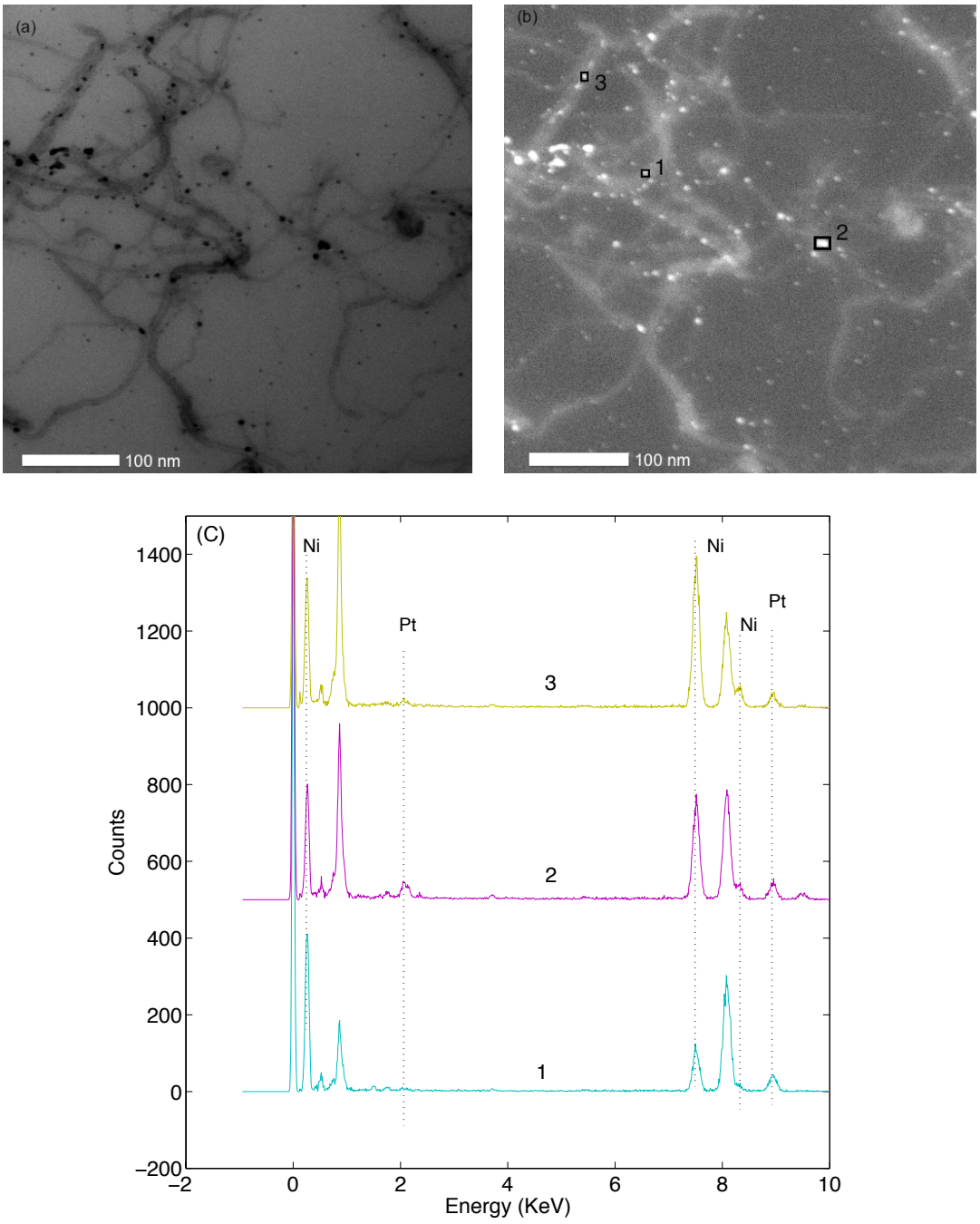

Figure 5-5 STEM micrographs of 1Pt-3Ni/MWNT (a) STEM dark field image of 1Pt-3Ni/MWNT (b) and the corresponding EDX spectra of point 1, 2 and 3 (c). Sample was calcined at 500 ºC for 60 min in flowing NO (1.5 vol.% in Ar)

The reducibility of monometallic Pt and Ni and bimetallic Pt-Ni supported on MWNT was studied with results shown in Figure 5-6. NiO and Pt-oxide were found as the precursor phases, and both could be completely reduced in 25 vol.% H_2 at 650 ^{0}C. The former presented a reduction that peaked at about 570 ^{0}C, and the latter underwent a reduction peak at 290 ^{0}C. However, bimetallic Pt-Ni was more easily reduced than monometallic Ni system. Bimetallic 1Pt-3Ni and 1Pt-6Ni showed reduction peak at 510 and 530 ^{0}C respectively, which are higher than monometallic Pt but lower than monometallic Ni catalyst, indecating Pt-Ni alloy formation. This result is consistent with XRD (Figure 5-3), XPS (Figure 5-4) and STEM-EDS result (Figure 5-5). Bimetallic Pt-Ni samples did not show two distinct peaks for Pt^0 and Ni^0, instead it showed one broad peak between Pt and Ni peaks

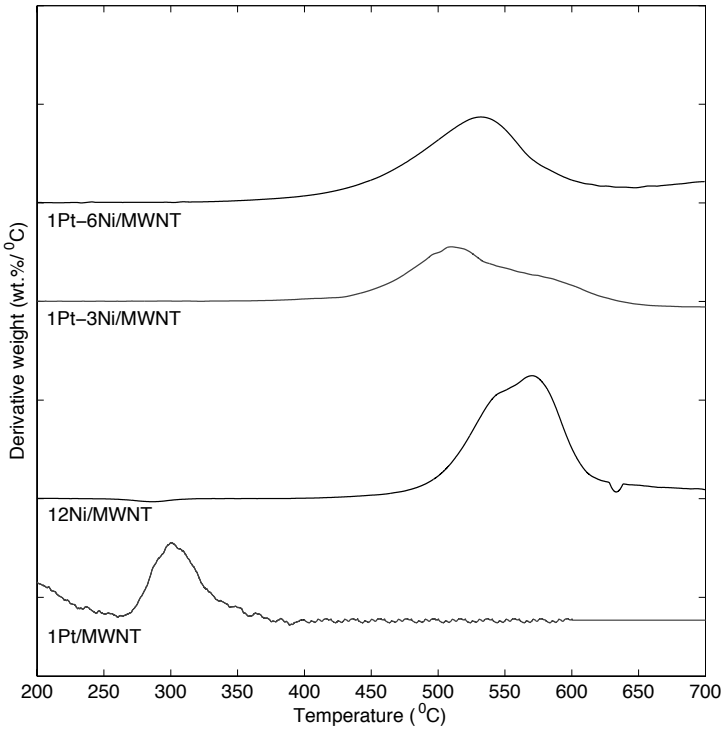

Figure 5-6 TGA study of catalyst reduction by H_2 (25 vol.% in Ar) at 5 ^{0}C/min.

5.3.2 Catalytic tests

5.3.2.1 Effect of support materials and glycerol concentration on the performance of the monometallic Pt catalysts

In order to study support effect in the APR of glycerol MWNT has been compared with two most popular commercial support γ-Al_2O_3 and MgO. Figure 5-7(a) shows the adsorption/desorption isotherms of the three different supported Pt catalysts. Among the supports, MWNT shows higher surface area and porosity as well (Table 5-4). For the γ-Al_2O_3 and MgO supported catalyst, the isotherm was type II, indicative of a non-porous (or macroporous) structure. However, slight hysteresis between adsorption and desorption at high pressures is suggestive of the existence of some meso-pores. According to the pore size distribution analysed by the BJH model (for both isotherms), the MWNT supported catalyst showed the narrowest range of pores size, with the majority around 3 nm. Both MgO and γ-Al_2O_3 supported catalyst showed a much wider distribution of pore sizes, between 4 and 9 nm (Figure 5-7b).

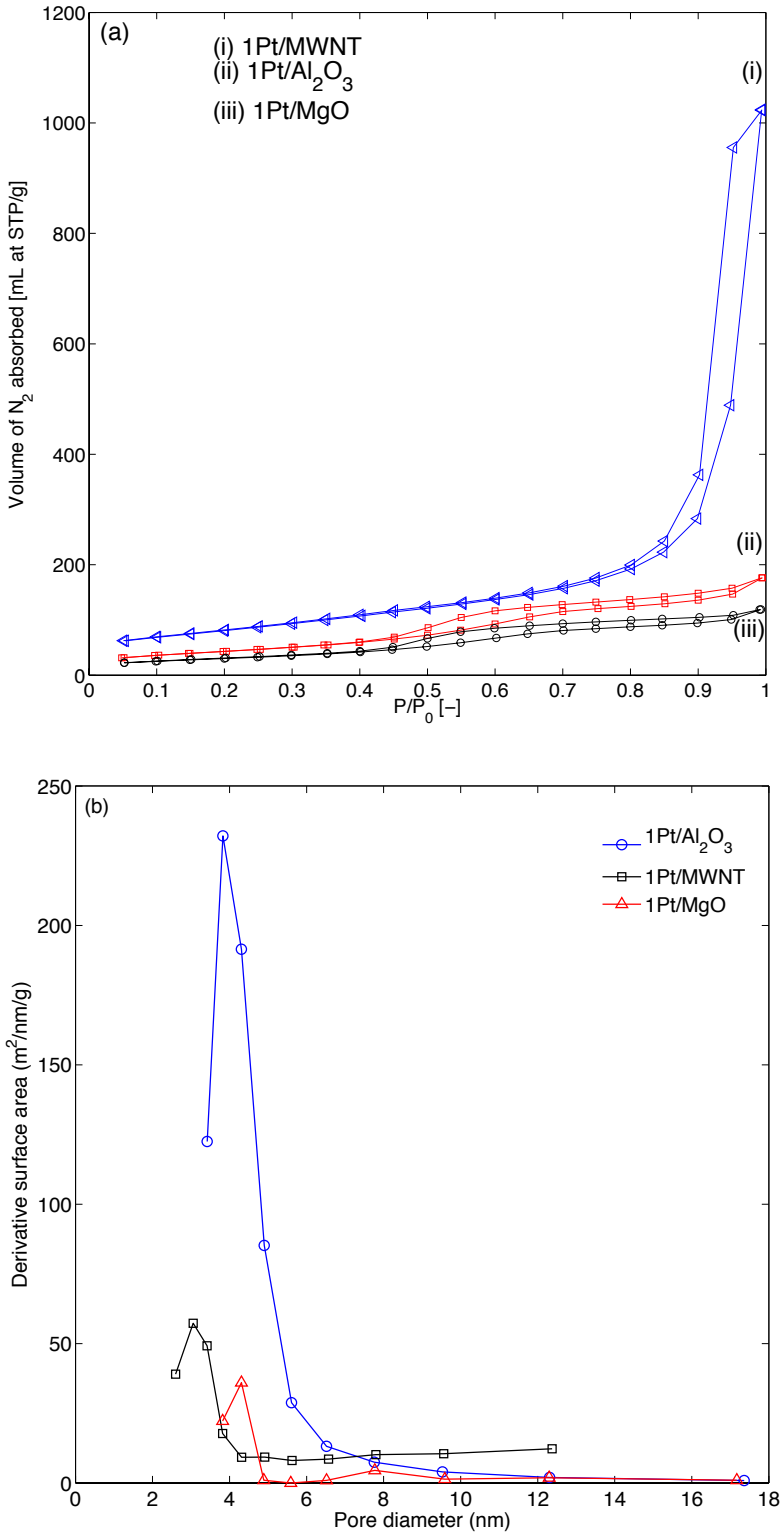

Figure 5-7 For 1Pt/MWNT, 1Pt/Al_2O_3 and 1Pt/MgO (a) N_2 adsorption/desorption isotherms, and (b) Pore size distribution (BJH model, desorption data was used)

An aqueous solution with 1 wt% glycerol was used to evaluate the performance of the catalysts. All reactions were performed at 240 °C, 40 bar, and with a feed flow rate of 0.05 mL/min irrespective of the catalyst used. The H_2 yield from the APR of glycerol was calculated as the ratio of the amount of H_2 produced divided by the amount of H_2 that could have been produced if all of the glycerol was completely reformed to H_2 (according to the stoichiometric reaction for APR of glycerol, 1 mol of glycerol produces 7 mol of H_2 (Davda et al., 2005)). The product yield of monometallic Pt catalysts supported on γ-Al_2O_3, MgO and MWNT in the APR of 1 wt% glycerol are compared in Table 5-3, also the physical properties of these catalysts are compared in Table 5-4. The result shows a higher H_2 yield (56.9%) and lowered methane production (5.7 mole%) for the 1Pt/MWNT catalyst. The results obtained from 1Pt/MWNT positively compare to the benchmark catalyst, 1Pt/Al_2O_3, in terms of H_2 yield, gas phase C yield, and methane production. The higher specific surface area (296 m^2/g) and metal dispersion (38%) and lower crystal size (10.3 nm) (Table 5-4) could be responsible for higher H_2 yield and gas phase C yield (Table 5-3) observed by 1Pt/MWNT catalysts. XRD patterns of these catalysts are shown in Figure 5-8

Table 5-3 Effect of the catalyst support on the catalytic performance of the monometallic Pt catalysts on the yield, gas phase conversion and gas phase composition of the aqueous phase reforming of glycerol (240 ºC, 40 bar, 1 wt% glycerol, 0.05 mL/min, 100 mg catalyst; data are mean values over t = 3–50 h)

Catalyst	1Pt/Al_2O_3	1Pt/MgO	1Pt/MWNT
H_2 yield (%)	39.4	42.7	56.9
Gas phase C yield (%)	41.7	44.7	46
Gas products (mol%)			
H_2	62.7	67.4	69.6
CO_2	26.9	27.7	25.8
CH_4	8.3	6.4	5.7

Table 5-4 Physical properties of the catalysts used for studying support effect. The catalysts were calcined under the flow of NO (1.5 vol.% in Ar) at 500 °C for 60 min

Catalysts	**S_{BET} ($m^2\ g^{-1}$)[a]**	**V_P ($cm^3\ g^{-1}$)[b]**	**D_P (nm)[c]**	**M_{disp} (%)[d]**	**Particle size (nm)[e]**
1Pt/Al_2O_3	155	0.25	4.50	11.3	15.7
1Pt/MgO	56	0.21	2.1	14	17
1Pt/MWNT	296	1.6	31.9	38	10.3

[a] Specific surface area (S_{BET}) was determined from the linear portion of the isotherm (P/P_0 = 0.05–0.35) (Brunauer et al., 1938).

[b] Pore volume (V_p) was calculated at P/P_0 = 0.995 of the desorption branch of isotherm.

[c] Predominant pore size (volume basis) (D_p) was calculated from the adsorption isotherm using the Barrett–Joyner–Halenda (BJH) formula (Barrett et al., 1951).

[d] Measured from H_2 chemisorption analysis (§ 5.3.1). Each catalyst was reduced in situ at 350 °C for 30 min in flowing pure H_2 (25 mL/min),

[e] Size of Pt particles, as measured from H_2 chemisorption analysis (§ 5.3.1).

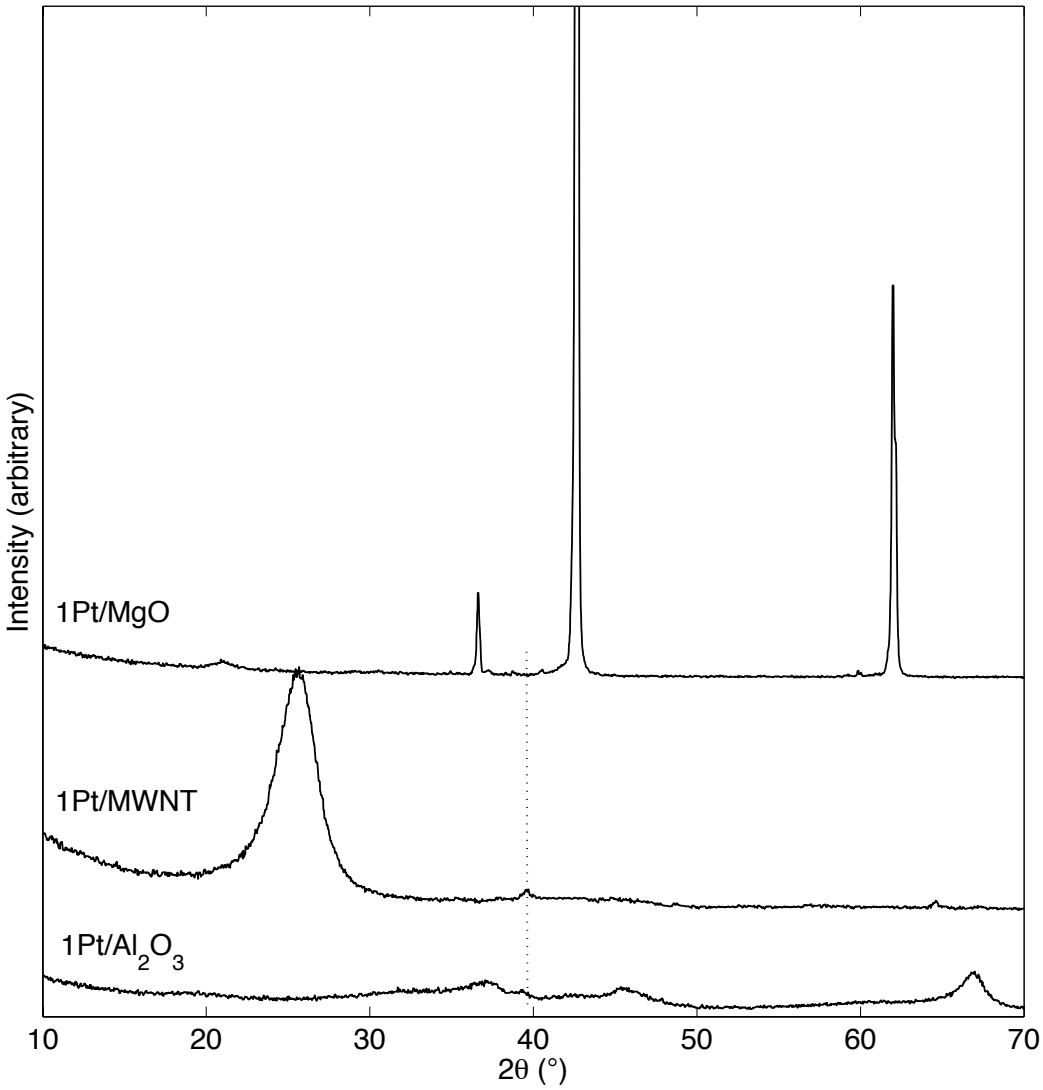

Figure 5-8 X-ray diffraction patterns of the monometallic Pt catalysts supported on Al_2O_3, MgO and MWNT that had been calcined at 500 °C for 60 min under the flow of NO (1.5 vol.% in Ar).

APR of high concentrated glycerol feeds leads to lower catalytic activity and selectivity for H_2 production (Table 5-5). As the glycerol concentration increases, H_2 yield and gas phase carbon yield decreeases tremendously, as the conversion rate of glycerol is very low (5% only).

Table **5-5** Effect of feed concentration on the catalytic performance of 1Pt/MWNT catalyst in the aqueous phase reforming of glycerol (240 °C, 40 bar, 0.05 mL/min, 100 mg catalyst; data are mean values over t = 3–50 h)

Glycerol concentration in feed	**1 wt%**	**20 wt%**	**40 wt%**
H_2 yield (%)	56.9	9.3	3.1
Gas phase C yield (%)	46	4.2	1.4
Gas products (mol%)			
H_2	69.6	81.6	87.6
CO_2	25.8	15.3	12.5
CH_4	5.7	4.5	2.4

5.3.2.2 Effect of nickel on the catalytic activity

Several bimetallic catalysts have been studied for APR of glycerol to date (Huber et al., 2006, Baker et al., 1986, Kunkes et al., 2008, Wang et al., 2009, Ko et al., 2006, Tupy et al., 2012). We chose to study the influence of Ni as the promoter element on the performance of 1Pt/MWNT catalyst for the APR of glycerol. The effect of the Ni loading in the catalyst on the gas phase yield is presented in Figure 5-9. The combination of Pt and Ni increased the hydrogen yield and selectivity compared to the monometallic Pt and Ni catalysts. Results shows that as the Pt:Ni ratio increases to 1:12, both the hydrogen yield and selectivity decreases, as the methane yield increases. The higher hydrogen yield (93%) and selectivity (91%) was achieved for 1 wt% Pt-3 wt% Ni loading than the benchmark 1Pt/MWNT catalyst. Even though, the non-noble metal catalyst, 12Ni/MWNT, showed

promising results compared to highly expensive noble metal catalyst, 1Pt/MWNT, but it showed severe deactivation after 40 hours on stream and significant CO yield (6.3%), infact H_2 peak was completely disappeared after 60 h on stream (Figure 5-10). Also traces of C_2H_6 and C_3H_8 were identified for 12Ni/MWNT catalyst, but were not further quantified.

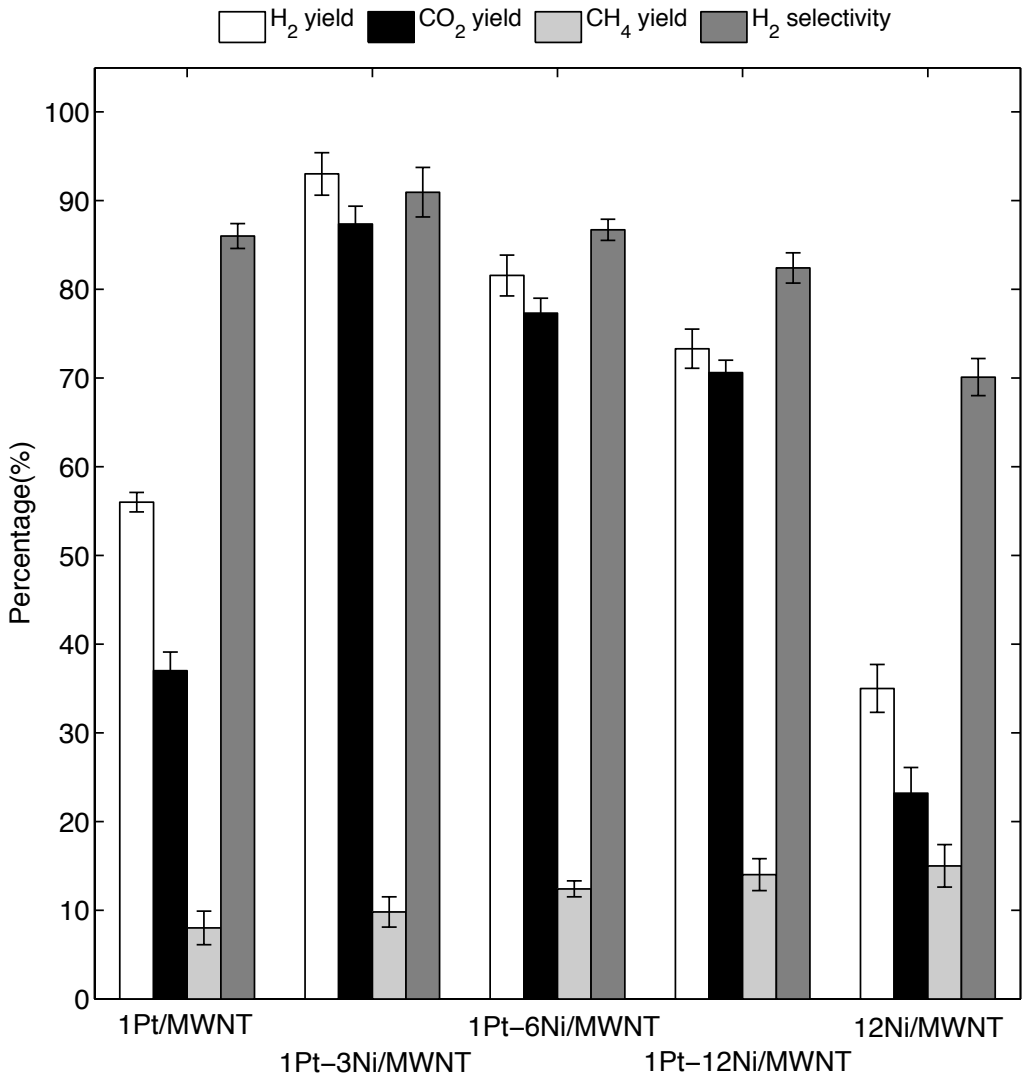

Figure 5-9 Effect of Ni addition to 1Pt/MWNT catalysts on yield and selectivity in the aqueous phase reforming of glycerol (240 ºC, 40 bar, 0.05 mL/min, 100 mg catalyst; data are mean values over t = 3–100 h). Error bars indicate one standard deviation; each bar is the average of ≥2 experiments

Table 5-6 Glycerol conversion, Gas phase C yield and system C balance in the aqueous-phase reforming of glycerol over MWNT supported catalysts (240 ºC, 40 bar, 0.05 mL/min, 100 mg catalyst; data are mean values over t = 3–100 h)

Catalysts	Glycerol Conv. (%)	Gas phase C yield (%)	C Balance, out/in (%)
1Pt/MWNT	53.6	46	97
1Pt-3Ni/MWNT	>99	99	98
1Pt-6Ni/MWNT	93.4	91	96.8
1Pt-12Ni/MWNT	89.7	88	103
12Ni/MWNT	44	41	96

The liquid phase after reaction was also analyzed for all the reactions. Apart from un-reacted glycerol, traces of some other compounds were also identified, particularly ethanol, ethylene glycol, acetic acid and propylene glycol, but were not further quantified. Glycerol conversion rate, gas phase C yield, and carbon balance are shown in Table 5-6. Compare to monometallic Pt and Ni catalyst, all bimetallic Pt-Ni catalysts showed much higher glycerol conversion and gas phase C yield, which might be due to the interaction between Pt and Ni. Similar phenomenon has been observed by Boga et al. (Boga et al., 2013) while studying the APR of glycerol over bimetallic Pt-Cu catalysts. The highest glycerol conversion rate (>99%) and gas phase C yield (99%) was observed for 3 wt% Ni loading in 1Pt/MWNT catalyst and as the Ni loading increased to 12 wt%, glycerol conversion rate and gas phase C yield decreased to 89.7% and 88% respectively. The lowest glycerol conversion rate (44%) and gas phase C yield (41%) was observed for 12Ni/MWNT catalyst. The interaction between Pt and Ni greatly

increased the conversion of the APR reaction, even the co-existence of individual Pt and Ni nanoparticles can greatly increase the conversion of the APR reaction, in good accordance with the literature (Wang et al., 2009).

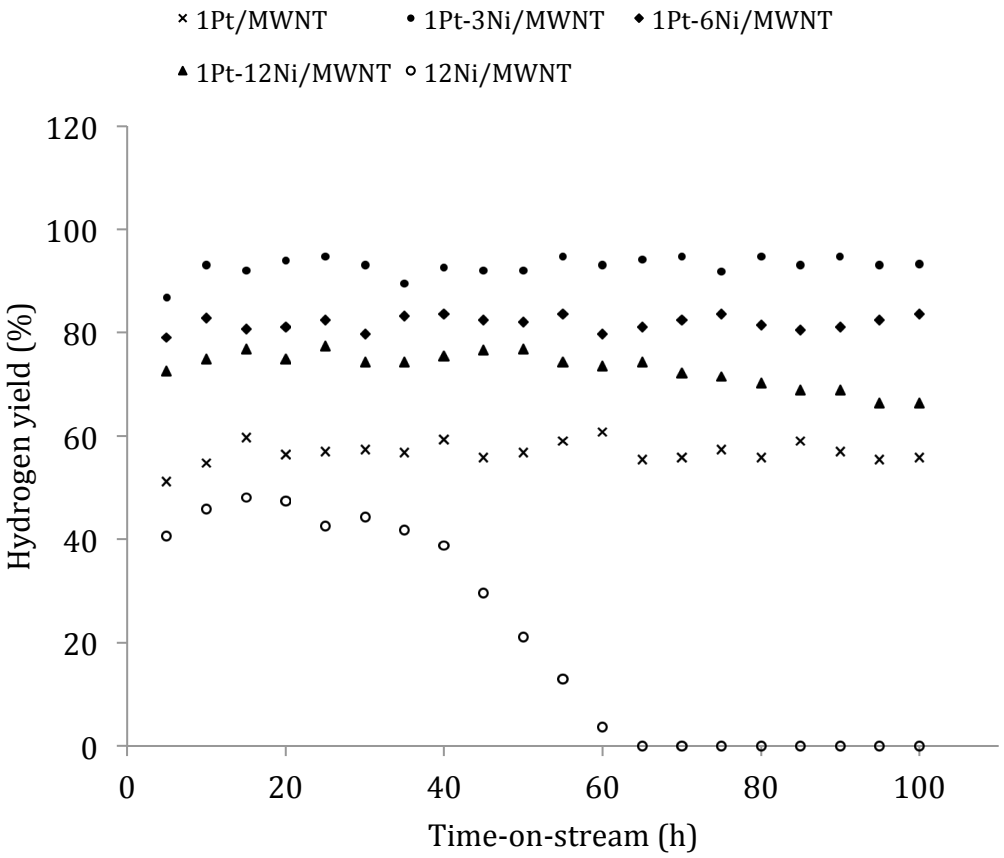

Figure 5-10 Variation of H_2 formation rate with time-on-stream in the APR of glycerol (240 °C, 40 bar, 1 wt% glycerol, 0.05 mL/min, 100 mg catalyst)

Figure 5-10 shows catalyst stability with time on-strem. Among the bimetallic catalysts we tested, 1Pt-3Ni/MWNT gave the highest H_2 yield, glycerol conversion, gas phase C yield, H_2 rate and lowest CH_4 yield. So to investigate the stability of the 1Pt-3Ni/MWNT catalyst, further 4 runs were made each with 100 h

on stream, the results were depicted in Figure 5-11. After the first run, the reactor was heated at 120 °C for 6 h and at the same time flushed with Ar to get ride of all the gaseous and liquid species trapped in the rig and the same procedure was followed before each run. As shown in Figure 5-11, H_2 yield was almost same for the first three runs and then decreased in 4^{th} and 5^{th} run. Over all after 5^{th} run (more than 500 h on strem) H_2 yield decreased 14% and glycerol conversion decreased about 17% of the 1^{st} run. XRD pattern of spent 1Pt-3Ni/MWNT catalyst (after 5^{th} run) showes diffraction peaks for NiO at $2\theta = 37.2$ and 62.9° representing the (111) and (220) planes (Figure 5-12), respectively (Iriondo et al., 2008, Manfro et al., 2011), means some of the metallic Ni particles were oxidized to NiO, which could be responsible for the minor deactivation of the catalyst (Figure 5-11). This oxidation could happen during pre-treatment before each run. Also the deactivation of the catalyst might be ascribed to the carbon deposition on the active phase (Davda and Dumesic, 2004, Yoshida et al., 2004). No sintering of the active phase was observed even after 5^{th} run (more than 500 h on-stream) of the 1Pt-3Ni/MWNT catalyst (Table 5-2). Also, inductively coupled plasma atomic emission spectrometry (ICP–AES) analysis of the liquid effluent showed no measurable leaching of Pt and Ni.

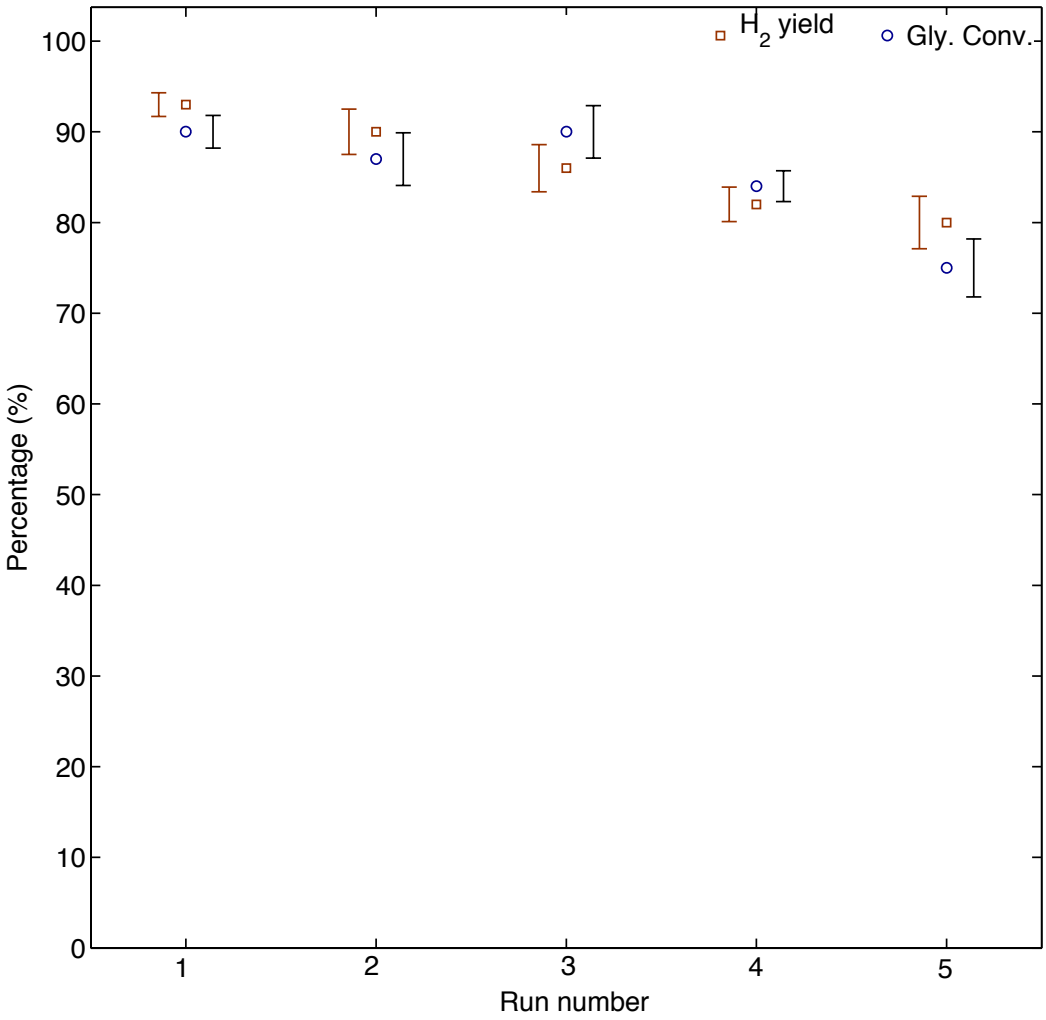

Figure 5-11 Repeated runs in the ARR of glycerol on 1Pt-3Ni/MWNT catalyst (240 °C, 40 bar, 1 wt% glycerol, 0.05 mL/min, 100 mg catalyst; data are mean values over t = 3–100 h). Error bars indicate one standard deviation; each bar is the average of ≥2 experiments

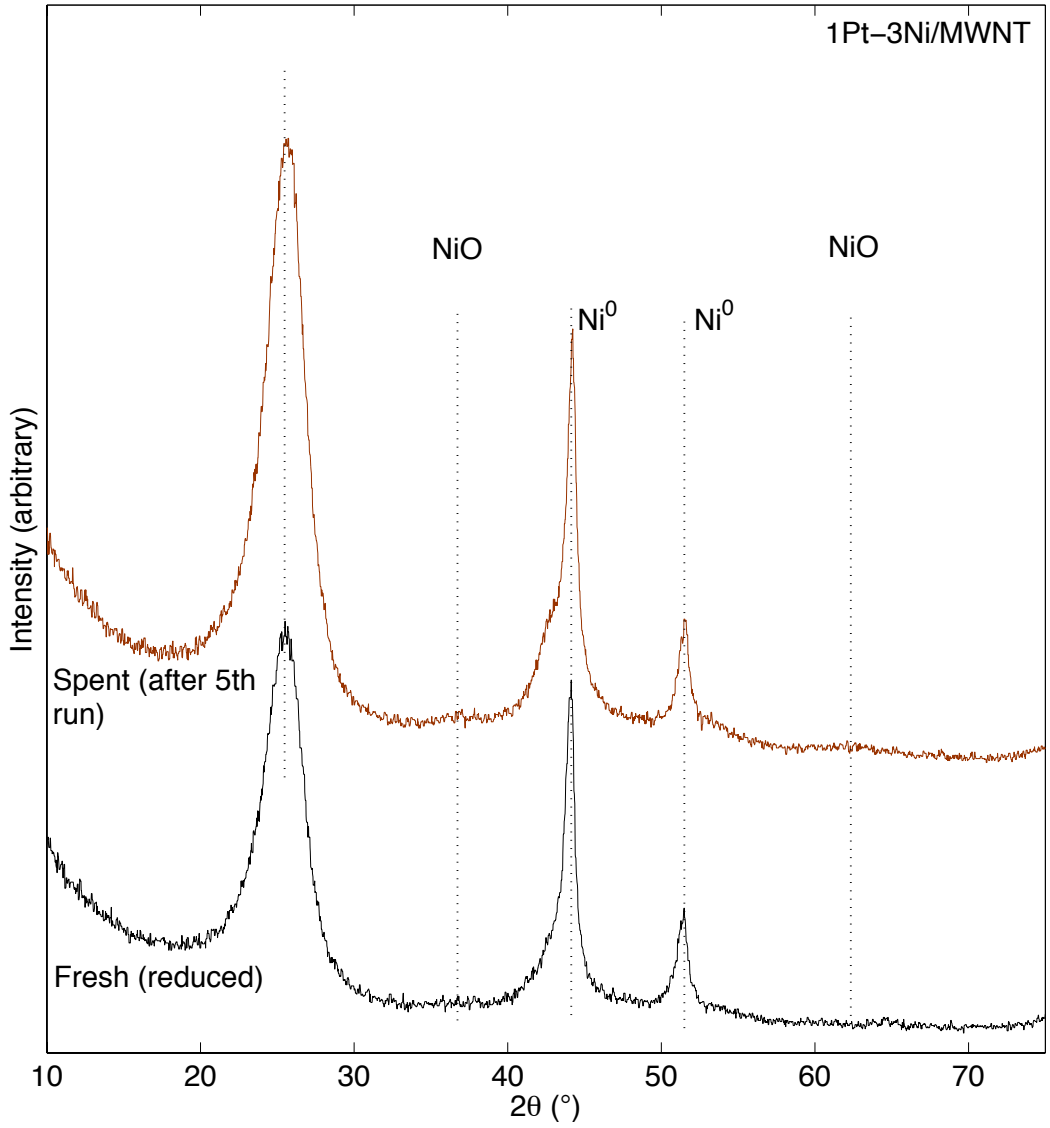

Figure 5-12 XRD patterns for fresh (reduced) and spent (after 5th run) 1Pt-3Ni/MWNT catalyst

5.3.2.3 Effect of WGS reaction on H_2 yield in ARR

An important advantage of APR (Eq. 4-3) is the ability of producing 7 moles of hydrogen per 1 mole of glycerol, 4 moles from glycerol reforming (Eq. 4-1) and 3 moles from WGS reaction (Eq. 4-2). To investigate the fact, WGS reaction was studied using the same reactor system and same reaction conditions (240 °C, 40

bar, 100 mg catalyst) was applied for APR process to investigate the catalyst performance. Instead of using 1 wt% glycerol in DI water, 0.05 ml min^{-1} DI water and 0.39 ml min^{-1} CO was introduced in the reactor as the reactant. The produced gas mixture was analyzed using an online gas chromatograph (Varian CP-3800). The carbon balance agreed within ±7 mol.%. Figure 5-13 shows the total CO conversion, H_2 yield and CH_4 yield. Supported Pt and Pt–Ni catalysts showed higher CO conversion and H_2 yield compare to WGS reaction without catalyst. In the case of Pt-Ni bimetallic catalysts, higher CO conversion was observed compare to 1Pt/MWNT catalyst. But CO conversion tends to decrease as the Ni loading increased.

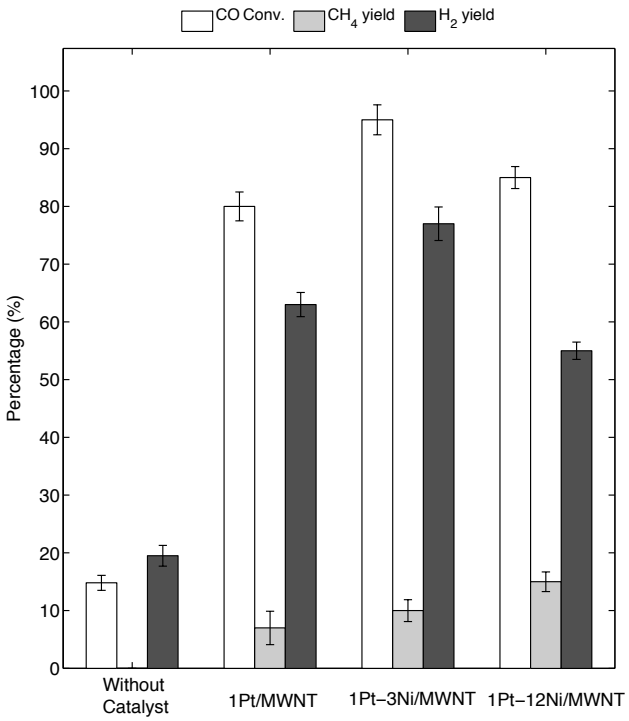

Figure 5-13 WGS study without catalyst and with catalysts (240 °C, 40 bar, 0.05 mL min–1 DI water, 0.39 mL/min CO, 100 mg catalyst; data are mean values over t = 3–20 h). Error bars indicate one standard deviation; each bar is the average of ≥2 experiments

When carrying out the WGS reaction, methane can be formed by CO/CO_2 hydrogenation in a methanation reaction (Haryanto et al., 2009). It has been reported that Ni is an effective catalyst for the methanation reaction (Takenaka et al., 2004). Since methanation consumes H_2 (Eq. 4-4), with higher Ni loading (12 wt%), H_2 yield decreases even though CO conversion is increased. Figure 5-13 shows methane yield during the WGS reaction and significant methane formation was observed for 12 wt% Ni loading with 1Pt/MWNT catalyst. This is an indication of the potential drawbacks of Ni as a WGS catalyst. Although CO conversion decreased with increased Ni loading into bimetallic Pt–Ni catalysts, but they showed higher activity compared to monometallic Pt catalys (Figure 5-13). The 1Pt–3Ni/MWNT catalyst showed highest CO conversion of about 100%. These results revealed important modifications of the surface properties of bimetallic catalysts, indicated by XRD and H_2–TPR. The 1Pt–3Ni/MWNT catalyst showed the best WGS performance among all catalysts. The presence of Pt produced favorable structural and electronic effects for enhancing the WGS activity.

5.4 Conclusions

In this work, monometallic Pt and bimetallic Pt-Ni catalysts having the same Pt loading but different Ni loading, supported on multi-walled carbon nanotubes (MWNT), were prepared and tested in the aqueous-phase reforming (APR) of glycerol. Amongst the catalysts tested, bimetallic 1Pt-3Ni/MWNT catalyst gave

the higher H_2 yield (93%) and selectivity (91%) than the bench mark 1Pt/MWNT catalyst. Irrespective of Pt and Ni ratio, bimetallic Pt-Ni catalysts showed higher activity and selectivity towards H_2 production than the monometallic Pt catalysts. To study the effect of support on the performance of monometallic Pt catalyst in APR process, two others supports Al_2O_3 and MgO was also tested. MWNT support showed a positive effect on APR process, which could be due to its hydrophobic nature. Catalyst characterization by XRD, XPS showed a peak shift of Pt in bimetallic Pt-Ni catalyst than the monometallic Pt catalyst. Also the presence of Pt and Ni emission lines, in STEM-EDS spectra, from both the bulk and the single crystal particles strongly suggests that Pt is present in close vicinity of Ni particle. The bimetallic interaction between Pt and Ni is thought to be responsible for the high glycerol conversion and gas phase C yield and, ultimately, the high H_2 yield observed. Also higher metal dispersion and smaller crystal size (Table 5-2) could be responsible for its better performance in APR process.

Chapter 6

Chapter 6 describes the effect of Cu addition to Ni catalyst supported on MWNT in the aqueous phase reforming of glycerol. The reaction was carried out in a continuous flow fixed bed reactor (240 °C, 40 atm) with a solution of 1 wt% glycerol in DI water at a flow rate of 0.05 mL/min. Catalysts characterized by XRD and XPS showed a significant peak shift of Ni in bimetallic Cu–Ni catalysts than the Ni catalyst, suggesting a strong interaction between Cu and Ni. Also H_2–TPR analysis showed that introducing Cu increased Ni reducibility. The bimetallic interaction is thought to be responsible for the lowered methane yield and ultimately, higher hydrogen yield observed.

6 Non-noble based Cu-Ni alloy catalyst for APR

6.1 Introduction

Chapter 3, 4 and 5 reports noble metal (Pt) and bimetallic noble metal (Pt-Ni) catalysts that significantly enhanced both the activity and selectivity of H_2 production from APR of glycerol. Though noble metals catalysts have both high activity for reforming reactions and resistance to carbon deposition as well (Wen et al., 2008, Cortright et al., 2002, Rahman et al., 2013, Rahman et al., 2014), however, considering the high cost, it is more economical to develop non-noble based metal catalysts. Sinfelt (Sinfelt, 1973) showed that among the metals, Ni has the highest C–C bond breaking reaction rates. On the other hand, Grenoble et al. (Grenoble et al., 1981) showed that Cu has the highest activity for water-gas shift reaction (contributes about 40% H_2 of total APR), but inactive for C–C bond cleavage. Currently, Cu-Ni bimetallic catalysts are receiving increased attention as these two metals are mutually soluble in each other and form a solid solution for all compositions (Chakrabart et al., 1991). In many reactions, compared to monometallic Ni catalysts, Ni-based catalysts containing Cu have already been found to have significantly different catalytic activity and selectivity. For example, the addition of Cu to Ni catalyst, in ethanol steam reforming reaction not only reduced CO production, but also improved resistance to coke formation on Ni catalysts (Vizcaíno et al., 2007). The addition of Cu to Ni/SiO_2 also led to a low conversion in the hydrodechlorination of 1,1,2-trichloroethane and a high selectivity to vinyl chloride monomer (Choi and Lee, 2001). Huang et al. studied

the WGS reaction during steam reforming of methane over supported Cu–Ni catalysts and showed the addition Cu to Ni catalysts enhanced the WGS activity (Huang et al., 2005). It is suggested that changes in the catalytic properties induced by Cu addition to Ni can be caused by changes in the electronic and/or geometric properties of the homogeneous bimetallic particles (Choi and Lee, 2001, Asedegbega-Nieto et al., 2005).

However, despite their promise, Cu–Ni bimetallic catalysts supported on carbon nanotubes (MWNT) have not been sufficiently investigated for APR of glycerol. Manfro et al. (Manfro et al., 2013) studied APR of glycerol using Ni–Cu catalysts prepared from hydrotalcite-like precursors and showed that the high activity of Ni–Cu catalysts is related to the formation of alloy phase after reduction and enhancement of metal dispersion and Ni reducibility. But they did not check catalyst stability for long run use. Kim et al. (Ji Yeon Kim et al., 2013) studied APR of glycerol by using Cu-promoted Ni catalysts supported on $LaAlO_3$. The highest glycerol conversion and H_2 selectivity was observed for 15Ni-5Cu/$LaAlO_3$ catalyst and this was attributed due to smallest crystal size, highest metal dispersion and highest surface area. Also, Cu increased Ni reducibility. Therefore, in this study, a number of bimetallic xCu–12Ni/MWNT catalysts have been prepared and compared as the APR catalysts to monometallic 12Ni/MWNT catalyst. The effect of Cu/Ni ratio, structural and morphological properties of the catalysts on the catalytic activity and hydrogen selectivity has been investigated. A detailed characterization of the Cu–Ni catalysts by N_2–physisorb, XRD, XPS and

H_2–TPR was conducted to elucidate the Cu–Ni interaction and catalytic performance and also the stability of the catalyst was checked.

6.2 Experimental

6.2.1 Catalyst preparation

The MWNT used in this research was purchased from SWeNT. At first, the nanotubes were treated with 1M HNO_3 at 25 °C (see §5.2.1). The surface modification of MWNT is necessary for metal deposition onto carbon (Ebbesen et al., 1996, Yu et al., 1998). The nanotubes were then filtered and dried for further use.

$CuN_2O_6.2.5H_2O$ (Sigma–Aldrich) and $Ni(NO_3)_2{\cdot}6H_2O$ (Strem chemical) were dissolved, individually or together, into Propylene Glycol (PG) to make monometallic or bimetallic catalysts, respectively. These were deposited on modified MWNT using reflux method. Specifically, to prepare 1Cu–12Ni/MWNT, 0.5 g of modified MWNT was mixed with a solution prepared by dissolving 214.6 mg CuN_2O_6. $2.5H_2O$ and 343.4 mg of $Ni(NO_3)_2{\cdot}6H_2O$ in 50 mL of PG in a 100-mL glass vial. The mixture was then sonicated for 15 min. and then NaOH was added to get the mixture P^H = 9.5~10. Refluxing of the total mixture was done with the help of a oil bath at 140 °C for 2 h and at the same time the mixture was stirred with the help of magnetic stirrer. After refluxing the sample was washed couple of times to get rid of PG and to get the P^H neutral. The sample was then dried in vacuum oven at 120 °C for 12 h and calcined under flowing NO (1.5

vol.% in Ar) at 500 °C for 2 h (heating rate 10 °C min^{-1}). Catalysts were reduced in situ in flowing H_2 (25 vol.% in Ar) at 650 °C for 1 h (heating rate 10 °C min^{-1}) at atmospheric pressure.

6.2.2 Catalyst testing

The APR of glycerol was studied in a continuous flow type fixed bed reactor system (see §2.2.1). The catalyst (150 mg) was loaded into a 5-mm i.d. stainless steel tubular reactor and held in position with quartz wool plugs. A backpressure regulator (0 to 1000 psig, Swagelok) attached to a pressure gauge was used to pressurize the system with Ar to 40 bar. A 1-wt% glycerol solution was introduced by a hplc digital pump (Waters 510) at a rate of 0.05 mL/min, and heating of the catalyst bed was initiated. When the reactor reached at 240 °C, Ar flow was set at 50 sccm using a Bronkhorst mass flow controller. The system was allowed to stabilize for about 2 h before analysis of the reaction products began. Gas products were analyzed at 25-min intervals using an online gas chromatograph (see §2.2.2). The calibration curves were developed, and the samples were analyzed, with the TCD at 200 °C and the FID at 300 °C. A representative GC trace (Figure 6-1) shows only four peaks, representing H_2, CO, CH_4 and CO_2, respectively, for each injection of product gas.

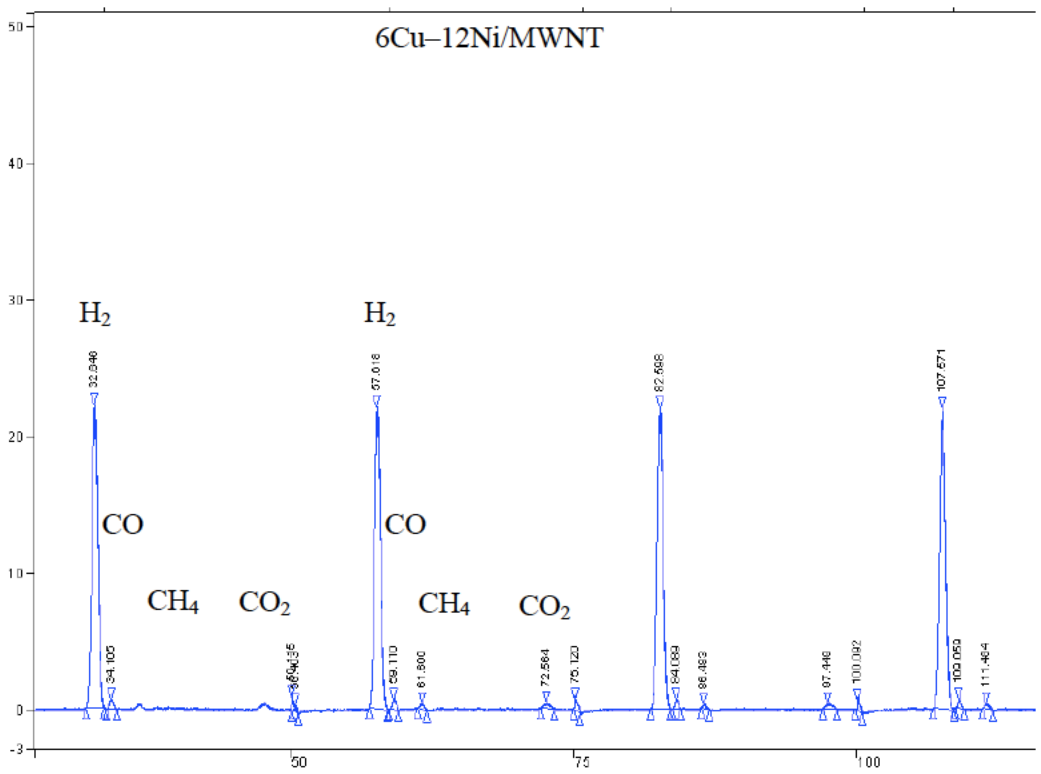

Figure 6-1 A representative GC curves from the APR of glycerol over 6Cu-12Ni/MWNT catalyst, as measured on the in-line Varian CP-3800 gas chromatograph. The product gas was sampled every 25 min; four successive injections are shown here

Liquid products were analyzed with a Shimadzu HPLC (see §2.2.3). The liquid products of the APR reaction were collected in a condenser downstream of the reactor bed (refer to Figure 2-1), and aliquot of the condensed liquid was used to determine the amount of un-reacted glycerol in the liquid phase. A representative HPLC trace is shown in Figure 6-2. Also Shimadzu TOC–L (with auto sampler ASI–L) was used to know the total organic carbon content of the liquid phase (see §2.2.4).

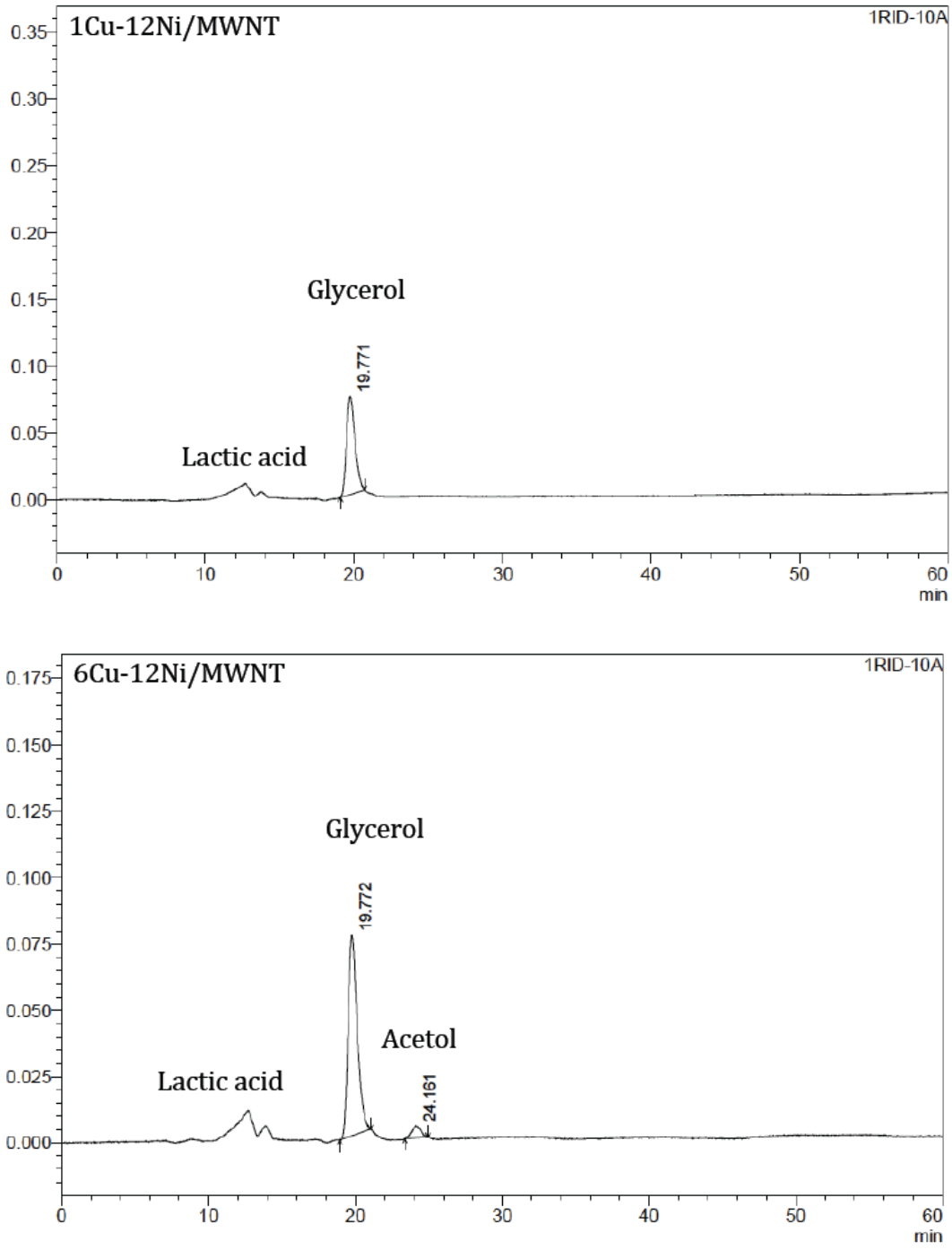

Figure 6-2 Representative HPLC curves for the APR of glycerol over 1Cu-12Ni/MWNT and 6Cu-12Ni/MWNT catalyst, reaction was carried out at T= 240 ^{0}C, P= 40 bar, flow rate 0.05 mL/min of 1 wt% aqueous glycerol

The catalysts were evaluated on the bases of H_2 yield, CO yield, CO_2 yield, CH_4 yield, and carbon conversion to gas, H_2 selectivity and glycerol conversion efficiency (see §2.2.1). Also the yield of liquid by-products are calculated by the below formula.

Yield of liquid species i = (moles of i produced) / (moles of glycerol in feed)

6.3 Results and Discussions

6.3.1 Catalyst characterization

From N_2 adsorption-desorption isotherms at −196 °C, a specific surface area of 254-278 m^2/g was obtained for the calcined catalysts. Prior to the analysis the samples were outgassed for 12 h at 140 °C (see §2.1.1). The results are summarized in Table 6-1. The pure support, MWNT, had S_{BET} = 296 m^2/g. Adding 12 wt% Ni lowered the surface area to 272 m^2/g. Again adding Cu (1,6 and 12 wt%) caused a gradual loss of surface area (Table 6-1). The reduction of specific surface area for all catalyst compared to pure support is mainly due to the presence of metals crystals. In addition, some blockage of part of the pores by metal particles might further decrease the specific surface area. The reduced catalysts did not show substantial difference in surface area or pore volume as compared to the calcined catalyst. Also no substantial difference in pore diameter was observed for pure support and impregnated catalyst (both calcined and reduced).

Table 6-1 N_2-physisorption analysis

Catalysts	S_{BET} (m^2/g)[a]		V_P (cm^3/g)[b]		D_P (nm)[c]	
	C[d]	R[e]	C[d]	R[e]	C[d]	R[e]
MWNT	296	–	1.60	–	31.9	–
12Ni/MWNT	272	260	1.41	1.38	31.0	31.1
1Cu-12Ni/MWNT	269	273	1.40	1.45	31.0	31.0
6Cu-12Ni/MWNT	261	265	1.36	1.40	30.6	30.9
12Cu-12Ni/MWNT	254	251	1.34	1.33	29.7	30.0
12Cu/MWNT	278	264	1.47	1.41	31.2	31.1

[a] Specific surface area (S_{BET}) was determined from the linear portion of the isotherm (P/P_0 = 0.05–0.35) (Brunauer et al., 1938).

[b] Pore volume (V_p) was calculated at $P/P_0 = 0.995$.

[c] Predominant pore size (volume basis) (D_p) was calculated from the adsorption isotherm using the Barrett–Joyner–Halenda (BJH) formula (Barrett et al., 1951).

[d] Prior to measurement, samples were calcined under flowing NO (1.5 vol.% in Ar) at 500 °C for 2 h (heating rate 10 °C min^{-1}).

[e] Catalysts were reduced in flowing H_2 (25 vol.% in Ar) at 650 °C for 1 h (heating rate 10 °C min^{-1}) at atmospheric pressure.

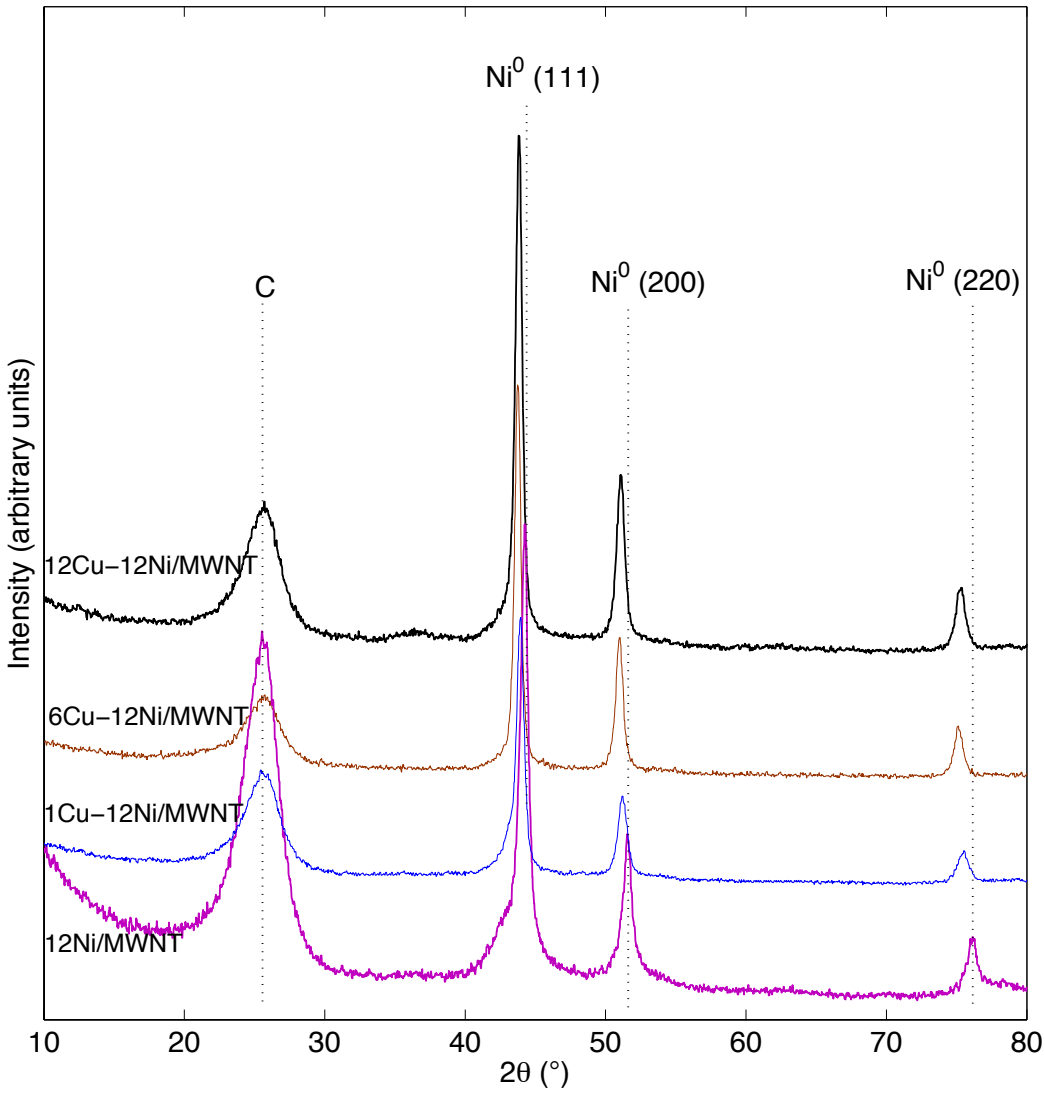

Figure 6-3 X-ray diffraction patterns of 12Ni/MWNT and xCu-12Ni/MWNT catalysts. Catalysts were reduced at 650 °C in flowing H_2 (25 vol.% in Ar) for 1 h (ramp rate of 10 °C/min)

In order to see any interaction between Cu and Ni, the catalysts were reduced at 650 °C in flowing H_2 (25 vol.% with Ar) for 1 h (ramp rate of 10 °C min^{-1}). XRD pattern of reduced catalysts have shown in Figure 6-3. The reduction resulted in the formation of metallic nickel (Ni^0) with diffraction peaks at 44.55, 51.84 and 76.31, corresponding to the (111), (200) and (220) planes respectively,

demonstrating that activation of the catalysts were effective (Iriondo et al., 2008). Also diffraction peaks (Figure 6-4) at about 43.18, 50.26 and 73.92 were observed for metallic copper (Cu^0) after reduction of 12Cu/MWNT. As we introduced Cu with 12Ni/MWNT sample, then peak shift of Ni was observed to lower diffraction angle (2θ) and the peak shift increases as the Cu loading (wt%) increases from 1 to 12 wt%. Since Cu and Ni are mutually soluble in each other for any compositions (Callister, 7 th edition, 2007), thus it is possible that copper formed an alloy with nickel. This might be the reason, why diffraction peaks related to metallic copper (Cu^0) were absent in the xCu–12Ni/MWNT sample after reduction (Figure 6-3) (Dussault et al., 2007, Lin et al., 2010)

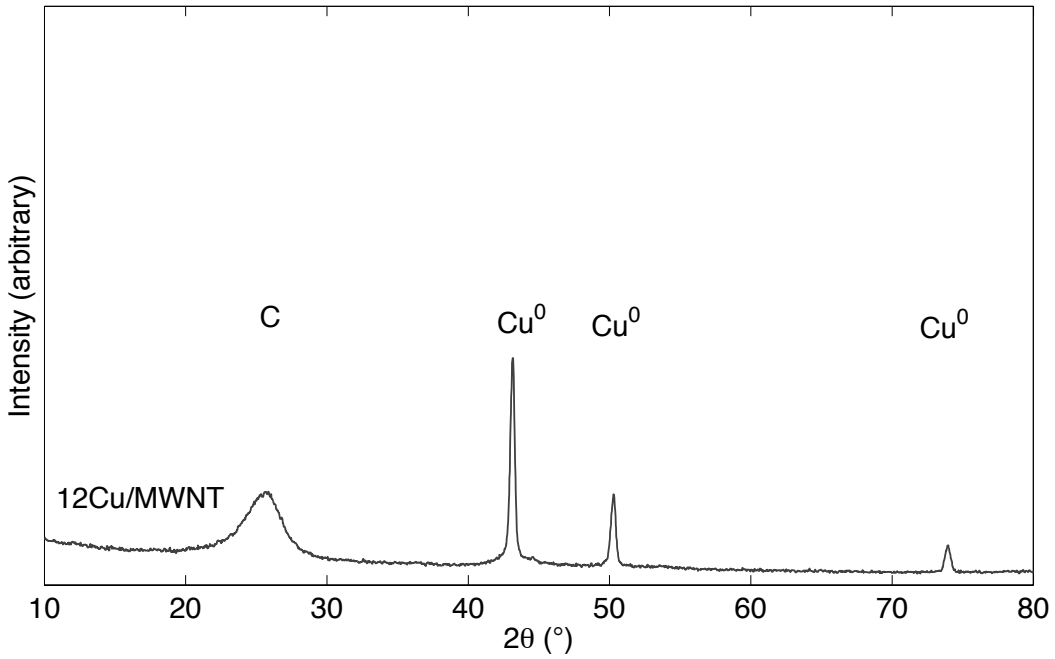

Figure 6-4 X-ray diffraction patterns of 12Cu/MWNT catalysts. Catalysts were reduced at 400 °C in flowing H_2 (25 vol.% in Ar) for 1 h (ramp rate of 10 °C min^{-1})

Ni (or Cu-Ni) crystallites size was calculated by the Scherrer equation (Eq. 2-4) (Scherrer, 1918), using the peak at $2\theta = 51.84$, which corresponds to the (200) plane (Figure 6-3). The results are shown in Table 6-2, together with the corresponding Ni (or Cu–Ni) dispersion calculated from Eq. 2-5, Where V is the Ni atomic volume (0.0109 nm^3), d is the crystallite size (nm) and A is the surface area of a single Ni atom (0.0649 nm^2) (Anderson, 1975). The addition of Cu to the Ni catalysts resulted in reduction of the crystallite size from 15.8 to 9.8 nm for 12Ni/MWNT and 1Cu–12Ni/MWNT samples, respectively. Also addition of 1 wt% Cu with 12 wt% Ni improved the Ni dispersion (Table 6-2). Unfortunately, higher amounts of Cu (6 and 12 wt%) did not promote further reduction in crystallite sizes of the Cu–Ni catalysts, and did not favour Ni dispersion as well. Investigation of the spent samples with XRD showed no detectable change for the 1Cu-12Ni/MWNT sample but substantial narrowing occurs for the 12Ni, 6Cu-12Ni and 12Cu-12Ni/MWNT catalysts. The average nickel crystallite size increased from 15.8 nm to 21.7 nm and the 12Cu-12Ni crystallites increased from 17.8 nm to 29.4 nm (Table 6-2). An increase in crystallite size from 13.7 nm to 24 nm was also detected for the spent 6Cu-12Ni/MWNT sample.

Table 6-2 Average crystalite size and metal dispertion

Catalysts	Crystal size (nm)[a]	M_{disp} (%)[b]	Crystal size (nm)[c]
12Ni/MWNT	15.8	6.4	21.7
1Cu-12Ni/MWNT	9.8	10.3	11.3
6Cu-12Ni/MWNT	13.7	7.4	24
12Cu-12Ni/MWNT	17.8	5.7	29.4
12Cu/MWNT	21.1	4.8	–

[a] Calculated by applying the Scherrer equation (§2.1.3) (Scherrer, 1918) to the XRD peak generated from the (200) plane of Ni and CuNi alloy in the freshly reduced catalysts (Figure 6-3).

[b] $\mathbf{M_{disp}}$ = metal dispersion of Ni and Cu-Ni alloy particles, calculated according to Eq. 2-5 (Anderson, 1975).

[c] Calculated by applying the Scherrer equation (§2.1.3) (Scherrer, 1918) to the XRD peak generated from the (200) plane of Ni and CuNi alloy in the spent catalysts after 110 h on-stream (Figure 6-11).

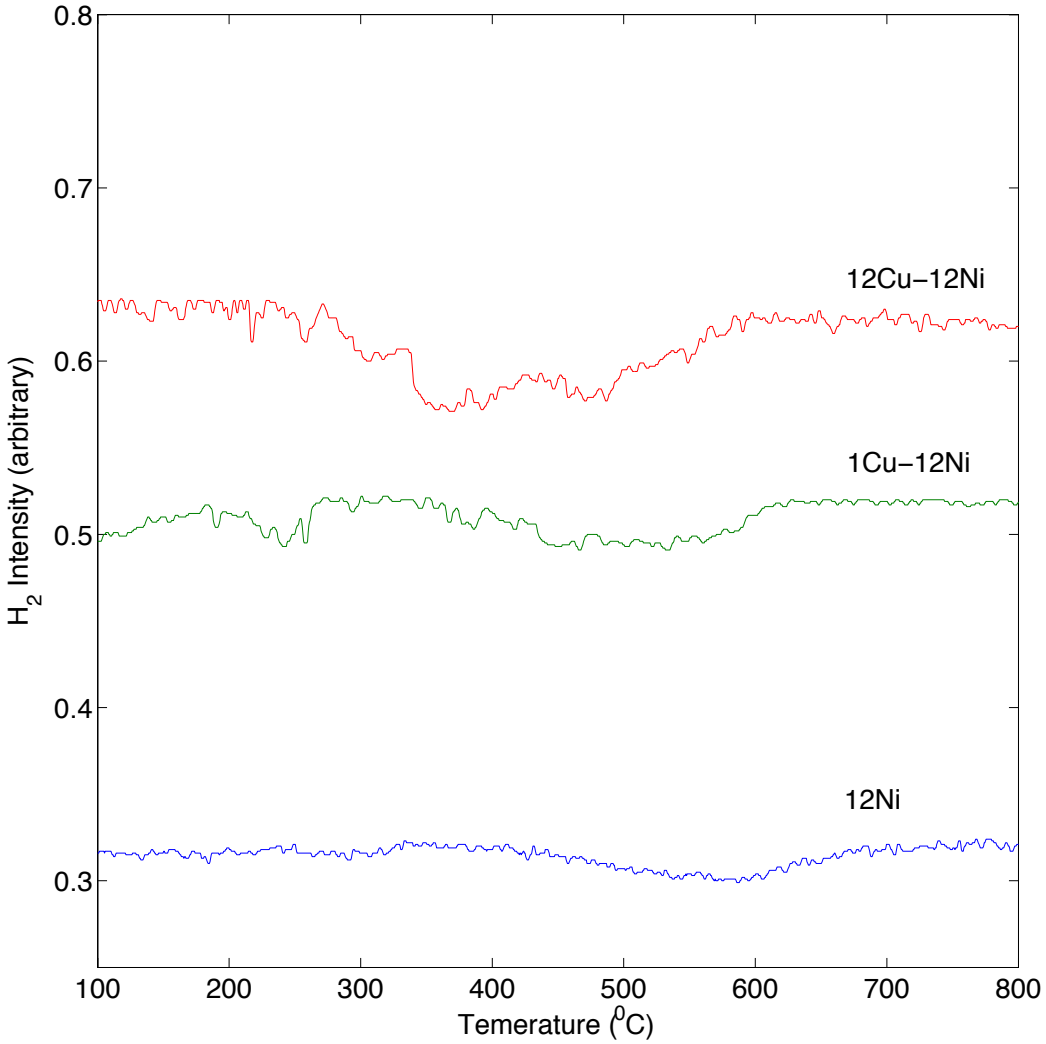

Figure 6-5 H_2-TPR profile of the xCu-12Ni/MWNT catalysts. Analysis conditions: ~50 mg sample, 1.6% H_2 in Ar, 30 sccm, heating at 10 °C/min over 100–800 °C, MS sampling at 15 scans/ min

H_2-TPR profiles of the calcined catalysts have shown in Figure 6-5. The 12Ni/MWNT sample showed reduction peak at about 580 °C, which corresponds to the reduction of the nickel species Ni^{2+} to Ni^0. This temperature is higher than that for pure NiO, which is reduced at 300–450 °C (Dussault et al., 2007), demonstrating an interaction of the nickel with the supported nanotubes. The 1Cu–

12Ni and 12Cu–12Ni/MWNT catalysts showed reduction peaks at lower temperature than the 12Ni/MWNT sample but at higher temperature than the pure 12Cu/MWNT sample (Pure CuO has a reduction temperature in the range of 200 to 400 °C (Dussault et al., 2005)), which indicates Cu-Ni alloy formation. This result is consistent with XRD result of Figure 6-3. TPR profile of xCu–12Ni/MWNT samples did not show two distinct peaks for Cu^0 and Ni^0, instead it showed one broad peak between Cu and Ni peaks. The TPR profiles (Figure 6-5) indicated that increasing the copper content results in a decrease in the reduction temperature of the nickel species, which can be associated with the spill over of hydrogen produced by Cu, accelerating the nucleation of the Ni metal, and increasing the reducibility (Ashok et al., 2008).

As shown in Figure 6-6, the Cu 2*p* XPS peak (Figure 6-6(a)) of xCu–12Ni catalysts shifted to higher binding energy compared to pure Cu catalyst, in particular to 1Cu-12Ni sample, indicating that the electronic structure of Cu was modified when Ni was introduced. Also Ni 2*p* peak (Figure 6-6(b)) intensity decreases as the Cu/Ni atomic ratio increases. The xCu–12Ni peak shifted to low binding energy compared to pure 12Ni peak. This result is similar to the results of Pt coated Au nanoparticles with core-shell structure (Zhao and Xu, 2006)

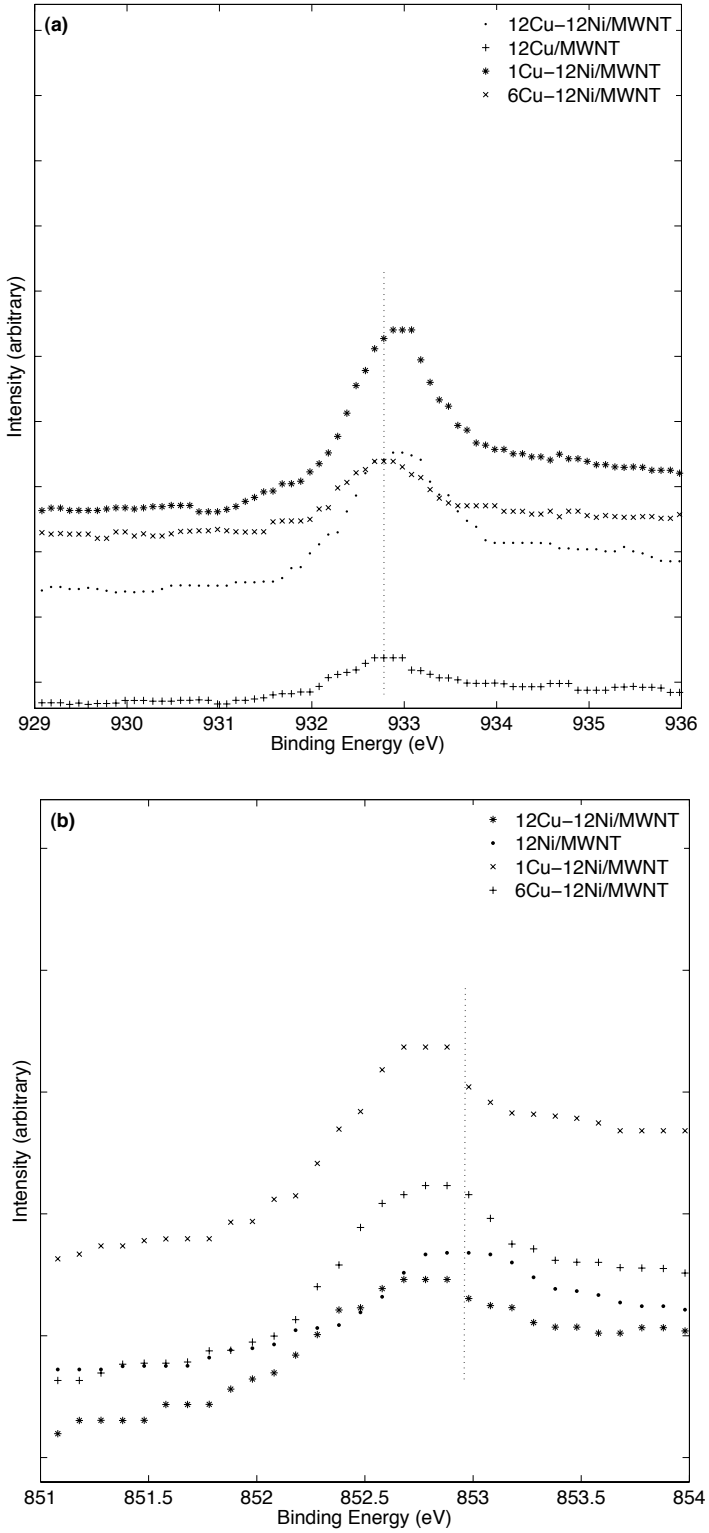

Figure 6-6 XPS patterns of Cu, Cu-Ni and Ni catalysts. Samples were reduced at 650 °C in flowing H_2 (25 vol.% in Ar) for 1 h (ramp rate of 10 °C min^{-1})

6.3.2 Catalytic tests

6.3.2.1 Effect of Cu on the catalytic activity

An aqueous solution with 1 wt% glycerol was used to evaluate the performance of the catalysts. All reactions were performed at 240 °C, 40 bar, and with a feed flow rate of 0.05 mL min^{-1}, irrespective of the catalyst used. Reaction results in terms of yield of gaseous products and H_2 selectivity are presented in Figure 6-7. Table 6-4 shows total glycerol conversion, gas phase carbon yield, system carbon balance and yield of acetol and lactic acid as the liquid by-products. The reaction data presented in Figure 6-7 and Table 6-4 shows that the aqueous-phase reforming of glycerol over any of the studied catalysts indeed leads to a hydrogen-rich gas phase. Alkanes other than methane (i.e ethane and propane) were only detected for 12Ni/MWNT and 12Cu–12Ni/MWNT catalyst in trace amounts and were not further quantified.

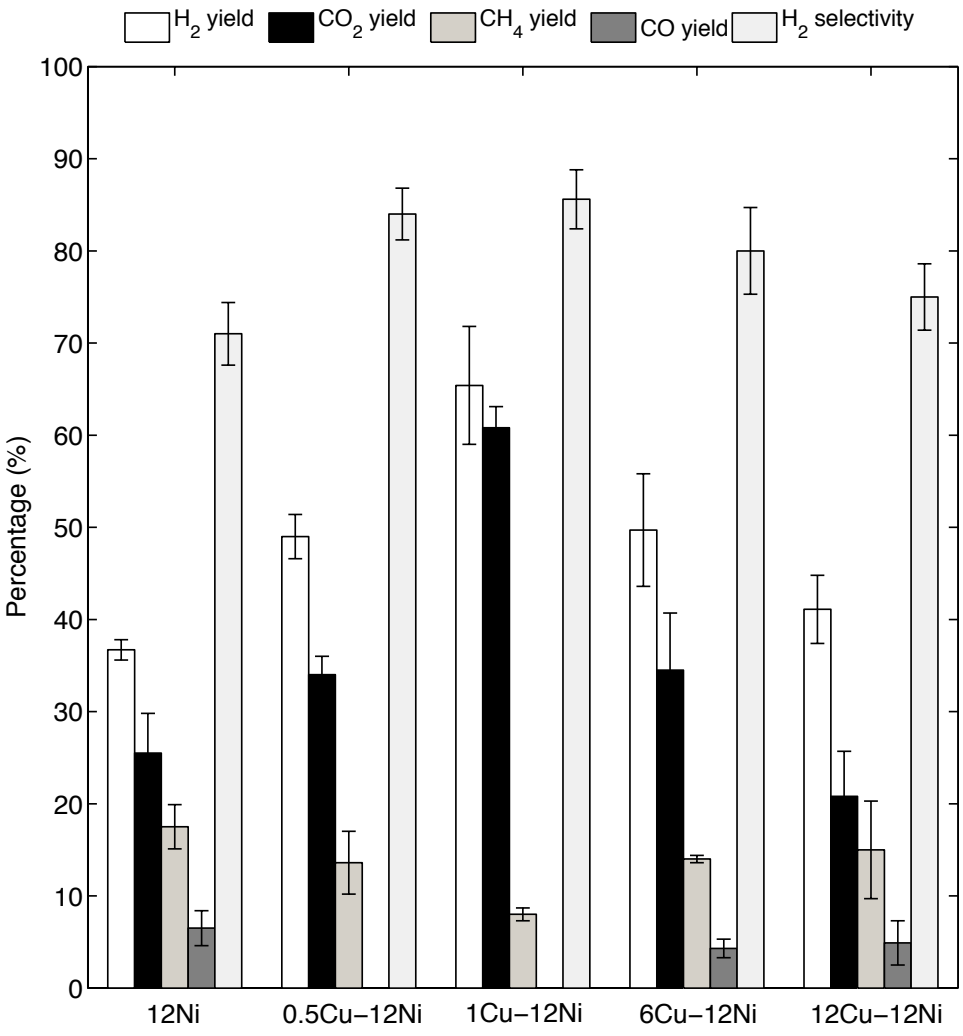

Figure 6-7 Effects of Cu addition to 12Ni/MWNT catalysts on yield and selectivity in the aqueous phase reforming of glycerol (240 °C, 40 bar, 0.05 mL/min, 150mg catalyst; data are mean values over t = 3–110 h). Error bars indicate one standard deviation; each bar is the average of ≥2 experiments

The H_2 yield from the APR of glycerol was calculated as the ratio of the amount of H_2 produced divided by the amount of H_2 that could have been produced if all of the glycerol was completely reformed to H_2 and CO_2 (i.e. 7 theoretical mol H_2/mol glycerol; refer to Eq. 4-3). Comparing the catalytic performance in terms of H_2 yield, all the Cu–Ni catalysts showed higher yield than Ni catalyst. Among the

Cu–Ni catalysts tested, 1Cu–12Ni catalyst showed highest H_2 yield (65.5%) and as the Cu loading increased H_2 yield decreased. H_2 yields reported in the literature are much lower than this, for example: <6% at 240 °C/40 bar for 12.5% Ni, 2.5% Pt and 12.5% Ni–2.5% Pt catalysts supported on alumina (Iriondo et al., 2011), and 22.6% at 250 °C/35 bar for 5 wt% Cu-20 wt% Ni catalyst supported on hydrotalcite-like compounds (HTLCs) (Manfro et al., 2013). The low concentration of feed (1 wt% glycerol in DI water) and optimised low flow rate (0.05mL/min) could be responsible for our reported high H_2 yield (65.5%). The same trend was observed for CO_2 yield, the main C-containing product in the gas phase, that could be due to high water gas shift reaction favoured by Cu (El Doukkali et al., 2012). Cu–Ni catalysts showed lower CO yield than the Ni catalyst as Cu is one of the most active metal in WGS reaction (Davda et al., 2005). No CO was detected for 0.5Cu-12Ni and 1Cu–12Ni catalyst, indicating that CO concentration in the product gas of these two catalysts was below the GC detection limit (i.e. [CO] ≤ 100 ppm) (Figure 6-8), and higher CO yield was observed for higher Cu loading (Figure 6-1). CH_4 formation was significant on the Ni catalyst, since Ni has high activity in methanation reaction (Davda et al., 2005), also Ni shows high activity in the cleavage of C–O bonds of oxygenated compounds (Cortright et al., 2002). The addition of Cu (up to 1 wt%) decreased the activity of the methanation reaction, which may be related to the formation of a Cu–Ni alloy, decreasing the number of clusters with multiple nickel atoms that are necessary for CO or H_2 dissociation. Also, there could be possibility that CO was just removed from the system by the WGS more efficiently when Cu was present,

and therefore less CO was available for methanation. Shabaker et al. (Shabaker et al., 2004) observed similar effect for Sn modified Ni catalysts. Lowest CH_4 yield was observed for 1Cu–12Ni/MWNT catalyst but CH_4 yield increased with higher (6 and 12 wt%) Cu loading.

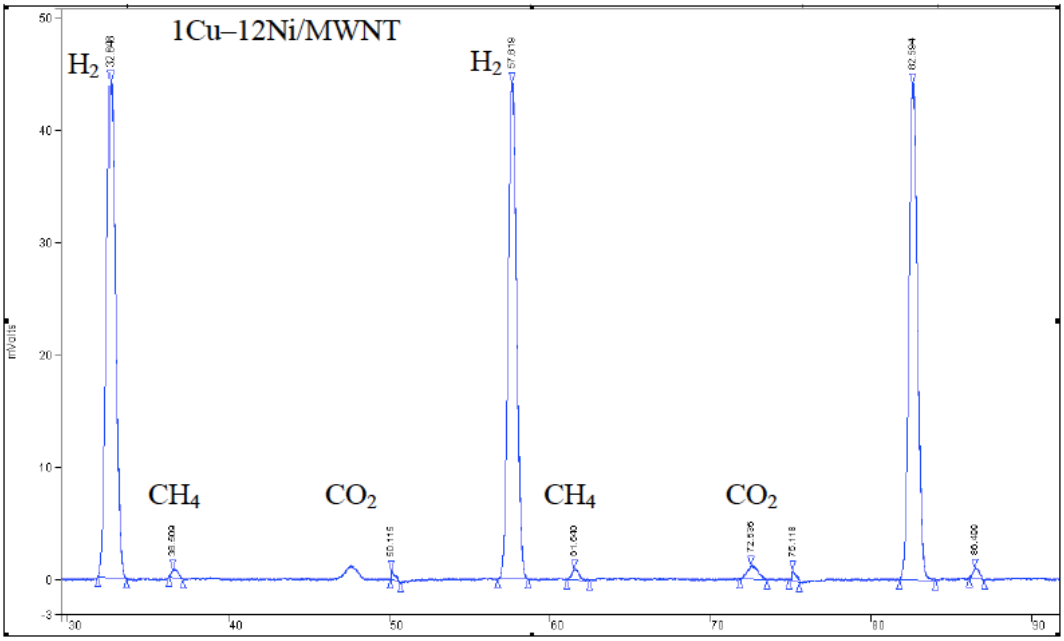

Figure 6-8 A representative GC curves from the APR of glycerol over 1Cu-12Ni/MWNT catalyst, as measured on the in-line Varian CP-3800 gas chromatograph. The product gas was sampled every 25 min.

Table 6-3 Gas phase composition over MWNT supported Ni and Cu-Ni catalysts (240 ºC, 40 bar, 0.05 mL/min, 150 mg catalyst; data are mean values over t = 3–110 h).

Catalysts	Gaseous products (v/v%)			
	H_2	CO_2	CH_4	CO
12Ni/MWNT	51.6	18.7	22.1	4.8
1Cu-12Ni/MWNT	77	16.5	6.5	0
6Cu-12Ni/MWNT	66.8	20.2	10.5	2.5
12Cu-12Ni/MWNT	65.3	15.8	13.4	3.7

The H_2 selectivity showed the same trend as H_2 yield; Cu-Ni catalysts were more selective towards H_2 production than Ni catalyst. 1Cu–12Ni catalyst showed higher (86%) H_2 selectivity but the selectivity decreased with higher (12 wt%) Cu loading. The H_2 selectivity obtained here are quite similar with those reported by Lehnert and Claus (Lehnert and Claus, 2008) for 3 wt% Pt catalysts supported on alumina (highest H_2 selectivity obtained was 85% at 250 °C/20 bar, 10 wt% glycerol at a flow rate of 0.5 ml min^{-1}) and Cortright et al. (Cortright et al., 2002) for 3 wt% Pt catalysts supported on nanofibers of γ-alumina (highest H_2 selectivity obtained was 75% at 225 °C/29 bar, 10 wt% glycerol at a flow rate of 0.06 ml min^{-1}). Also our observed H_2 selectivity was just double that reported by Manfro et al. (Manfro et al., 2013): 40% at 250 °C/35 bar, for 10 wt% glycerol through 1.25 gm catalyst (5 wt% Cu-20 wt% Ni supported on HTLCs). Compairing with C supported Pt and Pt-Re catalyst, H_2 selectivity was higher than reported by King et al. (King et al., 2010): 56% at 225 °C/30 bar, 10 wt% glycerol through 200 mg catalyst. Also, crystallite size and metal dispersion (Table 6-2) has an effect on the H_2 selectivity and catalytic activity. Wawrzetz et al. (Wawrzetz et al., 2010) showed that H_2 formation decreased in APR of glycerol with increasing Pt crystallite size. On the other hand, Lehnert and Claus (Lehnert and Claus, 2008) showed that bigger Pt crystallites led to a higher H_2 selectivity, concluding that adsorption of glycerol can be realized preferably at face positions. Iriondo et al. (Iriondo et al., 2011) also observed that lower dispersion of Ni and PtNi catalysts provided a higher activity for APR of glycerol. Considering that the Ni catalyst, which has the lowest dispersion but highest crystallite size (Table 6-2), presented

the lowest H_2 selectivities, our results seem to agree with Wawrzetz et al. (Wawrzetz et al., 2010).

The composition of gas phase is given in Table 6-3. Over 1Cu-12Ni/MWNT catalyst, the gas phase consists almost exclusively of H_2 and CO_2, and the highest H_2 yield (65.5%) was obtained for this catalyst (Figure 6-7). Also no CO was observed for this catalyst. The formation of large amount of undesired methane was observed for the 12Ni/MWNT catalyst. The addition of Cu to the Ni catalysts resulted in decrease of methane formation from 22 to 6.5% for 12Ni/MWNT and 1Cu–12Ni/MWNT samples, respectively. Unfortunately, higher amounts of Cu (6 and 12 wt%) did not promote further decrease of methane formation (Table 6-3), and did not favour H_2 yield as well (Figure 6-7).

Table 6-4 Glycerol conversion, Gas phase C yield, and Liquid by-products yield in the aqueous-phase reforming of glycerol over MWNT supported catalysts (240 ºC, 40 bar, 0.05 mL/min, 150 mg catalyst; data are mean values over t = 3–110 h).

Catalysts	Total Gly. Conv. (%)	Gas phase C yield (%)	C Balance, out/in (%)	H_2/CO_2 (molar)	Y_{acetol}	$Y_{lactic\ acid}$
12Ni/MWNT	44	39	96	1.4	0.0	0.03
0.5Cu-12Ni/MWNT	60	54	103	1.8	0.0	0.08
1Cu-12Ni/MWNT	84	76	101	1.9	0.0	0.10
6Cu-12Ni/MWNT	77	47	98	1.5	0.16	0.13
12Cu-12Ni/MWNT	68	34	95	1.7	0.22	0.09

Ni–Cu catalysts presented higher total glycerol conversion and gas phase C yield, although they also favored formation of liquid by-products, especially acetol and lactic acid (Table 6-4). The higher glycerol conversion (84%) and gas phase C

yield (76%) was observed by 1Cu–12Ni/MWNT catalyst but as the Cu loading increased both of them decreased gradually. Thus the total glycerol conversion and gas phase C yield reported here are higher than in the literature: 52.4% glycerol conversion for 3Pt–1Re/C catalyst at 225 °C/30 bar with 53.1% gas phase C yield (King et al., 2010) and 45% glycerol conversion for $3Pt/Al_2O_3$ catalyst at 250 °C/30 bar (Lehnert and Claus, 2008), always using 10 wt% glycerol solution at 0.5 ml min^{-1}. The observed H_2/CO_2 ratio is always below the theoretical ratio of 7/3, indicating that the overall reaction did not occur purely by APR process; many side reactions take place simultaneously (Luo et al., 2008, King et al., 2010). The H_2/CO_2 ratio observed by King et al. (King et al., 2010) with 3Pt-1Re/C catalysts at 225 °C/30 bar were quite similar (1.4 – 2.1) with those presented here.

Figure 6-9 shows catalyst stability with time on-stream. Even though, 12Ni/MWNT, showed promising results compared to highly expensive noble metal catalyst, $3Pt/Al_2O_3$, (Rahman et al., 2013) but it showed severe deactivation after 40 hours on stream, infact H_2 peak was completely disappeared after 70 h on stream (Figure 6-9). Also 6Cu-12Ni/MWNT and 12Cu-12Ni/MWNT catalyst showed deactivation and H_2 yield gradually decreased with time on-stream. High sintering of the active phase, as a result the particle size increased (Table 6-2) in relation to the fresh reduced phase could be partly responsible for their deactivation (Figure 6-9). Please note that these samples might also form a metal oxide layers on their surfaces which have diffraction lines with such low intensity that they are below the detection limit of XRD. On the other hand, no such deactivation was observed for 0.5Cu-12Ni/MWNT and 1Cu-12Ni/MWNT catalyst

for 110 h on-stream.

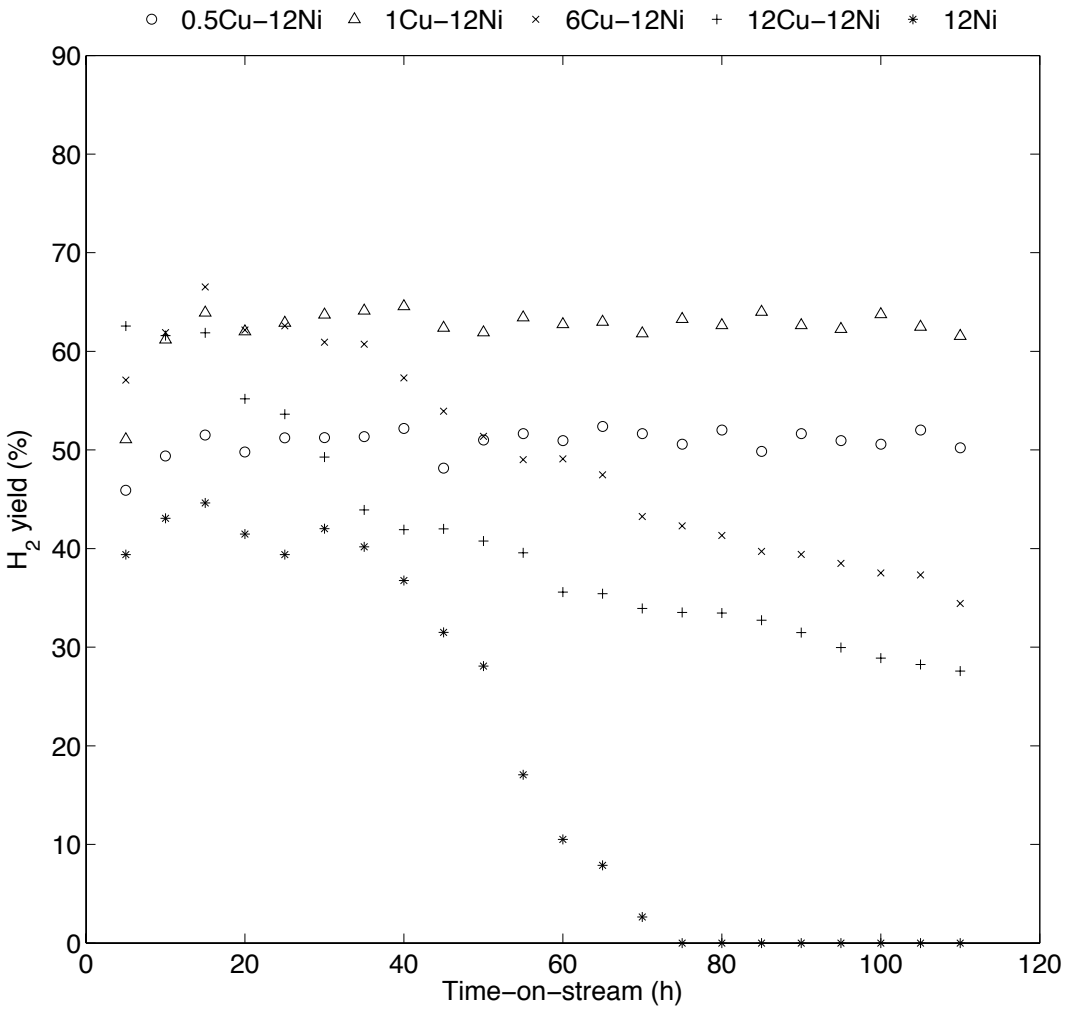

Figure 6-9 Variation of H_2 yield with time-on-stream in the APR of glycerol (240 °C, 40 bar, 1 wt% glycerol, 0.05 mL/min, 150 mg catalyst)

Among the bimetallic Cu-Ni catalysts we tested, 1Cu–12Ni/MWNT gave the highest H_2 yield, glycerol conversion, gas phase C yield, H_2 rate, lowest CH_4 yield and no CO concentration. So to further investigate the stability of the 1Cu–12Ni/MWNT catalyst, 2 more runs were made each with 110 h on stream, the

results were depicted in Figure 6-10. After the first run, the reactor was heated at 120 °C for 6 h and at the same time flushed with Ar to get ride of all the gaseous and liquid species in the reactor. As shown in Figure 6-10, no severe deactivation was observed even after 330 h on-stream (each run 110 h). XRD analysis of spent 1Cu-12Ni/MWNT catalysts (after 3rd run) showed no diffraction peaks for NiO and CuO phase (Figure 6-11). This means no metallic (Ni or Cu-Ni) phase was oxidized, which causes catalyst deactivation (Iriondo et al., 2008, Wen et al., 2008). Only an increase in particle size was observed in relation to the fresh reduced phase (based upon the Ni (200) plane, calculated particle sizes were 9.8, 11.3, 12.2 and 12.7 nm for the fresh, after 1st run, 2nd run and 3rd run, respectively), indicating a small sintering of the active phase. However, despite this sintering, no deactivation was observed with time on –stream (more than 330 h). Inductively coupled plasma atomic emission spectrometry (ICP–AES) analysis of the liquid effluent (1Cu–12Ni/MWNT catalyst, after 3RD run) showed no measurable leaching of Cu and Ni particles.

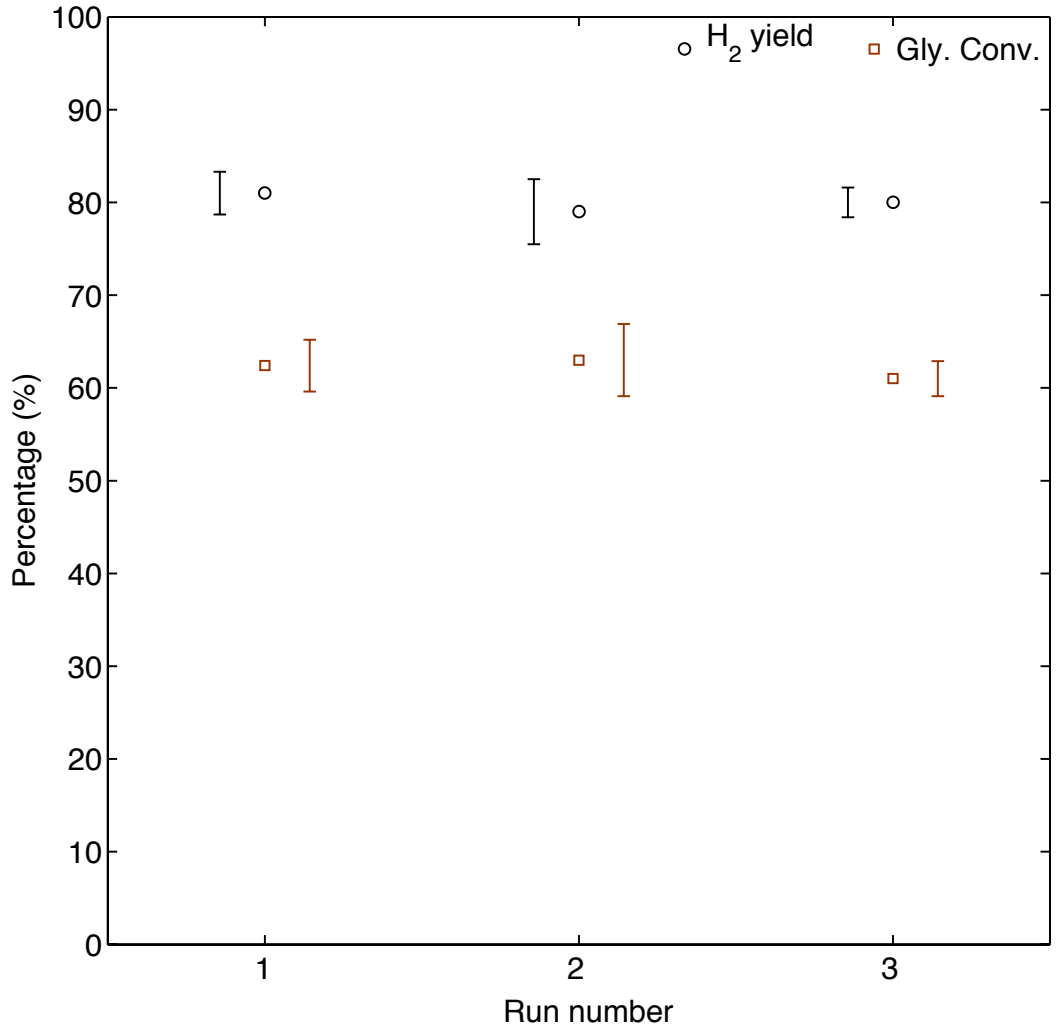

Figure 6-10 Repeated runs in the ARR of glycerol on 1Cu–12Ni/MWNT catalyst (240 °C, 40 bar, 1 wt% glycerol, 0.05 mL/min, 150 mg catalyst; data are mean values over t = 3–110 h). Error bars indicate one standard deviation; each bar is the average of ≥2 experiments

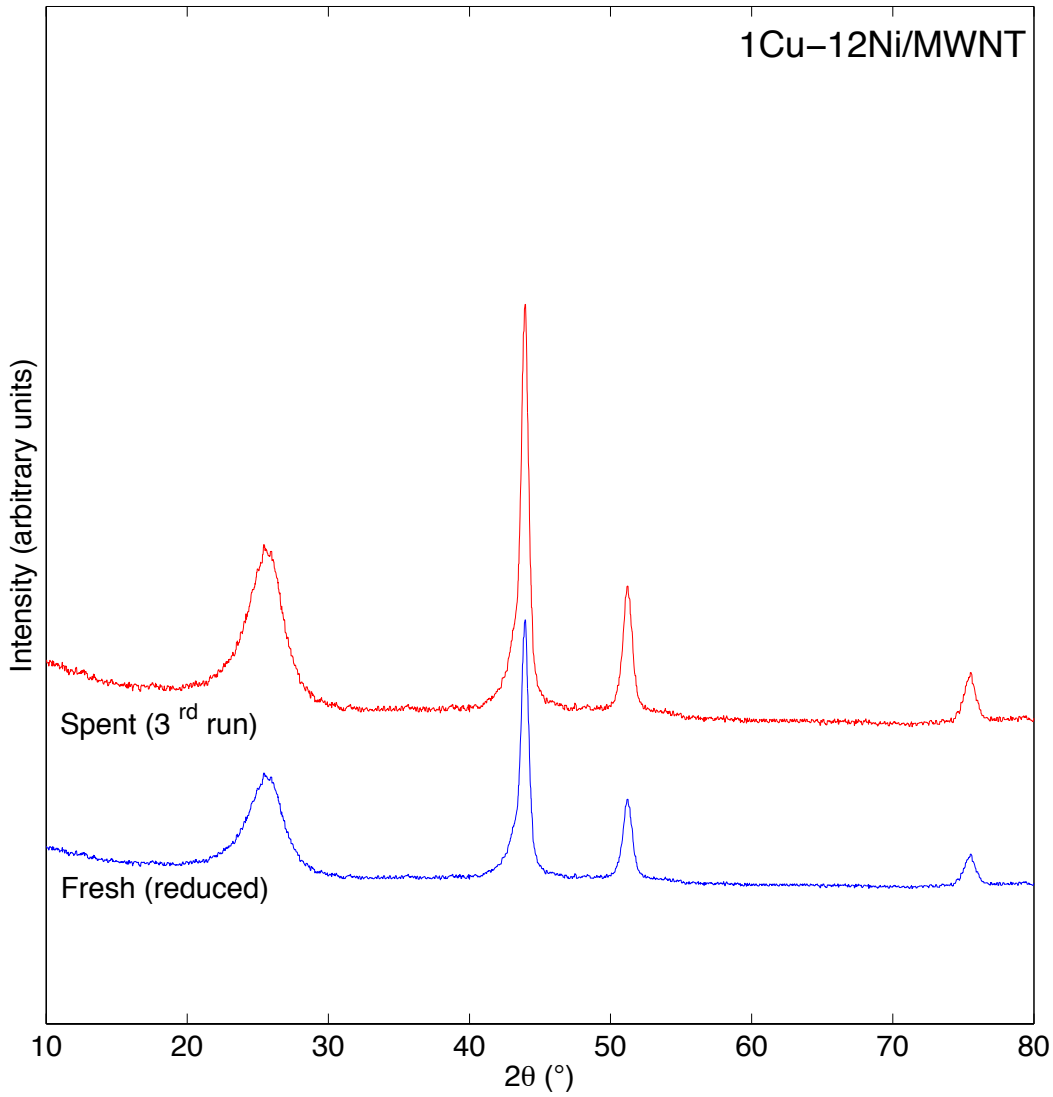

Figure 6-11 X-ray diffraction patterns of fresh (reduced at 650 °C in flowing H_2 for 1 h at 10 °C/min) and spent (after 3rd run of APR) 1Cu-12Ni/MWNT.

6.3.2.2 Effect of WGS reaction on H_2 yield in ARR

An important advantage of APR (Eq. 4-3) is the ability of producing 7 moles of hydrogen per 1 mole of glycerol– 4 moles from glycerol reforming (Eq. 4-1) and 3 moles from WGS reaction (Eq. 4-2). To investigate the fact, WGS reaction was

studied using the same reactor system and same reaction conditions (240 °C, 40 bar, 150 mg catalyst) was applied for APR process to investigate the catalyst performance. Instead of using 1 wt% glycerol in DI water, 0.05 ml/min DI water and 0.39 ml/min CO was introduced in the reactor as the reactant. The produced gas mixture was analyzed using an online gas chromatograph (Varian CP-3800). The carbon balance agreed within ±6 mol.%. Figure 6-12 shows the total CO conversion, H_2 yield and CH_4 yield. Supported Ni and Cu–Ni catalysts showed higher CO conversion and H_2 yield compare to WGS reaction without any catalyst (Figure 6-12). In the case of CuNi bimetallic catalysts, higher CO conversion and H_2 yield was observed as compared to 12Ni catalyst. But CO conversion tends to decrease as the Cu loading increased.

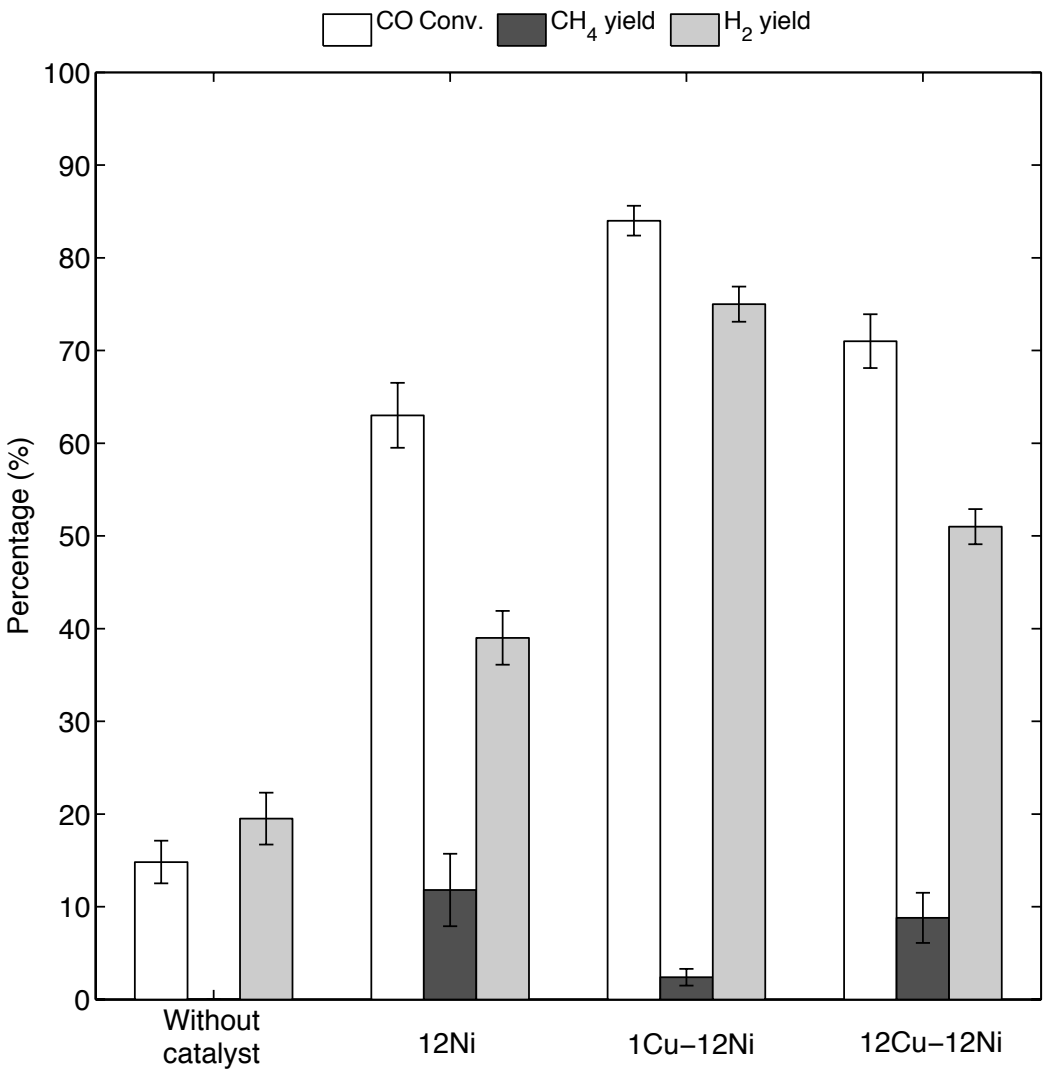

Figure 6-12 WGS study without catalyst and with catalysts (240 °C, 40 bar, 0.05 mL/min DI water, 0.39 mL/min CO, 150 mg catalyst; data are mean values over t = 3–20 h). Error bars indicate one standard deviation; each bar is the average of ≥2 experiments

When carrying out the WGS reaction, methane can be formed by CO/CO_2 hydrogenation in a methanation reaction (Haryanto et al., 2009). It has been reported that Ni is an effective catalyst for the methanation reaction (Takenaka et al., 2004). Since methanation consumes H_2 (Eq. 4-4), the higher the CH_4 yield, the lower the H_2 yield in the WGS reaction. Figure 6-12 shows methane yield during

the WGS reaction and significant methane formation was observed for the monometallic 12Ni catalyst. This is an indication of the potential drawbacks of Ni as a WGS catalyst. For supported bimetallic Cu–Ni catalysts, CO conversion progressively decreased with higher Cu content (Figure 6-12). However, supported Cu–Ni alloy catalysts were still highly active, the 1Cu–12Ni/MWNT catalyst showed the CO conversion about 84%. The addition of only 1wt% Cu, however, was sufficient to reduce methane yield from 12 to 3 %. The methanation reaction was further increased as the Cu content increased in the alloy catalysts. These results revealed important modifications of the surface properties of bimetallic catalysts, indicated by XRD and H_2–TPR. The 1Cu–12Ni/MWNT catalyst showed the best WGS performance among all catalysts. The presence of Cu produced favorable structural and electronic effects for enhancing the WGS activity and suppressed undesirable methanation side-reactions that resulted in greater H_2 yield in the WGS reaction.

6.4 Conclusions

Bimetallic Cu–Ni catalyst supported on carbon nanotubes showed higher activity and selectivity towards hydrogen than the monometallic Ni catalyst in the APR of glycerol. Bimetallic 1Cu–12Ni/MWNT catalyst gave the higher H_2 selectivity (86%) and glycerol conversion (84%) than the bench mark 12Ni/MWNT catalyst. Irrespective of Cu and Ni ratio, bimetallic Cu–Ni catalysts showed higher selectivity and glycerol conversion. The presence of Cu (1 wt%) in bimetallic

catalysts resulted in suppression of undesirable methanation reaction and enhancement of WGS reaction. The high activity and selectivity of Cu–Ni catalysts is related to the interaction between Cu and Ni, enhancement of metal dispersion and Ni reducibility.

This page intentionally left blank

Chapter 7 Summary and Recommendations

7.1 Summary

Glycerol is a biomass-derived by-product of biodiesel industry, produced from the transesterification of vegetable oils or animal fats. As world biodiesel production increases exponentially, the crude glycerol is also produced in a large amount. Consequently, the price of glycerol dropped down tremendously; only $0.02/kg for crude glycerol in 2010. One alternative use of glycerol is hydrogen and valuable chemical production by aqueous-phase reforming (APR). The APR process, pioneered by the Dumesic group, uses supported metal catalysts under mild reaction conditions (200–250 °C, 20–50 bar) for the production of hydrogen from oxygenated hydrocarbons in a single step. The APR process is promising because it gives higher energy efficiency, eliminates undesirable decomposition reactions, which are typically encountered at elevated temperatures and the less complex processing requirements associated with the single reactor APR reaction than the multi-reactor steam reforming system. Additionally, since water-gas-shift (WGS) reaction is an exothermic reaction, it favors low temperatures, resulting in low levels of CO (<300 ppm) than conventional steam reforming processes, a contaminant that poses well-known problems to the use of hydrogen in fuel cell applications. This study focuses on hydrogen and oxygenated products formation via the APR of glycerol over various supported catalysts that carried out at relatively low temperature and pressure.

Firstly, the effect of ceria doping with alumina support and various reaction parameters like Pressure, Temperature, Fed flow rate, Glycerol concentration in fed, and Weight hourly space velocity are examined and discussed in Chapter 3, to get a optimum condition for APR of glycerol. Here a series of Pt catalysts supported on Al_2O_3 doped with different amounts (in wt%) of CeO_2 were developed and tested in the aqueous-phase reforming of glycerol to H_2. The catalyst 3Pt/3CeAl showed the highest glycerol conversion (95%), carbon conversion to gas (85%) and hydrogen yield (80%) for a 1 wt% solution of glycerol fed at 0.05 mL/min, at 240 $^{\circ}$C under the corresponding system pressure (40 bar). Compared to 3Pt/Al, 1Pt/3CeAl showed higher H_2 selectivity and carbon conversion to gas, as well as much lower CH_4 yield, clearly evincing the effect of adding 3 wt% ceria to the alumina catalyst support in the Pt-catalyzed APR of glycerol. H_2-chemisorption results showed that highest metal dispersion (58%) and active surface area (4.3 m^2/g) was achieved for 3 wt% CeO_2 doping in the alumina support, and these are thought to be partly responsible for the high hydrogen yield and carbon conversion to gas. No CO could be detected in the product gas, meaning that it may be directly useable in a PEM fuel cell. Thus, Pt supported on ceria-doped alumina had both higher catalyst activity and higher selectivity towards H_2 generation from the APR of glycerol than an unpromoted alumina-supported Pt catalyst.

Secondly, bimetallic Pt-Ni catalysts are studied in Chapter 4. Although Pt is the most active catalyst for aqueous phase reforming (APR) of glycerol to generate H_2, it is expensive. We studied its possible minimization to levels where

acceptable H_2 yields are still maintained. When an additional catalytic metal, Ni, was introduced to our Pt/CeO_2–Al_2O_3 catalyst, the Pt content could be reduced from 3 to 1 wt%, with a slight increase in H_2 production. In Chapter 4, Pt and Ni in various ratios were supported on alumina doped with 3 wt% ceria, and the resulting materials were characterized and tested as catalysts for the APR of glycerol. Amongst the catalysts tested, bimetallic 1Pt-6Ni/3CeAl (containing 1 wt% Pt and 6 wt% Ni) gave the highest H_2 yield (86%) and gas-phase C yield (94%). Thus, although 3Pt/3CeAl (in chapter 3) and 1Pt-6Ni/3CeAl (in chapter 4) catalyst produced almost same amount of H_2 (1.8 and 1.9 mmol, respectively) per gram of catalyst per hour, the latter produced three times as much H_2 per gram of Pt per hour (195 mmol); this measure is crucial to the competitiveness of a catalyst in large-scale H_2 production. X-ray diffraction (XRD) patterns and thermogravimetric analyses of the spent catalysts showed no serious catalyst deactivation by carbon deposition after 30 h on stream, except in the case of Pt-free 6Ni/3CeAl, which ceased to produce H_2 after 15 h on stream. XRD and X-ray photoelectron spectroscopic analyses demonstrated that adding Ni impacted both the crystallite and electronic structure of Pt. These effects likely conspired to produce the high glycerol conversion and gas phase C yield and, ultimately, the high H_2 yield observed over 1Pt-6Ni/3CeAl.

In 3rd step, the influence of support in APR of glycerol is discussed in Chapter 5 using monometallic Pt catalysts supported on carbon nanotubes (MWNT), MgO, and Al_2O_3. Here, Pt/MWNT showed better APR performance with regards to H_2 yield, Gas phase C yield and products distribution. This could be due to high

porosity, higher metal dispersion and hydropobic nature of carbon nanotube. And then bimetallic Pt-Ni catalyst supported on MWNT and $3CeO_2–Al_2O_3$ is discussed. Amongst the catalysts tested, bimetallic 1Pt-3Ni supported on MWNT gave the higher H_2 yield (93%) and selectivity (91%). Irrespective of Pt and Ni ratio, bimetallic Pt-Ni catalysts showed about two times higher activity and selectivity towards H_2 production than the monometallic Pt catalysts. Catalyst characterization by XRD, XPS showed a peak shift of Pt in bimetallic Pt-Ni catalyst than the monometallic Pt catalyst. Also the presence of Pt and Ni emission lines, in STEM-EDS spectra, from both the bulk and the single crystal particles strongly suggests that Pt is present in close vicinity of Ni particle. Also H_2 chemisorption analysis showed higher metal dispersion (46%) for 1Pt-3Ni/MWNT catalyst.

Noble metals catalyst have high activity for reforming reactions and resistance to carbon deposition as discussed in Chapter 3, 4 and 5. However, considering the high cost, it is more economical to develop non-noble metals catalyst such as Ni, which shows a good activity for C–C bond scission. Cu, on the other hand, has high activity for the water-gas shift reaction, thus favoring the selectivity to hydrogen. In Chapter 6, Aqueous-phase reforming of glycerol is investigated over a series of Ni and Cu–Ni bimetallic catalysts supported on multiwalled carbon nanotubes (MWNT). Amongst the catalysts tested, bimetallic 1Cu–12Ni/MWNT catalyst gave the higher H_2 selectivity (86%) and glycerol conversion (84%) than the benchmark 12Ni/MWNT catalyst. Irrespective of Cu and Ni ratio, bimetallic Cu-Ni catalysts showed higher selectivity and glycerol conversion towards H_2

production than Ni catalyst. The presence of Cu in bimetallic catalysts resulted in suppression of undesirable methanation reaction. Catalysts characterized by XRD and XPS showed a significant peak shift of Ni in bimetallic Cu–Ni catalysts than the Ni catalyst, suggesting a strong interaction between Cu and Ni. Also H_2–TPR analysis showed that introducing Cu increased Ni reducibility.

7.2 Recommendations

Non-noble based bimetallic Cu-Ni catalyst showed promising results compared to highly expensive noble metal Pt, on catalytic activity and selectivity towards hydrogen production from APR of glycerol. However, some more work is recommended to do in future:

- To use as a commercial catalyst, the regenaration ability of Cu-Ni alloy should be studied;
- Although the reflux method worked well for Cu-Ni alloy catalyst, other methods are still expected to try to get higher metal dispersion;
- After 3rd successive run, the activity of Cu-Ni alloy catalyst decreased tremendously. The reasons should be studied for its commercial use;
- The application in large-scale reactors should be considered when a screening and fundamental research was fulfilled;
- In order to further lower the energy required for the process, higher concentrations of glycerol with greater flow rates should be studied;
- In order to lower CO concentration (< 5 ppm) in the product gas, further study should be made, so that product gas could be directly used in the PEM fuel cell;
- Real bio-glycerol, having very high concentration and impurities like Na, K and methanol etc., should be studied to see its affect on catalyst

performance.

- External metal deposition on nano-tubes has less catalytic effect than internal metal deposition, which is called confinement effect. This confinement effect of nano-tubes should be studied in APR of glycerol.

References

ADHIKARI, S., FERNANDO, S. D. & HARYANTO, A. 2008. Hydrogen production from glycerin by steam reforming over nickel catalysts. *Renewable Energy,* 33**,** 1097-1100.

ANA VALIENTE, JOS´E A. MEDRANO, MIRIAM OLIVA, JOAQUIN RUIZ, LUC´IA GARC´IA, A. & ARAUZO, J. 2010. Bioenergy II: Hydrogen Production by Aqueous-Phase Reforming. *INTERNATIONAL JOURNAL OF CHEMICAL REACTOR ENGINEERING,* 8.

ANDERSON, J. R. 1975. *Structure of Metallic Catalysts, Academic Press Inc., London*.

ASEDEGBEGA-NIETO, E., GUERRERO-RUÍZ, A. & RODRÍGUEZ-RAMOS, I. 2005. Study of CO chemisorption on graphite-supported Ru–Cu and Ni–Cu bimetallic catalysts. *Thermochimica Acta,* 434**,** 113-118.

ASHOK, J., SUBRAHMANYAM, M. & VENUGOPAL, A. 2008. Hydrotalcite structure derived Ni–Cu–Al catalysts for the production of H2 by CH4 decomposition. *International Journal of Hydrogen Energy,* 33**,** 2704-2713.

BAK, K. & HILAIRE, L. 1993. Quantitative XPS analysis of the oxidation state of cerium in Pt-CeO2/Al2O3 catalysts. *Applied Surface Science,* 70–71, Part 1**,** 191-195.

BAKER, R. T. K., DUMESIC, J. A. & CHLUDZINSKI JR, J. J. 1986. The effect of various bimetallics on the graphite-steam reaction. *Journal of Catalysis,* 101**,** 169-177.

BARBIER JR, J. & DUPREZ, D. 1993. Reactivity of steam in exhaust gas catalysis I. Steam and oxygen/steam conversions of carbon monoxide and of propane over PtRh catalysts. *Applied Catalysis B: Environmental,* 3**,** 61-83.

BARRETT, E. P., JOYNER, L. G. & HALENDA, P. P. 1951. The Determination of Pore Volume and Area Distributions in Porous Substances. I. Computations from Nitrogen Isotherms. *Journal of the American Chemical Society,* 73**,** 373-380.

BATES, S. P. & VAN SANTEN, R. A. 1998. The Molecular Basis of Zeolite Catalysis: A Review of Theoretical Simulations. *In:* D.D. ELEY, W. O. H. B. G. & HELMUT, K. (eds.) *Advances in Catalysis.* Academic Press.

BEHR, A., EILTING, J., IRAWADI, K., LESCHINSKI, J. & LINDNER, F. 2008. Improved utilisation of renewable resources: New important derivatives of glycerol. *Green Chemistry,* 10**,** 13-30.

BLOM, R., DAHL, I. M., SLAGTEM, Å., SORTLAND, B., SPJELKAVIK, A. & TANGSTAD, E. 1994. Carbon dioxide reforming of methane over lanthanum-modified catalysts in a fluidized-bed reactor. *Catalysis Today,* 21**,** 535-543.

BOGA, D. A., OORD, R., BEALE, A. M., CHUNG, Y.-M., BRUIJNINCX, P. C. A. & WECKHUYSEN, B. M. 2012. *CHEMCATCHEM***,** DOI: 10.1002/cctc.201200112.

BOGA, D. A., OORD, R., BEALE, A. M., CHUNG, Y.-M., BRUIJNINCX, P. C. A. & WECKHUYSEN, B. M. 2013. Highly Selective Bimetallic Pt-Cu/Mg(Al)O Catalysts for the Aqueous-Phase Reforming of Glycerol. *ChemCatChem,* 5**,** 529-537.

BRADFORD, M. C. J. & ALBERT VANNICE, M. 1999. The role of metal–support interactions in CO2 reforming of CH4. *Catalysis Today,* 50**,** 87-96.

BRUNAUER, S., EMMETT, P. H. & TELLER, E. 1938. Adsorption of Gases in Multimolecular Layers. *Journal of the American Chemical Society,* 60**,** 309-319.

ÇAĞLAYAN, B. S., AVCI, A. K., ÖNSAN, Z. İ. & AKSOYLU, A. E. 2005. Production of hydrogen over bimetallic Pt–Ni/δ-Al2O3: I. Indirect partial oxidation of propane. *Applied Catalysis A: General,* 280**,** 181-188.

CALLISTER, W. D. 7 th edition, 2007. Materials science and Engineering: An introduction. *John wiley & Sons, New YORK,* Ch. 9, Vil. 1**,** 184-257.

CHAKRABART, D. J., LAUGHLIN, D. E., CHEN, S. W. & CHANG, Y. A. 1991. *Desk Handbook: Phase Diagrams for Binary Alloys, ASM International***,** 85-95.

CHOI, Y. H. & LEE, W. Y. 2001. Effect of second metals and Cu content on catalyst performance of Ni–Cu/SiO2 in the hydrodechlorination of 1,1,2-trichloroethane into vinyl chloride monomer. *Journal of Molecular Catalysis A: Chemical,* 174**,** 193-204.

CHORNET, E., CZERNIK, S., FRENCH, R. & FEIK, C. 2002. *Ind. Eng. Chem. Res.,* 41**,** 4209.

COMAS, J., MARIÑO, F., LABORDE, M. & AMADEO, N. 2004. Bio-ethanol steam reforming on Ni/Al2O3 catalyst. *Chemical Engineering Journal,* 98**,** 61-68.

CORTRIGHT, R. D., DAVDA, R. R. & DUMESIC, J. A. 2002. Hydrogen from catalytic reforming of biomass-derived hydrocarbons in liquid water. *Nature,* 418**,** 964-967.

CRISAFULLI, C., SCIRÈ, S., MINICÒ, S. & SOLARINO, L. 2002. Ni–Ru bimetallic catalysts for the CO2 reforming of methane. *Applied Catalysis A: General,* 225**,** 1-9.

DAL SANTO, V., GALLO, A., NALDONI, A., GUIDOTTI, M. & PSARO, R. 2012. Bimetallic heterogeneous catalysts for hydrogen production. *Catalysis Today,* 197**,** 190-205.

DAMYANOVA, S. & BUENO, J. M. C. 2003. Effect of CeO2 loading on the surface and catalytic behaviors of CeO2-Al2O3-supported Pt catalysts. *Applied Catalysis A: General,* 253**,** 135-150.

DAVDA, R. R. & DUMESIC, J. A. 2004. Renewable hydrogen by aqueous-phase reforming of glucose. *Chemical Communications,* 0**,** 36-37.

DAVDA, R. R., SHABAKER, J. W., HUBER, G. W., CORTRIGHT, R. D. & DUMESIC, J. A. 2003. Aqueous-phase reforming of ethylene glycol on silica-supported metal catalysts. *Applied Catalysis B: Environmental,* 43**,** 13-26.

DAVDA, R. R., SHABAKER, J. W., HUBER, G. W., CORTRIGHT, R. D. & DUMESIC, J. A. 2005. A review of catalytic issues and process conditions

for renewable hydrogen and alkanes by aqueous-phase reforming of oxygenated hydrocarbons over supported metal catalysts. *Applied Catalysis B: Environmental,* 56**,** 171-186.

DUMESIC, J. Catalytic strategies for the conversion of biomass-derived carbohydrates to liquid hydrocarbon fuels. 2010. American Chemical Society, AETECH-2.

DUMESIC, J., SIMONETTI, D. A. & KUNKES, E. L. 2009. *Single-reactor process for producing liquid-phase organic compounds from biomass*. Copyright (C) 2012 American Chemical Society (ACS). All Rights Reserved.

DUMESIC, J. A. Award Address (George A. Olah Award in Hydrocarbon or Petroleum Chemistry sponsored by the George A. Olah Award Endowment). Strategies for catalytic conversion of lignocellulosic biomass to fuels and chemicals. 2012. American Chemical Society, CATL-35.

DUMESIC, J. A., ALONSO, D. M., BOND, J. Q. & WANG, D. 2011. *Integrated process and apparatus to produce hydrocarbons from aqueous solutions of lactones, hydroxy-carboxylic acids, alkene-carboxylic acids, and/or alcohols*. Copyright (C) 2012 American Chemical Society (ACS). All Rights Reserved.

DUNN, S. 2002. Hydrogen futures: toward a sustainable energy system. *International Journal of Hydrogen Energy,* 27**,** 235-264.

DUSSAULT, L., DUPIN, J. C., DUMITRIU, E., AUROUX, A. & GUIMON, C. 2005. Microcalorimetry, TPR and XPS studies of acid–base properties of NiCuMgAl mixed oxides using LDHs as precursors. *Thermochimica Acta,* 434**,** 93-99.

DUSSAULT, L., DUPIN, J. C., GUIMON, C., MONTHIOUX, M., LATORRE, N., UBIETO, T., ROMEO, E., ROYO, C. & MONZÓN, A. 2007. Development of Ni–Cu–Mg–Al catalysts for the synthesis of carbon nanofibers by catalytic decomposition of methane. *Journal of Catalysis,* 251**,** 223-232.

EBBESEN, T. W., HIURA, H., BISHER, M. E., TREACY, M. M. J., SHREEVE-KEYER, J. L. & HAUSHALTER, R. C. 1996. Decoration of carbon nanotubes. *Advanced Materials,* 8**,** 155-157.

EL DOUKKALI, M., IRIONDO, A., ARIAS, P. L., REQUIES, J., GANDARÍAS, I., JALOWIECKI-DUHAMEL, L. & DUMEIGNIL, F. 2012. A comparison of sol–gel and impregnated Pt or/and Ni based γ-alumina catalysts for bioglycerol aqueous phase reforming. *Applied Catalysis B: Environmental,* 125**,** 516-529.

ENERGILOGET 2007.

ESCH, U. & SCHNEIDER, A. 1944. Das System Nickel—Platin. *Zeitschrift für Elektrochemie und angewandte physikalische Chemie,* 50**,** 268-274.

EWAN, B. C. R. & ALLEN, R. W. K. 2005. A figure of merit assessment of the routes to hydrogen. *International Journal of Hydrogen Energy,* 30**,** 809-819.

FATHI, M., BJORGUM, E., VIIG, T. & ROKSTAD, O. A. 2000. Partial oxidation of methane to synthesis gas:: Elimination of gas phase oxygen. *Catalysis Today,* 63**,** 489-497.

FEIO, L. S. F., HORI, C. E., DAMYANOVA, S., NORONHA, F. B., CASSINELLI, W. H., MARQUES, C. M. P. & BUENO, J. M. C. 2007. The effect of ceria content on the properties of Pd/CeO2/Al2O3 catalysts for steam reforming of methane. *Applied Catalysis A: General,* 316**,** 107-116.

FRÜHBERGER, B., ENG, J., JR. & CHEN, J. G. 1997. Observation of anomalous reactivities of Ni/Pt(111) bimetallic surfaces. *Catalysis Letters,* 45**,** 85-92.

FU, X.-Z., LIANG, Y., CHEN, S.-P., LIN, J.-D. & LIAO, D.-W. 2009. Pt-rich shell coated Ni nanoparticles as catalysts for methanol electro-oxidation in alkaline media. *Catalysis Communications,* 10**,** 1893-1897.

GERMANI, G. & SCHUURMAN, Y. 2006. Water-gas shift reaction kinetics over μ-structured Pt/CeO2/Al2O3 catalysts. *AIChE Journal,* 52**,** 1806-1813.

GORTE, R. J. & ZHAO, S. 2005. Studies of the water-gas-shift reaction with ceria-supported precious metals. *Catalysis Today,* 104**,** 18-24.

GREELEY, J., MAVRIKAKIS, M. 2004. Alloy catalysts designed from first principles. *Nat Mater,* 3**,** 810-815.

GRENOBLE, D. C., ESTADT, M. M. & OLLIS, D. F. 1981. The chemistry and catalysis of the water gas shift reaction: 1. The kinetics over supported metal catalysts. *Journal of Catalysis,* 67**,** 90-102.

HARYANTO, A., FERNANDO, S. D., TO, S. D. F., STEELE, P. H., PORDESIMO, L. & ADHIKARI, S. 2009. Hydrogen Production through the Water−Gas Shift Reaction: Thermodynamic Equilibrium versus Experimental Results over Supported Ni Catalysts. *Energy & Fuels,* 23**,** 3097-3102.

HUANG, T.-J., YU, T.-C. & JHAO, S.-Y. 2005. Weighting Variation of Water−Gas Shift in Steam Reforming of Methane over Supported Ni and Ni−Cu Catalysts. *Industrial & Engineering Chemistry Research,* 45**,** 150-156.

HUBER, G. W., CORTRIGHT, R. D. & DUMESIC, J. A. 2004. Renewable Alkanes by Aqueous-Phase Reforming of Biomass-Derived Oxygenates. *Angewandte Chemie International Edition,* 43**,** 1549-1551.

HUBER, G. W. & DUMESIC, J. A. 2006. An overview of aqueous-phase catalytic processes for production of hydrogen and alkanes in a biorefinery. *catalysis today,* 111**,** 119-132.

HUBER, G. W., SHABAKER, J. W., EVANS, S. T. & DUMESIC, J. A. 2006. Aqueous-phase reforming of ethylene glycol over supported Pt and Pd bimetallic catalysts. *Applied Catalysis B: Environmental,* 62**,** 226-235.

HWU, H. H., ENG, J. & CHEN, J. G. 2002. Ni/Pt(111) Bimetallic Surfaces: Unique Chemistry at Monolayer Ni Coverage. *Journal of the American Chemical Society,* 124**,** 702-709.

IEA 2006.

IEA 2007a.

IGLESIA, E., SOLED, S. L. & FIATO, R. A. 1992. Fischer-Tropsch synthesis on cobalt and ruthenium. Metal dispersion and support effects on reaction rate and selectivity. *Journal of Catalysis,* 137**,** 212-224.

IPCC 2007.

IRIONDO, A., BARRIO, V. L., CAMBRA, J. F., ARIAS, P. L., GÜEMEZ, M. B., NAVARRO, R. M., SÁNCHEZ-SÁNCHEZ, M. C. & FIERRO, J. L. G. 2008. Hydrogen Production from Glycerol Over Nickel Catalysts Supported on Al2O3 Modified by Mg, Zr, Ce or La. *Topics in Catalysis,* 49**,** 46-58.

IRIONDO, A., CAMBRA, J. F., BARRIO, V. L., GUEMEZ, M. B., ARIAS, P. L., SANCHEZ-SANCHEZ, M. C., NAVARRO, R. M. & FIERRO, J. L. G. 2011. Glycerol liquid phase conversion over monometallic and bimetallic catalysts: Effect of metal, support type and reaction temperatures. *Applied Catalysis B: Environmental,* 106**,** 83-93.

JI YEON KIM, SEONG HAK KIM, DONG JU MOON, JONG HO KIM, NAM COOK PARK & YOUNG CHUL KIM 2013. Aqueous phase reforming of glycerol over nanosize Cu-Ni catalysts. *Journal of Nanoscience and Nanotechnology,* 13**,** 593-597.

KIM, Y. S. 1968. Crystallographic study of cerium aluminate (CeAlO3). *Acta Crystallographica Section B,* 24**,** 295-296.

KING, D. L., ZHANG, L., XIA, G., KARIM, A. M., HELDEBRANT, D. J., WANG, X., PETERSON, T. & WANG, Y. 2010. Aqueous phase reforming of glycerol for hydrogen production over Pt–Re supported on carbon. *Applied Catalysis B: Environmental,* 99**,** 206-213.

KO, E.-Y., PARK, E., SEO, K., LEE, H., LEE, D. & KIM, S. 2006. Pt–Ni/γ-Al2O3 catalyst for the preferential CO oxidation in the hydrogen stream. *Catalysis Letters,* 110**,** 275-279.

KUIPER, A. E. T., MEDEMA, J. & VAN BOKHOVEN, J. J. G. M. 1973. Infrared and Raman spectra of benzaldehyde adsorbed on alumina. *Journal of Catalysis,* 29**,** 40-48.

KUNKES, E. L., SIMONETTI, D. A., DUMESIC, J. A., PYRZ, W. D., MURILLO, L. E., CHEN, J. G. & BUTTREY, D. J. 2008. The role of rhenium in the conversion of glycerol to synthesis gas over carbon supported platinum–rhenium catalysts. *Journal of Catalysis,* 260**,** 164-177.

LEHNERT, K. & CLAUS, P. 2008. Influence of Pt particle size and support type on the aqueous-phase reforming of glycerol. *Catalysis Communications,* 9**,** 2543-2546.

LI, Y., YANG, X.-Y., TIAN, G., VANTOMME, A. L., YU, J., VAN TENDELOO, G. & SU, B.-L. 2010. Chemistry of Trimethyl Aluminum: A Spontaneous Route to Thermally Stable 3D Crystalline Macroporous Alumina Foams with a Hierarchy of Pore Sizes. *Chemistry of Materials,* 22**,** 3251-3258.

LIN, J.-H., BISWAS, P., GULIANTS, V. V. & MISTURE, S. 2010. Hydrogen production by water–gas shift reaction over bimetallic Cu–Ni catalysts supported on La-doped mesoporous ceria. *Applied Catalysis A: General,* 387**,** 87-94.

LIU, J., SUN, B., HU, J., PEI, Y., LI, H. & QIAO, M. 2010. Aqueous-phase reforming of ethylene glycol to hydrogen on Pd/Fe3O4 catalyst prepared by co-precipitation: Metal–support interaction and excellent intrinsic activity. *Journal of Catalysis,* 274**,** 287-295.

LUO, N., FU, X., CAO, F., XIAO, T. & EDWARDS, P. P. 2008. Glycerol aqueous phase reforming for hydrogen generation over Pt catalyst – Effect of catalyst composition and reaction conditions. *Fuel,* 87**,** 3483-3489.

LUO, N., OUYANG, K., CAO, F. & XIAO, T. 2010. Hydrogen generation from liquid reforming of glycerin over Ni–Co bimetallic catalyst. *Biomass and Bioenergy,* 34**,** 489-495.

MAGLINAO, R. L. & HE, B. B. 2011. Catalytic Thermochemical Conversion of Glycerol to Simple and Polyhydric Alcohols Using Raney Nickel Catalyst. *Industrial & Engineering Chemistry Research,* 50**,** 6028-6033.

MANFRO, R. L., DA COSTA, A. F., RIBEIRO, N. F. P. & SOUZA, M. M. V. M. 2011. Hydrogen production by aqueous-phase reforming of glycerol over nickel catalysts supported on CeO2. *Fuel Processing Technology,* 92**,** 330-335.

MANFRO, R. L., PIRES, T. P. M. D., RIBEIRO, N. F. P. & SOUZA, M. M. V. M. 2013. Aqueous-phase reforming of glycerol using Ni-Cu catalysts prepared from hydrotalcite-like precursors. *Catalysis Science & Technology,* 3**,** 1278-1287.

MARIS, E. P. & DAVIS, R. J. 2007. Hydrogenolysis of glycerol over carbon-supported Ru and Pt catalysts. *Journal of Catalysis,* 249**,** 328-337.

MARIS, E. P., KETCHIE, W. C., MURAYAMA, M. & DAVIS, R. J. 2007. Glycerol hydrogenolysis on carbon-supported PtRu and AuRu bimetallic catalysts. *Journal of Catalysis,* 251**,** 281-294.

MENDELOVICI, L. & STEINBERG, M. 1985. Methanation and water-gas shift reactions over PtCeO2. *Journal of Catalysis,* 96**,** 285-287.

MENEZES, A. O., RODRIGUES, M. T., ZIMMARO, A., BORGES, L. E. P. & FRAGA, M. A. 2010. Production of renewable hydrogen from aqueous-phase reforming of glycerol over Pt catalysts supported on different oxides. *Renewable Energy,* 36**,** 595-599.

MIYAO, T., YAMAUCHI, M., NARITA, H. & NAITO, S. 2006. Remarkable support effect for liquid phase methanol reforming with water over supported Pt–Ru catalysts. *Applied Catalysis A: General,* 299**,** 285-291.

MONTOYA, J. A., ROMERO-PASCUAL, E., GIMON, C., DEL ANGEL, P. & MONZÓN, A. 2000. Methane reforming with CO2 over Ni/ZrO2–CeO2 catalysts prepared by sol–gel. *Catalysis Today,* 63**,** 71-85.

NASH, P. & SINGLETON, M. F. 1989. The Ni-Pt (Nickel-Platinum) system. *Bulletin of Alloy Phase Diagrams,* 10**,** 258-262.

OZAWA, M. & KIMURA, M. 1990. Effect of cerium addition on the thermal stability of gamma alumina support. *Journal of Materials Science Letters,* 9**,** 291-293.

ÖZGÜR, D. Ö. & UYSAL, B. Z. 2011. Hydrogen production by aqueous phase catalytic reforming of glycerine. *Biomass and Bioenergy,* 35**,** 822-826.

PANAGIOTOPOULOU, P. & KONDARIDES, D. I. 2004. Effect of morphological characteristics of TiO2-supported noble metal catalysts on their activity for the water–gas shift reaction. *Journal of Catalysis,* 225**,** 327-336.

PARK, K.-W., CHOI, J.-H., KWON, B.-K., LEE, S.-A., SUNG, Y.-E., HA, H.-Y., HONG, S.-A., KIM, H. & WIECKOWSKI, A. 2002. Chemical and Electronic Effects of Ni in Pt/Ni and Pt/Ru/Ni Alloy Nanoparticles in Methanol Electrooxidation. *The Journal of Physical Chemistry B,* 106**,** 1869-1877.

PERRICHON, V., RETAILLEAU, L., BAZIN, P., DATURI, M. & LAVALLEY, J. C. 2004. Metal dispersion of CeO2–ZrO2 supported platinum catalysts measured by H2 or CO chemisorption. *Applied Catalysis A: General,* 260**,** 1-8.

PIRAS, A., TROVARELLI, A. & DOLCETTI, G. 2000. Remarkable stabilization of transition alumina operated by ceria under reducing and redox conditions. *Applied Catalysis B: Environmental,* 28**,** L77-L81.

RAHMAN, M. M., CHURCH, T. L., MINETT, A. I. & HARRIS, A. T. 2013. Effect of CeO2 Addition to Al2O3 Supports for Pt Catalysts on the Aqueous-Phase Reforming of Glycerol. *ChemSusChem,* 6**,** 1006-1013.

RAHMAN, M. M., CHURCH, T. L., VARIAVA, M. F., MINETT, A. I. & HARRIS, A. T. 2014. *RSC advances (Accepted for publishing)*.

RODRIGUEZ, J. A., LIU, P., HRBEK, J., EVANS, J. & PÉREZ, M. 2007. Water Gas Shift Reaction on Cu and Au Nanoparticles Supported on CeO2(111) and ZnO(000$\bar 1$): Intrinsic Activity and Importance of Support Interactions. *Angewandte Chemie International Edition,* 46**,** 1329-1332.

RYNKOWSKI, J. M., PARYJCZAK, T. & LENIK, M. 1995. Characterization of alumina supported nickel-ruthenium systems. *Applied Catalysis A: General,* 126**,** 257-271.

SALASC, S., PERRICHON, V., PRIMET, M., CHEVRIER, M., MATHIS, F. & MORAL, N. 1999. Magnetic study of the interaction of hydrogen with a Pt/CeO2–Al2O3 catalyst: influence of the presence of chlorine. *Catalysis Today,* 50**,** 227-235.

SCHERRER, P. 1918. *Göttinger Nachr. Math. Phys. ,* 2**,** 98-100.

SHABAKER, J. W., DAVDA, R. R., HUBER, G. W., CORTRIGHT, R. D. & DUMESIC, J. A. 2003a. Aqueous-phase reforming of methanol and ethylene glycol over alumina-supported platinum catalysts. *Journal of Catalysis,* 215**,** 344-352.

SHABAKER, J. W., HUBER, G. W., DAVDA, R. R., CORTRIGHT, R. D. & DUMESIC, J. A. 2003b. Aqueous-Phase Reforming of Ethylene Glycol Over Supported Platinum Catalysts. *Catalysis Letters,* 88**,** 1-8.

SHABAKER, J. W., HUBER, G. W. & DUMESIC, J. A. 2004. Aqueous-phase reforming of oxygenated hydrocarbons over Sn-modified Ni catalysts. *Journal of Catalysis,* 222**,** 180-191.

SHAPOURI, H., DUFFIELD, J. A. & WANG, M. 2002. The energy balance of corn: An update. *No. 814, Agriculture, USDo: Office of the chief Economist*.

SHEN, X., GARCES, L.-J., DING, Y., LAUBERNDS, K., ZERGER, R. P., AINDOW, M., NETH, E. J. & SUIB, S. L. 2008. Behavior of H2 chemisorption on Ru/TiO2 surface and its application in evaluation of Ru particle sizes compared with TEM and XRD analyses. *Applied Catalysis A: General,* 335**,** 187-195.

SHERRELL, P. C., ZHANG, W., ZHAO, J., WALLACE, G. G., CHEN, J. & MINETT, A. I. 2012. Microwave Decoration of Pt Nanoparticles on Entangled 3D Carbon Nanotube Architectures as PEM Fuel Cell Cathode. *ChemSusChem,* 5**,** 1233-1240.

SHYU, J. Z. & OTTO, K. 1989. Characterization of Pt/γ-alumina catalysts containing ceria. *Journal of Catalysis,* 115**,** 16-23.

SINFELT, J. H. 1973. Specificity in Catalytic Hydrogenolysis by Metals. *In:* D.D. ELEY, H. P. & PAUL, B. W. (eds.) *Advances in Catalysis.* Academic Press.

SOARES, R. R., SIMONETTI, D. A. & DUMESIC, J. A. 2006. Glycerol as a Source for Fuels and Chemicals by Low-Temperature Catalytic Processing. *Angewandte Chemie International Edition,* 45**,** 3982-3985.

TAKANABE, K., AIKA, K.-I., SESHAN, K. & LEFFERTS, L. 2004. Sustainable hydrogen from bio-oil—Steam reforming of acetic acid as a model oxygenate. *Journal of Catalysis,* 227**,** 101-108.

TAKENAKA, S., SHIMIZU, T. & OTSUKA, K. 2004. Complete removal of carbon monoxide in hydrogen-rich gas stream through methanation over supported metal catalysts. *International Journal of Hydrogen Energy,* 29**,** 1065-1073.

TANKSALE, A. 2010. A review of catalytic hydrogen production processes from biomass. *Renewable & sustainable energy reviews,* 14**,** 166.

TANKSALE, A., BELTRAMINI, J. N., DUMESIC, J. A. & LU, G. Q. 2008. Effect of Pt and Pd promoter on Ni supported catalysts—A TPR/TPO/TPD and microcalorimetry study. *Journal of Catalysis,* 258**,** 366-377.

TEGOU, A., PAPADIMITRIOU, S., MINTSOULI, I., ARMYANOV, S., VALOVA, E., KOKKINIDIS, G. & SOTIROPOULOS, S. 2011. Rotating disc electrode studies of borohydride oxidation at Pt and bimetallic Pt–Ni and Pt–Co electrodes. *Catalysis Today,* 170**,** 126-133.

TIERNAN, M. J. & FINLAYSON, O. E. 1998. Effects of ceria on the combustion activity and surface properties of Pt/Al2O3 catalysts. *Applied Catalysis B: Environmental,* 19**,** 23-35.

TROVARELLI, A. 1996. Catalytic Properties of Ceria and CeO2-Containing Materials. *Catal. Rev. - Sci. Eng.,* 38**,** 439-520.

TUPY, S. A., KARIM, A. M., BAGIA, C., DENG, W., HUANG, Y., VLACHOS, D. G. & CHEN, J. G. 2012. Correlating Ethylene Glycol Reforming Activity with In Situ EXAFS Detection of Ni Segregation in Supported NiPt Bimetallic Catalysts. *ACS Catalysis,* 2**,** 2290-2296.

TURNER 1999.

VAN HAASTERECHT, T., LUDDING, C. C. I., DE JONG, K. P. & BITTER, J. H. 2013. Stability and activity of carbon nanofiber-supported catalysts in

the aqueous phase reforming of ethylene glycol. *Journal of Energy Chemistry,* 22**,** 257-269.
VANNICE, M. A. 1977. The catalytic synthesis of hydrocarbons from H2CO mixtures over the Group VIII metals: V. The catalytic behavior of silica-supported metals. *Journal of Catalysis,* 50**,** 228-236.
VIZCAÍNO, A. J., CARRERO, A. & CALLES, J. A. 2007. Hydrogen production by ethanol steam reforming over Cu–Ni supported catalysts. *International Journal of Hydrogen Energy,* 32**,** 1450-1461.
WANG, D., MONTANÉ, D. & CHORNET, E. 1996. Catalytic steam reforming of biomass-derived oxygenates: acetic acid and hydroxyacetaldehyde. *Applied Catalysis A: General,* 143**,** 245-270.
WANG, S. & LU, G. Q. 1998. Role of CeO2 in Ni/CeO2–Al2O3 catalysts for carbon dioxide reforming of methane. *Applied Catalysis B: Environmental,* 19**,** 267-277.
WANG, X., LI, N., PFEFFERLE, L. D. & HALLER, G. L. 2009. Pt–Co bimetallic catalyst supported on single walled carbon nanotube: XAS and aqueous phase reforming activity studies. *catalysis today,* 146**,** 160-165.
WAWRZETZ, A., PENG, B., HRABAR, A., JENTYS, A., LEMONIDOU, A. A. & LERCHER, J. A. 2010. Towards understanding the bifunctional hydrodeoxygenation and aqueous phase reforming of glycerol. *Journal of Catalysis,* 269**,** 411-420.
WEN, G., XU, Y., MA, H., XU, Z. & TIAN, Z. 2008. Production of hydrogen by aqueous-phase reforming of glycerol. *International Journal of Hydrogen Energy,* 33**,** 6657-6666.
WEN, G., XU, Y., XU, Z. & TIAN, Z. 2009. Characterization and Catalytic Properties of the Ni/Al2O3 Catalysts for Aqueous-phase Reforming of Glucose. *Catalysis Letters,* 129**,** 250-257.
WHITTINGTON, B. I., JIANG, C. J. & TRIMM, D. L. 1995. Vehicle exhaust catalysis: I. The relative importance of catalytic oxidation, steam reforming and water-gas shift reactions. *Catalysis Today,* 26**,** 41-45.
WIDYANINGRUM, R. N., CHURCH, T. L. & HARRIS, A. T. 2013. Promoting effect of Pd on H2 production from cellulose pyrolysis over mesocellular-foam-supported Ni catalysts. *Catalysis Communications,* 35**,** 45-50.
YAO, H. C. & YAO, Y. F. Y. 1984. Ceria in automotive exhaust catalysts: I. Oxygen storage. *Journal of Catalysis,* 86**,** 254-265.
YAO, Y.-F. Y. 1980. Oxidation of Alkanes over Noble Metal Catalysts. *Industrial & Engineering Chemistry Product Research and Development,* 19**,** 293-298.
YOSHIDA, T., OSHIMA, Y. & MATSUMURA, Y. 2004. Gasification of biomass model compounds and real biomass in supercritical water. *Biomass and Bioenergy,* 26**,** 71-78.
YU, R., CHEN, L., LIU, Q., LIN, J., TAN, K.-L., NG, S. C., CHAN, H. S. O., XU, G.-Q. & HOR, T. S. A. 1998. Platinum Deposition on Carbon Nanotubes via Chemical Modification. *Chemistry of Materials,* 10**,** 718-722.

ZHAO, D. & XU, B.-Q. 2006. Enhancement of Pt Utilization in Electrocatalysts by Using Gold Nanoparticles. *Angewandte Chemie International Edition,* 45**,** 4955-4959.

ZHUANG, Q., QIN, Y. & CHANG, L. 1991. Promoting effect of cerium oxide in supported nickel catalyst for hydrocarbon steam-reforming. *Appl. Catal.,* 70**,** 1-8.